

**A CAPPED NANOPOROUS SPONGE FOR DURABLE  
OXIDASE BIOSENSORS AND ESTABLISHMENT  
OF AN ELECTROCHEMICAL READOUT  
FOR ENZYME ACTIVITY ASSAYS**



**Waraporn Rernglit**

**A Thesis Submitted in Partial Fulfillment of the Requirements for the  
Degree of Doctor of Philosophy in Chemistry  
Suranaree University of Technology**

**Academic Year 2017**

การตรึงเอนไซม์ออกซิเดสในไบโอเซนเซอร์ด้วยท่อนาโนรูพรุน  
และการตรวจหาปฏิกิริยาของเอนไซม์ด้วยวิธีทางไฟฟ้าเคมี

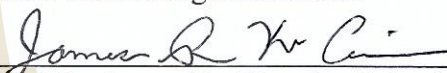


วิทยานิพนธ์นี้เป็นส่วนหนึ่งของการศึกษาตามหลักสูตรปริญญาวิทยาศาสตรดุษฎีบัณฑิต  
สาขาวิชาเคมี  
มหาวิทยาลัยเทคโนโลยีสุรนารี  
ปีการศึกษา 2560

**A CAPPED NANOPOROUS SPONGE FOR DURABLE OXIDASE  
BIOSENSORS AND ESTABLISHMENT OF AN  
ELECTROCHEMICAL READOUT FOR  
ENZYME ACTIVITY ASSAYS**

Suranaree University of Technology has approved this thesis submitted in partial fulfillment of the requirements for the Degree of Doctor of Philosophy.

Thesis Examining Committee

  
(Prof. Dr. James R. Ketudat-Cairns)

Chairperson

  
(Prof. Dr. Wipa Suginta)

Member (Thesis Advisor)

  
(Prof. Dr. Albert Schulte)

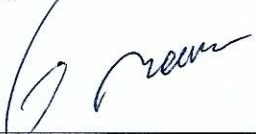
Member

  
(Asst. Prof. Dr. Jeerus Sucharitakul)

Member

  
(Assoc. Prof. Dr. Werasak Surareungchai)

Member

  
(Asst. Prof. Dr. Worawat Meevasana)

  
(Prof. Dr. Santi Maensiri)  
Vice Rector for Academic Affairs  
and Internationalization

Dean of Institute of Science

วารสาร วารสาร วารสาร : การตรึงเอนไซม์ออกซิเดสในไบโอเซนเซอร์ด้วยท่อนาโนรูพรุนและการตรวจหาปฏิกิริยาของเอนไซม์ด้วยวิธีทางไฟฟ้าเคมี (A CAPPED NANOPOROUS SPONGE FOR DURABLE OXIDASE BIOSENSORS AND ESTABLISHMENT OF AN ELECTROCHEMICAL READOUT FOR ENZYME ACTIVITY ASSAYS).

อาจารย์ที่ปรึกษา : ศาสตราจารย์ ดร.วิภา สุจินต์, 203 หน้า

งานวิจัยนี้ออกแบบการประดิษฐ์ไบโอเซนเซอร์สำหรับการตรวจวัดกลูโคสด้วยเทคนิควิเคราะห์แอมเพอร์โรเมทรีโดยใช้ท่อนาโนคาร์บอนซึ่งมีรูพรุนในการตรึงเอนไซม์กลูโคสออกซิเดส ซึ่งการตรึงเอนไซม์บนผิวหน้าอิเล็กโทรดโลหะแพลตตินัมหรือทองนั้นจะใช้วิธีการหยดท่อนาโนคาร์บอนและปล่อยให้แห้ง เพื่อให้ได้โครงข่ายของท่อนาโนคาร์บอนที่หนาแน่นและยึดติดกับอิเล็กโทรดได้ดี เมื่อท่อนาโนคาร์บอนที่หยดลงบนผิวหน้าอิเล็กโทรดแห้งแล้ว จากนั้นจึงหยดกลูโคสออกซิเดสเอนไซม์แล้วปล่อยให้แห้ง ในขั้นตอนสุดท้ายทำการปิดผิวหน้าของอิเล็กโทรดด้วยโพลีเมอร์ เพื่อเป็นการเก็บรักษาเอนไซม์ไว้ที่ผิวหน้าของอิเล็กโทรดให้ได้ยาวนานที่สุดระหว่างการทดลอง กลูโคสไบโอเซนเซอร์ที่พัฒนาขึ้น (CNT/GOx/EDP) ถูกนำมาใช้เป็นตัวตรวจวัดกลูโคสแบบแอมเพอร์โรเมทรี จากการทดลองพบว่าไบโอเซนเซอร์ชนิดนี้สามารถวัดความเข้มข้นของกลูโคสในช่วงที่สมการเป็นเส้นตรงได้สูงถึง 40 มิลลิโมลาร์ และสามารถวัดความเข้มข้นของน้ำตาลกลูโคสที่ต่ำที่สุดที่ 50 ไมโครโมลาร์ นอกจากนี้เมื่อนำไปใช้ในการทดลองในระบบฟลอสคานสำหรับตรวจวัดกลูโคสเพื่อทดสอบความแข็งแรงของโพลีเมอร์ที่ใช้สำหรับปิดผิวหน้าอิเล็กโทรด พบว่าไบโอเซนเซอร์นี้สามารถวัดความเข้มข้นของกลูโคสได้อย่างต่อเนื่อง ในระยะเวลามากกว่า 100 ชั่วโมง ซึ่งแสดงให้เห็นว่าเอนไซม์สามารถทำงานได้อย่างต่อเนื่องเมื่ออยู่ในรูพรุนของท่อนาโนคาร์บอนและโพลีเมอร์ที่ใช้ปิดผิวหน้าช่วยป้องกันไม่ให้เอนไซม์สูญหายออกไปจากผิวหน้าอิเล็กโทรดระหว่างการทดลอง

การตรวจหาปฏิกิริยาของเอนไซม์บีตา-เอ็น-อะซิติลกลูโคซามิเนส ( $\beta$ -N-acetylglucosaminidase) ที่ทำปฏิกิริยากับพาราเมทิลอัมเบอร์เฟอริน-เอ็น-อะซิติล-บีตา-ดี-กลูโคซามินสับสเตรต ด้วยวิธีทางไฟฟ้าเคมีแบบแอมเพอร์โรเมทรี พบว่าเมื่อสับสเตรตดังกล่าวเกิดปฏิกิริยากับเอนไซม์แล้วจะให้สารที่สามารถเกิดปฏิกิริยารีดอกซ์ได้ เทคนิคทางไฟฟ้าเคมีที่ใช้สำหรับ

ตรวจวัดการเกิดปฏิกิริยาระหว่างเอนไซม์และสับสเตรตคือการวัดปฏิกิริยาออกซิเดชันแบบแอมเพอร์โรเมทรี ด้วยอิเล็กโทรดใช้งานเพชรที่เจือโบรอน (Boron doped diamond electrode (BDD)) ซึ่งให้ศักย์ไฟฟ้าที่เหมาะสมกับอิเล็กโทรดใช้งานในขณะที่ตรวจวัดการเกิดปฏิกิริยา ในการทดลองจะแสดงสัญญาณออกมาในรูปของกระแสไฟฟ้าผ่านทางคอมพิวเตอร์ควบคุม ทำให้ทราบว่ามีการเกิดปฏิกิริยาระหว่างเอนไซม์กับสับสเตรตและสารที่เกิดขึ้นยังสามารถเกิดปฏิกิริยาออกซิเดชันได้ กระแสไฟฟ้าที่วัดได้จากการเกิดปฏิกิริยานั้นจะแปรผันตรงกับความเข้มข้นของสับสเตรต นอกจากนี้ยังสามารถสร้างกราฟแสดงความสัมพันธ์ของอัตราการเกิดปฏิกิริยาและความเข้มข้นของสับสเตรตแบบไฮเปอร์โบล่าฟังก์ชันได้ ซึ่งเป็นไปตามความสัมพันธ์ของสมการไมเคิลลิส-เมนเทน (Michaelis-Menten equation)

การศึกษากลไกการเกิดปฏิกิริยาระหว่างเอนไซม์เอ็น-อะซีติลกลูโคซามินิเดส ( $\beta$ -N-acetylglucosaminidase) จากเชื้อ *Vibrio harveyi* ที่มีผลต่อสับสเตรตพาราเมทิลอัมเบอร์เฟอริล-เอ็น-อะซีติล-บีตา-ดี-กลูโคซามิน (4-methylumbelliferyl-N-acetyl- $\beta$ -D-glucosaminide) โดย การวัดความเข้มของการวาวแสง (fluorescence) ที่เกิดจากการเปลี่ยนแปลงของความเข้มข้นของพาราเมทิลอัมเบอร์เฟอริล จากผลการศึกษาจนผลศาสตร์ก่อนเข้าสู่สถานะคงที่ พบว่ากลไกในการเกิดปฏิกิริยาระหว่างเอนไซม์และสับสเตรตดังกล่าวมาแล้วนั้นเป็นปฏิกิริยาที่เกิดขึ้นสองขั้นตอนคือขั้นแรกเป็นการจับกันระหว่างเอนไซม์กับสับสเตรต ขั้นที่สองเป็นการสลายพันธะระหว่าง 4-methylumbelliferyl กับ N-acetyl- $\beta$ -D-glucosaminide ด้วยค่า  $K_d$  (dissociate constant) เท่ากับ 99 ไมโครโมลาร์ ค่าคงที่  $k_{obs}$  เท่ากับ  $53 \pm 4$  ต่อวินาที และค่าคงที่  $k_{cat}$  เท่ากับ 11.5 ต่อวินาที

WARAPORN RERNGLIT : A CAPPED NANOPOROUS SPONGE FOR  
DURABLE OXIDASE BIOSENSORS AND ESTABLISHMENT OF AN  
ELECTROCHEMICAL READOUT FOR ENZYME ACTIVITY ASSAYS.  
THESIS ADVISOR : PROF. WIPA SUGINTA, Ph.D. 203 PP.

BIOSENSORS/CARBON NANOTUBES/IMMOBILIZATION/AMPEROMETRIC  
DETECTION/ENZYME ACTIVITY/CATALYTIC MECHANISM

This thesis approached advancements in the architecture of amperometric glucose biosensors with utilization of bare carbon nanotube (CNT) sensor deposits as a nanoporous immobilization matrix for glucose oxidase (GOx). A simple drop & dry procedure as used to create the dense and well-adhering conductive network of CNT nanowires on platinum (Pt) or gold (Au) disk electrodes. Fresh CNT surface films were then loaded in a subsequent drop & dry step with GOx as the biocatalytic unit. In a final step, an electrodeposition paint (EDP) was cathodically deposited as a biosensor top coat to prevent diffusional GOx loss during the desired long-term measurements and related prolonged measuring buffer exposure. CNT/GOx/EDP glucose biosensors have been tested and calibrated via common amperometry testing. The key performance characteristics of the generated biosensors were a literature-competitive glucose response linearity up to about 40 mM, a detection limit down to about 50  $\mu$ M, and over 100 hours of stable glucose signaling during continuous operation in an electrochemical flow cell, which is a remarkable CNT/GOx bilayer durability. The pronounced signal stability evidenced both the ability of the EDP glaze to block protein molecule escape from the trapping CNT matrix and decent CNT sponge biocompatibility.

Also established was a non-optical amperometric assay for the monitoring of  $\beta$ -*N*-acetylglucosaminidase action on a (4-MU)-labeled substrate. Here, advantage was taken of the redox activity of 4-MU, which creates electrochemical signals that can be detected on properly-charged noble metal or carbon working electrodes. Anodic 4-MU amperometry was operated in a reaction container in which enzyme and 4-MU-labeled substrate were brought together, while keeping a boron-doped diamond disk electrode at the 4-MU detection potential of + 700 mV vs. reference. In “real time” current recordings 4-MU liberation due to enzymatic substrate cleavage in the reaction buffer was visualized as a gradually increasing current signal and data from variations of substrate buffer levels made possible the construction of Michaelis Menten-type of enzyme activity plots.

Finally, the catalytic mechanism of the reaction of  $\beta$ -*N*-acetylglucosaminidase from *Vibrio harveyi* with 4-methylumbelliferyl- $\beta$ -*N*-acetyl-D-glucosaminide was inspected with a fluorimetric biochemical assay, executed in the stop-flow mode for fast kinetic data assessment of the enzymatic substrate hydrolysis reaction and related liberation of the fluorescent product 4-methylumbelliferone. From the result at pre-steady state kinetics found two-step process was revealed for the biocatalysis, first enzyme-substrate binding and second the bond break between 4-methylumbelliferyl and *N*-acetyl- $\beta$ -D-glucosaminide with  $K_d$  (dissociate constant) is 99  $\mu$ M,  $k_{obs}$  is  $53 \pm 4 \text{ s}^{-1}$  and  $k_{cat}$  is  $11.5 \text{ s}^{-1}$ .

School of Chemistry

Academic Year 2017

Student's Signature Waraporn Bernglit

Advisor's Signature Wipa Srit

## **ACKNOWLEDGEMENTS**

My time here at the Suranaree University of Technology had a great influence on me as a person and a scholar. I have learned a lot about myself in addition to the scientific skills which I have acquired. As my graduate studies come to an end and this thesis would not have been accomplished without the help of many people. I wish to give thanks to those who took part in this stage of my life. First of all, I would like to express my gratitude to my thesis advisor, Prof. Dr. Wipa Suginta and Prof. Dr. Albert Schulte. I am grateful for the support which they have supplied throughout my graduate career, including great advice, kindness, encouragement, and fruitful instructions throughout my Ph.D. thesis work and the most importantly for their giving me an opportunity to become a Ph.D. student.

Asst. Prof. Dr. Jeerus Sucharitakul is acknowledged for his kindness in accepting me to join for a total of a year at the Biochemistry Research Unit, Department of Dentistry, Chulalongkorn University, Bangkok, Thailand. I had a worthy time, gained a lot of data for my thesis and got the chance to gain additional knowledge and technical skills in biochemistry.

I am thankful to the SUT-Ph.D. grant by Suranaree University of Technology, Thailand for financial support through a Ph.D. scholarship.

Special thanks go to my committee members. I appreciate the time and effort they spent to evaluate my thesis. I am grateful for the advice and support that I have received from them.

I would be truly ungrateful if I did not acknowledge all my group members in the Biochemical-Electrochemistry Research Unit, especially, the group leaders, Prof. Dr. Wipa Suginta, Prof. Dr. Albert Schulte and Asst. Prof. Dr. Panida Khunkaewla. They were the forces behind a functional facility and always there for guidance of my work, if necessary. Moreover, I am grateful to our group members in the Biochemistry-Electrochemistry research unit for their help during my learning and doing experiments. I have gained a lot of effort, warmth and merriness at same time. I would also like to thank all of them that have been wonderful companions.

Last but not least, I would like to express my grateful admiration to my beloved parents and my sister for support, belief, understanding and encouragement all through the past five years. Not to forgot, my husband, Wiwat Yingsuttipan for his understanding, sharing happiness, sadness and standing beside me all the time. I could not have completed my education without the support and encouragement of all of those who stood with me. Thank you all very much.

มหาวิทยาลัยเทคโนโลยีสุรนารี

Waraporn Rernglit

# CONTENTS

	<b>Page</b>
ABSTRACT IN THAI.....	I
ABSTRACT IN ENGLISH .....	III
ACKNOWLEDGEMENTS.....	V
CONTENTS.....	VII
LIST OF TABLES .....	XV
LIST OF FIGURES .....	XVI
LIST OF ABBRIVIATION.....	XXV
<b>CHAPTER</b>	
<b>I INTRODUCTION.....</b>	<b>1</b>
1.1 Rationale of the study .....	1
1.2 General information on enzyme biosensors.....	4
1.2.1 Biosensors .....	4
1.2.2 First generation glucose biosensors.....	8
1.2.3 Second generation glucose biosensors.....	9
1.2.4 Third generation glucose biosensors.....	11
1.2.5 Direct electron transfer between redox active center of enzyme and electrode surface .....	12
1.2.6 Immobilizations of enzyme biosensor .....	14
1.2.7 Chitin and Chitosan as natural biocompatible material for enzyme immobilization.....	17

## CONTENTS (Continued)

	<b>Page</b>
1.2.8 Carbon nanotubes and biosensor applications .....	20
1.2.9 Principles amperometric glucose biosensor measurements .....	21
1.3 General characteristics of enzymes.....	25
1.3.1 What are enzymes? .....	25
1.3.2 Catalysis by enzymes .....	25
1.3.3 Enzyme kinetics .....	26
<b>II UNTAINTED CARBON NANOTUBES NETWORKS AS COMPETITIVE IMMOBILIZATION MATRIX FOR AMPEROMETRIC ENZYME BIOSENSORS .....</b>	<b>36</b>
2.1 Literature review .....	37
2.2 Experimental and methods.....	42
2.2.1 Chemicals.....	42
2.2.2 Electrochemical instrumentation .....	42
2.2.3 Fabrication of glucose biosensor by applying CNT/GOx/EDP onto platinum electrode.....	44
2.3 Results and discussion .....	46
2.3.1 Electrodes modified by carbon nanotubes .....	46
2.3.2 Morphology of carbon nanotubes modified platinum electrode....	49
2.3.3 Electrochemical capacitance measurements with carbon nanotube-modified platinum electrode .....	51

## CONTENTS (Continued)

	<b>Page</b>
2.3.4 Amperometric determination of glucose at CNT/GO <sub>x</sub> /EDP-based glucose biosensor .....	54
2.3.4.1 Platinum (Pt) electrode modification biosensor .....	54
2.3.5 The assessment of the detection limit for glucose quantifications with CNT/GO <sub>x</sub> /EDP-based glucose biosensors .....	61
2.3.6 Effect of electrochemically induced polymer precipitation.....	62
2.3.7 Reproducibility and long-term stability test with CNT/GO <sub>x</sub> /EDP glucose biosensors .....	66
2.3.8 Performance evaluation for quantitative measurements of model samples with pre-adjusted glucose levels .....	72
2.4 Conclusions.....	74
<b>III ADD-ON WORK WITH CNT/GOX/EDP-BASED BIOSENSOR .....</b>	<b>76</b>
3.1 Literature review .....	77
3.2 Experimental and methods.....	80
3.2.1 Chemicals.....	80
3.2.2 Electrochemical instruments.....	81
3.2.3 Fabrication of glucose biosensors by applying CNT/GO <sub>x</sub> /Chitin/EDP onto the electrode .....	82
3.2.4 Fabrication of glucose biosensors using CNT/(Fc+GO <sub>x</sub> +Chitosan)/EDP on the electrode .....	84

## CONTENTS (Continued)

	<b>Page</b>
3.3 Results and discussion .....	85
3.3.1 Amperometric determination of glucose at CNT/GO <sub>x</sub> /Chitin/ EDP-based glucose biosensor .....	89
3.3.1.1 Sensor variant based on modified platinum (Pt) electrodes .....	89
3.3.1.2 Sensor variant based on modified gold (Au) electrodes...	92
3.3.2 The assessment of the detection limit for glucose quantification with CNT/GO <sub>x</sub> /Chitin/EDP-based glucose biosensors .....	97
3.3.3 Direct electron transfer of glucose oxidase enzyme (GO <sub>x</sub> ).....	98
3.3.3.1 Test for biosensor with the ‘CNT/GO <sub>x</sub> /EDP’ design.....	98
3.3.3.2 Test for biosensor with the ‘CNT/GO <sub>x</sub> /chitin/EDP’ design .....	102
3.3.4 Effect of electrochemically induced polymer precipitation.....	105
3.3.5 Reproducibility and long-term stability tests with CNT/GO <sub>x</sub> /Chitin/EDP glucose biosensors.....	111
3.3.6 Performance evaluation for quantitative measurements of model samples with pre-adjusted glucose levels .....	116
3.3.7 Amperometric determination of glucose at CNT/(Fc- azide+Chitosan+GO <sub>x</sub> )/EDP-based glucose biosensor.....	118
3.4 Conclusions.....	126

## CONTENTS (Continued)

	Page
<b>IV ESTABLISHMENT OF AN ELECTROCHEMICAL READOUT FOR <math>\beta</math>- N-ACETYL GLUCOSAMINIDASE ENZYME ACTIVITY ASSAYS ....</b>	<b>128</b>
4.1 Literature review .....	129
4.2 Experimental and methods.....	134
4.2.1 Chemical .....	134
4.2.2 Electrochemical instruments .....	134
4.3 Results and discussion .....	135
4.3.1 Voltammetry and amperometry of dissolved 7-hydroxy-4- methylcoumarin (4-MU) .....	135
4.3.2 The amperometric <i>Vh</i> GlcNAcase activity assay.....	140
4.4 Conclusions.....	141
<b>V CATALYTIC REACTION OF 4MU-GLCNAC DEPENDENT BY <math>\beta</math>-N- ACETYL GLUCOSAMINIDASE FROM <i>VIBRIO HARVEYI</i>.....</b>	<b>143</b>
5.1 Literature review .....	144
5.2 Experimental and methods.....	149
5.2.1 Materials .....	149
5.2.2 Bacterial culture .....	149
5.2.3 Protein purification .....	150
5.2.4 Spectroscopic Studies .....	151
5.2.5 Pre-steady state kinetics .....	152
5.3 Results .....	153

## CONTENTS (Continued)

	<b>Page</b>
5.3.1 Steady-State Kinetics of <i>V<sub>h</sub></i> GlcNAc with fluorescence substrate .....	153
5.3.2 Pre-steady state kinetic and reaction mechanism with fluorescence substrate .....	154
5.3.3 Steady-State Kinetics of <i>V<sub>h</sub></i> GlcNAc with <i>p</i> NP-GlcNAc .....	156
5.4 Discussion .....	158
5.5 Conclusions.....	160
REFERENCES .....	161
APPENDICES .....	191
APPENDIX A STANDARD CURVE .....	192
APPENDIX B DERIVATION OF MECHANISM.....	194
APPENDIX C LIST OF PRESENTATION.....	200
APPENDIX D PUBICATION.....	202
CURRICULUM VITAE.....	203

## LIST OF TABLE

Table	Page
1.1 Existing immobilization procedures for enzymes – A comparison .....	16
1.2 Performance comparison of <i>p</i> -nitrophenol determination by various electrochemical modified electrodes.....	34
2.1 Summary performance of CNT/GOx/EDP biosensor.....	59
2.2 The recovery rate of CNT/GOx/EDP biosensor modified Pt electrode at various glucose concentration samples quantification by standard addition mode.....	73
3.1 Summary of performance of CNT/GOx/Chitin/EDP biosensor .....	95
3.2 The recovery rate of CNT/GOx/Chitin/EDP biosensor modified Pt electrode at various glucose concentrations of samples are quantified by standard addition mode .....	117

## LIST OF FIGURES

Figure	Page
1.1 A general schematic representation of a functional biosensor design .....	5
1.2 Three generations of glucose oxidase-based biosensor .....	7
1.3 The oxidation-reduction cascade of an active, “first-generation” glucose oxidase biosensor .....	9
1.4 Sequence of redox events that occur in ‘second generation’ glucose biosensors with redox recycling of the glucose oxidase supported by a dissolved artificial redox mediator.....	11
1.5 Simplified schematic representation of the third generation glucose biosensor system with direct electron transfer for enzyme re-oxidation .....	12
1.6 Importance of redox enzyme orientation on the transducing electrode surface for success with direct electron transfer from the electrode to the proteins redox site and back.....	13
1.7 Approaches to enzyme immobilization .....	15
1.8 Chemical structure of chitin and chitosan.....	18
1.9 Structure of carbon nanotube .....	21
1.10 Electrochemical set up for enzyme biosensor amperometry .....	23
1.11 Typical amperometric response of an enzyme biosensor .....	24
1.12 Free energy changes for an energetically favorable reaction showing the effects of a catalyst.....	26

## LIST OF FIGURES (Continued)

Figure	Page
1.13	Reaction progress curves for the loss of substrate and production of product during an enzyme-catalyzed reaction .....27
1.14	Progress curves of enzyme-catalyzed reactions with different starting concentrations of substrate.....28
1.15	Dependence of velocity ( $v$ ) on substrate concentration $[S]$ according to the Michaelis-Menten plot .....29
1.16	The experimental cycle of microplate-based enzyme assay with optical detection of enzyme-substrate interaction for kinetic parameter assessment.....31
1.17	Redox reaction of $p$ -nitrophenol at electrode surface .....32
1.18	Electrochemical behavior of $p$ NP at a carbon paste electrode and the proposed electrochemical reaction mechanism .....33
1.19	Enzymatic reactions followed by the electrooxidation of the liberated $p$ NP .....35
2.1	Illustration of bare commercial platinum 3-mm-diameter disk electrode and bare home-made gold 3-mm-diameter disk electrode.....43
2.2	The electrochemical workstation for long-term biosensor testing on flow mode .....44
2.3	Schematic diagram for the preparation of CNT/GO <sub>x</sub> /EDP modified platinum or gold as used in the biosensor measurement.....46

## LIST OF FIGURES (Continued)

Figure	Page
2.4	Schematic drawing of biosensor configuration modified by CNT comparison between normal glucose biosensor and the case of an utilization of a conductive CNT deposit as immobilization matrix.....48
2.5	Morphology of a carbon nanotubes modified platinum electrode .....50
2.6	Schematic diagram of the procedure used for the preparation of CNT-modified platinum in the capacitance measurement.....52
2.7	Electrode capacitance determinations for a bare and CNT-modified platinum electrode.....53
2.8	Current-time trace as acquired in the course of a calibration trial with a (CNT/GOx)/EDP-Pt glucose biosensor .....55
2.9	Electrochemical assessed biosensor calibration curve plot obtained from the amperometric recording measurement .....56
2.10	Current-time trace as acquired in the course of a calibration trial with a (CNT/GOx)/EDP-Au glucose biosensor and electrochemical assessed biosensor calibration curve plot .....58
2.11	Detection limits assessment for glucose quantification at CNT/GOx-modified platinum electrode .....62
2.12	Illustrated the partial step of glucose biosensor fabrication by CNT/GOx/EDP onto platinum or gold electrodes .....63
2.13	Typical amperometric response of an enzyme biosensor of CNT/GOx and electrochemical assessed biosensor calibration curve.....65

## LIST OF FIGURES (Continued)

Figure	Page
2.14	Performance comparison between CNT/GO <sub>x</sub> /EDP biosensor and CNT/GO <sub>x</sub> biosensor .....65
2.15	Performance comparison between CNT/GO <sub>x</sub> /EDP biosensor and CNT/GO <sub>x</sub> biosensor at different day measurement.....66
2.16	Electrochemical assessed biosensor calibration curve at CNT/GO <sub>x</sub> /EDP modified gold electrode which constructed by the analysis of the amperometric recording in batch experiment .....67
2.17	Long-time stability test with CNT/GO <sub>x</sub> /EDP glucose biosensors which established on a Au disk electrode transducer in an electrochemical flow cell measurement .....69
2.18	Typical amperometric response of a CNT/GO <sub>x</sub> /EDP glucose biosensor to successive additions of substrate for a flow-based calibration and a flow-based model sample analysis via standard addition .....71
2.19	Recovery rate assessments for glucose quantification in 1.0 mM model samples with CNT/GO <sub>x</sub> /EDP-based glucose biosensors modified Pt electrode .....73
3.1	Advantages of chitin and chitosan for biosensor applications.....79
3.2	Schematic diagram of the procedure used for the preparation of CNT/GO <sub>x</sub> /Chitin/EDP modified platinum or gold as used in the biosensor measurement.....83

## LIST OF FIGURES (Continued)

<b>Figure</b>	<b>Page</b>
3.3	Schematic diagram of the procedure used for the preparation of CNT/(Fc+Chitosan+GOx)/EDP modified platinum as used in the biosensor measurement.....85
3.4	Schematic drawing of biosensor configuration modified by CNT comparison between normal glucose biosensor and the case of an utilization of a conductive CNT and Chitin deposit as immobilization matrix .....87
3.5	Schematic drawing of biosensor configuration modified by CNT in the case of an utilization of a conductive carbon nanotubes chitosan polymer and ferrocene deposit as immobilization matrix.....89
3.6	Amperometric response of an enzyme biosensor and electrochemical assessed biosensor calibration curve at CNT/GOx/Chitin/EDP modified platinum electrode.....91
3.7	Amperometric response of an enzyme biosensor and electrochemical assessed biosensor calibration curve at CNT/GOx/Chitin/EDP modified gold electrode.....93
3.8	Performance comparison for electrochemical assessed biosensor calibration curves by the analysis of the amperometric recording at different electrode substrate between platinum and gold electrodes .....94
3.9	Detection limits assessment for glucose quantification at CNT/GOx/Chitin/EDP modified platinum electrode.....98

## LIST OF FIGURES (Continued)

<b>Figure</b>	<b>Page</b>
3.10 Cyclic voltammograms of CNT and CNT/GO <sub>x</sub> modified platinum electrode with de-aerated solution .....	100
3.11 Cyclic voltammograms of CNT/GO <sub>x</sub> modified platinum electrode with de-aerated solution at various scan rates and the analysis plots of anodic and cathodic peaks as a function of scan rates.....	102
3.12 Cyclic voltammograms of CNT and CNT/GO <sub>x</sub> /Chitin modified platinum electrodes with de-aerated solution .....	103
3.13 Cyclic voltammograms of CNT/GO <sub>x</sub> /Chitin modified platinum electrode with de-aerated solution at various scan rates and the analysis plots of anodic and cathodic peaks as a function of scan rates .....	105
3.14 Illustration of a partial series of the steps used in fabrication of glucose biosensor with CNT/GO <sub>x</sub> /Chitin/EDP on platinum or gold electrodes.....	106
3.15 Amperometric response of enzyme biosensor at CNT/GO <sub>x</sub> /Chitin-modified platinum electrode show the amperometric response of an enzyme biosensor and amperometric response of an enzyme biosensor .....	108
3.16 Electrochemically assessed biosensor calibration curve as constructed by the analysis of the amperometric recording in CNT/GO <sub>x</sub> /Chitin/EDP biosensor and CNT/GO <sub>x</sub> /Chitin biosensor .....	109

## LIST OF FIGURES (Continued)

<b>Figure</b>	<b>Page</b>
3.17 Electrochemical assessed biosensor calibration curve as constructed by the analysis of the amperometric recording show the performance comparison between CNT/GO <sub>x</sub> /Chitin/EDP biosensor and CNT/GO <sub>x</sub> /Chitin biosensor at different day measurement .....	110
3.18 Electrochemical assessed biosensor calibration curve as constructed by the analysis of the amperometric recording at CNT/GO <sub>x</sub> /Chitin/EDP modified platinum electrode at different days in batch measurement .....	112
3.19 Typical amperometric response of an enzyme biosensor to successive additions of substrate at different days and the experiment was performed in flow system .....	113
3.20 Amperometric response of an enzyme biosensor glucose quantification and model sample analysis via standard addition.....	115
3.21 Recovery rate assessments for glucose quantification in model samples with CNT/GO <sub>x</sub> /Chitin/EDP-based glucose biosensors modified on platinum electrode .....	117
3.22 Electrochemical assessed biosensor calibration curve as constructed by the analysis of the amperometric recording with CNT/(Fc-azide+Chitosan+GO <sub>x</sub> )/EDP biosensor .....	119
3.23 Performance comparison between CNT/(Chitosan+GO <sub>x</sub> )/EDP and (Chitosan+GO <sub>x</sub> )/EDP biosensor show the electrochemical assessed biosensor calibration curve .....	120

## LIST OF FIGURES (Continued)

Figure	Page
3.24	Performance comparison between CNT/(Fc+Chitosan+GOx)/EDP and CNT/(Chitosan+GOx)/EDP and (Chitosan+GOx)/EDP biosensors.....122
3.25	Typical amperometric response of an CNT/(Fc+Chitosan+GOx)/EDP biosensor to successive additions of substrate at different days performed in a flow system.....124
3.26	Amperometric response of an enzyme biosensor glucose quantification with a CNT/(Fc+Chitosan+GOx)/EDP modified electrode.....125
4.1	Amperometric monitoring of glucose oxidase activity in terms of glucose to gluconolactone/gluconic acid conversion.....131
4.2	Current-time profiles in a buffer solution containing the Prol $\beta$ -NA, the current increase after added PIP enzyme to the substrate solution and enzymatic reaction of proline iminopeptidase .....132
4.3	Enzyme kinetic assay utilizing 4-MU label attachment to sugar substrate and fluorescent spectrophotometry for visualization and determination of substrate/enzyme interaction .....133
4.4	Cyclic voltammograms responses of 4-MU obtained at a 3 mm disk-shaped boron doped diamond electrode.....136
4.5	Cyclic voltammograms responses of 100 $\mu$ M 4-MU as obtained at boron doped diamond electrode.....137

## LIST OF FIGURES (Continued)

Figure	Page
4.6	Collection of differential pulse voltammograms from a voltammetric 4-MU calibration trial with a disk-shaped boron-doped diamond electrode of 3 mm diameter .....138
4.7	Collection of 4-MU amperograms, acquired with a boron doped diamond electrode of diameter at +700 mV vs. reference electrode for different 4-MU concentrations.....139
4.8	Amperometric recordings of <i>VhGlcNAcase</i> cleavage activity on (4-MU)-labeled <i>N</i> -acetyl- $\beta$ -D-glucosaminide .....141
5.1	Chitin degradation pathway of <i>Vibrio harveyi</i> class involves the successive action of two classes of chitinolytic enzymes <i>VhChiA</i> and <i>VhGlcNAcases</i> .....146
5.2	The catalytic mechanisms of <i>GlcNAcases</i> .....147
5.3	Overall structure of GH20 <i>VhGlcNAcase</i> consists of three domains .....147
5.4	The steady-state kinetic of <i>VhGlcNAc</i> with 4MU- <i>GlcNAc</i> .....153
5.5	Pre-steady state kinetics of <i>VhGlcNAc</i> with 4MU- <i>GlcNAc</i> .....155
5.6	The catalytic mechanism of $\beta$ - <i>N</i> -acetylglucosaminidase enzyme toward 4-methylumbelliferyl- <i>N</i> -acetyl- $\beta$ -D-glucosaminide substrate.....156
5.7	The steady-state kinetic of <i>VhGlcNAc</i> with <i>pNP-GlcNAc</i> .....157
5.8	The kinetic mechanism for the reaction of <i>VhGlcNAcase</i> catalyzed fluorogenic substrate .....159

## LIST OF ABBREVIATIONS

BREs	Biological recognition elements
CE	Counter electrode
CNT	Carbon nanotubes
DMF	Dimethylformamide
DNA	Deoxyribonucleic acid
EC	Electrochemical
EDC	1-Ethyl-3-(3-dimethylaminopropyl) carbodiimide
Fc	Ferrocene
GCE	Glassy carbon electrode
GH3	Glycoside hydrolase family 3
GH18	Glycoside hydrolase family 18
GH20	Glycoside hydrolase family 20
GI	Gelatin
GlcNAc	<i>N</i> -acetylglucosamine
GOx	Glucose oxidase
HPLC	High-performance liquid chromatography
HRP	Horseradish peroxidase
$I_{\max}$	Maximum current
IPTG	Isopropyl thio- $\beta$ -D-galactoside
LB	Luria-Bertani lysogeny broth
PMSF	Phenylmethylsulfonylfluoride

**LIST OF ABBREVIATIONS (Continued)**

$K_m$	Michaelis-Menten constant
$k_{cat}$	Catalytic constant
MWCNTs	Multi-walled carbon nanotubes
NHS	N-Hydroxysuccinimide
NEEs	Nanoelectrode ensembles
PIP	prolineiminopeptidase
PMSF	phenylmethylsulfonyl fluoride
<i>p</i> NP	<i>p</i> -Nitrophenol
<i>p</i> NP-GlcNAc	<i>para</i> -nitrophenyl-N-acetyl-glucosaminide
PUCNTs	Partially unzipped carbon nanotubes
RE	Reference electrode
RGO	Graphene oxide
SWCNTs	Single-walled carbon nanotubes
SPE	Screen print electrode
SPCEs	screen-printed carbon electrodes
SDS	Sodium dodecyl sulfate
$V_{max}$	Maximum velocity
WE	Working electrode
$\beta$ -NA	$\beta$ -naphthyamine
4MU-GlcNAc	4-Methylumbelliferyl N-acetyl- $\beta$ -D-glucosaminide

# CHAPTER I

## INTRODUCTION

### 1.1 Rationale of the study

In the past few decades tremendous progress has been made with respect to the quality of electrochemical instrumentation and potentiostat with picoampere current and submicrosecond time resolution are through the advancements in the hard- and software of the electronics behind potentiostat operation with reasonable price levels on the market. At the same time the fields of Material and Nanotechnology Science made available a plethora of micro- and nanomaterials with potential to be utilized on electrochemical sensor platforms for enhancements of analytical performance. Taking advantage of these two favorable technology trends, modern electrochemical detection schemes were capable to establish themselves as an important fragment of Analytical Chemistry and prominent examples of application success cases are the trace analysis of environmental pollutants, the quantification of healthy or toxic food ingredients, the measurement of clinical disease biomarkers and the monitoring of industrial synthesis product formation. In the frame of the upsurge of the field of electroanalysis the themes of this Ph.D. thesis covered four distinct subjects. Firstly, work was done with relation to the manufacture of efficient amperometric glucose oxidase (GOx)-based glucose biosensors. More specifically the objective was to demonstrate that pure carbon nanotube (CNT) electrode surface deposits with no additional nanomaterial could

function as well for glucose determinations as the many published CNT/GO<sub>x</sub>-based glucose biosensors with complicated multi-component sensing layer arrangements. As valuable gain was expected a pronounced simplification of the sensor fabrication, of course with no concession in terms of analytical performance. Success with the initial work assumed, the second thesis part considered the incorporation of biocompatible chitin and/or chitosan as polymeric supplementation and ferrocene as a redox-active material into bare CNT electrode modifications. Motivation for the chitin/chitosan consideration was the predictable chance to prolong the life time of sensors via provision of a gentler biopolymeric environment while ferrocene addition offered the possibility to be independent on the presence of dissolved oxygen for measurements in de-aerated samples. Part three was designed to approach the development of an electrochemical assay for the determination of kinetic enzyme properties. Here, the main motivation was to establish the novel electrochemical assay as an alternative option to the optical microplate assays that are current the lone standard for biochemists and enzymologists for enzyme kinetic studies. And in the last part, the activity of  $\beta$ -N-acetylglucosaminidase from *Vibrio harveyi* (VhGlcNAcase), the model enzyme for electrochemical assay development, has been looked at with standard biochemical screening to facilitate better understanding of the kinetics of this protein.

The research objectives of this Ph.D. thesis, briefed in an itemized list, were:

- (1) Establishment of pure CNT-based amperometric glucose biosensors that are competitive with respect to analytical performance to published options but significantly simpler in their architecture. Tasks included completion of an easy to perform and highly reproducible procedure for the fabrication of the sensor

targets and then their thorough functional characterization via electrochemical performance tests.

- (2) The blending of CNT immobilization matrices with the two biomaterials chitin and/or chitosan and the redox compound ferrocene with aim on improved long-term stability and functioning in de-aerated sample solutions. Tasks included completion of the blended CNT sensor modifications and again their functional characterization via electrochemical performance tests.
- (3) Development of a quantitative electrochemical enzyme kinetic assay via utilization of redox labeled enzyme substrates that release their electrochemically detectable functionality in course of cleaving interaction with the biocatalyst. Model enzyme for this study part was  $\beta$ -N-acetylglucosaminidase from *Vibrio harveyi* (*VhGlcNAcase*) and tasks included the establishment of the electrochemical detection of the redox labels of choice, proof of principle of real-time electrochemical visualization of enzymic substrate conversion and finally the generation of enzyme activity vs. substrate concentration plots for kinetic analysis and comparison of the novel electrochemical with the routine optical microplate methodology.
- (4) A final thesis part addressed for the model enzyme of task (3) the inspection of the kinetics of its catalytic action via biochemical assays with optical detection.

The following sections will handle in sequential order the presentation of comprehensive general information on the background relevant for the three thesis subjects, a review of literature-known work with importance to the thesis topics, namely CNT-based biosensor constructions and optical and electrochemical enzyme activity

measurements, a summary of the applied research methodologies, the offer of obtained results with discussion and finally a conclusion, comments on possible future work and the list of the references.

## **1.2 General information on enzyme biosensors**

The first part of this work dealt with the development of an effective enzyme immobilization on the electrode platforms of amperometric biosensors. Therefore, the following sub-section will inform about general features of enzyme biosensors, in particular of glucose biosensor. Covered will be the principle of biosensor functioning, a coverage of possible strategies for enzyme immobilization, insights in enzyme biosensor signal generation including hints on direct electron transfer between an electrode surface and a protein biocatalyst and finally a description of the methodology of electrochemical enzyme biosensor testing and calibration.

### **1.2.1 Biosensors**

Biosensors are generally defined as analytical tools which connect a biological recognition element (BRE) to a solid transducer surface to convert an observed response due to interfacial BRE/analyte interaction into a measurable electrical signal, whose magnitude is proportional to analyte concentrations. Based on the type of transducer used, biosensors have been divided into optical, calorimetric, piezoelectric, thermometric and electrochemical biosensors (Chaubey and Malhotra, 2002; Monošík *et al.*, 2012; Newman and Turner, 1992; Perumal and Hashim, 2014).

Typical biosensors are comprised of three main functional components: (i) the biological recognition element (BRE) that are specific for the target molecules (analyte) and provide selectivity in the presence of other chemicals, (ii) a solid transducer that converts the interaction of the BREs with its affinity partner into signal and (iii) a signal processing system that converts the signal further into readable and storable form (Niraj *et al.*, 2012; Yoo and Lee, 2010). This constellation is depicted in Figure 1.1, which shows a general functional design of a biosensor with the specified components. Biosensors can be applied to a large variety of samples including body fluids, food samples, cell cultures and environmental samples (Fracione *et al.*, 2012; Grieshaber *et al.*, 2008; Prodromidis and Karayannis, 2002).

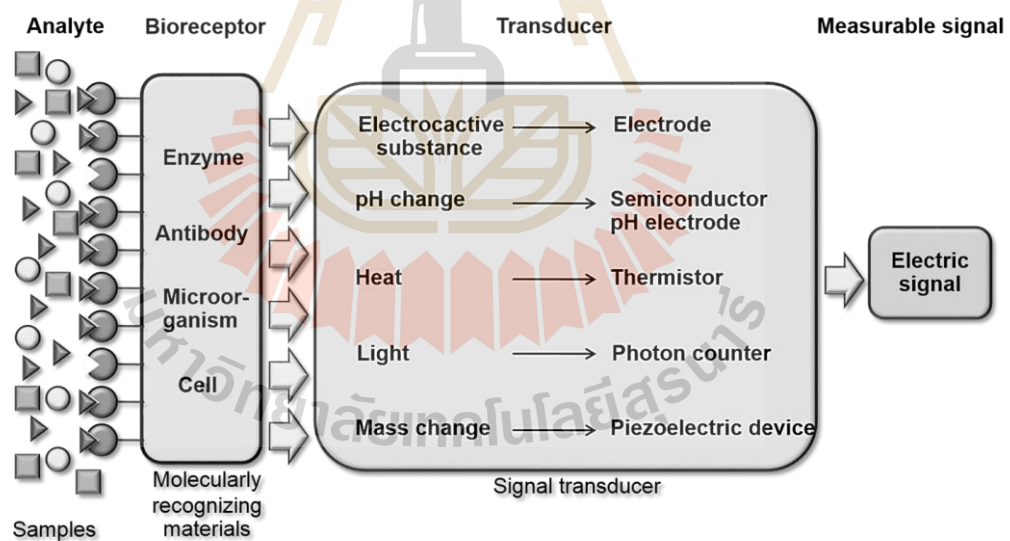


**Figure 1.1** A general schematic representation of a functional biosensor design. Shown are the biological recognition element (BRE) in contact with a transducer element which detects a physical, chemical or electrical change when the recognition element binds analyte from the solutions.

Most used biological recognition elements in biosensors are enzymes, antibodies, and single-stranded DNA fragments and the corresponding sensors are called enzyme biosensors, immunosensors and DNA sensors, respectively. The variety of sensing opportunities that an electrochemical signal transduction offers for analyte detection with an enzyme biosensor can be best exemplified with the common case of glucose quantification with glucose oxidase (*GOx*) biosensors (J. Wang, 2008). In an electrochemical (amperometric) *GOx* biosensor, most often the generation of hydrogen peroxide ( $H_2O_2$ ) (the product of enzymatic glucose conversion into gluconolacton/gluconic acid) or the consumption of oxygen (the cofactor used for enzyme recycling at the end of a catalytic cycle) is measured with the transducer, an  $H_2O_2$  or  $O_2$  sensitive electrode. Alternatively, the pH change due to gluconic acid formation may be traced via potentiometric proton-sensitive detection. In this PhD study *GOx* was chosen a favored model enzyme for the biosensor preparation and characterization work since this enzyme is (1) widely used as in (glucose) biosensor research and development (R&D) and thus has a lot of literature cases for comparison available, (2) easily commercially available at high quality and rather low price and (3) robust and stable in dissolved and immobilized state.

Sensitivity and stability of (glucose) biosensors are key features for quantitative analysis applications (J. Wang and Musameh, 2003). Such key properties depend on the effective recycling of the enzyme after a substrate conversion event and a reasonable life time of the functional biomacromolecule in the immobilization layer on the sensor surface. After reaction with a substrate molecule, the enzyme is in a reduced state and needs to be re-oxidized to be ready for the next cycle of substrate conversion.

Figure 1.2 is a representation of the 1<sup>st</sup>, 2<sup>nd</sup> and finally 3<sup>rd</sup> generation of glucose biosensors. As can be seen, the biosensing process involves a dissolved cofactor in the first two designs, more specifically a native or a synthetic redox species for the 1<sup>st</sup> and 2<sup>nd</sup> generation biosensor, respectively (Figures 1.2A and B). For the 3<sup>rd</sup> generation glucose biosensor, the cofactor is either represented by the electrode itself, employing direct electron transfer (DET) for reduced to oxidized enzyme transformation (Figure 1.2C) or a chain of redox equivalents that are covalently fixed to the polymeric structure of the immobilization layer and electrically wired (connected) to the electrode via electron hopping from enzyme to redox site and then from redox site to redox site with the electrode being destination for electron delivery (Figure 1.2D).

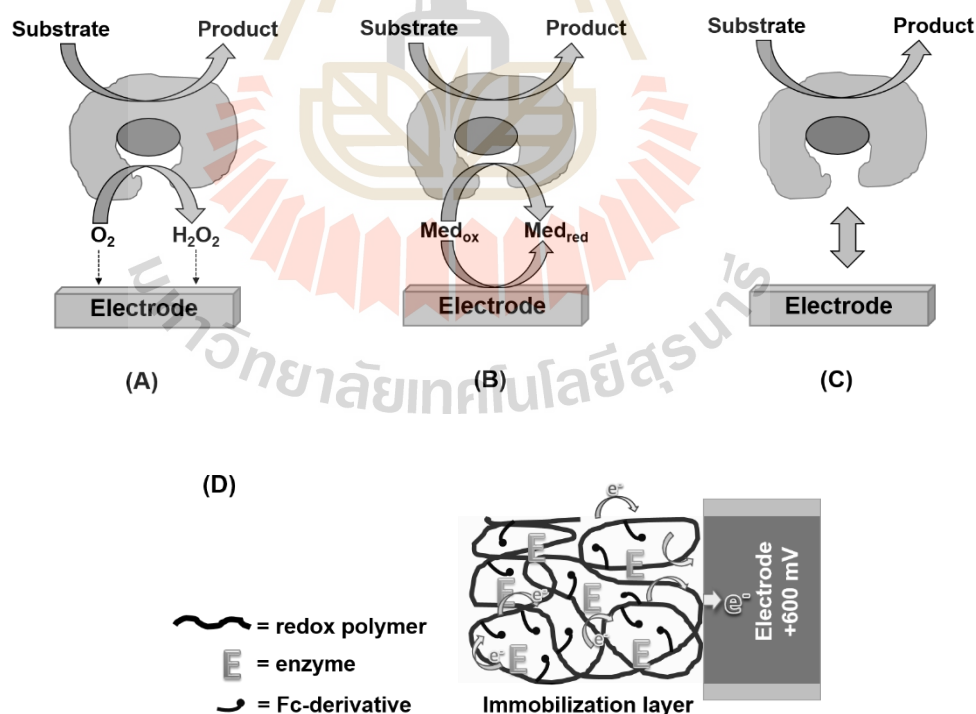
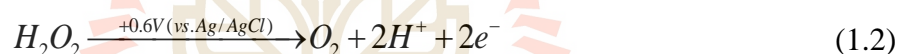


**Figure 1.2** Three generations of a glucose oxidase-based biosensor based on (A) the use of natural oxygen as cofactor, (B) the use of an artificial redox mediators as

cofactor, (C) the direct electron transfer (DET) between GOx and the electrode or enzyme electrode (J. Wang, 2008) and the exploitation of a redox polymer (here with ferrocene-based active sites) for GOx recycling (D).

### 1.2.2 First generation glucose biosensors

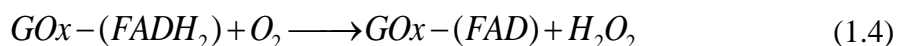
First generation glucose biosensors rely on the use of dissolved oxygen as natural co-substrate. Cyclic enzyme/sugar interaction in cofactor presence leads to the generation of hydrogen peroxide following equation 1.1. The concentration of  $H_2O_2$  is quantifiable through, for instance, amperometry at constant potential (equation 1.2).



The biocatalytic reaction happens in a first step and involves the reduction of the oxidized flavin group in the enzyme structure  $GOx-(FAD)$  and oxidation of substrate glucose, yielding the reduced form of the enzyme  $GOx-(FADH_2)$  and gluconolactone (equation 1.3).



In the subsequent step, the re-oxidation of the reduced flavin unit by molecular oxygen regenerates the oxidized form of the enzyme  $GOx-(FAD)$  (equation 1.4), which prepare the enzyme for the next catalytic glucose conversion.



$H_2O_2$  is a side product of the catalytic glucose→gluconolactone conversion. As species that can be oxidized or reduced it is detectable at appropriately polarized electrode surface. Figure 1.3 shows a schematic cascade of oxidation and reduction reactions of glucose in a “first-generation”  $GOx$  biosensor. The anodic electrooxidation of  $H_2O_2$  liberates electrons for current flow.  $H_2O_2$  and glucose are produced in a 1:1 ratio in the enzyme action and produced  $H_2O_2$  levels are thus proportional to the glucose concentrations seen by  $GOx$ . Therefore, measured  $H_2O_2$  currents can be used for a ‘biosensor-type’ of quantification of glucose (J. Wang, 2008).

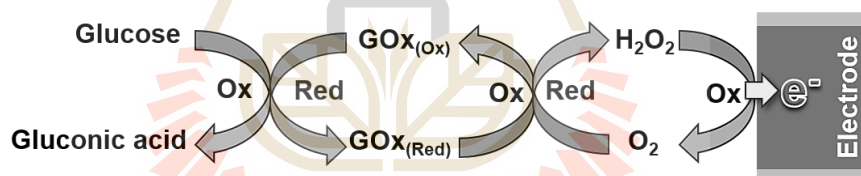
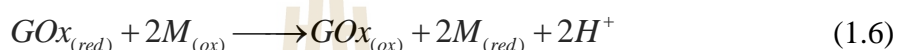
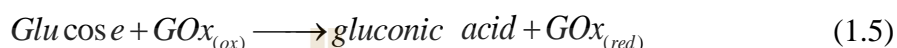


**Figure 1.3** The oxidation-reduction cascade that happens if a  $GOx$ -covered electrode is exposed to an aerated glucose-containing sample solution and the sensor is operated as 1<sup>st</sup> generation biosensor.

### 1.2.3 Second generation glucose biosensors

Second generation glucose biosensors are designed for detection of glucose in a complete absence of dissolved oxygen (de-aerated samples). Oxygen-independent  $GOx$  biosensors can be obtained by replacing the native cofactor oxygen with a non-physiological (synthetic) electron acceptor capable of shuttling electrons

from the redox center of the enzyme to the surface of the electrode. A comparison of equations 1.5-1.7 with equations 1.3 and 1.4 illustrates the replacement of oxygen as a redox partner of glucose oxidase in a glucose biosensor. Instead of oxygen, the artificial compound (e.g. the  $[\text{Fe}(\text{CN})_6]^{3-}$  ion with a complexed iron (III) reducible to Fe(II)) is used as a redox partner of the reduced enzyme to induce re-oxidation.



As shown in equations 1.6 and 1.7,  $\text{M}_{(ox)}$  and  $\text{M}_{(red)}$  are the oxidized and reduced forms of the synthetic mediator. The reduced form of the mediator ( $[\text{Fe}(\text{CN})_6]^{4-}$ , in case of use of supplemented  $[\text{Fe}(\text{CN})_6]^{3-}$ ), is reoxidized at the electrode, giving a current signal proportional to the glucose concentration level in similar manner as the hydrogen peroxide for the oxygen cofactor case (equation 1.7). The related synthetic redox mediator-supported enzyme/substrate conversion cycle between substrate and enzyme is displayed in Figure 1.4. Successfully working non-native redox mediators for glucose biosensors include ferrocene-derivatives, potassium ferricyanide and Os(III) complexes (J. Wang, 2008).

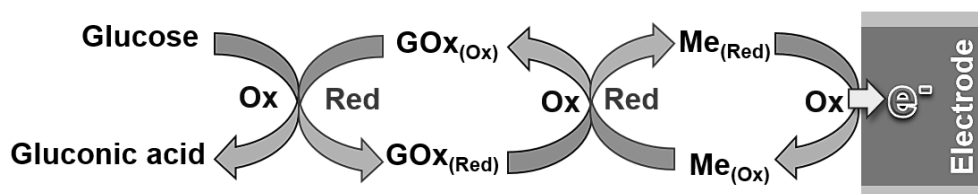


**Figure 1.4** Sequence of redox events that occur in ‘second generation’ glucose biosensors with redox recycling of the glucose oxidase supported by a dissolved artificial redox mediator.

#### 1.2.4 Third generation glucose biosensors

In contrast to 1<sup>st</sup> and 2<sup>nd</sup> generation biosensors, 3<sup>rd</sup> generation biosensors are “reagentless” sensing devices as they are designed not to require dissolved native or synthetic co-factors as effective electron transfer mediators in the measuring buffer for the requisite regeneration of the enzyme’s redox state. Freedom from redox mediator supplementation is the result of either an employment of the electrode as electron donor/acceptor via direct charge transfer with the enzyme in the need of reduction/oxidation (Figure 1.5A; Jose *et al.*, 2012; Q. Liu *et al.*, 2007; Y. Wang and Yao, 2012; Y. Wang *et al.*, 2011)) or a gain by covalently binding redox active chemical entities to the polymeric strands that serve as the immobilization matrix entrapping the enzyme (Figure 1.5B) (J. Wang, 2008).



an optimal structural orientation of the macromolecule on the polarized sensor surface. Important for the achievement of DET between an enzyme with reasonably well exposed redox site and the transducing electrode is nearness of the redox site to protein surface and a proper orientation of the biocatalytic macromolecule with the enzymatic redox site facing straight to the electron-accepting/donating liquid/solid interface. Obviously, optimal immobilization strategies are required for the fulfilment of that demand of protein positioning (Figure 1.6).

Though it was not the main goal here to establish a DET-type of biosensing or to work with synthetic mediators for GOx recycling, a part of the experiments with the CNT-based biosensors of this thesis was carried out with the intention to check whether DET for was feasible and hether the proposed CNT-based biosensor design was functional in de-aeraeted buffers, e.g. with intentional ferrocene derivative addition to the immobilization layer. For more information refer to the relevant later section in the Results and Discussion section.

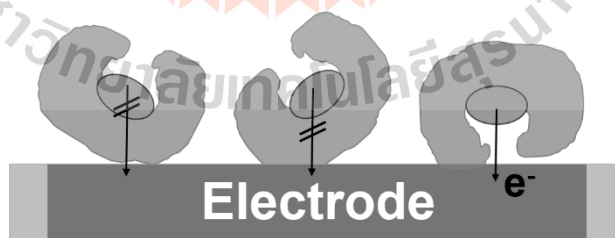


**Figure 1.6** Importance of redox enzyme orientation on the transducing electrode surface for success with direct electron transfer from the electrode to the proteins redox site and back.

### 1.2.6 Immobilizations of enzyme biosensor

A biosensor makes exquisite use of a biological molecule that is immobilized in proximity to a transducer to detect an analyte, and ultimately getting a storable electrical signal for quantification. A critical step in the fabrication of well-working biosensors is thus the reproducible and biocompatible functional fixation of enzyme molecules onto the surface of the the measuring solid electrode surface (Scouten *et al.*, 1995).

The term “immobilized enzymes” refers to “enzymes physically confined or localized in a certain defined region of space with retention of their catalytic activities, and which can be used repeatedly and continuously”. Enzymes may be attached to the solid electrode carrier by physical adsorption, electrostatic charge attractions or stable covalent bonding. The most common procedures for irreversible enzyme immobilization are, however, covalent coupling, entrapment or encapsulation into thin-film polymer surface deposits and protein molecule cross-linking (Figure 1.7). Information on the pros and cons of the various options of enzyme immobilization on electrodes are provided in Table 1.1 (Brena *et al.*, 2013; Datta *et al.*, 2013; Scouten *et al.*, 1995). Natural polymers, synthetic polymers and inorganic materials have been exploited to achieve enzyme immobilization on sensors. The quality of gentle but firm immobilization of the analyte-selective biological component is certainly a major factor determining analytical biosensor performance, and use of chitin or chitosan films with sound biocompatibility, for instance, proved to be beneficial transducer surface modifiers (Suginta *et al.*, 2013b). Based on that some preliminary experiments with natural shrimp chitin as supplementation of the GO<sub>x</sub>/CNT-based biosensors of this study have been conducted to test whether sensor life time indeed would be be extended

by the accomplished CNT/chitin composite or not. More information on this issue is available in the related section of the Results and Discussion section.

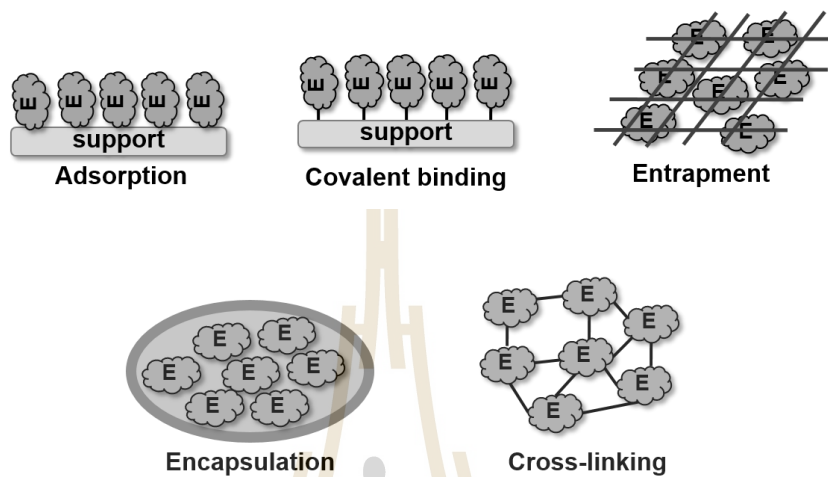


**Figure 1.7** Approaches to enzyme immobilization, irreversible methods.

**Table 1.1** Existing immobilization procedures for enzymes – A comparison.

Method	Advantages	Disadvantages
<b>Adsorption</b> on insoluble matrices (e.g. by van der Waals forces, ionic binding or hydrophobic forces)	Simple, mild conditions, less disruptive to enzyme protein	Enzyme linkages are highly dependent on pH, solvent and temperature; insensitive
<b>Entrapment</b> in a gel (eventually behind a semipermeable membrane)	Universal for any enzyme, mild procedure	Large diffusional barriers, loss of enzyme activity by leakage, possible denaturation of the enzyme molecules as a result of free radicals
<b>Crosslinking</b> by a multifunctional reagent (such as glutaraldehyde bis-isocyanate derivatives or bis-diazobenzidine)	Simple procedure, strong chemical binding of the biomolecules; widely used in stabilizing physically adsorbed enzymes or proteins that are covalently bound onto a support	Difficult to control the reaction, requires a large amount of enzyme, the protein layer has a gelatinous nature (lack of rigidity), relatively low enzyme activity
<b>Covalent</b> bonding onto a membrane, insoluble supports	Stable enzyme-support complex, leakage of the biomolecule is very unlikely, ideal for mass production and commercialization	Complicated and time-consuming: possibility of activity losses due to the reaction involving groups essential for the biological activity

### 1.2.7 Chitin and Chitosan as natural biocompatible material for enzyme immobilization

Although chitosan-based electrochemical biosensor fabrications have been intensively worked at over the past few decades (Suginta *et al.*, 2013b), 3<sup>rd</sup> generation enzyme biosensor fabrication using the chitosan precursor chitin as biological immobilization matrix has been barely approached. Chitin, is actually the second most abundant biopolymer in nature after cellulose (Pillai *et al.*, 2009; Rinaudo, 2006). It is an exceptional polysaccharide formed through a tight entanglement of long strings of chained *N*-acetylglucosamine (GlcNAc) units and as such the main structural component of marine animals such as crab, shrimp, and squids (W. R. Chen, 2013; Nakorn, 2017). As reviewed by Suginta *et al.* (2013), only a limited number of reports addressed so far the utilization of chitin for electrochemical and optical biosensor fabrication. An initial study from as early as 1992, for instance, succeeded in the spreading of thin enzyme-loaded membranes from squid pen  $\beta$ -type crystalline chitin (Ohashi and Koriyama, 1992), a material that was later successfully served as an immobilization matrix for glucose oxidase in implantable glucose biosensors with good stability (Ohashi and Karube, 1995).

In 2000, chitin was then made a supplementary modifier of carbon paste enzyme biosensors: GOx was entrapped into the chitin/carbon paste via interaction of anionic sulfide groups in the protein and protonated positively charged nitrogen functionalities in the chitin biomaterial, an immobilization strategy that produced well-working glucose biosensors (Sugawara *et al.*, 2000). Brondani *et al.* used a glyoxal/carbodiimide coupling chemistry to covalently fix the amino-groups of chitin to each other or to the ones available in a corn peroxidase enzyme (Brondani *et al.*,

2009). The obtained enzyme-modified and cross-linked chitin was mixed into carbon paste electrodes and successful biosensor measurements of adrenaline in pharmaceuticals could be carried out with the preparation. And thin chitin films were studied as bovine serum albumin adsorbing material on the surface of sensors designed for a quartz crystal microbalance with dissipation monitoring and surface plasmon resonance studies (Kittle *et al.*, 2012). The promising achievements of the available studies with a chitin-partaking biosensor design and the capabilities of chitin known from its frequent use in the biomedical, food, cosmetic, and textile industries (Mincea *et al.*, 2012) makes the material a promising resource from the marine environment for biosensor fabrication. Advancing the use of chitin for biosensors seems sensible bearing in mind its great ease of access, outstanding biocompatibility, film-forming properties and abundance of amino groups for cross-linking chemistry.

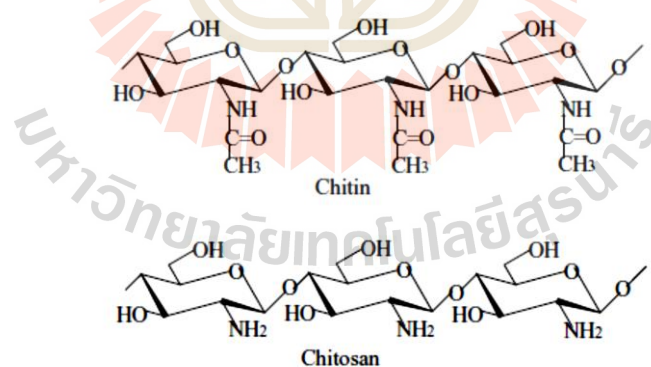


**Figure 1.8** Chemical structure (A) of chitin and (B) chitosan. (modified from Krajewska, 2004).

Chitin and its synthetic derivative chitosan are structurally quite similar (refer to Figure 1.8), given that in chitosan some of the many acetylated nitrogen functionalities is chemically modified via deacetylation into amino groups and others not. Different between the two biopolymers is accordingly just the ratio of the number of acetylated to the number of deacetylated nitrogen groups at the C2 carbon of the sugar ring. In chitin there are actually more acetylated than amino groups while in chitosan the situation is the opposite and the amino functional groups are dominant.

More recently, Yang and coworkers reported the successful synthesis of ferrocene (Fc)-modified chitosan (Fc-CHITO) and used the resulting redox polysaccharides for the establishment of reagentless GOx-based glucose biosensors (Fatoni *et al.*, 2013; Garcia *et al.*, 2007; Qiu *et al.*, 2009; Shukla *et al.*, 2013; Weiwei Yang *et al.*, 2007b; Yilmaz *et al.*, 2012). Upon solvent evaporation, films of the initially suspended Fc-CHIT hybrid material firmly immobilized GOx entities via electrostatic interaction on the surface of glassy carbon electrodes (GCE). Biosensors made with this design were superbly sensitive during the electroanalysis of glucose and thanks to the biocompatibility of the main matrix component chitosan had a good lifetime, too.

Since chitin has, though to a lower extent, amino groups for redox mediator cross-linking available the material should, in principle, be adaptable for the Yang's type of chemical modification strategy. Chitin has, however, not the same solubility, hydrophobicity, film-forming tendency and NH<sub>2</sub>-group density as chitosan and the distinct difference in the various chemical and physical material properties is likely to play a role for determining the analytical performance quality of, for instance, Chitin-Fc-GOx glucose biosensors.

### 1.2.8 Carbon nanotubes and biosensor applications

There has been an explosion of interest in the use of nanomaterials for the development of biosensors, and carbon nanotubes (CNT) are at the forefront of this trend (Agüí *et al.*, 2008; Pumera *et al.*, 2007; Wenrong Yang *et al.*, 2007a). The interest is partly motivated by the ability to improve macroscale biosensor behavior by incorporating nanoscale sensing components, leading to an enhanced detection of the targeted analytes (Wenrong Yang *et al.*, 2010).

CNTs are tube-shaped graphitic filaments with a diameter on the few nanometer scale (J. Wang, 2005). CNT is a promising material for sensing applications as they offer several excellent properties including high mechanical strength, high surface area, excellent chemical and thermal stability, and a very good of electrical conductivity (Ahammad *et al.*, 2009; Ajayan, 1999; Balasubramanian and Burghard, 2006; Gupta *et al.*, 2017; Lyons and Keeley, 2008). CNT thus became an important component of enzyme biosensor architectures (Gooding *et al.*, 2007; Heller *et al.*, 2006; Krapf *et al.*, 2006).

CNT tubes are prepared as single-walled or multi-walled versions (Figure 1.9) and have been utilized as nanoscopic functional component of the analytical tools since their discovery. Apart from already mentioned assets CNT became attractive for biosensor fabrication/application because it was discovered that they can promote direct electrode/protein electron-transfer. Representative examples of biosensor work with CNT include the work with single-walled carbon nanotubes decorated with Au-coated Pd (Au/Pd) nanocubes (Claussen *et al.*, 2009), incorporation of single-walled carbon nanotubes modified with enzyme into redox polymer hydrogels (Joshi *et al.*, 2005), CNT with nanoelectrode ensembles (NEEs) (Lin *et al.*, 2004),

glucose oxidase is entrapped in the composite of carbon nanotubes suspension mixed with chitosan solution was used for entrapped enzyme (Ying Liu *et al.*, 2005), carbon nanotube/Teflon composite was mixed with and glucose oxidase enzyme by hand mixing in the dry state (J. Wang and Musameh, 2003). Here, bare thin-film CNT electrode deposits and composites of CNT with chitin and chitin/ferrocene have been trialed as options for the immobilization of GOx on noble metal disk electrodes. For detailed information refer to the related Results and Discussion section.

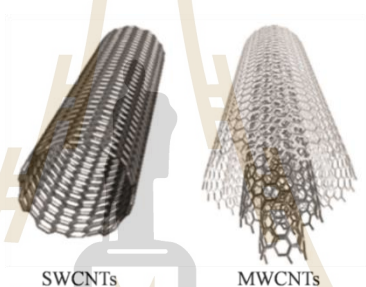


**Figure 1.9** Structure of single-walled carbon nanotubes (SWCNTs) and multi-walled carbon nanotubes (MWCNTs).

### 1.2.9 Principles of amperometric glucose biosensor measurements

Electrochemical enzyme biosensors measure the current produced from oxidation and reduction reactions. The current that is monitored can be quantitatively correlated to either the concentration of the measured electroactive species or to its rate of production/consumption. The resulting electrical signal is proportionally related to the recognition process of the immobilized enzyme with respect to substrate (target analyte) and, via suitable calibration can be used to determine substrate in sample

solutions. Reviews of this strategy are available from Wang et al. (2008) (Perumal and Hashim, 2014).

With enzyme-based biosensors most often amperometry is the electrochemical method used for the generation of the electrical signal that allows analyte (substrate) detection and quantification. At constant potential, suitably chosen in amplitude for the electro-reduction or oxidation of a product or educt (cofactor) of the enzymatic substrate conversion, the biosensor current is monitored as function of time and concentration of substrate. Popular platforms onto which enzymes are immobilized include gold (Au), platinum (Pt) and carbon (C) disk electrodes. Reference electrodes is usually the silver/silver chloride (Ag/AgCl) system and as counter electrode used are usually inert platinum spirals or wires or graphite sticks). Figure 1.10 represents the conventional three electrode cell arrangement for such system for enzyme biosensor amperometry. The cell has to be connected to a computer-controlled electrochemical amplifier ('potentiostat'), and to obtain an amperometric biosensor recording the current is continuously measured by the machine as function of time at constant potential. With a glucose biosensor, for example, the time course of the generation of hydrogen peroxide is usually monitored via the anodic oxidation of the molecule at + 600 mV vs. a reference electrode during additions of aliquots of glucose standard solution to the measuring buffer (Figure 1.11A) and the corresponding anodic peroxide current steps of a calibration trial are translated into the corresponding calibration plots (Figure 1.11B). Important biosensor properties that can be extracted from the amperometric calibration curves include the sensor's linear range, the sensor sensitivity, the sensors maximum current ( $I_{max}$ ) and the sensors apparent Michaelis-Menten ( $K_m$ ) value.

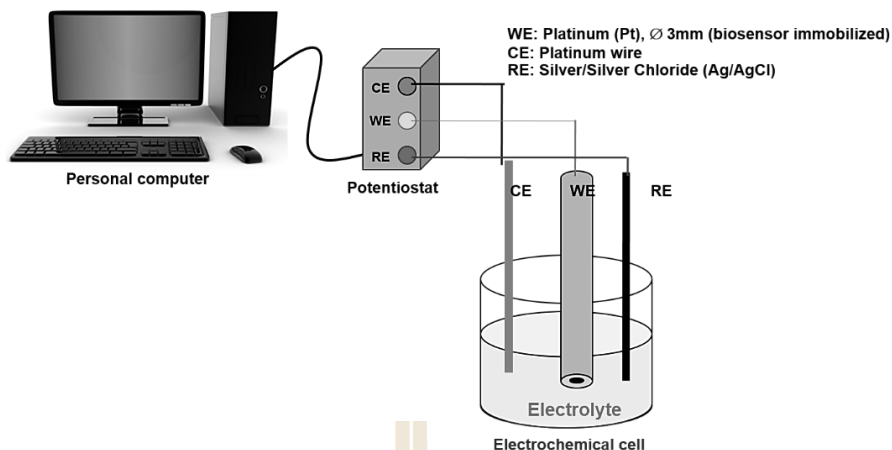


**Figure 1.10** Electrochemical set up for ‘enzyme biosensor amperometry’, in three-electrode configuration and with a potentiostat and computer used for amperometric current measurement, data acquisition and data storage.

Figure 1.11A shows an example of a current vs. time trace for an amperometric calibration trial with a GOx-based glucose biosensor. Measured was the hydrogen peroxide current in dependence of the glucose concentration in the measuring buffer. The variation of current values within the amperometric trace upon glucose spiking of the measuring buffer can be translated into a calibration curve (Figure 1.11B) from which the parameters  $K_m$  and  $I_{max}$  as well as the linear range for the particular biosensor and its sensitivity can be extracted.

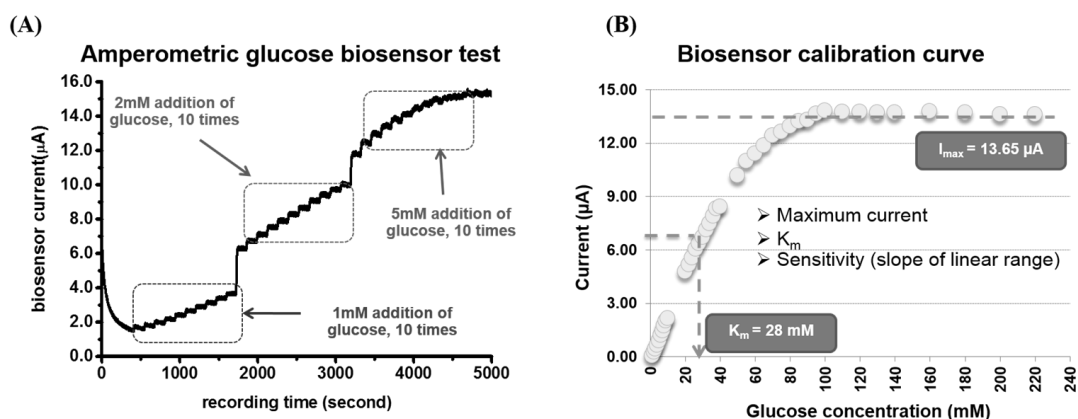


**Figure 1.11** Typical amperometric response of an enzyme biosensor to successive additions of substrate (A). Electrochemical assessed biosensor calibration curve as constructed by the analysis of the amperometric recording in A (B).

Based on principles as valid for amperometric enzyme biosensing in an independent part of this thesis a novel non-optical amperometric assay for the monitoring of  $\beta$ -N-acetylglucosaminidase action on a redox-labeled substrate was worked on. Advantage was taking here of the pronounced electroactivity of the redox labels for the generation of an electrochemical signals that reflects cleavage activity of the chosen biocatalyst. Further details of this particular piece of work on electrochemical enzyme kinetic assay establishments are available in the following Introduction section and in the related Results and Discussion section.

## 1.3 General characteristics of enzymes

### 1.3.1 What are enzymes?

Enzymes are biological catalysts. They increase the rate of chemical reactions taking place within living cells without themselves suffering any overall change. The reactants of enzymes-catalysed reactions are termed substrates and each enzyme is quite specific in character, acting on a particular substrate or substrate to produce a particular product (Palmer, 1991). A characteristic feature of enzymes is that they are specific in action. Some enzymes exhibit group specificity, i.e. they may act on several different, though closely related, substrates to catalyse a reaction involving a particular chemical group.

### 1.3.2 Catalysis by enzymes

A catalyst accelerates a chemical reaction without changing its extent and can be removed unchanged amongst the end-products of the reaction. It has no overall thermodynamic effect: the amount of free energy liberated or taken up when a reaction has been completed will be the same whether a catalyst is present or not.

In most cases, a catalyst acts by reducing the energy of activation. The catalyst, or part of it, combines with the reactants to form a different transition-state from that involved in the uncatalysed reaction; one which is more stable and, therefore, of lower energy (Figure 1.12) (Palmer and Bonner, 2007).

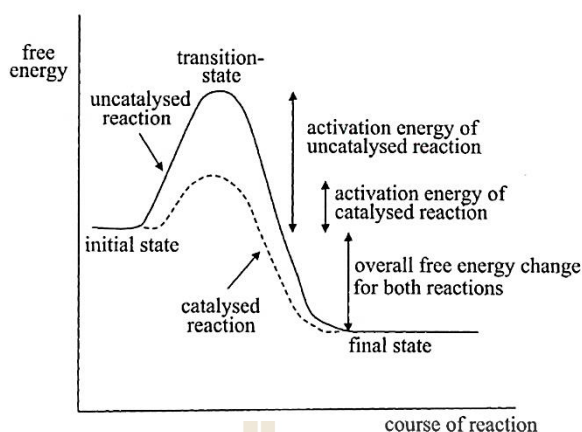


**Figure 1.12** Free energy changes for an energetically favorable reaction, showing the effects of a catalyst.

Note that the initial and final states are at the same free energy levels for the catalysed and uncatalysed reaction, and the overall free energy changes as the reaction proceeds is also the same.

### 1.3.3 Enzyme kinetics

Enzyme kinetics is the study of chemical reactions that are catalyzed by enzymes. The reactions rate is measured by following the loss of substrate [S] or the generation of product [P]. Observations will be in progress curves similar to shown in Figure 1.13A. At early times substrate loss and product appearance change rapidly but the reaction proceeds these rates diminish, reaching zero when all the substrate has been converted to product by the enzyme (Robert A Copeland, 2004). In the typical product profile which shown in Figure 1.13B, the linear increase in the product concentration

at early times refer to an initial velocity  $v_0$  (which is the slope of product increase as a function of time).

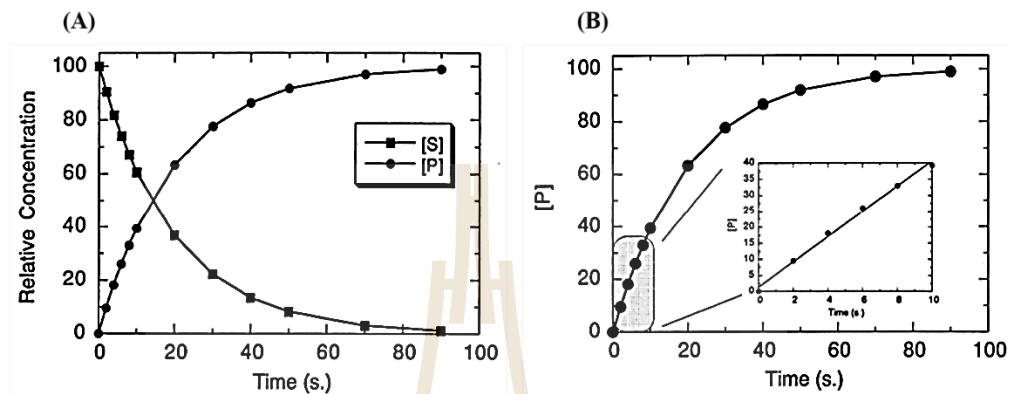


**Figure 1.13** (A) Reaction progress curves for the loss of substrate and production of product during an enzyme-catalyzed reaction, (B) Reaction progress curve only for the production of product. Inset highlights the early time points at which the initial velocity can be determined from the slope of the linear plot of [P] versus time (Robert A Copeland, 2004).

For different starting concentrations of substrate, the initial velocity ( $v_0$ ) for each substrate concentration is measured by means of the slope at which the product formation is a linear function of time as shown in Figure 1.14A. Each slope represents each velocity. Figure 1.14B presents typical “Michaelis-Menten” plot of the reaction velocity as a function of substrate concentration, with a single-substrate reaction model.

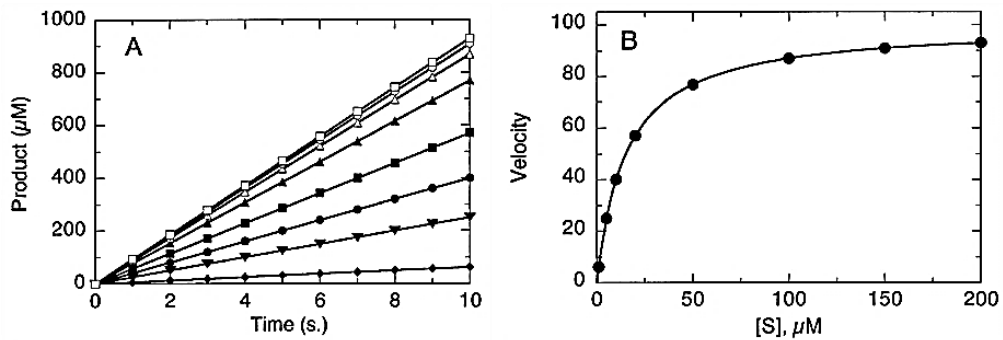


**Figure 1.14** (A) Progress curves for a set of enzyme-catalyzed reactions with different starting concentrations of substrate [S]. (B) Plot of the reaction velocities, measured as the slopes of the lines from (A), as a function of substrate concentrations (Robert A Copeland, 2004).

In 1902, the velocity of enzyme-catalyzed reaction was explained by Brown. The kinetic characteristics of enzyme-catalyzed reaction are best described by the following reaction scheme in equation 1.9 (Robert A Copeland, 2004).



Where E is concentration of enzyme, S is concentration of substrate, ES is concentration of enzyme-substrate complex, and P is concentration of product. This scheme predicts that the reaction velocity will be proportional to the concentration of the ES complex as:  $v = k_2[ES]$ .

From reaction scheme, the reaction rate (velocity,  $v$ ) can be derived by one of two types of assumption, (i) the rapid-equilibrium assumption, and (ii) the steady-state assumption. The equation 1.10 is “Michaelis-Menten” equation; which represents both assumptions and describes the rate of reaction.

$$v = \frac{V_{\max} [S]}{K_m + [S]} \quad (1.10)$$

Where  $V_{\max}$  and  $K_m$  represent maximum velocity of reaction and Michaelis constant, respectively. Figure 1.15 represent the reaction rate as a function of substrate concentration according to Michaelis-Menten equation which already mentioned above.

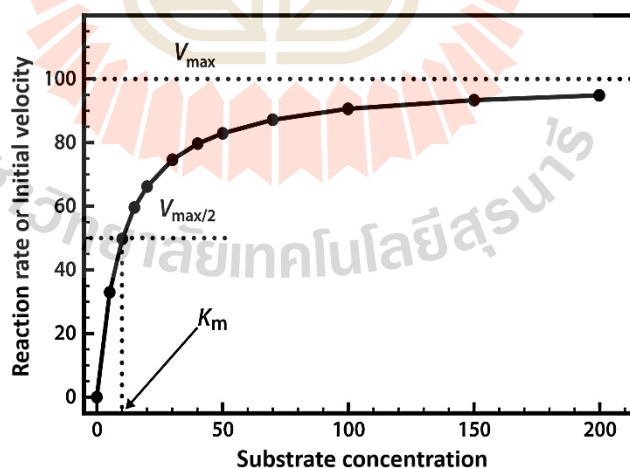


**Figure 1.15** Dependence of velocity ( $v$ ) on substrate concentration  $[S]$ , according to Michaelis-Menten equation (Robinson, 2015).

The kinetic constant  $K_m$  is defined as the substrate concentration at half-maximal velocity for the enzymatic reaction.  $V_{max}$  is defined as  $k_{cat}[E]$ , where the value of  $k_{cat}$  is referred to as the turnover number for the enzyme, since it defines the number of catalytic turnover events that occur per unit time (Robert A Copeland, 2004).

Usually, optical assays based on spectrophotometry are the methods of choice to follow enzyme activity (Harris and Keshwani, 2009; Kricka *et al.*, 2000; Nagy *et al.*, 1998). Absorption spectroscopy (Sirimontree *et al.*, 2014; Sritho and Suginta, 2012; Suginta *et al.*, 2010) and fluorescence spectroscopy (Linko-Löppönen and Mäkinen, 1985) are common schemes for enzyme activity detection. Both techniques measure, changes in electronic configuration of a target molecule resulting from its absorption of light energy at a specific wavelength (Robert Allen Copeland, 1997). The experimental procedure for a routine assessment of kinetics parameter of enzyme-catalyzed reaction via microplate-based optical measurements is schematically represented in Figure 1.16. The advantage of such an approach is a rather simple handling of the sample solutions. However, among the drawbacks are the limited detection limit of standard absorption spectroscopy and the inability of the assay to monitor the ongoing changes in substrate or product that do not show optical activity in terms of absorption, fluorescence or chemiluminescence properties. Furthermore, many steps have to be executed sequentially in course of a microplate-based optical activity screening experiment and strong chemicals have to be used for stopping enzyme action on substrate at desired time points, which to certain extent are practical and/or environmental disadvantage.

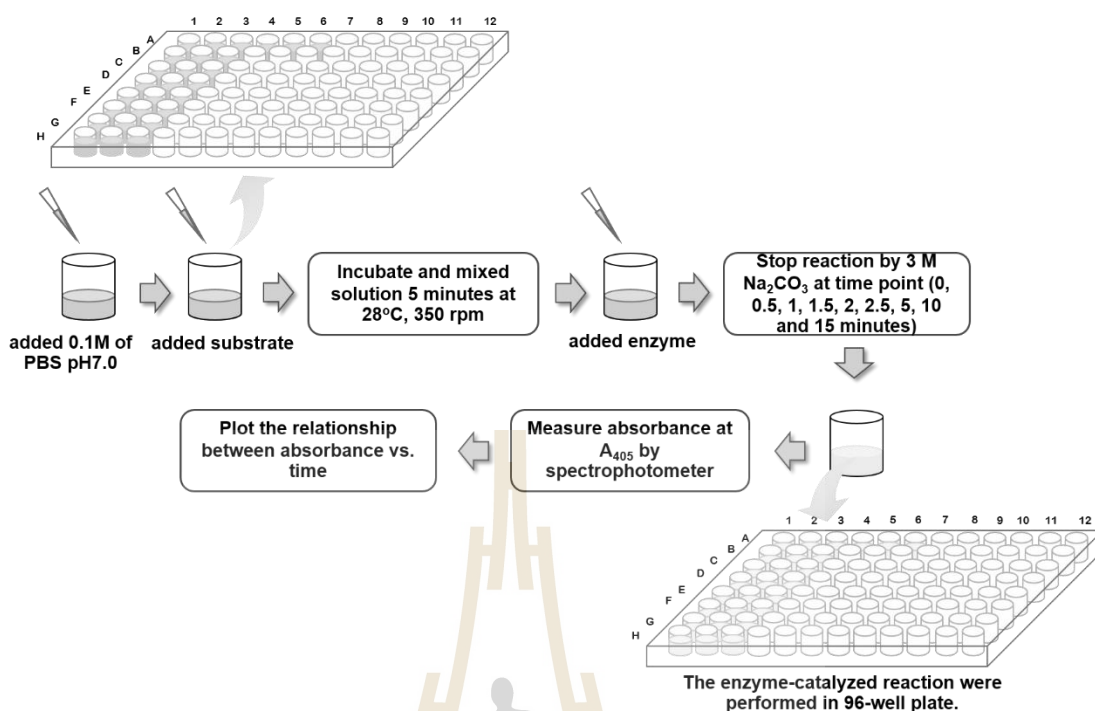


**Figure 1.16** The experimental cycle of a microplate-based enzyme assay with optical detection of enzyme-substrate interaction for kinetic parameter assessment.

Since simple-to-do and sensitive voltammetry or amperometry has been shown for a lot of redox active compounds as capable of ultralow trace detection, an electrochemical detection of enzyme-substrate interaction may in one or the other case be the better choice for kinetic parameter assessment, compared to work with optical assaying. As detailed below reports are available in that direction. In one study case an Advantage was taken of the pronounced electrochemical activity of *p*-nitrophenol (*p*NP) that, served in spectroscopic assays as efficient optical reporter for the activity of various enzymes, including glycoside hydrolases, phosphatases, lipases, etc (Hasan *et al.*, 2009; Ren *et al.*, 2014; Suginta *et al.*, 2010). Figure 1.17A and 1.17B show the reduction and oxidation of the optical marker molecule *p*NP at anodic or cathodic

electrode surface. Figure 1.17C shows the possible redox reaction of *p*NP, in which electrons are shuttled between the oxidized and reduced form of the molecule.

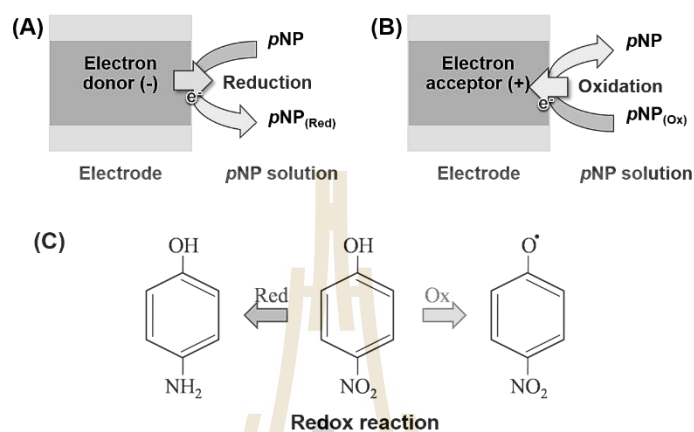


**Figure 1.17** Redox reaction of *p*-nitrophenol at electrode surfaces. (A) reduction and (B) oxidation of *p*-nitrophenol (*p*NP) at an anodically (A) or cathodically polarized (B) electrode surface, and the related redox reactions of *p*NP via electron ejection or uptake, expressed in a redox equation (C).

Figure 1.18, on the other hand, represents the suitability of the *p*NP redox for establishment of an electrochemical activity assay through the presentation of the outcome of a cyclic voltammetry recording on *p*NP with assignment of a proposed mechanism of *p*NP oxidation/reduction, here valid for a disk-shaped carbon paste electrode (Alizadeh *et al.*, 2009). *p*NP is actually a phenolic compound that has on the benzene ring a nitro group in opposite position of its hydroxyl group, and it may be added to an enzymatically cleavable several substrates as optically and electrochemically active label, e.g. in form of 4-nitrophenyl- $\beta$ -*D*-glucopyranoside. According to fingerprint voltammogram in the Alizadeh study, *p*NP could be measured

via cyclic voltammetry or amperometry, via exploitation of its electroreduction or -oxidation. Cleavage activity of enzyme on the *p*NP-labeled sugar substrate releases the tag, which is quantifiable via spectroscopy (in the common way), or via voltammetry/amperometry (in an alternative electrochemical mode). For the latter sensitive *p*NP electroanalysis is important and Table 1.3 summarizes for a selection of research studies that dealt with *p*NP voltammetry or amperometry at various types of electrodes possible analytical figures of merit.

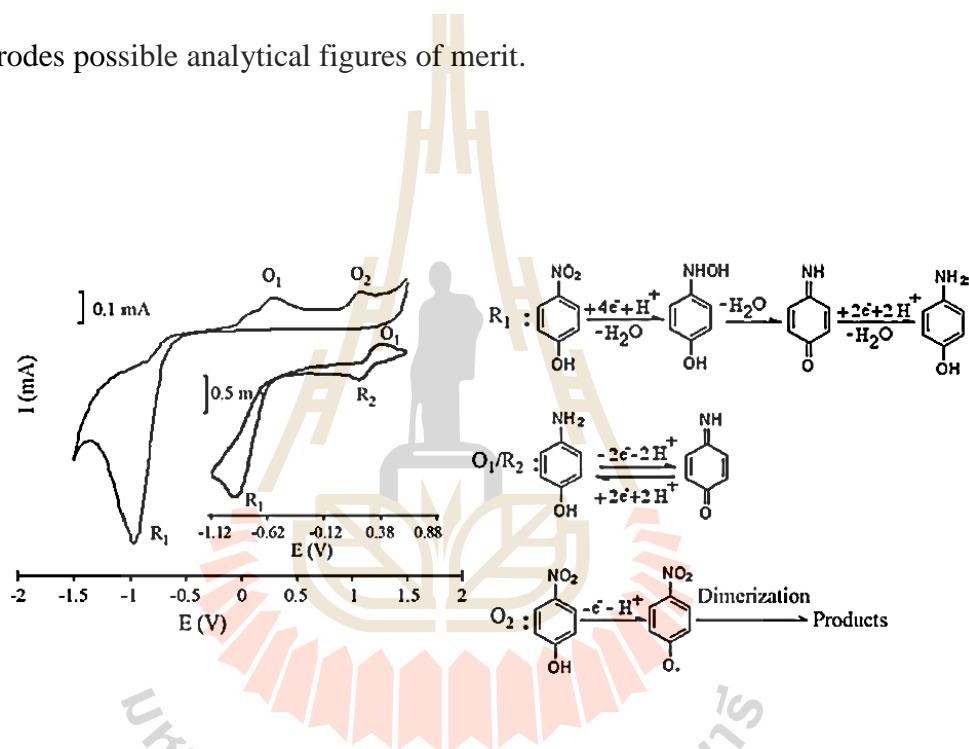


**Figure 1.18** Electrochemical behavior of *p*NP at a carbon paste electrode (left panel) and the proposed electrochemical reaction mechanism (right panel) (Alizadeh *et al.*, 2009).

**Table 1.2** A comparison of *p*-nitrophenol determination by various electrochemical modified electrodes.

Electrode type	Linear range ( $\mu\text{M}$ )	Sensitivity ( $\mu\text{A M}^{-1} \text{cm}^{-2}$ )	LOD ( $\mu\text{M}$ )	Type of measurement	Reference
HA-NP/GCE	1.0 – 300.0	41.73	0.60	DPV	(Yin <i>et al.</i> , 2010)
Graphene-Nafion/SPE	10.0 – 620.0	24.16	0.60	DPV	(Arvinte <i>et al.</i> , 2011)
MWCNTs-Nafion/SPE	25.0– 620.0	25.75	1.30	DPV	(Arvinte <i>et al.</i> , 2011)
PDPA-MWCNTs/GCE	3.96 – 177.8	8.71	0.50	Amperometry	(C.-Y. Yang <i>et al.</i> , 2012)

In the past decade, Tangkuaram *et al.*, (2006) indeed have been demonstrated that amperometry is suitable to follow an enzyme-catalyzed reaction using the electrooxidation of liberated *p*-nitrophenol at constant potential +1.15V. The electrochemical assay was shown functional for two glycosidases and relied on the anodic detection of the enzymatically-generated *p*-nitrophenol for a fixed concentration of the *p*NP-glycoside substrate (refer to Figure 1.19). Successive additions of substrate to solutions containing the enzyme of choice at desired concentration triggered well-pronounced signal increases in current vs. time recordings. The study proved for  $\beta$ -1,3-galactosidase and *endo*- $\alpha$ -N-acetylgalactosaminidase as enzyme models that simple and low-cost electrochemical analysis is suitable for monitoring enzyme activity, enzymatic reaction. However, quantitative enzyme assaying has not been performed related Results and Discussion section for further details.

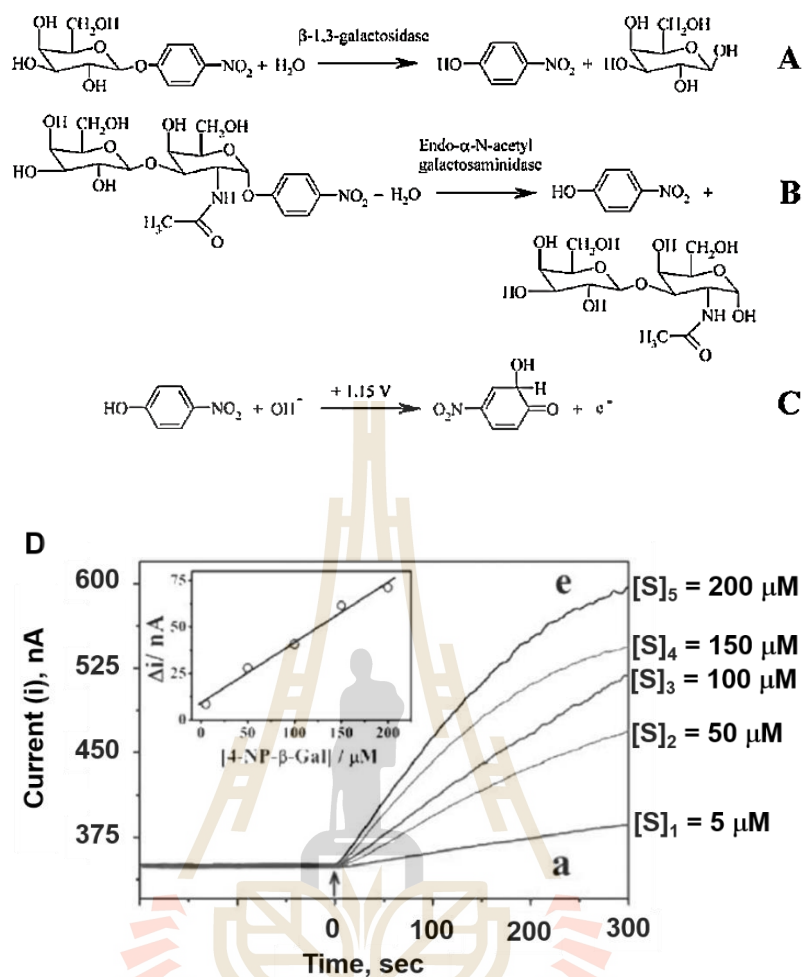


**Figure 1.19** Enzymatic reaction followed by the electrooxidation of the liberated *pNP* (A) Enzymatic reaction of  $\beta$ -1,3-galactosidase and (B) *endo*- $\alpha$ -N-acetyl-galactosaminidase. The equation in support of an electrochemical galactosidase or galactosaminidase substrate conversion assaying via electrooxidation of liberated *pNP* (C) and amperometric responses of 0.2 U successive additions from 0.2 (a) to 1.0 U (e) of  $\beta$ -1,3-galactosidase at GCE in a 1.5 mL of stirred solution of 133 mM of 4-NP- $\beta$ -Gal (D) (Tangkuaram *et al.*, 2006).

## CHAPTER II

# UNTAINTED CARBON NANOTUBES NETWORKS AS COMPETITIVE IMMOBILIZATION MATRIX FOR AMPEROMETRIC ENZYME BIOSENSORS

A Mid of July, 2018 Web of Science search combining the appearance of the phrases “carbon nanotube”, “CNT”, “glucose” and “biosensor or biosensors” is linked to 182 publication hits. Surprisingly, almost the entire set of biosensor studies did not use carbon nanotubes on their own as functional immobilization matrix for glucose oxidase or dehydrogenase as biocatalyst but worked with rather complex multi-component blends of CNT with other functional materials and various types of metal, metal oxide or polymer nanoparticles and organic or inorganic nanoclusters have been suggested as sensor performance enhancers. In the period 2015 to date, for instance, 19 reports appeared on the topic and they all made use of a biosensing layer design that combined CNT with various extras. Additive examples included polyoxometalate nanoclusters (Boussema *et al.*, 2018), high molecular weight, heavily glycosylated proteins (Comba *et al.*, 2018), synthetic or biological polymers (Cogal *et al.*, 2018; Kamyabi *et al.*, 2016; J. Liu *et al.*, 2016; Mason *et al.*, 2016; Shrestha *et al.*, 2016; Shrestha *et al.*, 2017; Uwimbabazi *et al.*, 2017), metal, metal oxide or metal organic framework particles (Guzsvany *et al.*, 2017; Ibrahim *et al.*, 2016; Song *et al.*, 2017) and carbon/graphite foams (Fan *et al.*, 2017). Own preliminary tests with biosensors that

had GOx trapped into bare CNT electrode deposits disclosed a promising performance for glucose detection. Objective of this thesis part was thus to demonstrate with a thorough study that glucose biosensors with competitive analytical performance levels indeed can be prepared just with CNT, via simple practical procedures. In contrast to the published options, a tedious preparation of micro- or nanomaterial additives and the establishment of complex functional sensing layers could then be spared and valuable time and budget be saved for other purposes.

In brief, the plan was to involve simple drop/dry coating procedures to first spread a nanoporous coating of carbon nanotubes (CNT) over the surface of disk-shaped platinum electrodes and then infuse the dried CNT deposits solution of glucose oxidase (GOx) to finally form the active layer of glucose biosensors. An undesired but expected enzyme leakage out of the electrode surface coating into storage or measuring buffer was planned to be prevented by finally applying an extra protective top layer of a commercially available easy to apply cathodic electrodeposition paint (EDP), which served as effective diffusion barrier for the entrapped GOx biomacromolecules. Information on the performance level of the novel GOx immobilization design was supposed to come from cyclic voltammetry inspections with completed sensors and from amperometric calibration, recovery rate and sensor stability measurements.

## **2.1 Literature review**

Electrochemical enzyme biosensors are valued bioanalytical tools, in particular for the inspection of complex samples in medical and clinical laboratories and test centers of the pharmacy, biotechnology, food technology and environmental

monitoring control sectors (Sett *et al.*, 2012; Van Dorst *et al.*, 2010; J. Wang, 2008; S. Wang *et al.*, 2003). The great popularity is based on the highly selective interaction of the immobilized protein biocatalyst on the detecting electrode surface with matching substrate and the related chance to exploit the high-affinity substrate binding with subsequent enzymatic turnover into product via rather simple signal generation for target-specific substrate (analyte) quantification, even in difficult heterogeneous sample matrices. Most prominent and also best perfected case of enzyme-assisted electroanalysis is the commercialized amperometric glucose biosensor (Arslan *et al.*, 2011; Castillo *et al.*, 2004; Che *et al.*, 2010; Kong *et al.*, 2009; Newman and Turner, 2005; Şenel and Nergiz, 2012) that, in mass-produced screen-printed electrode format and with immobilized glucose oxidase (GOx) in charge of glucose capture and conversion, since decades is in widespread use as sophisticated miniaturized measuring strip of handheld devices for life-saving daily home blood glucose tests by individuals with diabetes or hypoglycemia. However, not only prominent glucose but also other analytes can be measured selectively with fittingly enzyme-modified electrodes. Functional versions exist, for instance, with various oxidases (e.g., galactose, lactate, glutamate, cholesterol, alcohol oxidase) (Batra and Pundir, 2013; Boujtita *et al.*, 2000; Cosnier, 1999; Cui *et al.*, 2007; Gülce *et al.*, 2002; Odaci *et al.*, 2008; Tan *et al.*, 2005; Tkac *et al.*, 2007) or dehydrogenases (e.g., fructose, glutamate, lactate, cellobiose, formaldehyde, and alcohol dehydrogenases) (Alpat and Telefoncu, 2010; Batra *et al.*, 2016; Chaubey *et al.*, 2001; Herschkovitz *et al.*, 2000; Liang *et al.*, 2015; Paredes *et al.*, 1997; Stoica *et al.*, 2004; Tang *et al.*, 2007; Trivedi *et al.*, 2009; Yakovleva *et al.*, 2012) as biological recognition element and they worked well for quantification of a variety of analytically relevant species including ethanol, cholesterol, dopamine,

xanthine, glutamate, lactate, putrescine, galactose, choline, l-lysine, benzaldehyde, glycerol; and catechol, to name just a few out of the collection of success cases in the scientific literature databases.

Continuous performance improvements for analyte quantification, simplification of fabrication procedures and miniaturization of completed detectors are permanent challenging targets of modern makers of amperometric enzyme biosensors, whether for bio-analysis applications in academic research or for commercial purpose. Known routes to superior sensor sensitivity, response stability and overall life time take advantage of adaptations of the entire sensor design and usually they jointly address the layout of the enzyme immobilization matrix and type of signal transduction as well as the choice and chemical pre-modification of the carrier electrode structures. With regard to immobilization layer optimization considerate supplementation with nanoscopic materials of high catalytic activity, large surface area, and exceptional electronic features became in recent times one of the prime strategies in support of the preparation of amperometric enzyme biosensors with advanced analytical figures of merit. Tested in a copious numbers of studies since about new millennium start as functional biosensor components were metal and metal oxide nanoparticles (NPs) (Kaushik *et al.*, 2008; Luo *et al.*, 2006; Solanki *et al.*, 2011) and -wires, semiconductor quantum dots (Frasco and Chaniotakis, 2009; Sapsford *et al.*, 2006) and high-tech graphitic matter such as spherical C60-type fullerenes (bucky-balls) (Afreen *et al.*, 2015; Pilehvar and De Wael, 2015), molecular graphene nanoplatelets, graphitic single-walled nano-cages, and multi- or single-walled carbon nanotubes (CNT) (Lin *et al.*, 2004; So *et al.*, 2005; Sotiropoulou and Chaniotakis, 2003; J. Wang, 2005; N. Yang *et al.*, 2015). Relevant for this study is the pool of reports describing CNT exploitations

for amperometric (glucose) oxidase biosensor development. A look through the about 150+ (Devasenathipathy *et al.*, 2015; Guzsavány *et al.*, 2017; Mani *et al.*, 2013; Masoomi-Godarzi *et al.*, 2014; Oliveira *et al.*, 2012) proposed options reveals that interestingly most of the issued cases actually do not rely on straight utilization of bare CNT electrode modifications but involve the formation of more or less complex composites of the nanotubular graphite with other functional (nano-) materials. Tried CNT immobilization matrix additions range from natural or synthetic polymers (e.g. chitosan, gelatin, poly-aniline, poly-pyrrole, poly-thionine, poly-toluidine, poly-acrylonitrile, poly-lactic acid, Teflon) (Periasamy *et al.*, 2011; J. Wang and Musameh, 2003; M. Zhang *et al.*, 2004b) to nanoscale silicon dioxide sol-gel structures, small-scale redox entities (e.g. Prussian blue, cobalt/nickel phthalocyanines, poly-brilliant green, ferrocene-derivatives, and organic Os (III) complexes) and nano-catalysts (e.g. platinum (Pt) and gold (Au) NPs, zinc oxide and zirconium oxide NPs, and graphene) (Che *et al.*, 2011; X. Chen *et al.*, 2003; Dong *et al.*, 1992; L. Li *et al.*, 2008; F.-F. Zhang *et al.*, 2004a; S. Zhang *et al.*, 2005). Though biosensors with multicomponent enzyme/CNT/add-on hybrid layers delivered in the disclosed pioneering studies reasonable performances, their successful completion is in the need of extra synthesis of the special raw materials and/or multiple assembly steps, two demands which make sensor reproduction by inexperienced others and widespread routine application difficult. From the viewpoint of fabrication simplicity a well-working biosensor design based on bare CNT surface layers obtained via uncomplicated (drop) casting procedures would certainly be the better, at least as long as no significant concession regarding detection quality has to be made. Claims of such an uncomplicated tactic are rare. In one of the listed cases microliter volumes of a CNT suspension were dropped onto a

glassy carbon (GC) disc electrode surface and solvent was allowed to evaporate (Hu *et al.*, 2015; TermehYousefi *et al.*, 2015; H. Yang *et al.*, 2017). Well-dried graphitic nanomaterial electrode spreads were then drop-dry loaded with enzyme through placement of a microliter splash of GOx solution and the finally gained porous CNT/GOx structure protected against protein loss with a dropped and dried Nafion top coat.

Apparently, the above-mentioned studies were in favor of the potential of a plain CNT biosensor modification; however, with the attention in the biosensor community moving to trendy multi-component sensor matrices the promising trail was actually not further checked and optimized. In this thesis untainted thin film CNT deposits have therefore been thoroughly explored as simple but effective immobilization matrix of GOx biosensors. To be with the realization of the sensor design easy CNT placement and subsequent CNT layer loading with enzyme was restricted to undemanding manual drop and dry coating procedures while the user-friendly process of cathodic electrodeposition of paint (EDP) generated the polymer top coat that protected just accomplished CNT/GOx blends against undesirable protein leakage. Data from voltammetric tests, amperometric calibration trials and applications for quantitative glucose model analysis will be provided in the following subsections as proof of a biosensor performance characteristic that is competitive to literature-known other variants of CNT-based glucose biosensors with more complex multi-component sensing layer architectures. Strength of the minimalistic sensor option here are the simplicity of their construction procedure with the capacity to be further developed into automated production of large quantities, the restriction to commercially available

starting materials, the wide dynamic range for target valuations and very good long-term response stability.

## 2.2 Experimental and methods

### 2.2.1 Chemicals

Glucose oxidase (GOx, EC 1.1.3.4, from *Aspergillus niger*) was obtained through S.M. Chemical Supplies Co., Ltd. (Bangkok, Thailand) as product of Sigma-Aldrich® (St. Louis, MO, USA, product no. G1741, lyophilized, 75% protein, 136300 units/g).  $\beta$ -D (+) glucose anhydrous (C<sub>6</sub>H<sub>12</sub>O<sub>6</sub>) was obtained through Italmar (THAILAND) Co., Ltd. (Bangkok, Thailand) as a product of CARLO ERBA Reagents S.A.S. (Val-de-Reuil, France). Purified carboxylated single-walled CNT, with an about 1.0 - 3.0 at-% carboxylic acid entities were obtained from Carbon Solutions, Inc., (Riverside, CA, USA). The commercial cathodic electrodeposition paint (EDP) system Clearclad® was a kind gift for research purpose from LHV Coatings Ltd., (Birmingham, England). All other chemicals were Sigma-Aldrich® products and of analytical grade. Routinely, aqueous solution preparation used ultrapure de-ionized water. Supporting electrolyte for all biosensor tests was 0.1 M phosphate buffer solutions, pH 7.0.

### 2.2.2 Electrochemical instrumentation

Cyclic voltammetry and amperometry trials with prepared biosensors were carried out with a computer-controlled three-electrode galvanostat/potentiostat

type Reference 600® from Gamry Instruments Inc. (Warminster, PA, USA). If not otherwise mentioned, the working electrode for the tests was a CNT/GOx/EDP-modified 3-mm-diameter Pt or Au disk electrode (bare electrode of Pt and Au which show in Figure 2.1) while a Pt and Ag/AgCl wire were in service as counter and reference electrode, respectively. For long-term continuous response tests the gold disk versions of the biosensors were used in an electrochemical flow cell that was run by the EA163/ED410 potentiostat/e-corder system from eDAQ Pty. Ltd. (Denistone East, Australia). RE of the flow system was a fritted Ag/AgCl (3M KCl) while the tubular stainless steel cell outlet was the CE. Flow cell supply with glucose-free or glucose-loaded 0.1 M phosphate buffer solution, pH 7.0 at about 20  $\mu\text{L/s}$  was duty of peristaltic pump Miniplus-3® from Gilson (Middleton, WI, US). Figure 2.2 represent the flow system of electrochemical cell set up for long-term continuous experiment.



**Figure 2.1** Illustration of bare commercial platinum 3-mm-diameter disk electrode (A) and bare home-made gold (Au) 3-mm-diameter disk electrode (B).

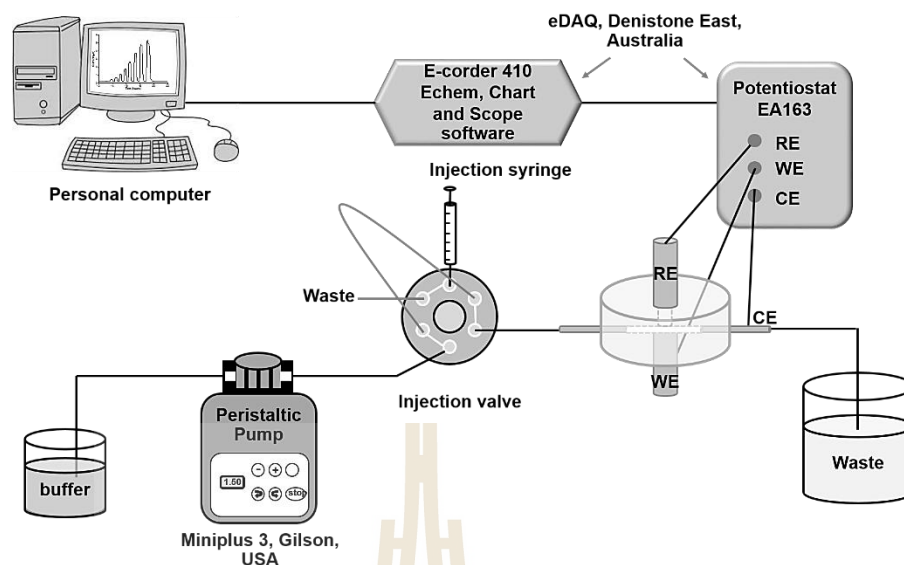


**Figure 2.2** The electrochemical workstation for long-term biosensor testing on flow mode.

### 2.2.3 Fabrication of glucose biosensor by applying CNT/GOx/EDP onto electrode

To begin with, a commercial 3-mm-diameter Pt disk electrode (Gamry Instruments Inc., Warminster, PA, USA, Kel-F® body, outer diameter 7 mm) was polished on a soft textile pad that was soaked with alumina slurry of first 5 and then 1  $\mu\text{m}$  particle size. Pt disk polishing was followed by complete removal of the polishing paste via thorough water rinsing and electrode air-drying at room temperature (RT). Then, a 5.0  $\mu\text{L}$  drop of a suspension of 5.0 mg CNT in 1 mL  $\text{H}_2\text{O}$  was dropped onto the cleaned Pt disk and dried minute air at RT. Four time's repetition of the CNT drop coating step placed a thin film of the black graphitic nanomaterial on the noble metal surface. Next was the careful placement of a 5.0  $\mu\text{L}$  drop of a 5.0 mg  $\text{mL}^{-1}$  solution of GOx in  $\text{H}_2\text{O}$  straight onto just dried CNT deposits and again RT air-drying. Three

time's repetition of the GOx drip treatment loaded the pores in the CNT layer on the Pt surface efficiently with the biocatalyst. Final step was the deposition of a protein leak-protecting polymer cover, which was accomplished in a two-electrode electrochemical cell with a Pt wire counter electrode via cathodic EDP at a potential of negative 7 Volt for 2 minutes. Please note that heat curing of a fresh EDP deposit - as usually done in related industry to induce transformation of fresh paint coats into dry insulating and thus corrosion protecting material - was avoided here not to harm the enzyme and make the paint impermeable for dissolved molecules and ions. Completed biosensors were stirred for 30 minutes in 0.1 M phosphate buffer solution, pH 7.0 and overnight stored at 4°C in the same solution to allow sensor settling. When not used, CNT/GOx/EDP glucose biosensors were stored at 4°C in 0.1 M phosphate buffer solution, pH 7.0. Note that for the home-made 3-mm-diameter Au disk electrode the same procedure was applied to reach glucose sensitivity. The steps to go through during the preparation of the Pt disc-modified CNT/GOx/EDP are shown in Figure 2.3.

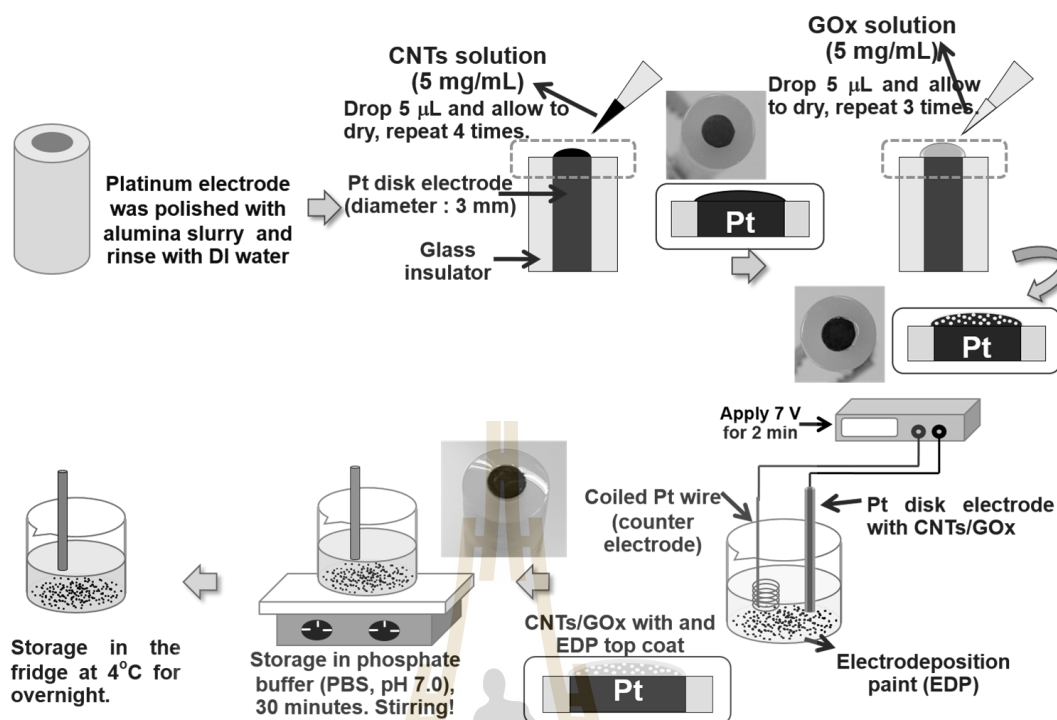


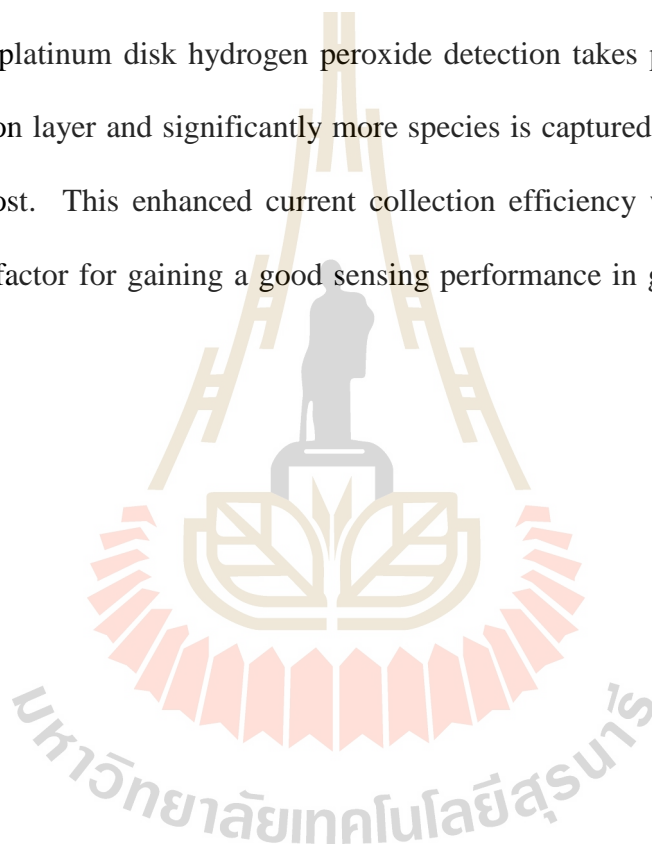
**Figure 2.3** Schematic diagram of the procedure used for the preparation of CNT/GOx/EDP modified platinum or gold as used in the biosensor measurement.

## 2.3 Results and discussion

### 2.3.1 Electrodes modified by carbon nanotubes

Carbon nanotubes (CNT) exhibit a unique combination of excellent structural, mechanical, electrical and electrochemical properties and this stimulated increasing interest in the application of CNT as components of biosensors (Balasubramanian and Burghard, 2006; Rivas *et al.*, 2007; J. Wang, 2005; Wenrong Yang *et al.*, 2010). Figure 2.4A represents the anodic hydrogen peroxide collection at a normal glucose biosensor with non-conducting polymer coating act as immobilization matrix. Only a few GOx molecules happens to have an orientation which their active center in close contact with substrate electrode, and the manifestation of direct electron

transfer for enzyme redox recycling is very unlikely. If the enzyme is considered as a point source of hydrogen peroxide evolution about half of produced hydrogen peroxide will diffuse away from the detecting platinum electrode surface while the other half may reach the sensor for current signal generation. In the case of the utilization of a conductive CNT deposit act as immobilization matrix (refer to Figure 2.4B) enzyme is fixed within the pores of the CNT network. Since the CNT filaments are electrically wired to the platinum disk hydrogen peroxide detection takes place all through the immobilization layer and significantly more species is captured for signal production and less is lost. This enhanced current collection efficiency was expected to be a contributing factor for gaining a good sensing performance in glucose quantification trials.



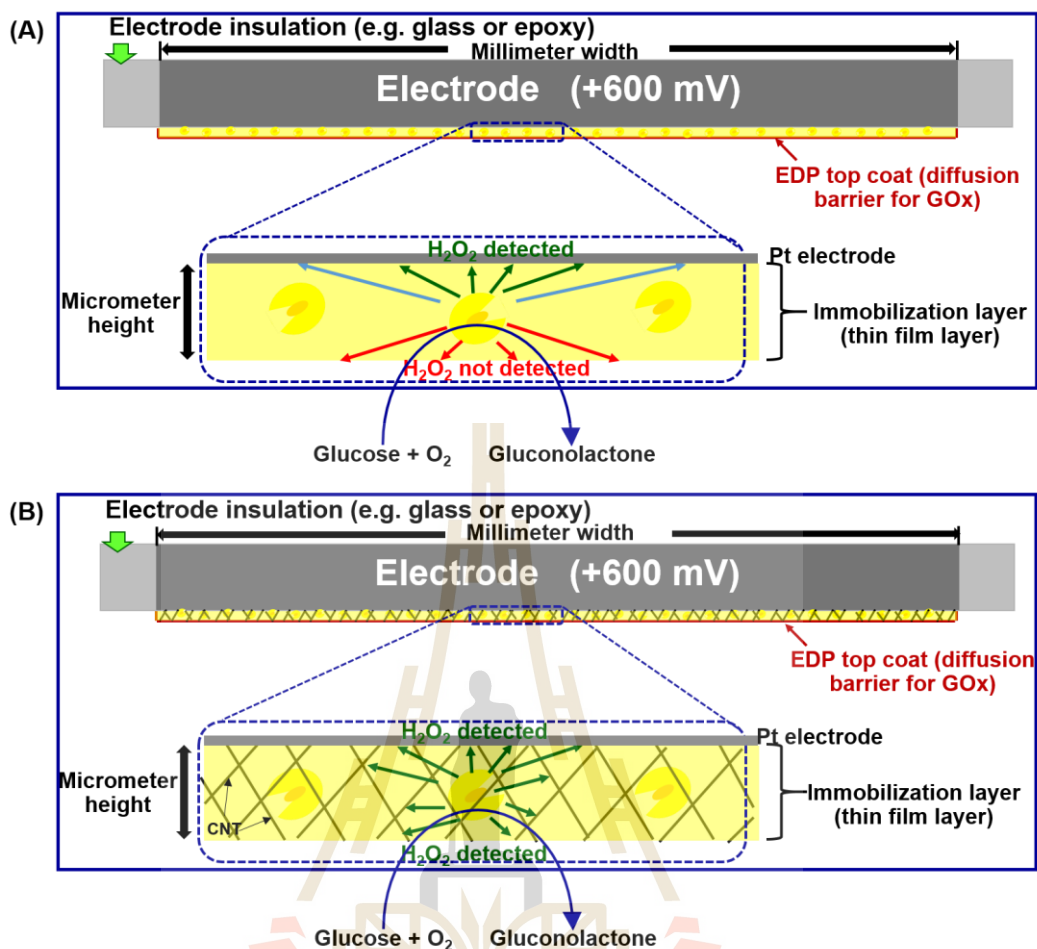


**Figure 2.4** Immobilization of GOx on platinum electrodes in a non-conducting polymer film (A) and a network of electrically wired carbon nanotube thin-film deposit (B). In case (A) about 50 % of hydrogen peroxide from enzymatic glucose to gluconolactone conversion is lost as detection takes place only at the platinum disk that carries the functional layer. In case (B) the collection efficiency is raised as the individual filaments of the immobilization carbon nanotube network are electrically wired to the carrying Pt disk and can serve as detector for hydrogen peroxide.

### 2.3.2 Morphology of carbon nanotubes modified platinum electrode

Measured with ordinary *GOx* driven glucose biosensors is at suitable anodic detection potential the Faradaic current,  $i$ , for the electrochemical oxidation of hydrogen peroxide ( $H_2O_2$ ), which is proportional side product of the biocatalytic conversion of glucose into glucono-lactone/gluconic acid at enzyme spots inside in the sensing layer of the gadget. Elevations in dissolved glucose levels,  $[G]$ , intensify the diffusional delivery of substrate to immobilized bio-catalytic sites and hence raise signal level. Accordingly, plots of the background-corrected biosensor response as function of  $[G]$ , prepared from amperometric raw data ( $i_{H_2O_2}$  vs.  $t$ ) of test trials, serve as calibration curves; observed is usually manifestation of an initial linear segment at lower glucose levels and then gradual transition into a current plateau at stronger challenge with analyte. Obviously, the quality of such a biosensor signaling depends much on the cooperative impacts of enzyme properties (e.g. substrate affinity and turnover rate in the state of immobilization), diffusional access of substrate and molecular oxygen to entrapped enzyme entities and the  $H_2O_2$  capture and oxidation efficiency of the detecting sensor surface. Such a complex multi-parameter situation is for biosensor developers' challenge and opportunity at the same time. Smart arrangement of the biosensor design is, for instance, the practical route for advancements of the analytical performance of the diagnostic tool. Here, freshly polished 3-mm-diameter Pt disk electrodes with mirror-like surface appearance (Figure 2.5A-a) were armed with pure CNT deposits into which biocatalytic *GOx* molecules could be blended as selective analytical component.

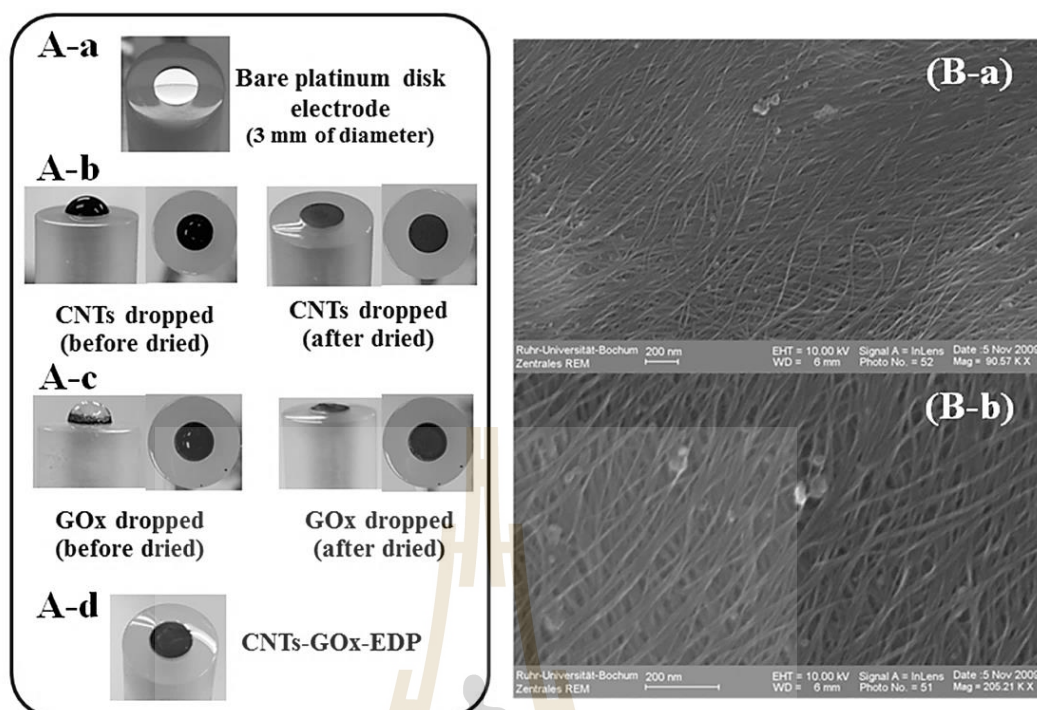


**Figure 2.5** Morphology of carbon nanotubes modified platinum electrode (A-a). Bare platinum disk electrode (3-mm of diameter), (A-b). Placement of carbon nanotube deposits via drop-coating, (A-c). Loading of CNT layers with GOx via drop-coating, (A-d) GOx/CNT surface layer after placement of a thin film of a cathodic electrodeposition paint. (B-a). and (B-b). Dried carbon nanotubes coatings on a metal substrate surface in scanning electron microscope (SEM) images at two different magnifications.

Establishment of the functional biosensor surface modification involved a comfortable sequence of two manual drop & dry casting steps, one for a suspension of carboxylated CNT in water (Figure 2.5A-b, left) and one for an aqueous *GOx* solution (Figure 2.5A-c, left). Formed on the polished Pt disk was in step 1 an even and well-adhering spongy network of CNT filaments (Figure 2.5A-b, right & 2.5B-a),

which are electrically chain-wired to each other and, important for efficient signal generation (= anodic hydrogen peroxide detection) to the Pt surface, too. A scanning electron microscopy examination verified an abundance of irregularly distributed nanopores in the CNT deposit (Figure 2.5B-b) while cyclic voltammetry in pure 0.1 M KCl revealed the predictable large surface area of the spongy Pt disk adaptation via visualization of considerable capacitance currents (which discuss in section 2.3.3). The placement of  $\mu\text{L}$  drops of a *GOx* stock with subsequent solvent evaporation loaded the nanopores of a CNT sensor layer in step 2 with *GOx* molecules. Firmly attached CNT/*GOx* (Figure 2.5A-c, right) was finally glazed with cathodic EDP paint (Figure 2.5A-d). The polymer top coat was conveniently formed in a 2-electrode electrochemical cell with which the CNT/*GOx*-covered Pt disc and a coiled Pt wire were coupled to the negative and positive terminals of a simple laboratory power supply, respectively. During sensor use and storage in aqueous media the role of the EDP glaze was protection of trapped *GOx* against escape from the CNT sponge and thus guarantee of good sensor response stability.

### **2.3.3 Electrochemical capacitance measurements with carbon nanotube-modified platinum electrodes**

The capacitance of electrode surfaces is proportional to their surface area. The placement of a highly porous carbon nanotube deposit onto an otherwise smooth Pt disk electrode was thus expected to increase noticeably the capacitance of the sensors. A good way to get access to the capacitance of electrode surfaces is the execution of cyclic voltammetry (CV) in inert electrolytes with no redox active species present as supplementation. Here, bare and CNT-modified Pt disc electrodes were

inspected via CV in oxygen-free since Argon-purged 0.1 M phosphate buffer solutions of pH 7.0. The Pt disk electrodes for the capacitance measurement were modified with a thin film of a carbon nanotubes (CNT) network following the procedure displayed in Figure 2.6.

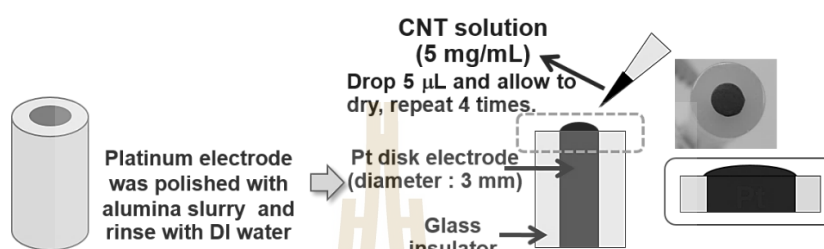


**Figure 2.6** The procedure used for the preparation of CNT-modified platinum disk electrodes as used for the capacitance measurement.

The results of the cyclic voltammetry assessment of the intrinsic capacitance properties of bare and CNT-modified Platinum electrode are shown in Figures 2.7. Cyclic potential scans with the electrodes in redox-mediator-free electrolyte produced the expected quasi-rectangular voltammograms, typical of a purely capacitive sensor response (Figure 2.7(A) and (C)). As expected, the anodic and cathodic charging currents ( $I$ ) were directly proportional to scan speed ( $\nu$ ) (graphs not shown). Plots of  $\Delta I$  (ie, the difference between the currents for the two scan direction as extracted from the recordings at the same potential) against scan speed,  $\nu$ , were also linear ( $R^2 = 0.99$ , refer to Figure 2.7(B) and (D)). Measurement of  $\Delta I$  as a function of  $\nu$  allowed calculation of the individual electrode double-layer capacitance  $C$  from the formula  $C = \Delta I / (2\nu)$ . The average values for otherwise identical Platinum disc electrodes, with and without CNT, were  $1.870 \pm 0.146 \mu\text{F}$  and  $0.016 \pm 0.002 \mu\text{F}$ ,

respectively. Since the capacitance of an electrode is directly proportional to its effective area, the  $\sim 119.7$ -fold larger C-value for the CNT-modified platinum electrode indicated nicely that the porosity of the thin-layer films of the carbon filaments created an electrode structure with enlarged contact area for the electrolyte.

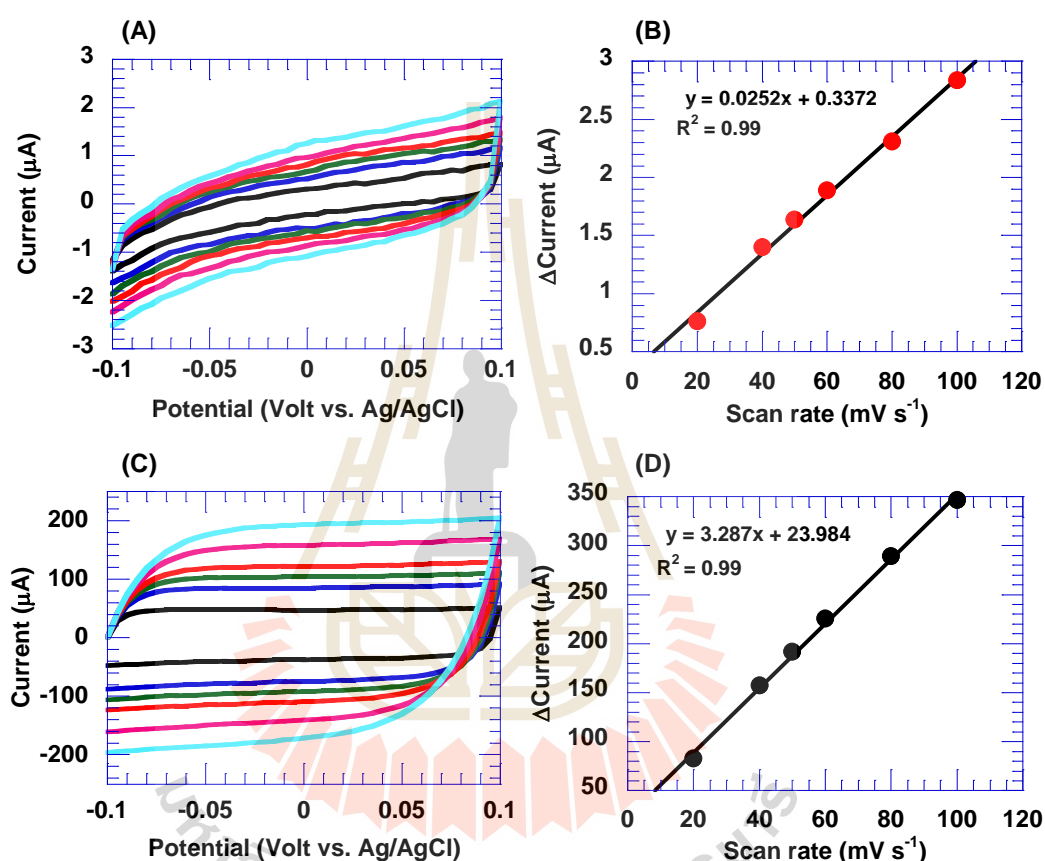


**Figure 2.7** Electrode capacitance determinations for a bare and CNT-modified platinum disk electrode by cyclic voltammetry in oxygen-free, Argon-purged, in 0.1 M phosphate buffer solution, pH 7.0. (A) and (C) are the original voltammograms as recorded at six scan rate in between 20  $\text{mV/s}$  and 100  $\text{mV/s}$  (from inner to outer traces). Plot (B) and (D) are plots of the width of the quasi-rectangular CVs at 0.035 V vs. Ag/AgCl, against the scan speed.

## **2.3.4 Amperometric determination of glucose at CNT/GOx/EDP-based glucose biosensor**

### **2.3.4.1 Platinum (Pt) electrode modification biosensor**

As already mentioned in section 1.2.9 chronoamperometry is the normal electrochemical technique used for the characterization of glucose-oxidase-based glucose biosensors. Obtained through analysis of the original amperometric recordings of the biosensor response to sequential additions of small glucose aliquots are the calibration curves that are requisite for judgements on analytical figures of merits such as the sensor's linear range width and sensitivity etc. Chronoamperometry with the sensors of this study was carried out in an aqueous 0.1 M phosphate buffer solution (pH 7.0) with a conventional three-electrode cell. A magnetic stirrer provided the convective transport during the measurements. The anodic current responses of the biosensor electrodes were measured at applied constant potentials +600 mV versus Ag/AgCl. When glucose stock solution was added in the bulk solution, the enzymatic reaction created hydrogen peroxide, which was measured as current via anodic oxidation of the molecule at the positively polarized Pt/CNT electrolyte interfaces.

Actually, the biosensors of the established CNT/GOx/EDP design offered in their calibration trials reproducibly a marked glucose receptiveness with reasonably fast response time, adequate sensitivity and a linear range that stretched broadly over tenths of mM analyte concentrations. Figure 2.8A displays as proof of the good performance a typical example of an amperometric recording that was acquired with a prototype of a CNT/GOx/EDP-modified 3-mm-diameter Pt disk electrode in course of successive additions of small aliquots of a glucose stock solution. Evident in the trace is a series of well-defined step-like rises in the continuously acquired anodic

$H_2O_2$  current, with an about 10 s interval needed to reach 90 % of the finally established steady-state signal value (Figure 2.8B plus inset).

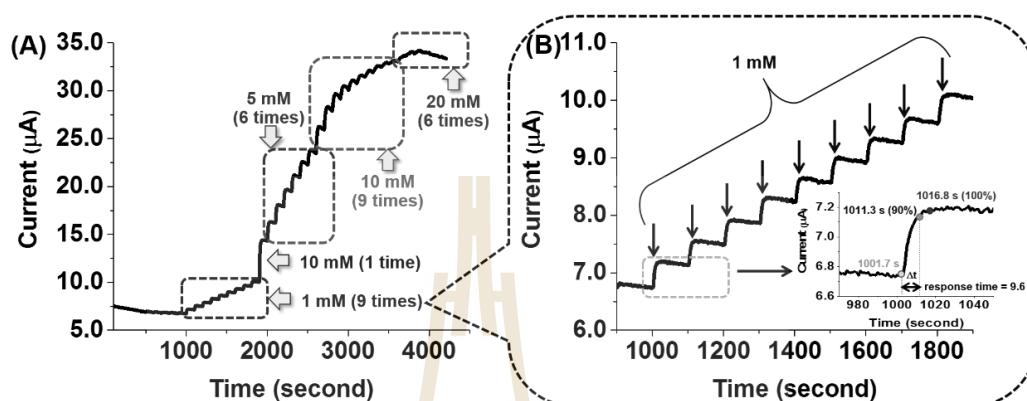


**Figure 2.8** (A) Representative current-time trace as acquired in the course of a calibration trial with a (CNT/GOx)/EDP-Pt glucose biosensor; aliquots of a glucose stock solution were added to stirred 0.1 M phosphate buffer solution (pH 7.0); The recording was made at ambient temperature of 25°C with a  $H_2O_2$  detection potential of +0.6 V vs. Ag/AgCl. (B) Zoom into the initial section of the current trace in (A) and, as inset, the example of response time estimation for the 1<sup>st</sup> of the 9 steps included in the zoom.

Extracted from current-time traces as in Figure 2.8 was then the amplitude of the current steps for the individual glucose additions. The obtained values allowed construction of so-called glucose sensor calibration curves, which are actually plots of the current increments as function of the actual glucose concentration in the measuring buffer. Figure 2.9 is the graphical illustration of such a calibration curve. In good agreement with the common behavior of enzyme-based biosensors the current

initially increased linearly with glucose concentrations, however, at higher levels of substrate the curve flattened and finally went into saturation. Figure 2.9A shown amperometric response of an enzyme biosensor to successive additions of various substrate concentrations, which displayed Michaelis-Menten type behavior was constructed by the analysis of the amperometric recording from Figure 2.8A, Exposed for this particular case is a plateau current,  $i_{\max}$ , of 30  $\mu\text{A}$ , response linearity up to an outstanding 60.0 mM glucose ( $r^2 = 0.99$ ) and a sensitivity of 0.41  $\mu\text{A mM}^{-1}$  ( $5.76 \mu\text{A mM}^{-1} \text{cm}^{-2}$ , normalized to the geometric surface area of the Pt disk transducer). For a compilation of 12 identically prepared biosensors  $28.0 \pm 5.9 \mu\text{A}$ , competitive  $42.1 \pm 8.1 \text{ mM}$  and  $6.54 \pm 3.0 \mu\text{A mM}^{-1} \text{cm}^{-2}$  were the average and standard deviation values for  $i_{\max}$ , linear range width and sensitivity, respectively.

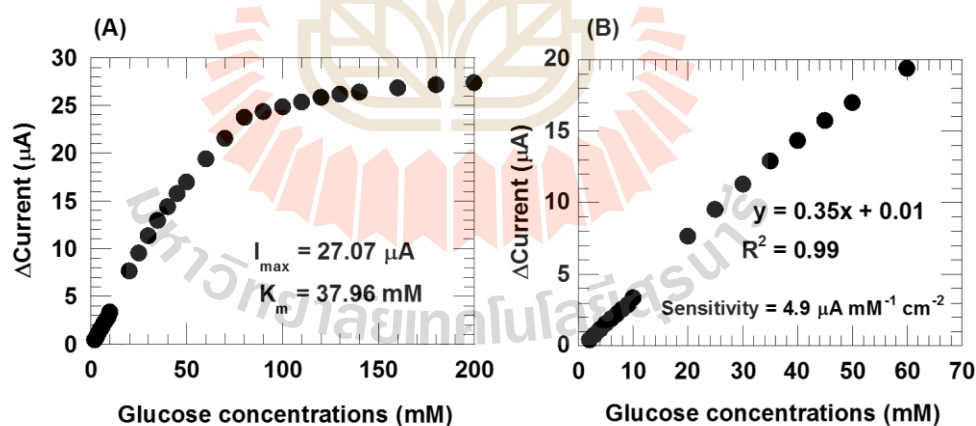


**Figure 2.9** (A) Electrochemically assessed CNT/GOx/EDP-based biosensor calibration curve plot obtained with data from the amperometric recording measurement in Figure 2.8A. (B) Illustration of the widely dynamic linear range of the response of CNT/GOx/EDP biosensors to glucose exposure, with regression coefficient of 0.99.

Later described stability testing for CNT/GO<sub>x</sub>/EDP biosensors had to be carried out with gold disk electrodes as these were available in a geometry and size suitable for incorporation into an electrochemical flow cell designed for continuous long-term measurements. Figure 2.10A and B represents the amperometric response of a prototype of a CNT/GO<sub>x</sub>/EDP-modified 3-mm-diameter Au disk electrode to successive additions of small aliquots of a glucose stock solution. A look at the calibration curve for this variant of the novel biosensors (refer to 2.10 C and D) confirmed that the CNT/GO<sub>x</sub>-modified Au disc electrode also had a wide linear range and a reasonable sensitivity. Exposed for this particular case was, for instance, a plateau current,  $i_{\max}$ , of 13.05  $\mu\text{A}$ , response linearity up to 40.0 mM glucose ( $r^2 = 0.99$ ) and a sensitivity of 0.18  $\mu\text{A mM}^{-1}$  (2.50  $\mu\text{A mM}^{-1} \text{cm}^{-2}$ , normalized to the geometric surface area of the Au disk transducer) which show in Figure 2.10D. For a compilation of 4 identically prepared biosensors  $18.1 \pm 7.4 \mu\text{A}$ ,  $25.0 \pm 17.3 \text{mM}$  and  $5.2 \pm 4.5 \mu\text{A mM}^{-1} \text{cm}^{-2}$  were the average and standard deviation values for  $i_{\max}$ , linear range width and sensitivity, respectively.

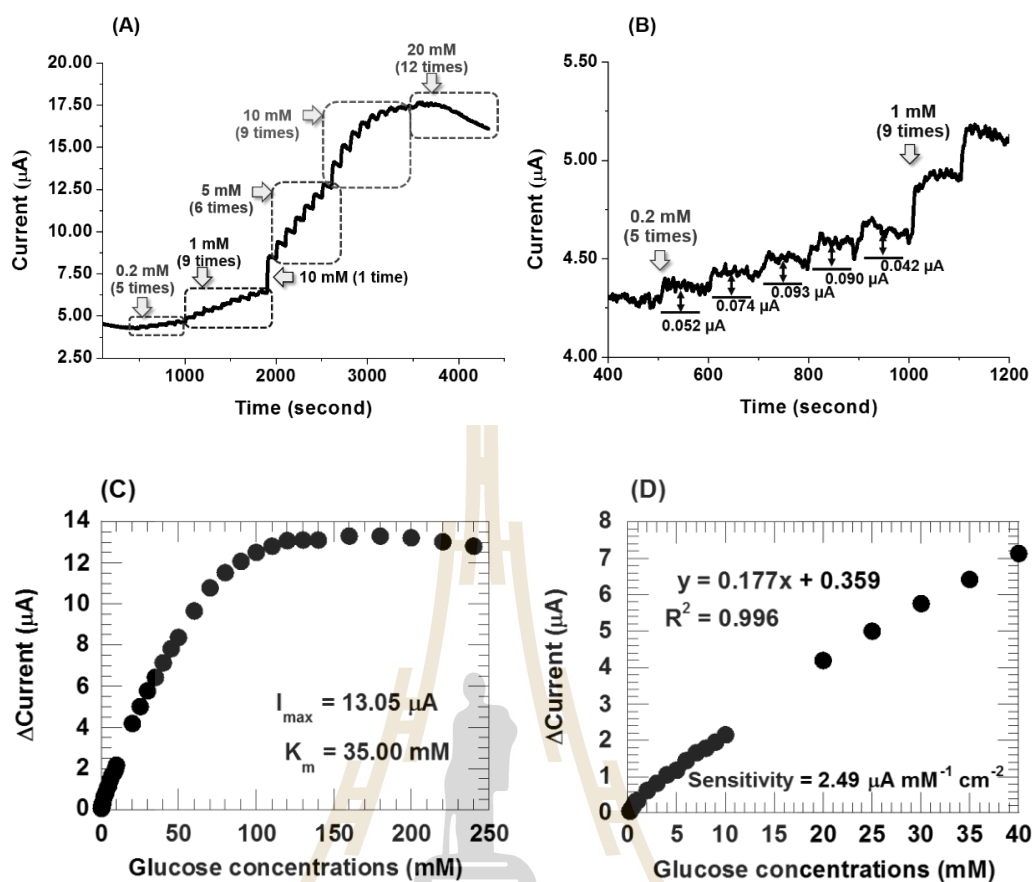


**Figure 2.10** (A) Representative current-time trace as acquired in the course of a calibration trial with a (CNT/GOx)/EDP-Au glucose biosensor; aliquots of a glucose stock solution were added to stirred 0.1 M PBS (pH 7.0). (B) Zoom into the initial section of the current trace in (A). (C) Electrochemical assessed biosensor calibration curve as constructed by the examination of the amperometric recording in (A). (D) Manifestation of the wide linear range response at biosensor with a regression coefficient of 0.99.

A summary of the analytical figures of merit for both CNT/GOx/EDP-modified Pt and Au disk electrodes is available in following Table 2.1.

**Table 2.1** Summary performance of CNT/GO<sub>x</sub>/EDP biosensor.

Characteristics	Platinum electrode												
	#1	#2	#3	#4	#5	#6	#7	#8	#9	#10	#11	#12	Average
<b>I<sub>max</sub> (μA)</b>	19.28	32.72	27.12	24.19	27.07	21.57	36.02	20.1	36.9	30.28	28.45	32.31	28.0±5.9
<b>K<sub>m</sub><sup>app</sup> (mM)</b>	29.8	27.24	32.59	35.08	37.96	44.17	18.01	110	21.91	33.15	30.84	28.60	-
<b>Linear range (mM)</b>	35	40	50	50	50	50	25	40	40	35	40	50	42.1±8.1
<b>Regression Coefficient (R<sup>2</sup>)</b>	0.996	0.995	0.996	0.995	0.995	0.995	0.997	0.996	0.996	0.998	0.995	0.996	-
<b>Sensitivity (μA mM<sup>-1</sup> cm<sup>-2</sup>)</b>	4.64	8.60	5.80	4.99	5.11	3.35	12.83	2.05	10.79	6.56	6.43	7.34	6.5±3.0

**Table 2.1** Summary performance of CNT/GOx/EDP biosensor (Continuous).

Characteristics	Gold electrode				
	#1	#2	#3	#4	Average
$I_{\max}$ ( $\mu\text{A}$ )	17.58	13.1	28.66	13.05	$18.1 \pm 7.4$
$K_m^{app}$ (mM)	29.25	55.00	22.00	35.03	-
Linear range (mM)	40	10	10	40	$25.0 \pm 17.3$
Regression coefficient ( $R^2$ )	0.997	0.996	0.966	0.995	-
Sensitivity ( $\mu\text{A mM}^{-1} \text{cm}^{-2}$ )	4.44	2.26	11.77	2.49	$5.2 \pm 4.5$

### **2.3.5 The assessment of the detection limit for glucose quantifications with CNT/GO<sub>x</sub>/EDP-based glucose biosensors**

An important analytical feature of amperometric biosensors is its practical detection limit, which for the biosensors of this study shall be defined as the smallest glucose concentration change that is related to a measurable ('visible') raise in current above baseline signal valid for glucose-free electrolyte. To determine the practical detection limit glucose was added to the measuring solution at smaller and smaller increments and the smallest increment that still was able to create a visible step in the current trace was judged on as "LOD". Actually, small aliquots of a 1.0 M glucose stock solution were added into 5 mL in the measuring buffer, a 0.1 M phosphate buffer solution (pH 7.0) while the biosensors hydrogen peroxide oxidation current was recorded at constant working potential + 600 mV. Tested triplicate glucose additions raised the solution level by either 200, 100, 50 or 25  $\mu\text{M}$ , respectively. Figure 2.11 shows a typical amperometric recording of such a trial in search for the practical LOD. Triplicate identical changes in glucose buffer levels caused as desired current elevations of identical height, which confirmed the reproducibility of the biosensor response to analyte variations. For the platinum-based CNT/GO<sub>x</sub>/EDP glucose biosensors 50.0  $\mu\text{M}$  concentration changes were the lowest that could be clearly resolved in the amperometric recordings and 50  $\mu\text{M}$  is thus referred to as practical LOD.

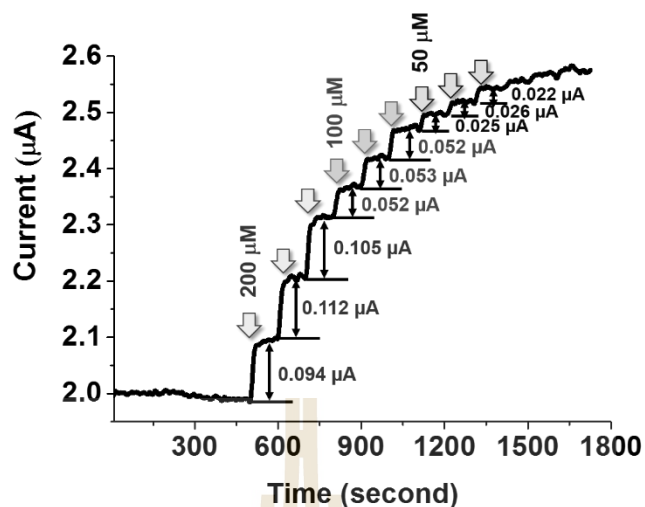


**Figure 2.11** Detection limits assessment for glucose quantification with biosensor. Glucose was added to the measuring solution at smaller and smaller increments and the smallest increment determined that still was able to create a visible step in the current trace, glucose concentration solution: 200, 100, 50 and 25  $\mu\text{M}$ , respectively.

### 2.3.6 Effect of electrochemically induced polymer precipitation

Aqueous suspensions of anodic paints or cathodic paints are commercially available and widely used for corrosion protection in the car and can industry. First use for biosensor construction was reported for anodic paints (Kurzawa *et al.*, 2002) and the entrapment of GOx into the thin film polymer electrodeposits lead to functional glucose detectors. A clear asset of electrodeposition paints (EDP) is that their deposition is electrochemically induced and thus non-manual. This simplifies the procedure and makes it a user-friendly strategy for polymer placement on sensor surfaces. Here the function of EDP was not to immobilize GOx onto the noble metal disk electrodes (this was the prominent role of the nanoporous CNT modification) but

to work as a barrier against diffusional loss of enzyme that was soaked into the prime CNT deposit. Figure 2.12 illustrates the electrochemical cell arrangement for the glazing of CNT/GOx layers on Pt or Au disk electrodes, and as here the cathodic EDP version was used, the modified electrode to be further coated with a thin polymer top layer as protection for diffusional GOx loss had to be connected to the negative terminal of the laboratory power supply.

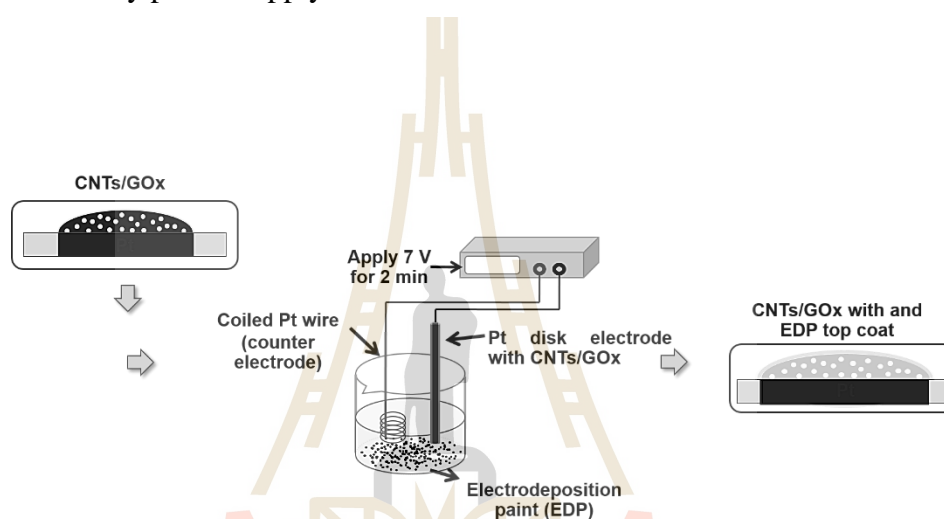


**Figure 2.12** Setup used for the placement of a thin film of electrodeposition paint on top of the CNT/GOx modification of platinum or gold electrodes as enzyme leak protection.

The need for a leak protection becomes immediately evident through a look to Figure 2.13A. Shown is the outcome of an amperometric calibration trial for a CNT/GOx biosensor that lacked the EDP glaze and that before measurement was stored overnight in refrigerated phosphate buffer, just as the CNT/GOx/EDP equivalents with polymer film leak protection. From the raw amperometric recording in Figure 2.13A the calibration curve for the biosensor without leak protection was constructed and is displayed in Figure 2.13B. Indeed, the maximum current at sensor

saturation was for the CNT/GOx biosensor almost 10 times less than for CNT/GOx/EDP biosensors and also the width of linear range was greatly reduced. This is also nicely visible of in one and the same graph the calibration curves of an EDP-coated and an “naked” CNT/GOx biosensor are jointly presented (refer to Figure 2.14). Apparently a significant portion of initially entrapped enzyme had been lost during overnight storage and was not anymore available for signaling of the presence of glucose.

The vital role of the EDP glaze of the proposed biosensors in stopping GOx leakage from the CNT matrix is also highlighted in Figure 2.15, correlating the responses of sensors prepared by the standard protocol, with and without the final EDP coating. Amperometric calibrations were for both sensor types carried out after the usual overnight refrigerator storage of completed sensors in PBS/KCl and after a further 24 h cooled storage. In the performance tests on day 1 and day 2 both (CNT/GOx)/EDP-Pt and (CNT/GOx)-Pt biosensors produced amperometric glucose calibration curves of the classic shape (Figures 2.15A and B). Unsurprisingly, the omission of the EDP leak protection allowed diffusional loss of GOx from the matrix, resulting in a major reduction in anodic  $H_2O_2$  current and a contraction of the linear range. The close similarity of the responses on days 1 and 2 for the EDP-coated glucose biosensor (Figure 2.15B) demonstrated, on the other hand, the ability of the thin electropaint coverage to stop leak of biocatalyst, and hence to preserve signal stability.

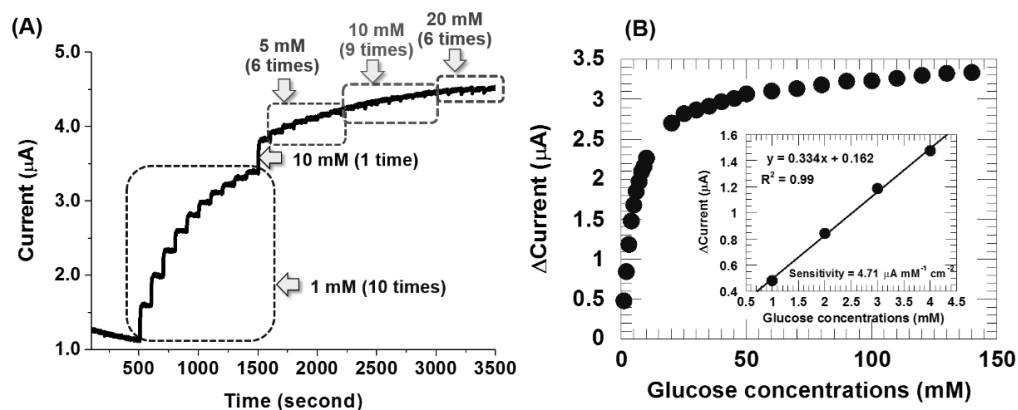


**Figure 2.13** Typical amperometric response of a CNT/GOx biosensor without EDP top coat to successive additions of substrate in aerated solution (A). Computed biosensor calibration curve as constructed by the analysis of the amperometric recording in A, the inset show linear range with good regression coefficient (B).

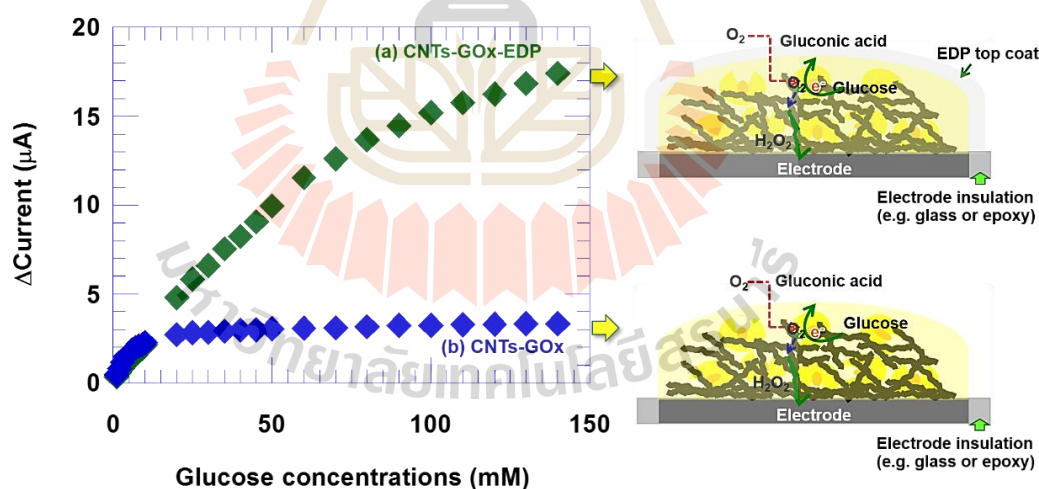


**Figure 2.14** Comparison of "day 1" glucose calibration curves for (a) a CNT/GOx/EDP and (b) a CNT/GOx biosensor. Both sensors were prepared via identical procedures, with the exception that for the sensor (a) EDP top coat was applied and sensor (b) was left uncovered. Both sensors went through a one-night refrigerator storage before measurement.

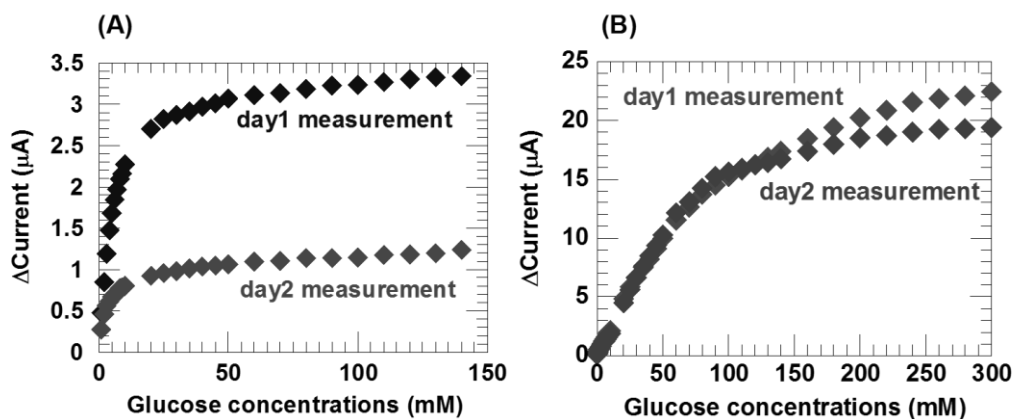


**Figure 2.15** (A) Electrochemical assessed biosensor calibration curve as constructed by analysis of the amperometric recording. Performance of CNT/GO<sub>x</sub> modified platinum electrode at day one vs. day two. (B) Performance of CNT/GO<sub>x</sub>/EDP modified platinum electrode at day one vs. day two. Please note the difference in the scaling of the x and y axes in (A) and (B).

### 2.3.7 Reproducibility and long-term stability tests with CNT/GO<sub>x</sub>/EDP glucose biosensors

Apart from their capability to measure their target analyte accurately also desired for sensors in general and enzyme biosensors in particular is the offer of a good reproducibility and life time. Initial tests regarding the quality of the sensor life time involved a look at calibration data for measurements carried out at day 1 and 7 after preparation, with refrigerator storage in phosphate buffer solution (pH 7.0) applied in the resting period between measurements. Since the proposed sensors are easy to make with cheap materials and are not meant for commercial applications longer storage periods have not been considered here. Instead, after a week of storage fresh preparations were preferred, in case the biosensors were needed. Figure 2.16 displays

a typical set of “day 1” and “day 7” calibration curves for a CNT/GOx/EDP glucose biosensor, as derived from the corresponding raw data of their amperometric calibration trials. Carrier of the enzyme sensor modification was in this particular case a 3 mm gold disk electrode. Evident are on first sight (1) a minor, about 10 % decrease in the value of the maximum current at sensor saturation and (2) an almost perfect overlay of the traces in the range of linear response to glucose variations, up to a competitive level of 40 mM. The latter positive finding is the more important issue for analytical application of this type of biosensors and suggests that within the tested period of one week an adverse degradation of the detector, for instance because of a loss or inactivation of entrapped GOx entities, is not a problem at all. Apparently, the EDP glaze served well as protecting layer against diffusional GOx leak and the CNT matrix was a biocompatible enough to work for non-toxic immobilization of the delicate protein biocatalyst molecules.

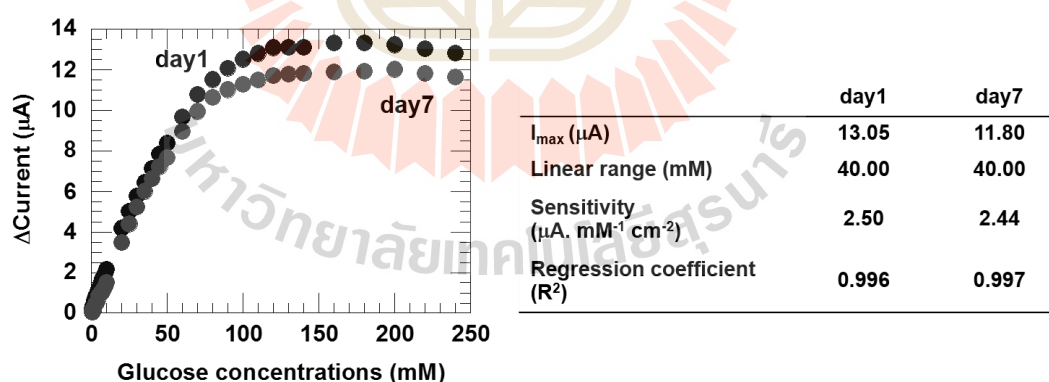


**Figure 2.16** Comparison of “day 1” and “day 7” calibration curve for one and the same CNT/GOx/EDP glucose biosensors, with refrigerator storage in phosphate buffer solution (pH 7.0) applied in the resting period between measurements. Carrier system in this particular case was a 3 mm Au disk electrode.

To further demonstrate the effectiveness of the EDP top coat as barrier against GOx loss and the undamaging function of a CNT matrix for GOx electrode surface fixation freshly prepared CNT/GOx/EDP glucose biosensor were inspected via continuous operation in a flow electrochemical cell as shown in Figure 2.17. In such a trial the biosensor was incorporated as working electrode into the small-volume cell section of the system and for the duration of the experiment - ranging from hours to many days – continuously exposed to the stream of running buffer (here: the usual phosphate buffer, pH 7) and to polarization of + 600 mV, as needed for amperometric detection of GOx/glucose produced hydrogen peroxide in calibration trials or for recovery rate measurements. Before used for a test in the flow systems sensors went through a “day 1” and “day 7” testing and only if they appeared well-working they were further processed into the flow system. Figure 2.17 displays, as typical example, an about 200 hour-long stretch of an uninterrupted amperometric recording that followed a “day 7” pre-calibration trial and for the duration of which the CNT/GOx/EDP-Au biosensor was in flow mode continuously polarized to + 600 mV vs. Ag/AgCl/3M KCl and subjected to constant passage of phosphate buffer solutions without or, in six calibration and two model sample analysis efforts, with glucose at various molarities. Response generation for the stepped glucose changes was with the minimalistic sensor design for the first four calibrations and thus remarkable 94 hours of flow operation possible on virtually 100 % reproducibility level. Only then a signal drop to 92 % and further to 70 % evolved for the 5<sup>th</sup> (120+ hours) and 6<sup>th</sup> (180+ hours) calibration, respectively.

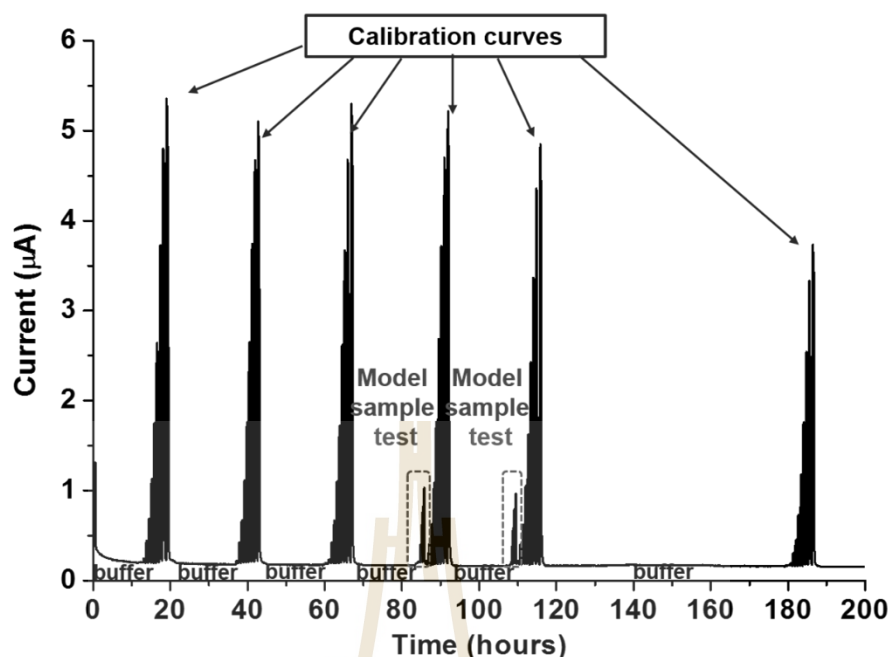


**Figure 2.17** Long-time stability test with CNT/GO<sub>x</sub>/EDP glucose biosensors, established on a Au disk electrode transducer, in an electrochemical flow cell arrangement. For the duration of the trial, the sensors were continuously polarized to +600 mV for hydrogen peroxide detection and exposed to a non-stop flow of phosphate buffer as running solution. Six biosensor calibrations were executed with glucose concentrations spanning from 0.1, 0.5, 1, 2, 4, 8, 16, 32 to 50 mM, respectively. Also, two model sample were assessed, before calibrations 4 and 5.

Figure 2.18A is a zoom of the current trace for the period of the 4<sup>th</sup> calibration while Figure 2.18B is the calibration curve that corresponds to that calibration data. All applied sequential elevations in running buffer glucose levels got well translated into visible columnar trails in the monitored flow cell current and plots of signal column heights as function of the related glucose content correctly portrayed typical Michaelis-Menten enzyme biosensor behavior with initial manifestation of a

linear section followed by curve flattening at saturating substrate values. Predictable from the known practical detection limit of the beaker-type measurements of this study the lowest trialed glucose level of 100  $\mu\text{M}$  produced a clearly visible anodic  $\text{H}_2\text{O}_2$  footprint. Maximum sensor currents at saturation (4.6 vs. 13.1  $\mu\text{A}$ ), linear range (4 vs. 40 mM) and sensitivity (5.4 vs. 2.5  $\mu\text{A mM}^{-1} \text{cm}^{-2}$ ) were on the other hand not as closely mimicked (Figure 2.18B). Instead, the glucose response linearity window got considerably narrowed while sensor sensitivity increased about two-fold. The exact bases for these trends is unclear but likely responsible is the special hydrodynamics in the small dead volume flow cell and related differences in balances of diffusional and convectional glucose and/or molecular oxygen delivery to enzyme sites on the electrode, as compared to mass transport conditions in the stirred bulk of a large-volume container. Despite of the observed concession in the linear range width CNT/GOx/EDP-Au biosensors did in the flow cell even above 100 hours of continuous contact to buffer stream very well for accurate glucose determinations in samples of known content. A standard addition mode assessment of a 500  $\mu\text{M}$  model glucose sample, just prior to the 4<sup>th</sup> and 5<sup>th</sup> calibration at about 84-86 and 108-110 hours after trial start, worked, for instance, via standard addition plot analysis (Figure 2.18C is an example) with recovery rates of 102 and 100 % very close to ideal level.

Important message of the stability tests in flow mode is that on the one hand the EDP hinders GOx effectively to diffuse out of the immobilizing CNT thin films into the aqueous surrounding while on the other hand the graphitic nanotube network itself is a healthy host for GOx in support of protracted life time.

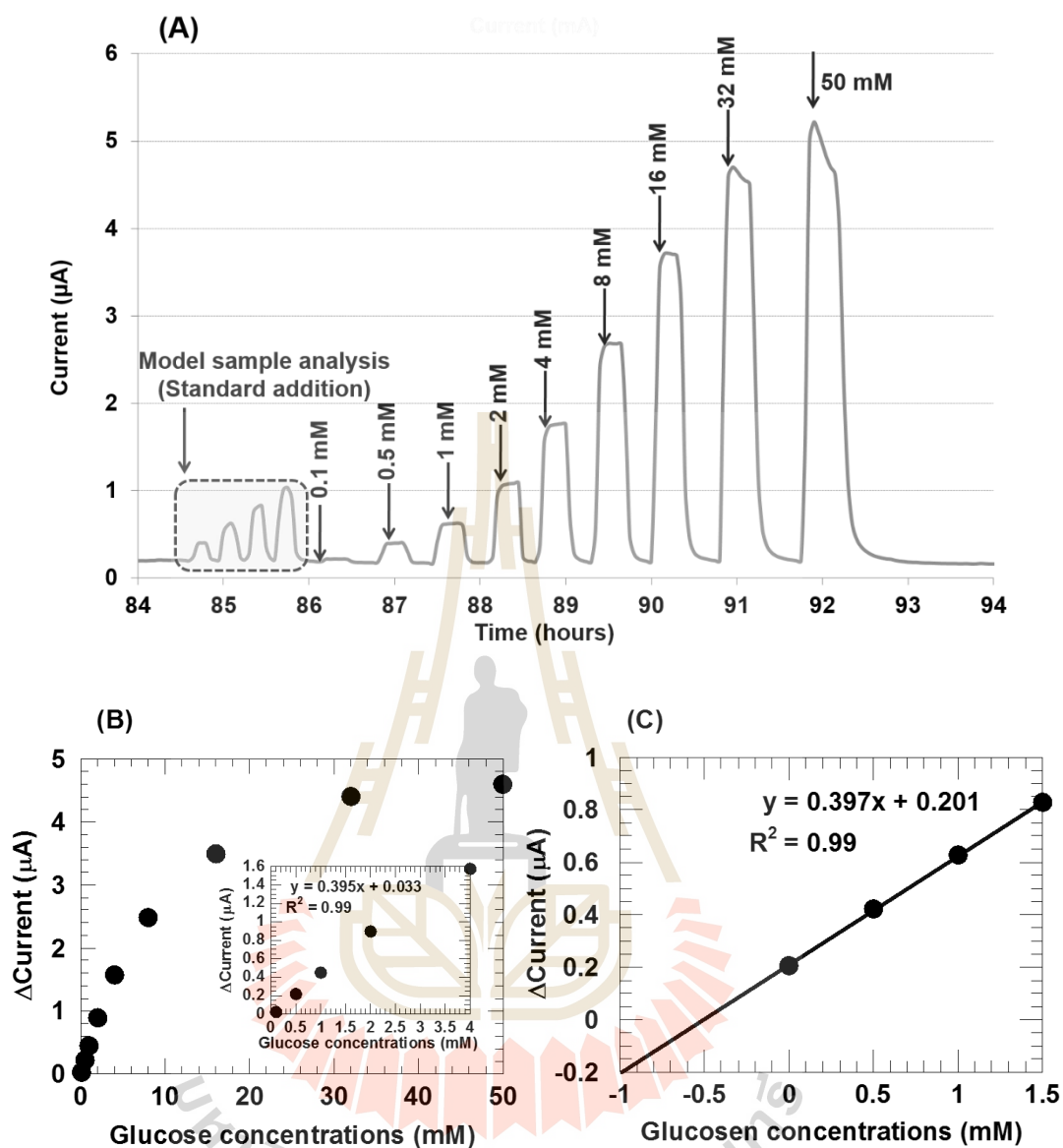


**Figure 2.18** (A) Typical amperometric response of a CNT/GOx/EDP glucose biosensor to successive additions of substrate for a flow-based calibration (here the 4<sup>th</sup> one in Figure 2.17) and a flow-based model sample analysis via standard addition. (B) Electrochemical assessed biosensor calibration curve as constructed by the analysis of the amperometric recording in A. (C) Recovery rates assessments for glucose quantification in 0.5 mM model samples with CNT/GOx/EDP-based glucose biosensors modified on gold electrode via standard addition method.

### 2.3.8 Performance evaluation for quantitative measurements of model samples with pre-adjusted glucose levels

Established CNT/GOx/EDP-based glucose biosensors with Pt disk electrode signal transduction were checked with respect to their ability to recover the known levels of glucose in model samples accurately, with reasonable recovery rates. The recovery rate assessments used the routine strategy of standard addition and targeted with six-fold repetitions model samples with low (1 or 2 mM), medium (5 mM, equivalent to the normal, healthy human blood glucose content) and high (15 mM, equivalent to the glucose content of seriously diabetic blood). Figure 2.19A shows the original amperometric recording of a recovery rate trial for a 1 mM model sample while Figure 2.19B displays the corresponding standard addition plot from which the model sample glucose level can be graphically or mathematically extracted. In the particular case of the 1 mM model sample of Figure 2.19A, the experimentally determined glucose levels were visibly very close to the expected value of 1.0 mM. Statistical analysis of the data for all six 1 mM samples revealed  $0.97 \pm 0.08$  mM ( $n=6$ ) as measured average and standard deviation, which corresponds to an excellent average recovery rate of  $97.84 \pm 8.02$  %. Table 2.2 summarizes the recovery rate performance for glucose quantifications with CNT/GOx/EDP-based glucose biosensors. Apparently, the measured concentrations for the various model samples did not deviate more than 10 % from the expected since adjusted value reflecting acceptable recovery rates for the determinations in the range of 90 – 110 %.

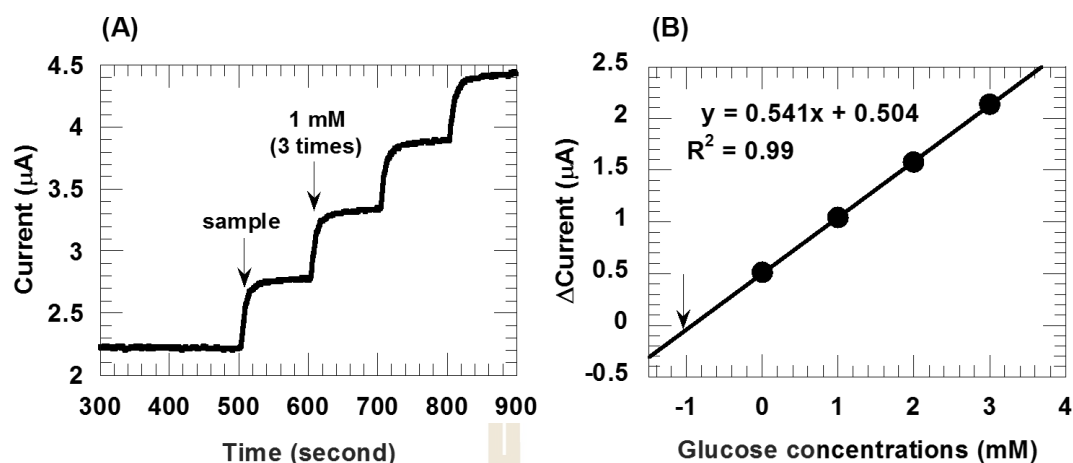


**Figure 2.19** Recovery rate assessments for glucose quantification in 1.0 mM model samples with CNT/GOx/EDP-based glucose biosensors modified on Pt electrode. The standard addition method was employed, amperometric response of an enzyme biosensor to successive additions in 0.1 M phosphate buffer solution (pH7.0) at + 600 mV.

**Table 2.2** The recovery rate of CNT/GOx/EDP biosensor modified Pt electrode at various glucose concentration samples quantification by standard addition mode.

Adjust (mM)	Found (mM) (n=6)	Found (mM) (n=6)
1.00	$0.98 \pm 0.08$	$97.84 \pm 8.02$
2.00	$1.97 \pm 0.13$	$98.40 \pm 6.31$
5.00	$5.51 \pm 0.18$	$110.17 \pm 3.60$
15.00	$15.85 \pm 1.20$	$105.64 \pm 7.97$

## 2.4 Conclusions

Serial drop/drying of  $\mu\text{L}$  volumes of first an aqueous CNT suspension and then a GOx solution led to firm but gentle immobilization of the macromolecular protein biocatalyst in entirely additive-free well-adhering nanoporous CNT films on Pt or Au electrode disks. A brief electrochemical post-treatment with cathodic EDP capped just dried CNT/GOx blends finally protected the established glucose biosensors with a thin polymeric top coat as GOx leak protection. Held in test trials at + 600 mV vs. reference for anodic  $\text{H}_2\text{O}_2$  detection CNT/GOx/EDP-modified Pt and Au electrodes both were in amperometric recordings capable to consistently and fast convert glucose additions to measuring buffer into proportional steps of continuously monitored  $\text{H}_2\text{O}_2$  current. Glucose and  $\text{O}_2$ , the substrate and native redox recycler of embedded GOx hence could diffuse easily through the EDP top coat into the nanoporous CNT matrix to become available at randomly dispersed enzyme sites for biocatalytic action. A more than 100 hours long adequate response stability during continuous use as electrochemical flow cell detector indicated, on the other hand, remarkable CNT/GOx bilayer durability as the biosensors EDP glaze effectively suppressed adverse loss of functional enzyme molecules from the interior of the CNT network into bulk solution and the graphitic CNT sponge itself was suitably biocompatible. In glucose valuation trials CNT/GOx/EDP biosensors showed wide analyte response linearity up to the order of 40 mM, a low detection limit down to 50  $\mu\text{M}$  and a reasonable recovery of known analyte levels. Advantage of the suggested biosensor version is that their highly competitive analytical figures of merit are reached with a minimalistic immobilization layer design, excluding in contrast to many previously published other options an integration of any signal-producing (nano-) materials other than bare CNTs. Key

deliveries were a general route for very simple oxidase biosensor assembly, a novel EDP-based polymeric diffusion barrier as enzyme leak protection, glucose biosensors with very good detection performance and the important take-home message that untainted CNT matrices can serve as good for biosensor enzyme immobilization as multicomponent complex CNT/additive composites. A not yet explored extra plus of the proposed design is its feasibility for robotic sensor mass production with readily available commercial starting materials.



## CHAPTER III

### Add-on work with CNT/GO<sub>x</sub>/EDP-based biosensors

The previous chapter dealt with detailed characterization of CNT/GO<sub>x</sub>/EDP biosensors and evidence has been provided that bare CNT deposits soaked with GOX and leak-protected via EDP polymer glaze were enough for the reach of competitive linear range, detection limit, sensor sensitivity and sensor life time. This chapter describes preliminary work that was carried out with the following three motivations:

1. Chitin and chitosan are biopolymers with well-known biocompatibility and they are matrix component of many published biosensor versions. Tests were conducted here to check whether the life time of CNT/GO<sub>x</sub>/EDP glucose biosensors could be further stretched through blending of the enzyme-entrapping CNT matrix with chitin/chitosan as extra matrix modifier that is gentle to entrapped protein biocatalyst molecules.
2. For glucose enzyme that was immobilized on single CNT filaments or in CNT networks direct electron transfer between the enzyme and the surface of the graphitic nanotubes was observed in several published studies. Tests were conducted here to check whether this effect happened for the CNT/GO<sub>x</sub>/EDP glucose biosensors of this study, too.
3. CNT/GO<sub>x</sub>/EDP glucose biosensors use oxygen as mediator of enzyme redox recycling and thus depend on aeration of the measuring buffer and presence of

O<sub>2</sub>. To make the sensor design suitable for work in deaerated solutions with no O<sub>2</sub> thought of was incorporation of ferrocene derivatives into the GOx entrapping CNT matrix and thus let the iron compound instead of molecular oxygen do the job of GOx oxidation after one cycle of glucose to gluconolactone conversion. Tests to evaluate the suitability of this mediator replacements have been carried out here and related data will be presented as final part of this chapter

What follows is first a presentation of the background literature for above issues 1-3 and then a description of the measurements and results that were obtained with CNT/GOx/EDP glucose biosensors with additional chitin/chitosan or ferrocene modification of their functional sensing layer.

### **3.1 Literature review**

In recent years research and development of electrochemical biosensors has been studies on enzyme immobilization of detector design and enhancement of signal generation. Several methods have been proposed to achieve immobilization of enzymes, theirs may be immobilized by a variety of methods, which may be broadly classified as physical and chemical, where covalent bonds are formed with the enzyme (Bullock, 1995; Chaplin and Bucke, 1990; Scouten *et al.*, 1995; Tischer and Wedekind, 1999; Woodley, 1992). Regarding immobilization layer optimization integration of with nanoscopic materials of high catalytic activity, large surface area and unique electronic features became a prime strategy for the preparation of amperometric enzyme

biosensors with advanced analytical figures of merit. Tested in many studies since about new millennium start as functional sensor components were metal and metal oxide nanoparticles and -wires, semiconductor quantum dots, high-tech graphitic matter such as fullerenes and carbon nanotubes (CNT) and few-layered nanosheets of graphene, graphene oxide or transition metal di-chalcogenides (Frasco and Chaniotakis, 2009; Gavalas and Chaniotakis, 2000; Guo *et al.*, 2011; Xinyu Li *et al.*, 2009; Q. Liu *et al.*, 2007; Yong Liu *et al.*, 2010; Mani *et al.*, 2013; Razmi and Mohammad-Rezaei, 2013). Whether final goal is utilization for bio-analysis in academic research or commercial distribution for health, biotech and environmental monitoring, continuing tasks of makers of biosensors are performance perfection, simplification of fabrication and miniaturization. Carbon nanotubes (CNT), for instance, have been utilized almost since their discovery as nanoscopic functional component of the analytical tools. The reason for the attraction of the field towards CNT is that the high-tech material has not only the capacity to enhance the electrochemical sensor sensitivity for the signaling molecule but also the potential to promote direct electrode/protein electron-transfer.

Chitin and chitosan are natural polyaminosaccharides, structurally quite similar and possess good biocompatibility, have potential to form uniform films and hydrogels, and contain multiple oxygen- and nitrogen-based functional groups that can be chemically modified. However, in chitosan a good portion of the acetylated nitrogen functionalities is chemically modified via deacetylation into amino groups. Different between the two biopolymers is only the ratio of the number of acetylated to the number of deacetylated nitrogen groups at the C2 carbon of the sugar ring. In chitin there are actually more acetylated than amino groups while in chitosan the situation is the opposite and the amino functional groups are dominant.

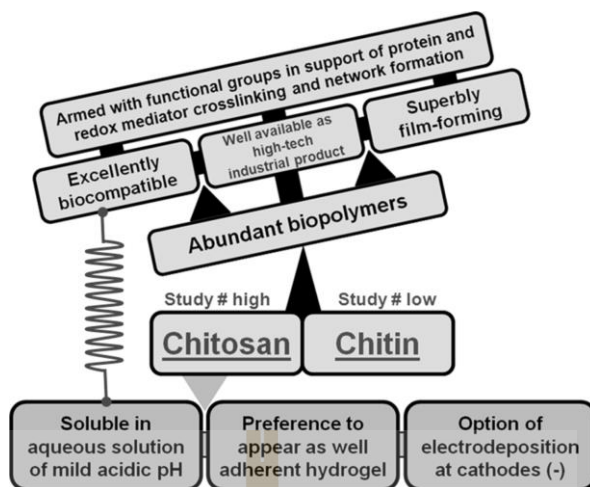


**Figure 3.1** Advantages of chitin and chitosan for biosensor applications. Chitosan, with its higher solubility and its hydrogel-forming characteristics, is by far the more widely used material in this field; balance between the number of published studies with the two materials is thus firmly on the side of chitosan. (Suginta *et al.*, 2013b).

Although chitosan-based fabrications have been studied intensively, 3<sup>rd</sup> generation enzyme biosensor fabrication using chitin biomaterial has been barely described. Chitin is a long-chain polymer of *N*-acetylglucosamine (GlcNAc) units and the structural component of marine animals, such as crab, shrimp, and squids (Li *et al.*, 2012). As reviewed by Suginta *et al.* (2013), only five reports appeared so far on chitin applications in biosensor research. Motivation behind an integration of the marine biopolymer chitin into the desired biosensor architecture was a gain of matrix biocompatibility and, as a consequence, a good GOx survival and related analytical response stability. Then, own thesis work on an exploration of CNT incorporation into enzyme biosensor immobilization matrices will be introduced. The target biosensor design was actually realized via simple drop/dry coating steps, namely via serial load

of the electrode disks with  $\mu\text{L}$  droplets. Successful with close to ideal recovery rates were quantitative assessments of spiked model samples and continuous biosensor use in a flow-based three-electrode electrochemical cell with scheduled on-line glucose calibration measurements during uninterrupted flow cell operation. Apparently, electrode surface-immobilized GOx entities were in the CNT/chitin environment kept healthily in place and thus able to maintain their pronounced bio-catalytic activity for long. Possible was as a result an electrochemical biosensing service on an extended time scale for glucose quantifications, with adequate analytical figures of merit for analyte quantifications.

## 3.2 Experimental and methods

### 3.2.1 Chemicals

Glucose oxidase (GOx, EC 1.1.3.4, from *Aspergillus niger*) was obtained through S.M. Chemical Supplies Co., Ltd. (Bangkok, Thailand) as product of Sigma-Aldrich® (St. Louis, MO, USA, product no. G1741, lyophilized, 75% protein, 136300 units/g).  $\beta$ -D (+) glucose anhydrous ( $\text{C}_6\text{H}_{12}\text{O}_6$ ) was obtained through Italmar (THAILAND) Co., Ltd. (Bangkok, Thailand) as a product of CARLO ERBA Reagents S.A.S. (Val-de-Reuil, France). Purified carboxylated single-walled CNT, with an about 1.0 - 3.0 at-% carboxylic acid entities were obtained from Carbon Solutions, Inc., (Riverside, CA, USA). The commercial cathodic electrodeposition paint (EDP) system Clearclad® was a kind gift for research purpose from LHV Coatings Ltd., (Birmingham, England). Colloidal chitin was available in Biochemistry-Electrochemistry Research Unit & Center of Excellence in Advanced Functional

Materials, Schools of Chemistry from Prof.Dr.Wipa research unit. All other chemicals were Sigma-Aldrich® products and of analytical grade. Routinely, aqueous solution preparation used ultrapure de-ionized water. Supporting electrolyte for all biosensor tests was 0.1 M phosphate buffer solutions, pH 7.0.

### 3.2.2 Electrochemical instruments

Cyclic voltammetry and amperometry trials with prepared biosensors were carried out with a computer-controlled three-electrode galvanostat/potentiostat type Reference 600® from Gamry Instruments Inc. (Warminster, PA, USA). If not otherwise mentioned, the working electrode for the tests was a CNT/GOx/Chitin/EDP-modified 3-mm-diameter Pt or Au disk electrode while a Pt and Ag/AgCl wire were in service as counter and reference electrode, respectively. For long-term continuous amperometric response tests the developed biosensors were operated in a three-electrode electrochemical flow cell that was under control of the galvanostat/potentiostat EA163 and e-corder ED410, both from eDAQ Pty Ltd. (Denistone East, Australia). Duty of the peristaltic pump Miniplus-3® from Gilson (Middleton, WI, USA) was to deliver glucose-free or glucose-containing 0.1 M phosphate buffer solution, pH 7.0 to the flow cell, which had a home-made CNT/GOX/Chitin/EDP-modified 3-mm-diameter home-made gold disk electrode incorporated as the working electrode. Reference electrode of this system was a home-made Ag/AgCl (3 M KCl) while the tubular stainless steel cell outlet functioned as counter electrode, flow system of electrochemical cell set up was use same as in

CNT/GOx/EDP biosensor modification operation (refer Figure 2.1 and 2.2 in chapter II).

### **3.2.3 Fabrication of glucose biosensors by applying CNT/GOx/Chitin/EDP onto the electrode**

To begin with, a commercial 3-mm-diameter Pt disk electrode (Gamry Instruments Inc., Warminster, PA, USA, Kel-F® body, outer diameter 7 mm) was polished on a soft textile pad that was soaked with alumina slurry of first 5 and then 1  $\mu\text{m}$  particle size. Pt disk polishing was followed by complete removal of the polishing paste via thorough water rinsing and electrode air-drying at room temperature (RT). Then, a 5.0  $\mu\text{L}$  drop of a suspension of 5.0 mg CNT in 1 mL  $\text{H}_2\text{O}$  was dropped onto the cleaned Pt disk and dried min air at RT. Four time's repetition of the CNT drop coating step placed a thin film of the black graphitic nanomaterial on the noble metal surface. Next was the careful placement of a 5.0  $\mu\text{L}$  drop of a 5.0  $\text{mg mL}^{-1}$  solution of GOx in  $\text{H}_2\text{O}$  straight onto just dried CNT deposits and again RT air-drying. Three time's repetition of the GOx drip treatment loaded the pores in the CNT layer on the Pt surface efficiently with the biocatalyst. Next was the careful placement of a 5.0  $\mu\text{L}$  drip of a 10.0  $\text{mg mL}^{-1}$  solution of Colloidal Chitin in  $\text{H}_2\text{O}$  straight onto just dried GOx deposits and again RT air-drying. Two time's repetition of the Colloidal Chitin drip treatment loaded the pores in the CNT and GOx layer on the Pt surface efficiently with the biocatalyst. Final step was the deposition of a protein leak-protecting polymer cover, which was accomplished in a two-electrode electrochemical cell with a Pt wire counter electrode via cathodic EDP at a potential of negative 7 Volt for 2 minutes. Please note

that heat curing of a fresh EDP deposit - as usually done in related industry to induce transformation of fresh paint coats into dry insulating and thus corrosion protecting material - was avoided here not to harm the enzyme and make the paint impermeable for dissolved molecules and ions. Completed biosensors were stirred for 30 minutes in 0.1 M phosphate buffer solution, pH 7.0 and overnight stored at 4°C in the same solution to allow sensor settling. When not used, CNT/GOx/Chitin/EDP glucose biosensors were stored at 4°C in 0.1 M phosphate buffer solution, pH 7.0. Note that for the home-made 3-mm-diameter Au disk electrode the same procedure was applied to reach glucose sensitivity. The steps to go through during the preparation of the Pt disc-modified CNT/GOx/Chitin/EDP are shown in Figure 3.2.

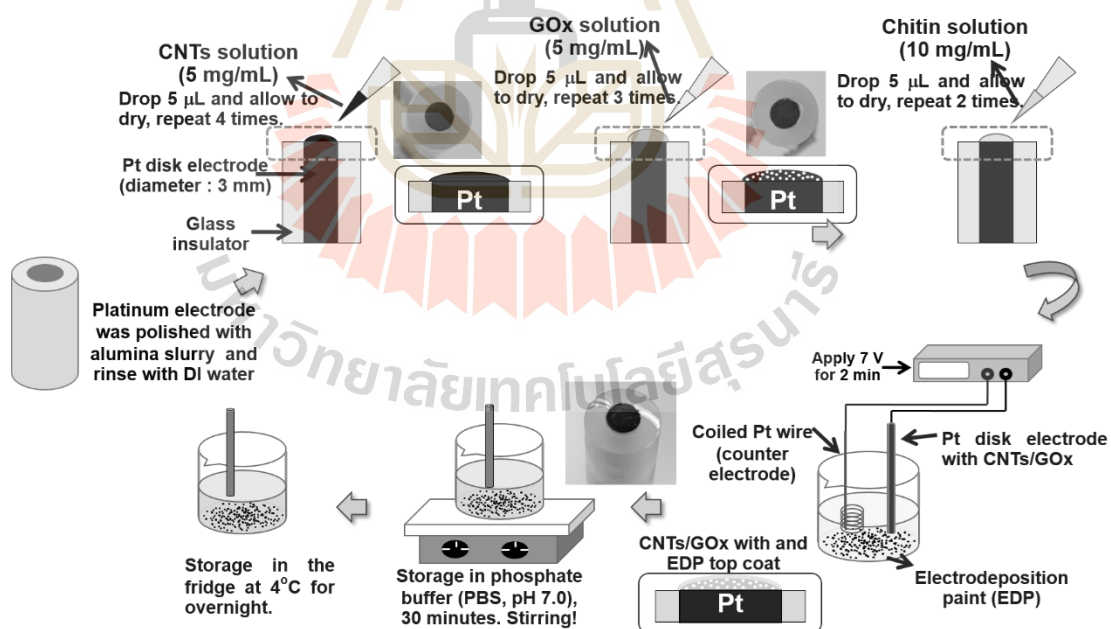


**Figure 3.2** Schematic diagram of the procedure used for the preparation of CNT/GOx/Chitin/EDP modified platinum or gold as used in the biosensor measurement.

### 3.2.4 Fabrication of glucose biosensors using CNT/(Fc+GOx+Chitosan)/EDP on electrode

To begin with, a commercial 3-mm-diameter Pt disk electrode (Gamry Instruments Inc., Warminster, PA, USA, Kel-F® body, outer diameter 7 mm) was polished on a soft textile pad that was soaked with alumina slurry of first 5 and then 1  $\mu\text{m}$  particle size. Pt disk polishing was followed by complete removal of the polishing paste via thorough water rinsing and electrode air-drying at room temperature (RT). Then, a 5.0  $\mu\text{L}$  drop of a suspension of 2.5 mg CNT in 1 mL  $\text{H}_2\text{O}$  was dropped onto the cleaned Pt disk and dried in air at RT. Four time's repetition of the CNT drop coating step placed a thin film of the black graphitic nanomaterial on the noble metal surface. Next was careful placement of a 5.0  $\mu\text{L}$  drop a mixture of Ferrocene azide (3.0  $\text{mg mL}^{-1}$  in  $\text{H}_2\text{O}$  stock), Chitosan (commercial) and GOx (15.0  $\text{mg mL}^{-1}$  in  $\text{H}_2\text{O}$  stock) onto just dried CNT deposits and again RT air-drying. Three time's repetition of the mixture drop treatment loaded the pores in the CNT layer on the Pt surface efficiently with the biocatalyst. Final step was the deposition of a protein leak-protecting polymer cover, which was accomplished in a two-electrode electrochemical cell with a Pt wire counter electrode via cathodic EDP at a potential of negative 7 Volt for 2 minutes. Please note that heat curing of a fresh EDP deposit - as usually done in related industry to induce transformation of fresh paint coats into dry insulating and thus corrosion protecting material - was avoided here not to harm the enzyme and make the paint impermeable for dissolved molecules and ions. Completed biosensors were stirred for 30 minutes in 0.1 M phosphate buffer solution, pH 7.0 and overnight stored at 4°C in the same solution to allow sensor settling. When not used, CNT/(Fc+GOx+Chitosan)/EDP glucose biosensors were stored at 4°C in 0.1 M

phosphate buffer solution, pH 7.0. Note that for the home-made 3-mm-diameter Au disk electrode the same procedure was applied to reach glucose sensitivity. The steps to go through during the preparation of the Pt disc-modified CNT/(Fc+GOx+Chitosan)/EDP are shown in Figure 3.3.

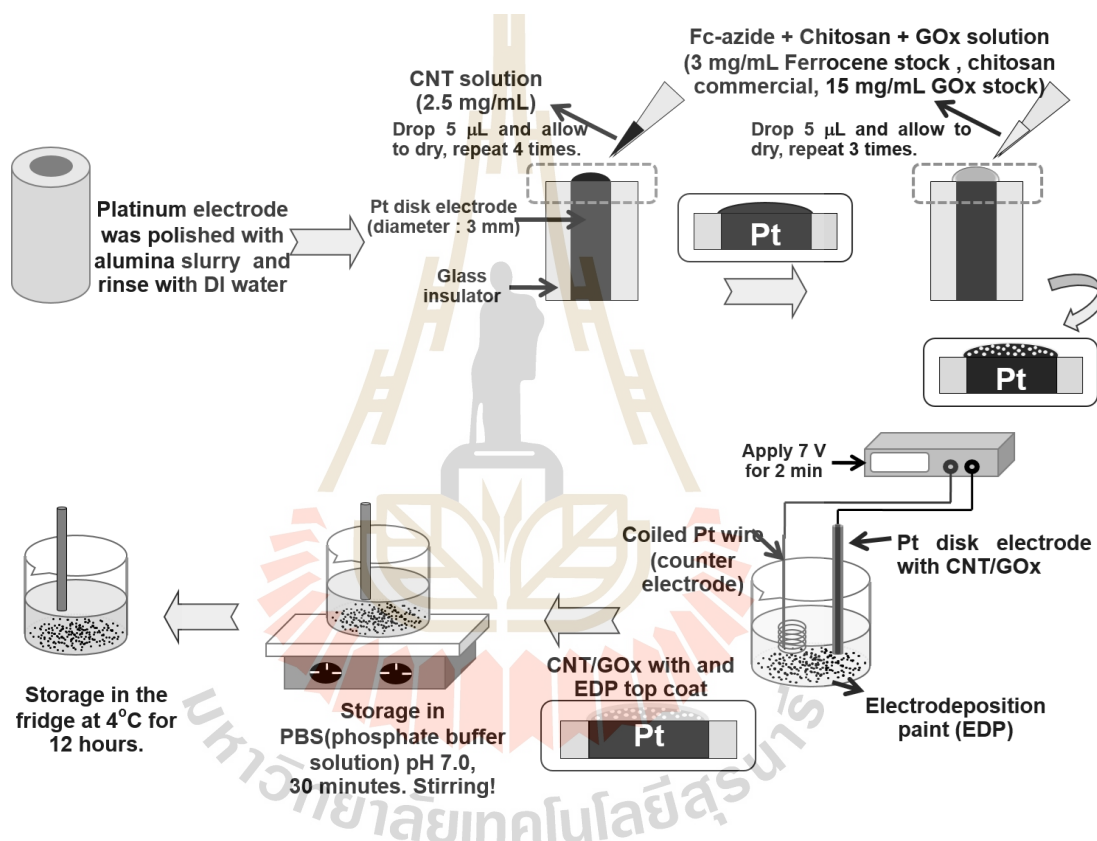


**Figure 3.3** Schematic diagram of the procedure used for the preparation of CNT/(Fc+Chitosan+GOx)/EDP modified platinum as used in the biosensor measurement.

### 3.3 Results and discussion

As mentioned before, carbon nanotubes (CNT) have gained considerable attention in more ten years past due to of their remarkable electronic and

mechanical properties, which have made them extremely attractive for a wide range of sensing applications from structural material to nanoelectronic components (Agüí *et al.*, 2008; Cai and Chen, 2004; Pumera *et al.*, 2007; Schlittler *et al.*, 2001; Wenrong Yang *et al.*, 2007a) especially conductive network components in biosensor.

Many researcher have been considered and studied for immobilizing enzymes, organic or inorganic, natural or synthetic, chitin and chitosan are of interest due to their properties consist of high affinity to proteins, availability of reactive functional groups for direct reactions with enzymes and for chemical modifications, mechanical stability and rigidity, regenerability and provide the system with permeability and surface area suitable for a chosen biotransformation (Krajewska, 2004; Nakorn, 2017; Pillai *et al.*, 2009; Prashanth and Tharanathan, 2007; Rinaudo, 2006). The schematics drawing in Figure 3.4A represents the anodic hydrogen peroxide collection at a normal glucose biosensor with non-conducting polymer coating in use as immobilization matrix: only a few GOx molecules happen to have an orientation of their diffusional move towards the substrate electrode. Figure 3.4B represents the case of a utilization of a conductive CNT/Chitin deposit as immobilization matrix with a platinum disk electrode still acting as the substrate electrode. Now, anodic hydrogen peroxide collection can take place within the immobilization matrix at the conducting CNT network. However, since the possibility of DET between enzyme and CNT filaments has been claimed in a series of publications, DET may contribute to GOx redox recycling on top of recycling through molecular oxygen.

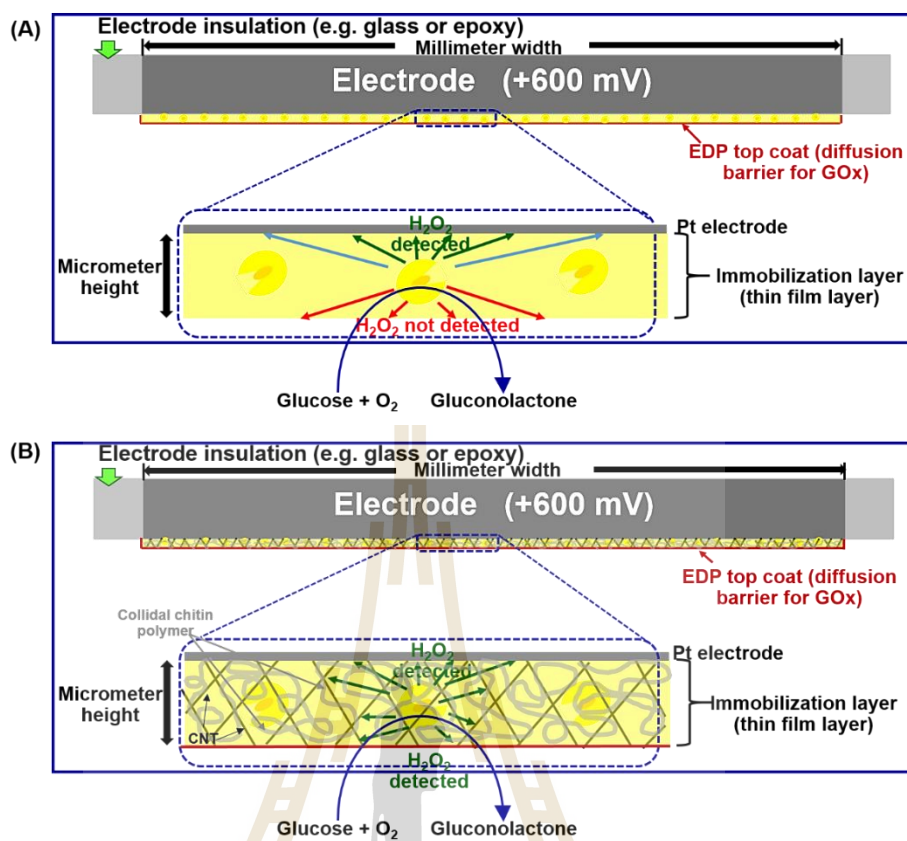


**Figure 3.4** Comparison between the anodic hydrogen peroxide detection at a “normal” glucose biosensor with a non-conducting polymer electrode coating acting as immobilization matrix (A) and the case of a utilization of a conductive CNT/colloidal chitin deposit as immobilization matrix (B). In either case a platinum disk electrode is assumed to be the substrate electrode. Physical contact of the CNT network with the electrode surface and among conductive individual filaments extends the electrode surface into the immobilization matrix facilitating larger collection efficiency for the anodic peroxide detection. Colloidal Chitin in the CNT network may provide extra biocompatibility to entrapped enzyme entities, which may in turn help extend sensor life time. Very close physical contact of GOx molecules to CNT surfaces may additionally facilitate the manifestation of direct electron transfer as extra pathway for GOx redox recycling, at least if CNT contact is in appropriate molecular orientation.

CNT is the the main component of the biosensor of this study and chitin or chitosan (commercially available as product of partial deacetylation of chitin, the most abundant polysaccharide after cellulose in the world (Yilmaz *et al.*, 2012) was a first functional additive of the basic design. Considered as another modification option was the addition of a ferrocene derivative (Fc) to a CNT/e.g. chitosan. Ferrocene (Fc) and its derivatives have attractive properties such as rapid responses to many electroactive substances and fast electron transfer that make them the most widely used class of mediators in the development of chemically modified electrodes (Cass *et al.*, 1984; Chaubey and Malhotra, 2002; Pandey *et al.*, 2003; Raof *et al.*, 2009; Zhilei *et al.*, 2010). When ferrocene is incorporated into the CNT/chitin-chitosan immobilization matrix molecular oxygen and/or DET GOx recycling is expected to become accompanied or, depending on the efficiencies, even fully replaced by redox interaction between reduced GOx and oxidized ferrocene entities and the requisite reprocessing of GOx in oxidized state, as needed for the oxidation of substrate glucose (refer to Figure 3.5).

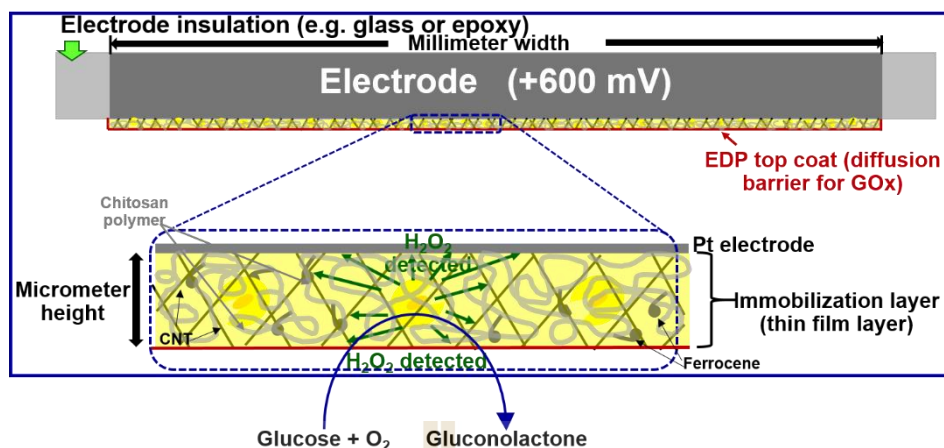


**Figure 3.5** Schematic drawing of biosensor configuration modified by CNT in the case of an utilization of a conductive carbon nanotubes, chitosan polymer and Ferrocene deposit as immobilization matrix. A platinum disk electrode is assumed to be the substrate electrode. Physical contact of the CNT network with the electrode surface and among conductive individual filaments extends the electrode surface into the immobilization matrix facilitating larger collection efficiency for the anodic peroxide detection. Chitosan polymer network which consist of in porous of conductive CNT assisting to support enzyme to stay extended in the immobilization matrix. Ferrocene derivative help to support electron transfer.

### 3.3.1 Amperometric determination of glucose at CNT/GOx/Chitin/EDP-based glucose biosensor

#### 3.3.1.1 Sensor variant based on modified platinum (Pt) electrodes

Chronoamperometric measurement for characterization of the glucose biosensors by CNT/GOx/Chitin/EDP immobilization biosensor, the design offered in calibration trials reproducibly a marked glucose receptiveness with

reasonably fast response time, adequate sensitivity and a linear range that stretched broadly over tenths of mM analyte concentrations. Figure 3.6 represent the outcome of original trace amperometric calibration measurements that have been obtained in course of trials with the CNT/GOx/Chitin/EDP-based glucose biosensors. The experiments were carried out in an aqueous 0.1 M phosphate buffer solution (pH 7.0) with a conventional three-electrode cell. A magnetic stirrer provided the convective transport during the measurements. Figure 3.6A shows whole trace of a typical current-time curve response for successive adding 1.0 M glucose stock solution into 5 mL phosphate buffer solution (pH7.0) at applied constant potential +600 mV *versus* Ag/AgCl start from low to high glucose concentration. A display as proof of the good performance a typical example of an amperometric recording that was acquired with a prototype of a CNT/GOx/Chitin/EDP-modified 3-mm-diameter Pt disk electrode in course of successive additions of small aliquots of a glucose stock solution. Evident in the trace is a series of well-defined step-like rises in the continuously acquired anodic H<sub>2</sub>O<sub>2</sub> current, with an about 13.9 second interval needed to reach 90 % of the finally established steady-state signal value (Figure 3.6B plus inset). Figure 3.6C shown amperometric response of an enzyme biosensor to successive additions of various substrate concentrations, which displayed Michaelis-Menten type behavior was constructed by the analysis of the amperometric recording from Figure 3.6A, Exposed for this particular case is a plateau current,  $i_{\max}$ , of 22.1  $\mu\text{A}$ , response linearity up to 30.0 mM glucose ( $r^2 = 0.995$ ) and a sensitivity of 0.45  $\mu\text{A mM}^{-1}$  (6.34  $\mu\text{A mM}^{-1} \text{cm}^{-2}$ , normalized to the geometric surface area of the Pt disk transducer). For a compilation of 10 identically prepared biosensors  $18.5 \pm 7.7 \mu\text{A}$ ,  $30.4 \pm 12.0 \text{ mM}$  and

$4.0 \pm 18.3 \mu\text{A mM}^{-1} \text{cm}^{-2}$  were the average and standard deviation values for  $i_{\text{max}}$ , linear range width and sensitivity, respectively.

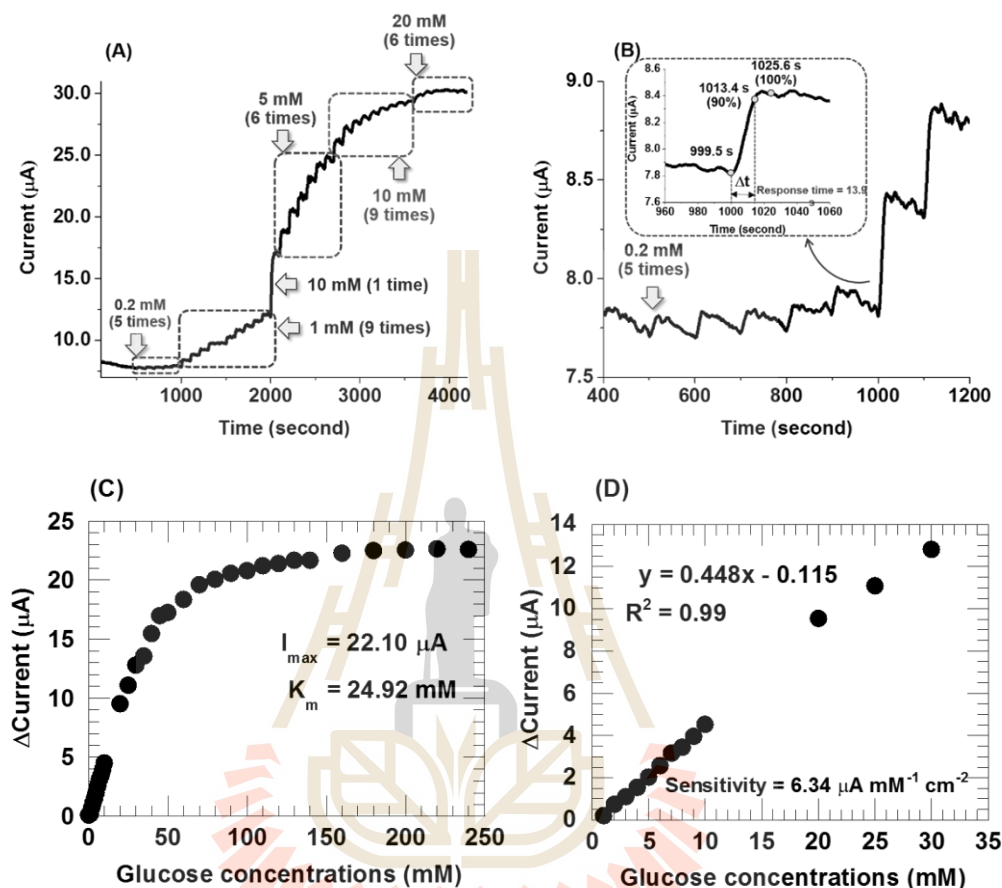


**Figure 3.6** (A) Representative current-time trace as acquired in the course of a calibration trial with a (CNT/GOx/Chitin)/EDP-Pt glucose biosensor; aliquots of a glucose stock solution were added to stirred 0.1 M phosphate buffer solution (pH 7.0); The recording was made at ambient temperature of 25°C with a H<sub>2</sub>O<sub>2</sub> detection potential of +0.6 V vs. Ag/AgCl. (B) Zoom into the initial section of the current trace in (A) and, as inset, the example of response time estimation for the step included in the zoom. (C) Electrochemical assessed biosensor calibration curve as constructed by the analysis of the amperometric recording in A and (D) Widely dynamic linear range response at CNT/GOx/Chitin/EDP biosensor with regression coefficient of 0.99.

### 3.3.1.2 Sensor variant based on modified gold (Au) electrodes

Later described stability testing for CNT/GOx/Chitin/EDP biosensors had to be carried out with gold disk electrodes as these were available in a geometry and size suitable for incorporation into an electrochemical flow cell designed for continuous long-term measurements. Figure 3.7A and B represents the amperometric response of a prototype of a CNT/GOx/Chitin/EDP-modified 3-mm-diameter Au disk electrode to successive additions of small aliquots of a glucose stock solution. A look at the calibration curve for this variant of the novel biosensors (refer to 3.7C and D) confirmed that the CNT/GOx/Chitin-modified Au disc electrode also had a wide linear range and a reasonable sensitivity. Exposed for this particular case is a plateau current,  $i_{\max}$ , of 11.3  $\mu\text{A}$ , response linearity up to 35.0 mM glucose ( $r^2 = 0.996$ ) and a sensitivity of 0.16  $\mu\text{A mM}^{-1}$  (2.26  $\mu\text{A mM}^{-1} \text{cm}^{-2}$ , normalized to the geometric surface area of the Au disk transducer). For a compilation of 3 identically prepared biosensors  $12.9 \pm 1.8 \mu\text{A}$ ,  $36.7 \pm 2.9 \text{mM}$  and  $3.2 \pm 1.1 \mu\text{A mM}^{-1} \text{cm}^{-2}$  were the average and standard deviation values for  $i_{\max}$ , linear range width and sensitivity, respectively.

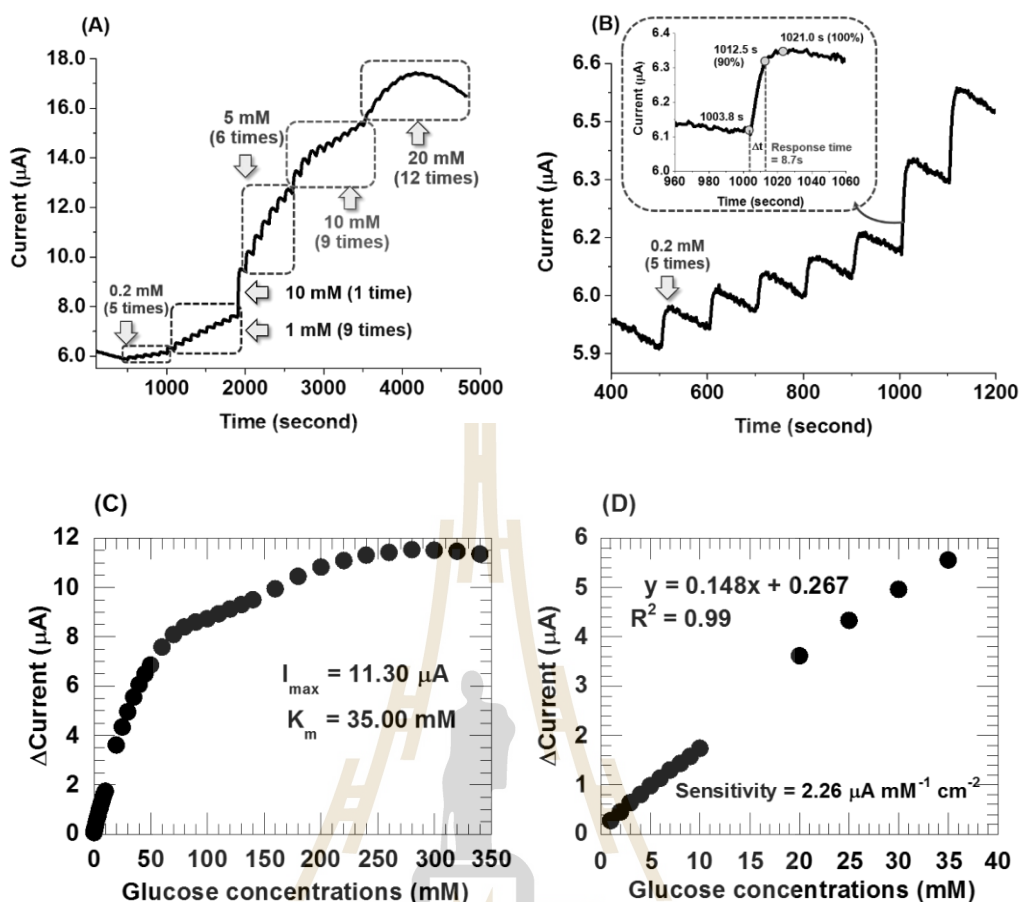


**Figure 3.7** (A) Representative current-time trace as acquired in the course of a calibration trial with a (CNT/GOx/Chitin)/EDP-Pt glucose biosensor; aliquots of a glucose stock solution were added to stirred 0.1 M phosphate buffer solution (pH 7.0); The recording was made at ambient temperature of 25°C with a  $\text{H}_2\text{O}_2$  detection potential of +0.6 V vs. Ag/AgCl. (B) Zoom into the initial section of the current trace in (A) and, as inset, the example of response time estimation for the step included in the zoom. (C) Electrochemical assessed biosensor calibration curve as constructed by the analysis of the amperometric recording in A and (D) Widely dynamic linear range response at CNT/GOx/Chitin/EDP biosensor with regression coefficient of 0.99.

Figure 3.8 represent the graphical illustration of a performance comparison calibration curves at different electrode substrate between platinum (Pt) and gold (Au). A plot displayed Michaelis-Menten type behavior was constructed by the analysis of the amperometric recording. The maximum current ( $i_{max}$ ) and sensitivity are evaluated to be 22.10  $\mu\text{A}$  and 6.34  $\mu\text{A mM}^{-1} \text{cm}^{-2}$  at Pt disk electrode, 11.30  $\mu\text{A}$  and 2.26  $\mu\text{A mM}^{-1} \text{cm}^{-2}$  at Au disk electrode for CNT/GOx/Chitin/EDP immobilized. While both of them show comparable value at the dynamic linear range response.

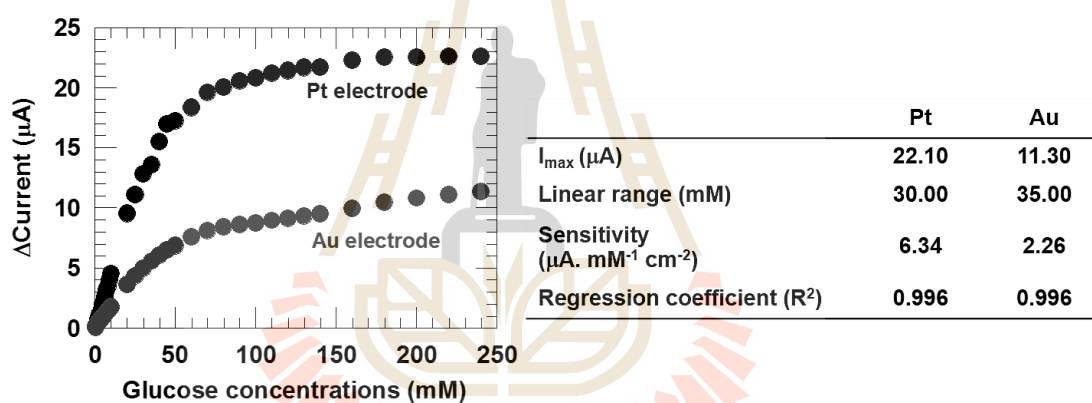


**Figure 3.8** Performance comparison for electrochemical assessed biosensor calibration curves as constructed by the analysis of the amperometric recording at different electrode substrate between platinum (Pt) and gold (Au).

A summary of the analytical figures of merit for both CNT/GOx/EDP/Chitin-modified Pt and Au disk electrodes is available in following Table 3.1.

**Table 3.1** Summary performance of CNT/GOx/Chitin/EDP biosensor.

Characteristics	Platinum electrode										
	#1	#2	#3	#4	#5	#6	#7	#8	#9	#10	Average
<b><math>I_{\max}</math> (<math>\mu\text{A}</math>)</b>	14.92	22.51	11.84	20.15	29.24	24.28	12.13	7.35	13.71	29.17	18.5±7.6
<b><math>K_m^{app}</math> (mM)</b>	33.00	25.00	25.00	35.00	37.00	90.00	20.00	30.00	27.00	77.00	-
<b>Linear range (mM)</b>	24	30	10	40	35	40	10	40	40	35	30.4±12.0
<b>Regression coefficient (<math>R^2</math>)</b>	0.996	0.995	0.994	0.996	0.996	0.998	0.997	0.995	0.996	0.996	-
<b>Sensitivity (<math>\mu\text{A mM}^{-1} \text{cm}^{-2}</math>)</b>	3.86	6.34	4.58	3.97	5.88	1.74	4.77	1.41	3.54	3.40	4.0±18.3



**Table 3.1** Summary performance of CNT/GOx/Chitin/EDP biosensor (Continuous).

Characteristics	Gold electrode			
	#1	#2	#3	Average
$I_{\max}$ ( $\mu\text{A}$ )	11.30	12.59	14.88	12.9 $\pm$ 1.8
$K_m^{app}$ (mM)	35.00	19.34	36.28	-
Linear range (mM)	35	40	35	36.7 $\pm$ 2.9
Regression coefficient ( $R^2$ )	0.996	0.996	0.996	-
Sensitivity ( $\mu\text{A mM}^{-1} \text{cm}^{-2}$ )	2.26	4.41	3.01	3.2 $\pm$ 1.1

### 3.3.2 The assessment of the detection limit for glucose quantification with CNT/GOx/Chitin/EDP-based glucose biosensors

An important analytical feature of amperometric biosensors is its practical detection limit, which for the biosensors of this study shall be defined as the smallest glucose concentration change that is related to a measurable (“visible”) raise in current above baseline signal valid for glucose-free electrolyte. To determine the practical detection limit glucose was added to the measuring solution at smaller and smaller increments and the smallest increment that still was able to create a visible step in the current trace was judged on as “LOD”. Actually, small aliquots of a 1.0 M glucose stock solution were added into 5 mL in the measuring buffer, a 0.1 M phosphate buffer solution (pH 7.0) while the biosensors hydrogen peroxide oxidation current was recorded at constant working potential + 600 mV. Tested triplicate glucose additions raised the solution level by either 200, 100, 50, 25, 12.5 and 200  $\mu\text{M}$ , respectively. Figure 3.9 shows a typical amperometric recording of such a trial in search for the practical LOD. Triplicate identical changes in glucose buffer levels caused as desired current elevations of identical height, which confirmed the reproducibility of the biosensor response to analyte variations. For the platinum-based CNT-GOx-EDP glucose biosensors 50.0  $\mu\text{M}$  concentration changes were the lowest that could be clearly resolved in the amperometric recordings and 50  $\mu\text{M}$  is thus referred to as practical LOD.

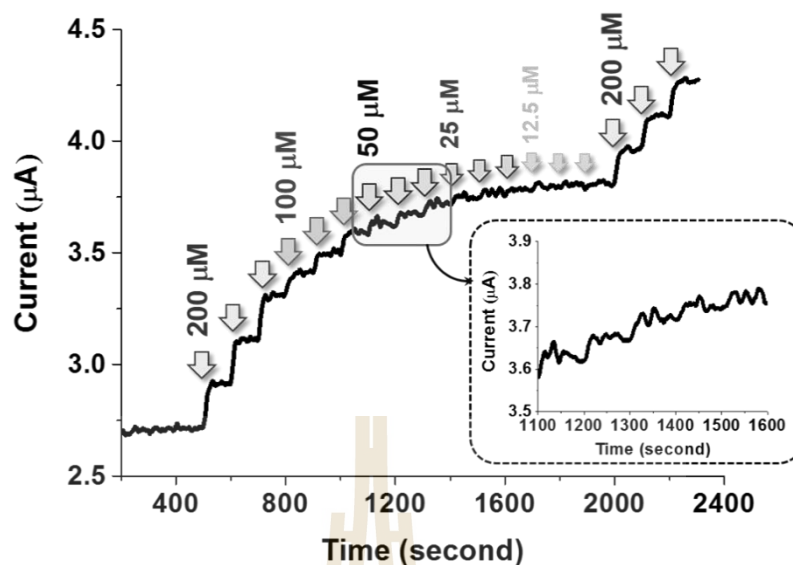


**Figure 3.9** Detection limits assessment for glucose quantification with biosensor. Glucose was added to the measuring solution at smaller and smaller increments and the smallest increment determined that still was able to create a visible step in the current trace, glucose concentration solution: 200, 100, 50, 25, 12.5 and 200  $\mu\text{M}$ , respectively.

### 3.3.3 Direct electron transfer of glucose oxidase enzyme (GOx)

#### 3.3.3.1 Test for biosensor with the 'CNT/GOx/EDP' design

As already mention in section 1.2.5 the redox center in biomolecules is usually embedded deeply into the large three dimensional structures of enzyme molecules; it is difficult to achieve protein DET from the active sites to the electrode surface. Controlling the interactions of enzymes with the substrate to optimize the electron transfer processes remains a challenge. Variety of methods and electrodes materials have been studied to immobilize enzymes and promote electron transfer of redox enzymes on the surface of electrodes (Cai *et al.*, 2004; Frew and Hill, 1988; Kang

*et al.*, 2009; Palanisamy *et al.*, 2012; Velmurugan *et al.*, 2015; Y. Wang and Yao, 2012; Zhao *et al.*, 2006).

In this part the direct electron transfer (DET) of glucose oxidase enzyme (GOx) was evaluated at the platinum electrode modified, the experiment was examined by cyclic voltammetry to studies the mechanical properties of protein electron transfer between active redox centers and the electrode surface. Figure 3.10 shows cyclic voltammogram of the CNT-modified and CNT/GOx-modified (Figure 3.10(a) and (b)) onto platinum electrode in 0.1 M phosphate buffer solution (pH 7.0), the scan started at - 0.8 V vs Ag/AgCl, moved into the positive direction to +0.3 V and went back to starting point with the scan rate at 10 mV s<sup>-1</sup>. Curve (a) found no any observable voltammetric response are obtained while curve (b) shown the cyclic voltammogram of CNT/GOx modified platinum electrode in the same buffer solution and the same scan rate at that for curve (a), the results show a pair of well-defined and nearly symmetric redox peaks are observed. These results suggest that the redox peaks in curve b can be ascribed to the redox reaction of the prosthetic group (FAD) bound to the GOx and not to free FAD, which may have dissociated away from GOx due to conformational changes during immobilized, adsorbed on the surface of CNT (Cai *et al.*, 2004).

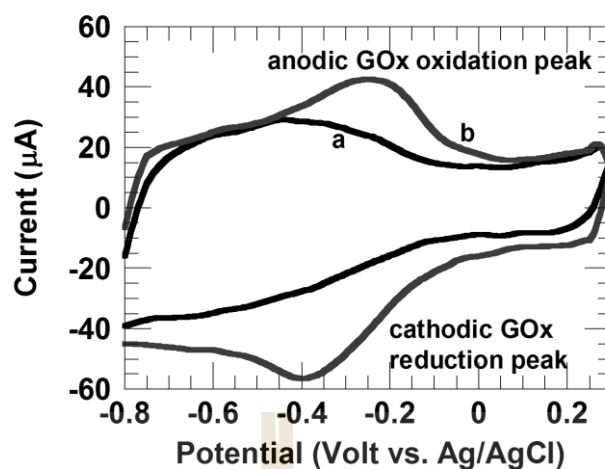


**Figure 3.10** Cyclic voltammograms of CNT (a) and CNT/GOx (b) modified platinum electrode in 0.1 M phosphate buffer solution (pH 7.0) with de-aerated solution at the scan rate  $10 \text{ mV}\cdot\text{s}^{-1}$ , and the scan potential in the range of  $-0.8 \text{ V}$  to  $+0.3 \text{ V}$ .

Figure 3.11A illustrates the cyclic voltammograms obtained to the effect of scan rates at CNT/GOx modified platinum electrode in de-aerated solution, the experiment was performed in phosphate buffer solutions (pH7.0) at different scan rates. The scan started at  $+0.5 \text{ V}$  vs Ag/AgCl, moved into the negative direction to  $-0.8 \text{ V}$  and went back to starting point. A pair of well-defined and nearly symmetric redox peaks are observed with a formal potential of  $-0.14 \text{ V}$  (vs. Ag/AgCl). Both the anodic and cathodic peak currents were increased linearly proportional to the scan rate in the range from  $2$  to  $50 \text{ mV s}^{-1}$ , the results suggesting that the reaction is not a diffusion-controlled process but a surface-controlled electrode reaction as expected for immobilized systems which show in Figure 3.11B. The results confirm that the redox couple was due to the oxidation and reduction of the bound prosthetic group  $FAD/FADH_2$  of the glucose oxidase enzyme ( $GOx$ ), and can be ascribed to the DET

of  $GOx$  (mediating reaction) which shown in following as in equation 3.1 (Y. Wang and Yao, 2012).



The heterogeneous electron transfer rate constant ( $k_s$ ) for  $GOx$  immobilized at CNT modified electrode is calculated by Laviron equation (Laviron E., 1979). Two straight lines were obtained from the slope of anodic potential (equation 3.2) and cathodic potential (equation 3.3) vs. logarithm of scan rate which shown in Figure 3.11C and Figure 3.11D. The electron transfer coefficient ( $\alpha$ ) value calculated to be 0.0002 by using Laviron theory, which is measured by the slope of the two straight line in Figure 3.11D following as;

$$\text{Anodic:} \quad \frac{2.303RT}{(1-\alpha)nF} \quad (3.2)$$

$$\text{Cathodic:} \quad \frac{-2.303RT}{\alpha nF} \quad (3.3)$$

According to the equation 3.4, the  $k_s$  value of  $GOx$  immobilized CNT modified electrode was estimated to be  $60.3 \text{ s}^{-1}$  (at scan rate  $50 \text{ mV.s}^{-1}$ ).

$$\log k_s = \alpha \log(1-\alpha) + (1-\alpha) \log \alpha - \log \frac{RT}{nFv} - \frac{\alpha(1-\alpha)nF\Delta E_p}{2.303RT} \quad (3.4)$$

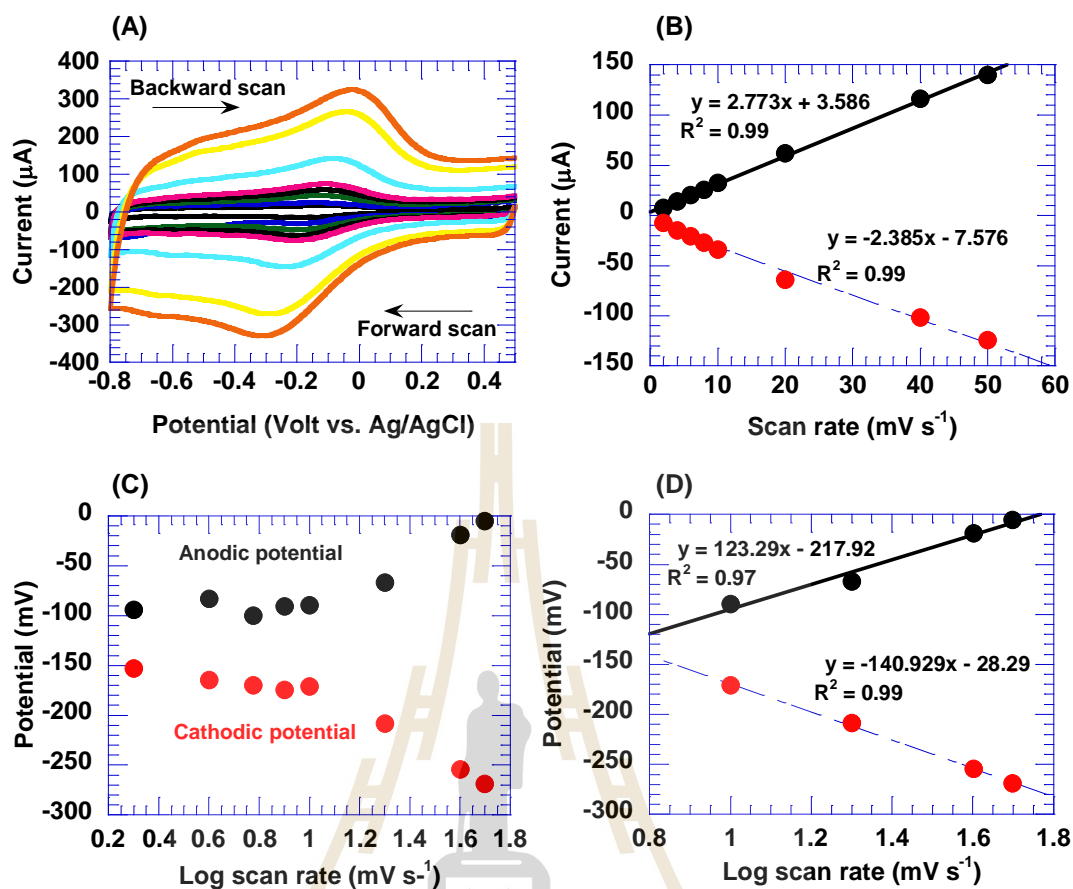


**Figure 3.11** Cyclic voltammograms of CNT/GOx modified platinum electrode in 0.1 M phosphate buffer solution (pH 7.0) with de-aerated solution at various scan rates. The scan rate are from inner to outer curves: 2, 4, 6, 8, 10, 20, 40 and 50  $\text{mV s}^{-1}$  (A). The analysis plots of anodic and cathodic peaks as a function of scan rates (B). The analysis plots of anodic and cathodic potential as a function of logarithm scan rates (C), linearity region of anodic and cathodic potential at high scan rate (D).

### 3.3.3.2 Test for biosensor with the ‘CNT/GOx/chitin/EDP’ design

Figure 3.12 shows cyclic voltammogram of the CNT-modified and CNT/GOx/Chitin/modified (Figure 3.12(a) and (b)) onto platinum electrode in 0.1 M phosphate buffer solution (pH 7.0), the scan started at -0.8 V vs Ag/AgCl, moved

into the positive direction to + 0.5 V and went back to starting point with the scan rate at  $10 \text{ mV s}^{-1}$ . Curve (a) found no any observable voltammetric response are obtained while curve (b) shown the cyclic voltammogram of CNT/GOx/Chitin modified platinum electrode in the same buffer solution and the same scan rate at that for curve (a), the results show a pair of well-defined and nearly symmetric redox peaks are observed.

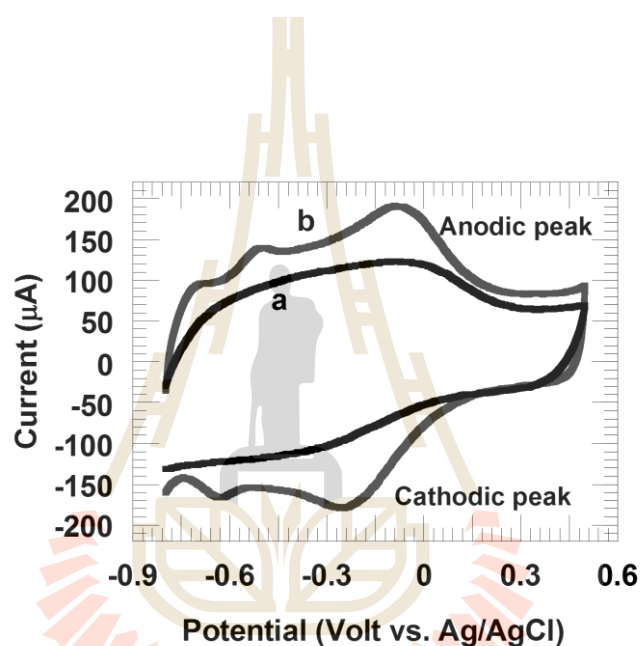


**Figure 3.12** Cyclic voltammograms of CNT (a) and CNT/GOx/Chitin (b) modified platinum electrodes. Readings were taken in 0.1 M phosphate buffer solution (pH 7.0) with de-aerated solution at scan rate  $10 \text{ mV}\cdot\text{s}^{-1}$ , the scan potential in the range of -0.8 V to +0.5 V.

Figure 3.13A illustrates the cyclic voltammograms obtained to the effect of scan rates at CNT/GOx/Chitin modified platinum electrode in de-aerated solution, the experiment was performed in phosphate buffer solutions (pH7.0) at

different scan rates. The scan started at - 0.8 V vs Ag/AgCl, moved into the positive direction to + 0.5 V and went back to starting point. A pair of well-defined and nearly symmetric redox peaks are observed with a formal potential of - 0.16 V (vs. Ag/AgCl). Both the anodic and cathodic peak currents were increased linearly proportional to the scan rate in the range from 2 to 80 mV s<sup>-1</sup>, the results suggesting that the reaction is not a diffusion-controlled process but a surface-controlled electrode reaction as expected for immobilized systems which show in Figure 3.13B.

The heterogeneous electron transfer rate constant ( $k_s$ ) for *GOx* immobilized at CNT modified electrode is calculated by Laviron equation (Laviron, 1979). Two straight lines were obtained from the slope of anodic potential and cathodic potential vs. logarithm of scan rate which shown in Figure 3.13C and Figure 3.13D. The electron transfer coefficient ( $\alpha$ ) value calculated to be 0.0003 by using Laviron theory.

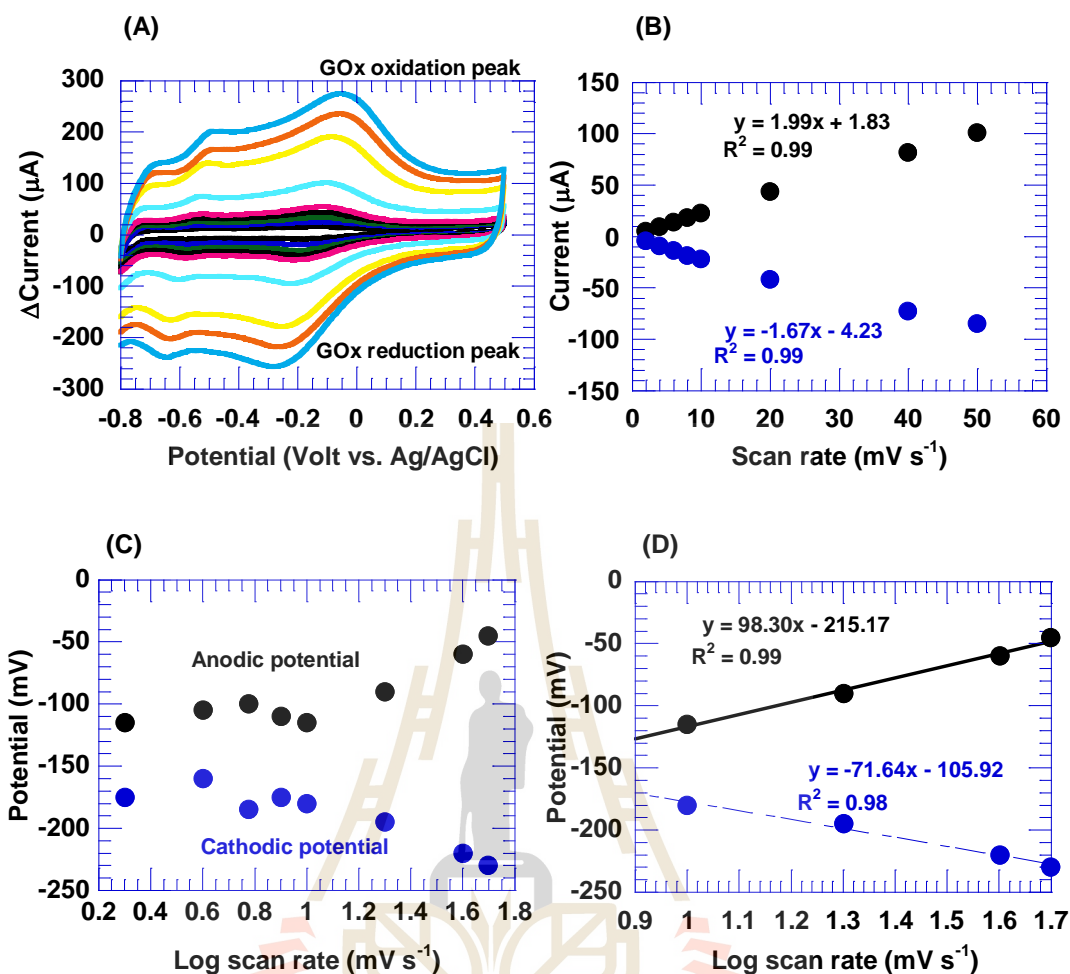


**Figure 3.13** Cyclic voltammograms of CNT/GOx/Chitin modified platinum electrode in 0.1 M phosphate buffer solution (pH 7.0) with de-aerated solution at various scan rates (from inner to outer curves: 2, 4, 6, 8, 10, 20, 40 and 50  $\text{mV s}^{-1}$ ) (A). The analysis plots of anodic and cathodic peaks as a function of scan rates (B). The analysis plots of anodic and cathodic potential as a function of logarithm scan rates (C), linearity region of anodic and cathodic potential at high scan rate (D).

### 3.3.4 Effect of electrochemically induced polymer precipitation

Aqueous suspensions of anodic paints or cathodic paints are commercially available and widely used for corrosion protection in the car and can

industry. First use for biosensor construction was reported for anodic paints (Kurzawa *et al.*, 2002) and the entrapment of GOx into the thin film polymer electrodeposits lead to functional glucose detectors. A clear asset of electrodeposition paints (EDP) is that their deposition is electrochemically induced and thus non-manual. This simplifies the procedure and makes it a user-friendly strategy for polymer placement on sensor surfaces. Here the function of EDP was not to immobilize GOx onto the noble metal disk electrodes (this was the prominent role of the nanoporous CNT modification) but to work as a barrier against diffusional loss of enzyme that was soaked into the prime CNT deposit. Figure 3.14 illustrates the electrochemical cell arrangement for the glazing of CNT/GOx/Chitin layers on Pt or Au disk electrodes, and as here the cathodic EDP version was used, the modified electrode to be further coated with a thin polymer top layer as protection for diffusional GOx loss had to be connected to the negative terminal of the laboratory power supply.

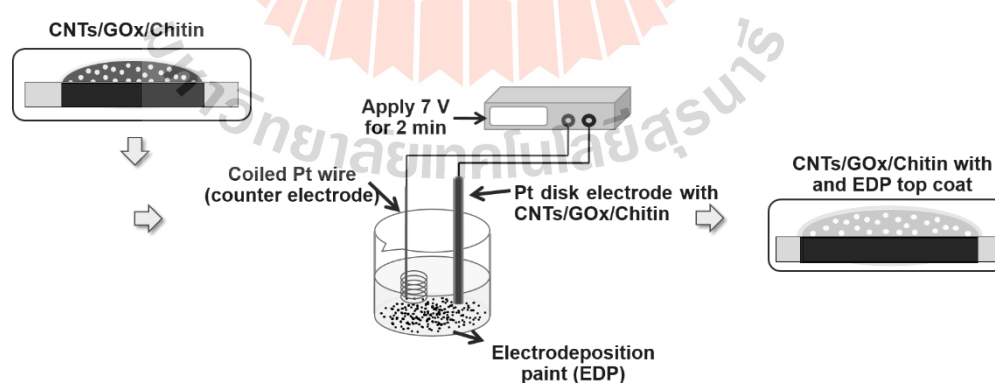


**Figure 3.14** Illustration of the partial series of steps used in fabrication of glucose biosensor with CNT/GOx/Chitin/EDP on platinum or gold electrodes.

Figure 3.15A shows a typical current-time curve response for successive adding glucose into 5 mL of phosphate buffer solution (pH7.0) at constant potential +600 mV at biosensor CNT/GOx/Chitin modified Pt electrode. At first concentration, 0.1 mM (final concentration) of glucose were added into the bulk solutions until 10 steps after that 1 mM (final concentration) were added 9 steps. The original trace show the current rapidly 6 steps at 0.1 mM and then slightly increase until 3 mM, for 4-10 mM the results show saturated of the current response. From the experiment indicated that all enzyme molecules at electrode surface already done at high turnover rate. The calibration curve in Figure 3.15B was constructed by the analysis of the amperometric recording from Figure 3.15A, which represent the experiment was performed at day one after electrode preparation. A linear relationship with a good regression coefficient of 0.99 was observed between current response and glucose concentrations span up to 0.6 mM, results show the apparent Michaelis-Menten constant ( $K_m^{app}$ ) is evaluated to be 0.53 mM with maximum current ( $I_{max}$ ) 4.03  $\mu$ A with a high sensitivity is 49.76  $\mu$ A. $\cdot$ mM<sup>-1</sup>.cm<sup>-2</sup> was obtained.

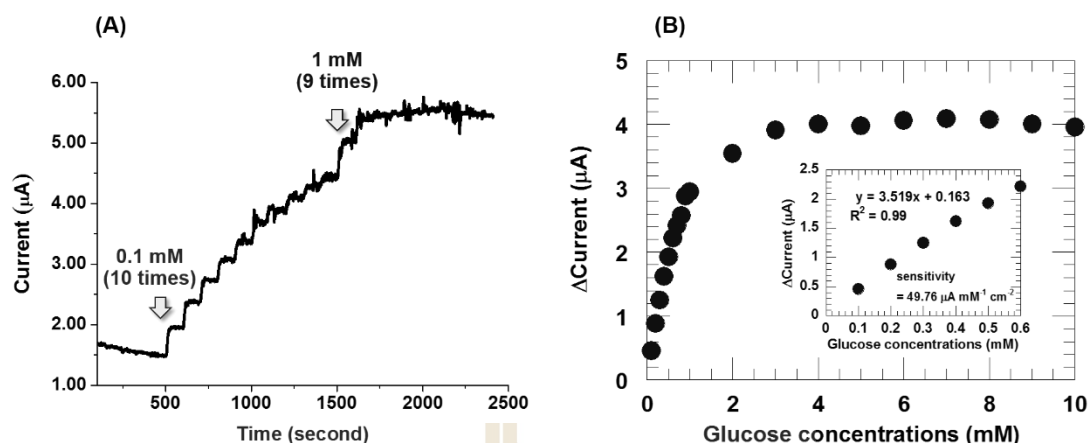


**Figure 3.15** Amperometric response of enzyme biosensor at CNT/GOx/Chitin-modified platinum electrode. (A) Typical amperometric response of an enzyme biosensor to successive additions of substrate at various glucose concentrations. (B) Electrochemical assessed biosensor calibration curve as constructed by the analysis of the amperometric recording in A with a good linearity which show in the inset.

The comparison of calibration curves in Figure 3.16 were constructed by the analysis of the amperometric recording (a) at CNT/GOx/Chitin/EDP biosensor and (b) at CNT/GOx/Chitin biosensor at day one (after electrode was prepared and stored in the fridge). The anodic current of CNT/GOx/Chitin/EDP biosensor should be from all of enzyme molecules which entrapped onto the electrode substrate do their work, while the anodic current of CNT/GOx/Chitin biosensor may come from all of enzyme molecules which can stay onto electrode surface after the sensor was kept in the fridge overnight do their work also. The schematic of both CNT/GOx/Chitin/EDP and CNT/GOx/Chitin which shown in the right hand side in Figure 3.16 should be help to clear idea how enzyme molecule can be stay onto the electrode surface by electrodeposition paints. The results show good agreement about our hypothesis that is

electrodeposition paints can be help to protect enzyme molecules on to the electrode surface due to the characteristics data from CNT/GOx/Chitin/EDP sensor show higher than CNT/GOx/Chitin sensor such as high maximum current ( $i_{max}$ , 22.10  $\mu\text{A}$ ) and widely linear range (30 mM) but CNT/GOx/Chitin sensor got higher sensitivity than CNT/GOx/Chitin/EDP sensor ( $49.76 \mu\text{A}\cdot\text{mM}^{-1} \text{cm}^{-2}$ ). The results indicated that biosensor with electrodeposition paint can help to keep all enzyme molecules onto electrode surface longer than biosensor which contained only chitin polymer, while biosensor which contained only chitin polymer can help to keep enzyme molecules which can stay into the pore of carbon nanotubes to do their work as fast as possible.

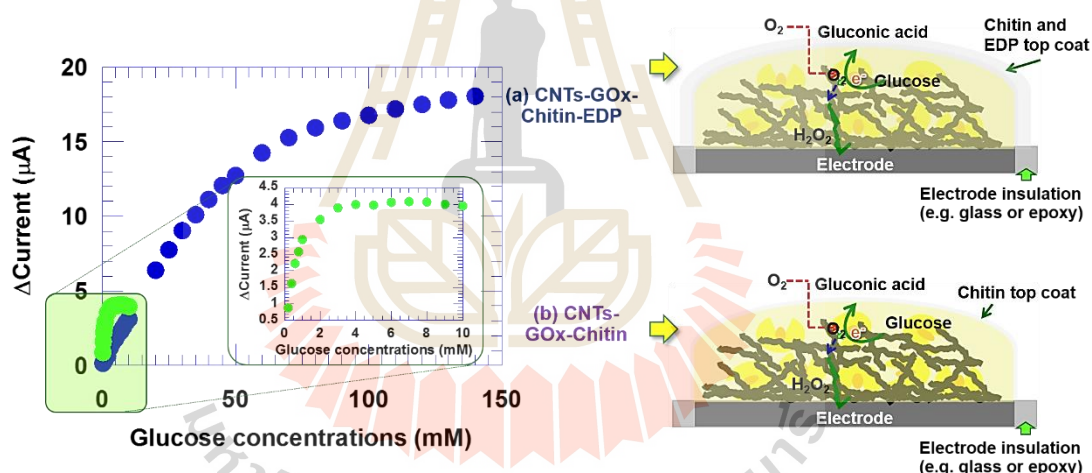


**Figure 3.16** Electrochemically assessed biosensor calibration curve as constructed by the analysis of the amperometric recording in (a) CNT/GOx/Chitin/EDP biosensor and (b) CNT/GOx/Chitin biosensor.

Glucose quantification by calibration curves at the day after electrode was prepared and kept in the fridge overnight recommend to call day one, when the electrode was kept overnight and did the calibration curve again recommend to call day

two and onward. Therefore, the performance comparison between EDP version and free EDP at different day would like to introduce the advantage why our work should have cathodic electrodeposition paints onto sensors. Figure 3.17A represent the electrochemical assessed biosensor calibration curve for CNT/GOx/Chitin modified platinum electrode, they were constructed by the analysis of the amperometric recording (data was not shown). The maximum current was lose around 22.08% from day one when electrode was not use by storage biosensors in the fridge. While the maximum current of CNT/GOx/Chitin/EDP was lose around 8.31% by storage biosensors overnight in the fridge which shows in Figure 3.17B. The results indicated that cathodic electrodeposition paints can be help to entrapped enzyme onto biosensor electrode surface, enzyme can be alive and show a good response with substrate over a week.

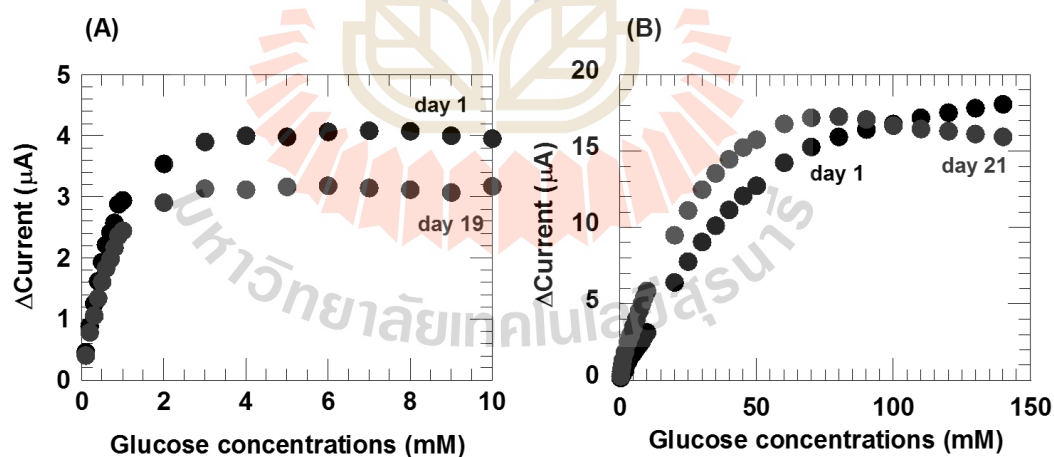


**Figure 3.17** Electrochemical assessed biosensor calibration curve as constructed by the analysis of the amperometric recording. (A) Performance of CNT/GOx/Chitin modified platinum electrode at different day. (B) Performance of CNT/GOx/Chitin/EDP modified platinum electrode at different day. Please note the difference in the scaling of the x and y axes in (A) and (B).

### 3.3.5 Reproducibility and long-term stability tests with CNT/GOx/Chitin/EDP glucose biosensors

Apart from their capability to measure their target analyte accurately also desired for sensors in general and enzyme biosensors in particular is the offer of a good reproducibility and life time. The tests regarding the quality of the sensor life time involved a look at calibration data for measurements carried out at day 1, 7, 21, 35 and 49 after preparation, with refrigerator storage in phosphate buffer solution (pH 7.0) applied in the resting period between measurements. The results show a plot relationship of the current as a function of time or typical of Michaelis-Menten plot. For clear idea how can studies the reproducibility and long-term stability via glucose quantification, Figure 3.18 show the results typical current-time response for successive adding glucose into 5 mL of phosphate buffer solution (pH7.0) with constant potential +600 mV at biosensor CNT/GOx/Chitin/EDP modified platinum electrode. The results show the maximum current at different day slightly decrease from day 1 to day 49, the sensor still response at day 49 around 41.1 % of the initial response with sensitivity of sensor show comparable for different day at the same linear range, which is 40 mM of glucose concentrations with good regression coefficient 0.99.

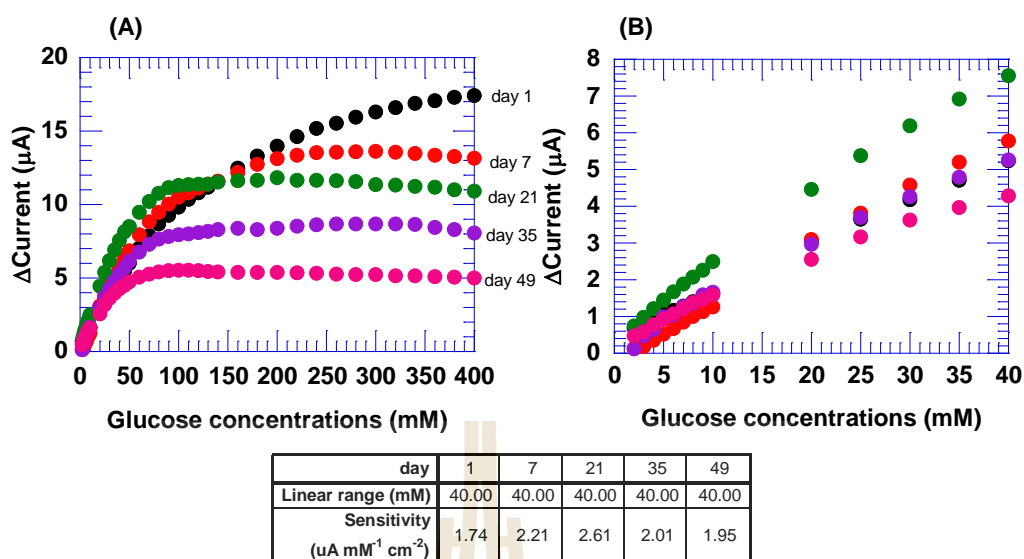


**Figure 3.18** Electrochemical assessed biosensor calibration curve as constructed by the analysis of the amperometric recording. Each calibration curve was produced on a different day for quantification of glucose.

In addition this communication would like to introduced glucose quantification which performed by continuous detection. Continuous measurement for the reproducibility and long-term stability test was performed in flow system recording the current response with glucose by operated in a three-electrode electrochemical flow cell that was under control of the galvanostat/potentiostat EA163 and e-corder ED410, both from eDAQ. The biosensors CNT/GOx/Chitin/EDP modified gold (homemade) electrode was operated for glucose quantification by continuous measurement. In this case the biosensor was inserted into the wall-jet cell, the control solution (0.1 M phosphate buffer solution, pH7.0) was continuous passed into the cell. The glucose response signal was recorded continuously when glucose solution was passed into the cell. Figure 3.19 displays an about 200 hour-long stretch of an uninterrupted

amperometric recording that followed a “day 1” pre-calibration trial and for the duration of which the CNT/GO<sub>x</sub>/Chitin/EDP-Au biosensor was in flow mode continuously polarized to + 600 mV vs. Ag/AgCl/3M KCl and subjected to constant passage of phosphate buffer solutions without or, in six calibration and one model sample analysis efforts, with glucose at various molarities. Response generation for the stepped glucose changes was with the minimalistic sensor design for the first three calibrations and thus remarkable 75 hours of flow operation possible on virtually 100 % reproducibility level. Only then a signal drop to 89 % evolved for the 6<sup>th</sup> (175+ hours).

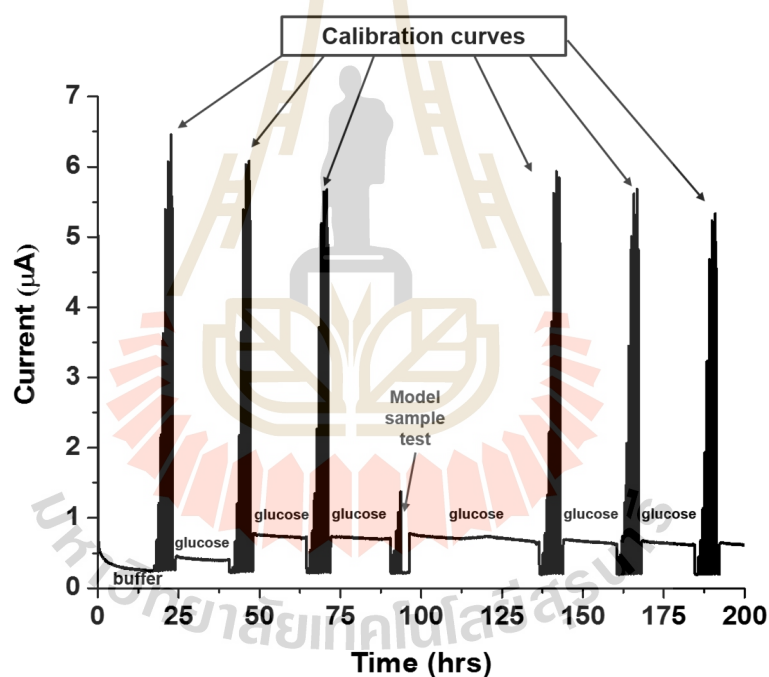


**Figure 3.19** Typical amperometric response of an enzyme biosensor to successive additions of substrate on different days, when performed in a flow system. The storage stability of CNT/GO<sub>x</sub>/Chitin/EDP electrode was investigated by keeping the electrode in 1 M glucose solution (pH7.0) was continuous passed into the cell at +600 mV between each calibration, the calibration curve was constructed follow glucose concentrations: 0.1, 0.5, 1, 2, 4, 8, 16, 32 and 50 mM, respectively.

Extracted from current-time traces was the amplitude of the current steps for the individual glucose additions. A zoomed of Figure 3.19 look at the CNT/GO<sub>x</sub>/Chitin/EDP-Au biosensor signal in the flow cell is for the 3<sup>rd</sup> repetition of sensor calibration provided in Figure 3.20A. All applied elevations in carrier buffer glucose levels got well translated into visible columnar trails in the monitored flow cell current and plots of signal column heights as function of the related glucose content correctly portrayed typical Michaelis-Menten enzyme biosensor behavior with initial manifestation of a linear section followed by curve flattening at saturating substrate values. Predictable from the known practical detection limit of the beaker-type measurements of this study the lowest trialed glucose level of 100  $\mu\text{M}$  produced a clearly visible anodic H<sub>2</sub>O<sub>2</sub> footprint. Sensor currents at saturation (4.8 vs. 12.6  $\mu\text{A}$ ), linear range (4 vs. 40 mM) and sensitivity (4.4 vs. 7.3  $\mu\text{A mM}^{-1} \text{cm}^{-2}$ ) were on the other hand not as closely mimicked (Figure 3.20C). Instead, the glucose response linearity window got considerably narrowed while sensor sensitivity increased about two-fold. The exact bases for these trends is unclear but likely responsible is the special hydrodynamics in the small dead volume flow cell and related differences in balances of diffusional and convectonal glucose and/or molecular oxygen delivery to enzyme sites on the electrode, as compared to mass transport conditions in the stirred bulk of a large-volume container. Despite of the observed concession in the linear range width CNT/GO<sub>x</sub>/Chitin/EDP-Au biosensors did in the flow cell even above 90 hours of continuous contact to buffer stream very well for accurate glucose determinations in samples of known content. A standard addition mode assessment of a 500  $\mu\text{M}$  model glucose sample, just prior after the 3<sup>rd</sup> calibration at about 91-95 hours after trial start,

worked, for instance, via standard addition plot analysis (Figure 3.20B and Figure 3.20D is an example) with recovery rates of 113 %.

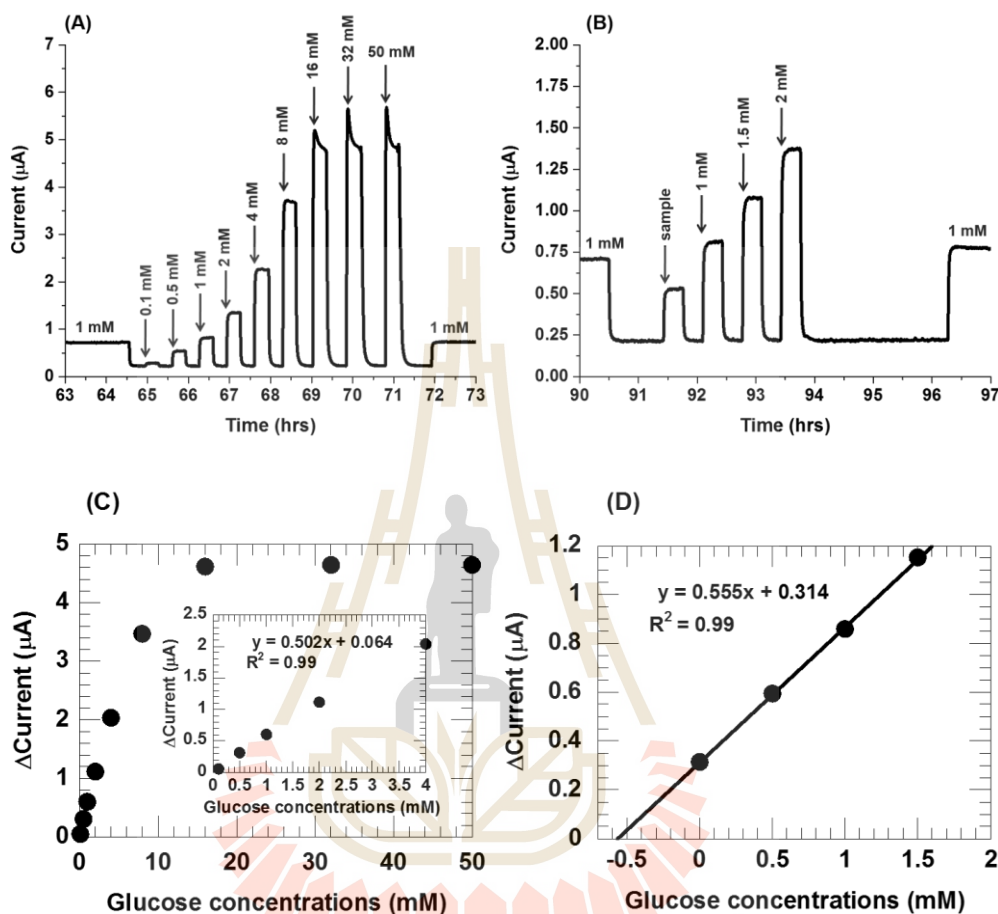


**Figure 3.20** Amperometric response of an enzyme biosensor glucose quantification and model sample analysis via standard addition. (A) Typical amperometric response of an enzyme biosensor to successive additions of substrate at 3<sup>rd</sup> glucose quantification and (B) model sample analysis via standard addition. (C) Electrochemical assessed biosensor calibration curve as constructed by the analysis of the amperometric recording in A. (D) Recovery rates assessments for glucose quantification in 0.5 mM model samples with CNT/GO<sub>x</sub>/Chitin/EDP -based glucose biosensors modified on gold electrode via standard addition method.

### 3.3.6 Performance evaluation for quantitative measurements of model samples with pre-adjusted glucose levels

The CNT/GO<sub>x</sub>/Chitin/EDP glucose biosensors with Pt disk electrode signal transduction were checked with respect to their ability to recover the known levels of glucose in model samples accurately, with reasonable recovery rates. Figure 3.21 shows the quantitative measurements obtained from glucose biosensors which had the CNT layer on a platinum electrode. A plot of peak current of the presented glucose was determined by amperometric response, current plot as a function of time. For the examples shown the experimentally determined glucose levels for the 1.0 mM samples was  $1.11 \pm 0.06$  mM (n=6) of the biosensors, which corresponded to excellent recovery rates of  $111.24 \pm 6.07$  %. The regression coefficient ( $R^2 = 0.99$ ) extrapolation to zero current and/or calculation based on the corresponding line equation ( $y = 0.424x + 0.468$ ) allowed to determination of the glucose level for the 1.0 mM. Table 3.2 represents the recovery rate at various glucose concentration samples at CNT/GO<sub>x</sub>/Chitin/EDP based glucose biosensors, the measured concentrations did not deviate more than 10 % from the true value reflecting recovery rates for the determinations in the range of 90 – 100 %.

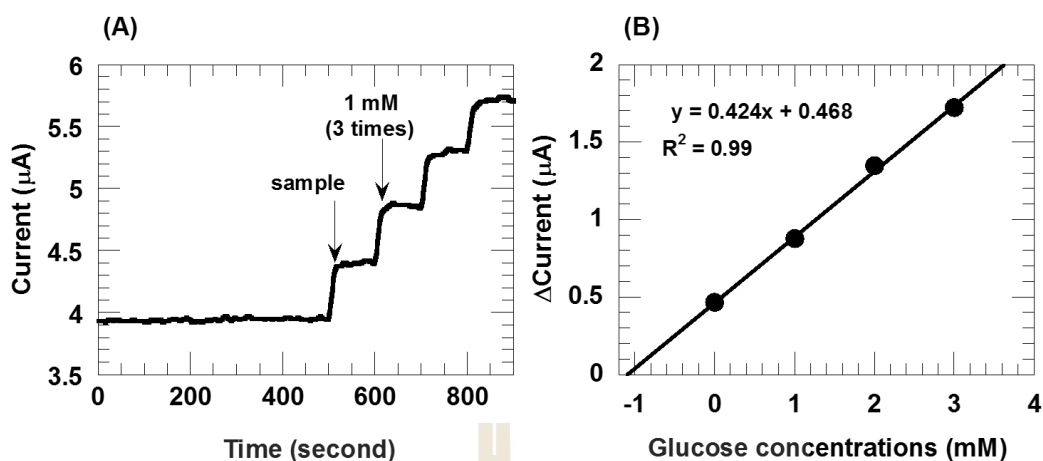


**Figure 3.21** Recovery rate assessments for glucose quantification in 1.0 mM model samples with CNT/GOx/Chitin/EDP-based glucose biosensors modified on Pt electrode. The standard addition method was employed, amperometric response of an enzyme biosensor to successive additions in 0.1 M phosphate buffer solution (pH7.0) at + 600 mV.

**Table 3.2** The recovery rate of CNT/GOx/Chitin/EDP biosensor modified Pt electrode at various glucose concentrations of samples quantified by standard addition mode.

Adjust (mM)	Found (mM)	%Recovery rate
1.00	1.11 ± 0.06 (n=6)	111.24 ± 6.07
2.00	1.97 ± 0.13 (n=3)	98.40 ± 6.31

### 3.3.7 Amperometric determination of glucose at CNT/(Fc-azide+Chitosan+GOx)/EDP-based glucose biosensor

Chronoamperometric measurement use for characterization of the glucose biosensors by CNT/(Fc-azide+Chitosan+GOx)/EDP immobilization biosensor. Figure 3.22 represent the outcome of amperometric calibration measurements that have been obtained in course of trials with the CNT/(Fc-azide+Chitosan+GOx)/EDP-based glucose biosensors. The experiments were carried out in an aqueous 0.1 M phosphate buffer solution (pH 7.0) with a conventional three-electrode cell. A magnetic stirrer provided the convective transport during the measurements. Original trace of a typical current-time curve response for successive adding 1.0 M glucose stock solution into 5 mL phosphate buffer solution (pH7.0) at applied constant potential +600 mV *versus* Ag/AgCl start from low to high glucose concentration (data was not shown). A displays as proof of the good performance a typical example of an amperometric recording that was acquired with a prototype of a CNT/(Fc-azide+Chitosan+GOx)/EDP-modified 3-mm-diameter Pt disk electrode in course of successive additions aliquots of a glucose stock solution. Figure 3.22A shown amperometric response of an enzyme biosensor to successive additions of various substrate concentrations, which displayed Michaelis-Menten type behavior was constructed by the analysis of the amperometric recording, Exposed for this particular case is a plateau current,  $i_{\max}$ , of 23.8  $\mu\text{A}$ , response linearity up to 60.0 mM glucose ( $r^2 = 0.98$ ) and a sensitivity of 0.23  $\mu\text{A mM}^{-1}$  (3.3  $\mu\text{A mM}^{-1} \text{cm}^{-2}$ , normalized to the geometric surface area of the Pt disk transducer) at aerated solutions. On the other hand, the characteristic parameters in case at de-aerated,  $i_{\max}$ , of 14.4  $\mu\text{A}$ , response linearity up to 60.0 mM glucose ( $r^2 = 0.98$ ) and a sensitivity of 0.12  $\mu\text{A mM}^{-1}$  (1.8  $\mu\text{A mM}^{-1} \text{cm}^{-2}$ , normalized to the geometric surface area of the Pt

disk transducer). A zoomed of Figure 3.22A look at the linear area of CNT/(Fc-azide+Chitosan+GOx)/EDP biosensor signal in both conditions of the sensor calibration provided in Figure 3.22B.

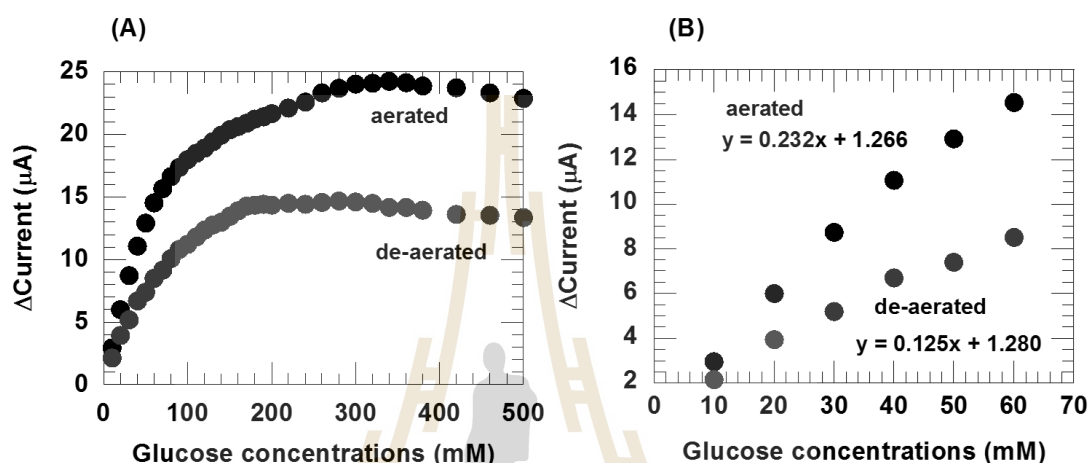


**Figure 3.22** (A) Electrochemical assessed biosensor calibration curve as constructed by the analysis of the amperometric recording with a CNT/(Fc-azide+Chitosan+GOx)/EDP biosensor at aerated (black) and de-aerated (red) solutions, respectively. (B) A zoomed at the same linear range of the sensor for both condition.

The experiment to find out effect of ferrocene-derivative, CNT/(Chitosan+GOx)/EDP and (Chitosan+GOx)/EDP were tried to quantification glucose solution by fabrication onto Pt electrode. All experiments were carried out in an aqueous 0.1 M phosphate buffer solution (pH 7.0) with a conventional three-electrode cell. A magnetic stirrer provided the convective transport during the measurements. Original trace of a typical current-time curve response for successive adding 1.0 M glucose stock solution into 5 mL phosphate buffer solution (pH 7.0) at

applied constant potential +600 mV versus Ag/AgCl start from low to high glucose concentration (data was not shown). A displays as proof of the performance a typical example of an amperometric recording that was acquired with a prototype of a CNT/(Chitosan+GOx)/EDP and (Chitosan+GOx)/EDP -modified 3-mm-diameter Pt disk electrode in course of successive additions aliquots of a glucose stock solution.

Figure 3.23 shown amperometric response of an enzyme biosensor to successive additions of various substrate concentrations, which displayed Michaelis-Menten type behavior was constructed by the analysis of the amperometric recording for CNT/(Chitosan+GOx)/EDP (Figure 3.23A) and (Chitosan+GOx)/EDP (Figure 3.23B), respectively. Both of them represent the measurement in aerated (curve a) and de-aerated (curve b).

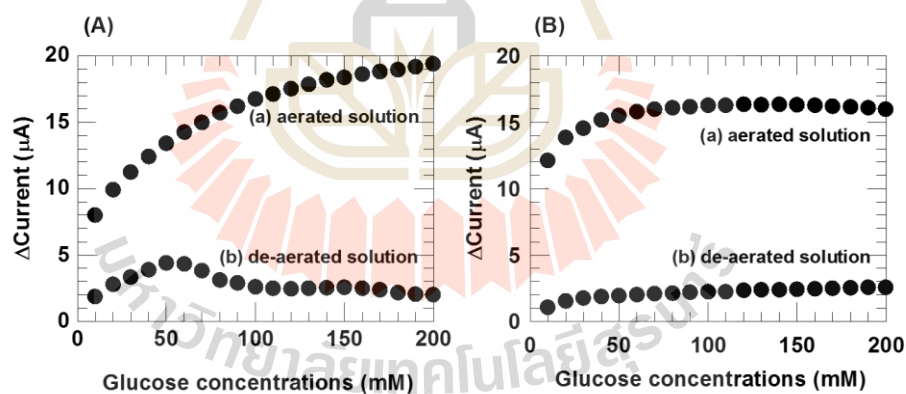


**Figure 3.23** Performance comparison between CNT/(Chitosan+GOx)/EDP and (Chitosan+GOx)/EDP biosensor.(A) Electrochemical assessed biosensor calibration curve as constructed by the analysis of the amperometric recording at CNT/(Chitosan+GOx)/EDP biosensor and (B) at (Chitosan+GOx)/EDP biosensor. Both of them show the current response in aerated (a) and de-aerated (b) solutions, respectively.

Ferrocene derivative immobilized biosensor CNT/(Fc-azide+Chitosan+GOx)/EDP onto Pt electrode, via drop/drying of  $\mu\text{L}$  volumes. Figure 3.24 displays as proof of the good performance a typical example of an amperometric recording in de-aerated solution that was acquired with the three prototype of biosensor, such as CNT/(Fc-azide+Chitosan+GOx)/EDP, CNT/(Chitosan+GOx)/EDP and (Chitosan+GOx)/EDP-modified 3-mm-diameter Pt disk electrode in course of successive additions of small aliquots of a glucose stock solution. All experiments were carried out in an aqueous 0.1 M phosphate buffer solution (pH 7.0) with a conventional three-electrode cell. A magnetic stirrer provided the convective transport during the measurements. The current responses of the biosensor electrode were measured at applied constant potentials +600 mV *versus* Ag/AgCl.

Figure 3.24A show performance comparison at CNT/(Chitosan+GOx)/EDP and (Chitosan+GOx)/EDP-modified electrode. The current response of glucose quantification at CNT version could be came from direct electron transfer of GOx molecules are randomly oriented onto the surface. While comparison at CNT/(Fc+Chitosan+GOx)/EDP and (Chitosan+GOx)/EDP-modified electrode, the current response of glucose quantification at CNT plus ferrocene version could be came from direct electron transfer of GOx molecules are randomly oriented onto the surface and electron-shuttling in conductive network which show in Figure 3.24B. In case of, CNT/(Fc+Chitosan+GOx)/EDP *versus* CNT/(Chitosan+GOx)/EDP, the higher current response until saturated was observed at ferrocene version contained into the immobilization matrix, although both of them were contained CNT conductive network represent in Figure 3.24C. The result confirm hypothesis that is, ferrocene derivatives can help to achieve and gain of effects collection efficiency close to 100 %

by electron-shuttled via CNT conductive network when GOx/glucose interaction which already mention in section 3.3.2.

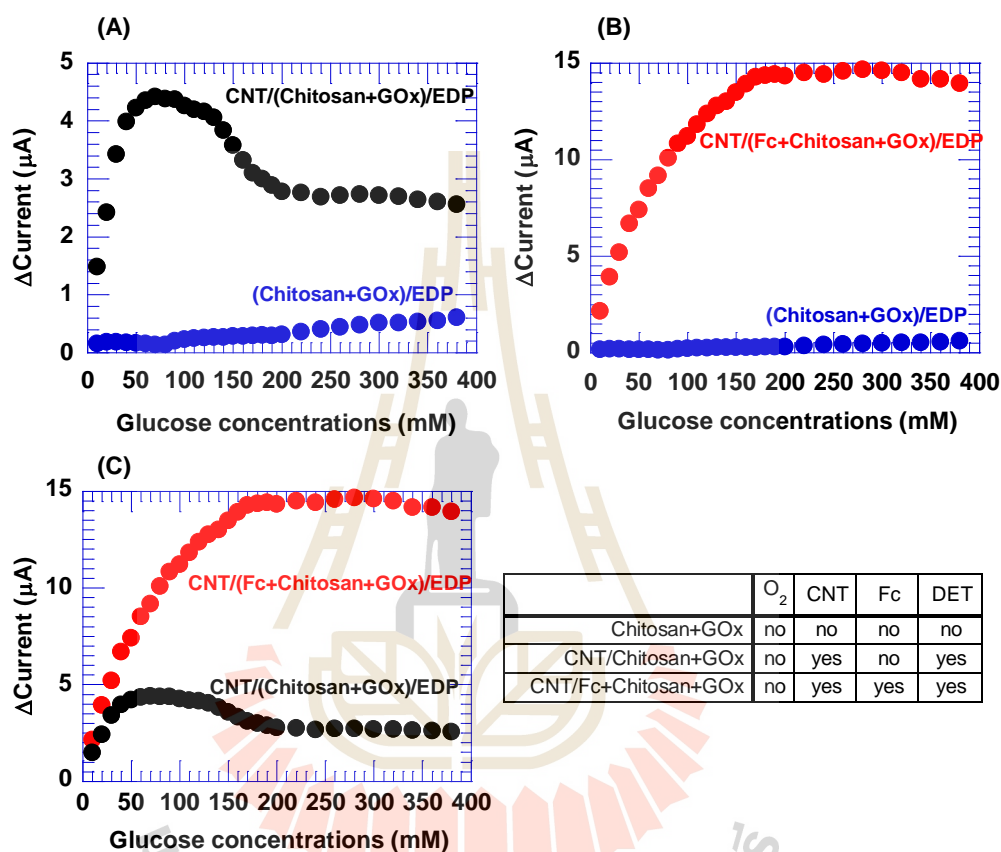


**Figure 3.24** (A), (B), and (C) represents the electrochemical assessed biosensor calibration curve as constructed by the analysis of the amperometric recording, comparison the performance at CNT/(Fc+Chitosan+GOx)/EDP (red curve), CNT/(Chitosan+GOx)/EDP (black curve) and (Chitosan+GOx)/EDP (blue curve) biosensor, respectively.

Continuous measurement for the reproducibility and long-term stability test was performed in flow system recording same as other biosensor configuration

which already described, the current response with glucose by operated in a three-electrode electrochemical flow cell that was under control of the galvanostat/potentiostat EA163 and e-corder ED410, both from eDAQ. The biosensors CNT-GOx-EDP modified gold electrode was operated for glucose quantification by continuous measurement. In this case the biosensor was inserted into the wall-jet cell, the control solution (0.1 M phosphate buffer solution, pH7.0) was continuous passed into the cell. The glucose response signal was recorded continuously when glucose solution was passed into the cell. Figure 3.25 displays an about 180 hour-long stretch of an uninterrupted amperometric recording that followed a 'day 1' pre-calibration trial and for the duration of which the CNT/(Fc+Chitosan+GOx)/EDP-Au biosensor was in flow mode continuously polarized to + 600 mV vs. Ag/AgCl/3M KCl and subjected to constant passage of phosphate buffer solutions without or, in five calibration, with glucose at various molarities. Response generation for the stepped glucose changes was with the minimalistic sensor design for the first four calibrations and thus remarkable 80 hours of flow operation possible on virtually 100 % reproducibility level. Then a signal drop to 73 % and further to 52 % evolved for the 5<sup>th</sup> (120+ hours) and 6<sup>th</sup> (180+ hours) calibration, respectively.

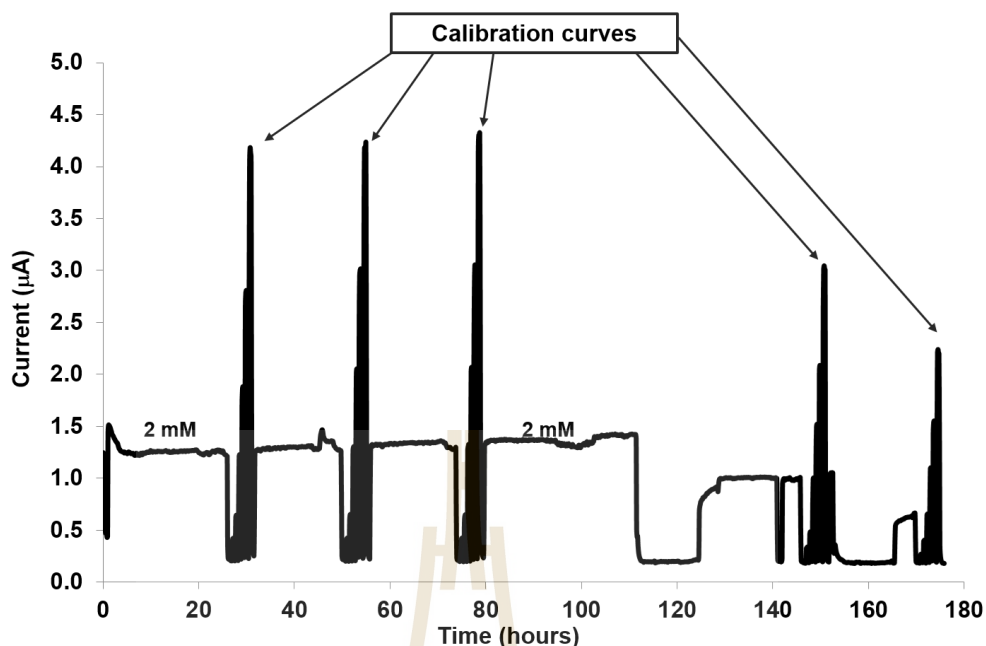


**Figure 3.25** Typical amperometric response of an enzyme biosensor to successive additions of substrate at different days performed in a flow system. The storage stability of CNT/(Fc+Chitosan+GOx)/EDP electrode was investigated by keeping the electrode in 2 mM (in 0.1 M phosphate buffer solution, pH7.0), was continuous passed into the cell at + 600 mV between each calibration, the calibration curve was constructed follow glucose concentrations: 0.5, 1, 2, 5, 10 and 25 mM, respectively.

Extracted from Current-time traces was the amplitude of the current steps for the individual glucose additions. A zoomed of Figure 3.26 look at the CNT/(Fc+Chitosan+GOx)/EDP-Au biosensor signal in the flow cell is for the 1st repetition of sensor calibration provided in Figure 3.26A. All applied elevations in carrier buffer glucose levels got well translated into visible columnar trails in the monitored flow cell current and plots of signal column heights as function of the related glucose content correctly portrayed typical Michaelis-Menten enzyme biosensor

behavior with initial manifestation of a linear section followed by curve flattening at saturating substrate values. Sensor currents at saturation (3.9 vs. 33.9  $\mu\text{A}$ ), linear range (2 vs. 30 mM) and sensitivity (7.6 vs. 7.5  $\mu\text{A mM}^{-1} \text{cm}^{-2}$ ) which show in Figure 3.26B. Instead, the glucose response sensitivity window got considerably narrowed while sensor linear increased about fifteen-fold. The exact bases for these trends is unclear but likely responsible is the special hydrodynamics in the small dead volume flow cell and related differences in balances of diffusional and convectional glucose and/or molecular oxygen delivery to enzyme sites on the electrode, as compared to mass transport conditions in the stirred bulk of a large-volume container.

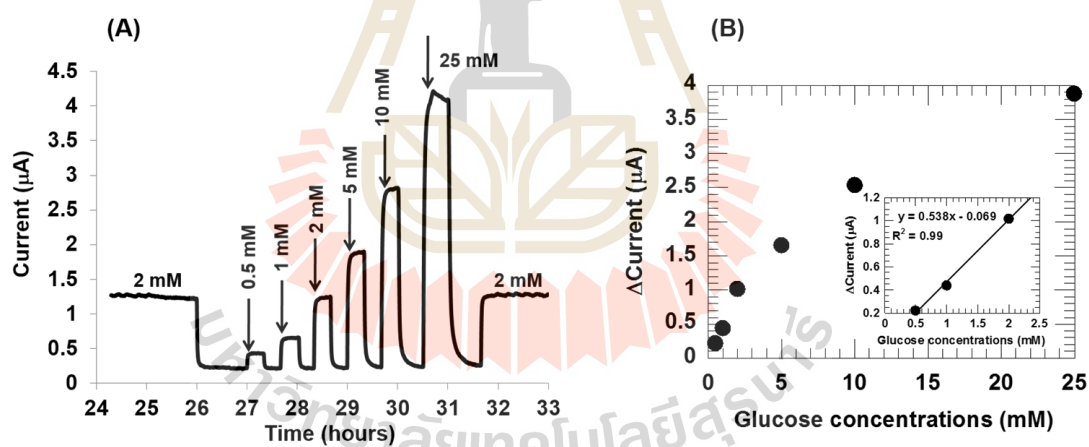


**Figure 3.26** Amperometric response of an enzyme biosensor glucose quantification at CNT/(Fc+Chitosan+GOx)/EDP. (A) Typical amperometric response of an enzyme biosensor to successive additions of substrate at 1<sup>st</sup> glucose quantification and model sample analysis via standard addition. (B) Electrochemical assessed biosensor calibration curve as constructed by the analysis of the amperometric recording in A, with the inset show a zoom at linear area.

### 3.4 Conclusions

From the previous main chapter 2, it was known that CNT/*GOx*/EDP glucose biosensors showed an exceptional high quality in terms of their performance for glucose analysis. In this chapter tested was whether the literature-known effect of a possible CNT↔*GOx* direct electron transfer was observed for biosensor of the CNT/*GOx*/EDP design and whether an incorporation of chitin or chitosan and ferrocene as functional additives to the otherwise bare ‘CNT’ immobilization matrix would help improving sensor life time and signal quality, respectively. The cyclic voltammetry inspections of relevant biosensor variants indeed offered signs of the possibility of DET on CNT filaments as alternative pathway for *GOx* redox recycling. Though this was not an objective of this PhD thesis it may thus be useful to explore in future experiments the potential of this effect for improving quantitative glucose analysis in model and real samples, with the fabricated biosensor operated at *GOx* instead of hydrogen peroxide oxidation potential to enhance protection against interference influence. The expected beneficial effect of a chitin or chitosan supplementation of the CNT immobilization matrix on sensor life time was unfortunately not observed. Biosensor with chitin or chitosan addition did not expose longer life times in the long-term test in continuous flow operation mode as the ones with a bare CNT deposit as entrapping environment for the *GOx* molecules. This observation was not expected but delivered, on the other hand, a valuable experimental evidence of an inherently good biocompatibility of CNT towards *GOx*, which is good enough to keep enzyme alive and functional for the stretch of a week of continuous use. Based on the outcome here, a chitin/chitosan supplementation is thus not necessary if the aim is just sensor life extension and not utilization of their functional ‘NH<sub>2</sub>’ groups for covalent matrix modification. And an

incorporation of ferrocene into the sensor matrix helped, as expected, with manifestation of an ‘dissolved oxygen’ independence and sensors with the ferrocene addition worked better in de-aerated solutions for glucose detections as the ferrocene-free ones. As for the DET case, further work must be carried out to utilize this observation optimally for glucose biosensing, in particular with respect to a covalent fixation of the ferrocene component to, for instance, chitosan polymer strings in a merged CNT/chitosan immobilization matrix, via utilization of their  $\text{NH}_2$  groups for crosslinking.



# CHAPTER IV

## ESTABLISHMENT OF AN ELECTROCHEMICAL READOUT FOR $\beta$ -*N*-ACETYL GLUCOSAMINIDASE ENZYME ACTIVITY ASSAYS

Kinetic assays for the enzymatic degradation of 4-methylumbelliferyl (4-MU)-labeled oligosaccharides normally work with a standard colorimetric optical detection of released 4-MU species. In this communication, the inherent redox activity of the valuable marker molecule was explored for prototyping an alternative analytical option for the quantification of the marker of enzyme action, namely 4-MU electroanalysis. Motivation for the efforts was the well-known redox activity of 4-MU, which is a species that in close physical contact with properly charged solid-state sensors readily undergoes electrochemical anodic oxidation through an equivalent current-producing interfacial electron transfer process. Used here for revealing the time course of enzymatic 4-MU release was actually amperometry at electrically positive disk-shaped working electrodes. Various sensor types have been screened regarding their quality as possible probes for this voltammetric/amperometric 4MU monitoring. Provided in the following paragraphs will be basic information on the enzyme that was used in this study part, namely  $\beta$ -*N*-acetyl-glucosaminidase. Then reviewed will be a selection of studies that deal with an electrochemical detection of organic molecules that are

exploited as labels of enzyme substrate, in particular of 4-MU and *p*-nitrophenol (*p*NP) and existing work on applications of electrochemical detection for an enzyme activity inspection. As first outcome of own thesis work on the subject will be reported the practical performance level of a 4-MU voltammetry/amperometry at the chosen electrode types, as evaluated via differential pulse and amperometry calibration trials. And finally demonstrated will be how the best choice of electrochemical 4-MU detection actually performed as monitoring tool of ongoing enzymatic cleavage action of  $\beta$ -*N*-acetyl-glucosaminidase on 4-MU-labeled *N*-acetyl- $\beta$ -*D*-glucosaminide and how ‘Michalis-Menten’-type of plots of enzyme kinetics can be derived via quantitative 4-MU electroanalysis. In the concluding segment of this thesis section the value of the electrochemical enzyme assay will be discussed and compared with the qualities of the standard colorimetric options.

#### 4.1 Literature review

The structure and hydrolytic cleavage activity of the enzyme  $\beta$ -*N*-acetylglucosaminidase or GlcNAcase (EC 3.2.1.52) from *Vibrio harveyi* 650 on various optically labeled oligosaccharides is well known (Meekrathok *et al.*, 2015a; Meekrathok *et al.*, 2015b; Meekrathok and Suginta, 2016; Sirimontree *et al.*, 2015; Suginta *et al.*, 2010). The enzyme actually catalyses the hydrolytic release of terminal  $\beta$ -(1-4)-linked *N*-acetyl-*D*-glucosamine residue from the non-reducing end to produce GlcNAc residue of a variety of substrates including glycoproteins, glycolipids and glycosaminoglycans (Cohen-Kupiec and Chet, 1998; Pemberton *et al.*, 2001). Most current methods to determine the activity of enzymes activity rely on colorimetric

and/or radiological measurements. Common synthetic chromogenic substrate labels include *p*-nitrophenyl (4-NP) and 4-methylumbelliferyl (4-MU) and, attached to particular oligosaccharide substrate of glycosidases, they are commonly used in optical assays for the visualization and quantification of the activity of glycosidases (Kitchen *et al.*, 1978; Linko-Löppönen and Mäkinen, 1985; Lo *et al.*, 1979; Umemoto *et al.*, 1978).

As reasonably priced electrochemical detection schemes offer a unique combination of simplicity, speed and high sensitivity for accurate measurement of a variety of species the methodology was also considered as an analytical tool for enzyme kinetic studies. The standard hydrogen peroxide amperometry, as implemented in many published glucose biosensor studies, was, for instance, used for visualizing and quantifying the substrate conversion activity of glucose oxidase, creatine kinase, and putrescine oxidase (Nagy *et al.*, 1998). Hydrogen peroxide as formed in the enzyme-catalyzed reaction was actually detected via common amperometry at anodic working electrodes and the amperometric signal evolution in response to successive additions of substrate to the enzyme-containing electrochemical cell was found to be proportional to substrate concentrations. The shapes of the current plot as a function of time recordings showed similar characteristics for all three enzymes reactions, with its linear range dissimilar, depending on the activity range of each enzyme (Figure 4.1)

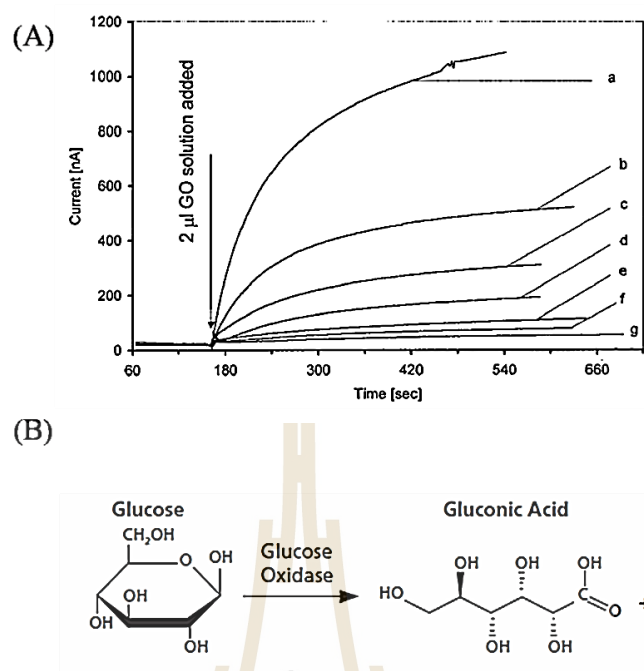


**Figure 4.1** Amperometric monitoring of glucose oxidase activity in terms of glucose to gluconolactone/gluconic acid conversion (A). Current-time curve acquisition is valid for the addition of 2  $\mu$ L aliquots of glucose oxidase solutions of different activities to 5  $\mu$ L of 100 mM glucose solution in the electrochemical cell: (a) 5.70, (b) 3.80, (c) 1.90, (d) 1.26, (e) 0.58, (f) 0.39, and (g) 0.19 unit/mL (Nagy *et al.*, 1998). (B) Enzymatic reaction of glucose oxidase.

Amperometry was used for activity measurements of proline-iminopeptidase (PIP), a specific hydrolase enzyme that catalyses the proline-liberating hydrolysis of Pro-NH-R type peptides (Figure 4.2B). In this work, the PIP activity was assessed through the detection of  $\beta$ -naphthylamine ( $\beta$ -NA), the reaction product of the enzyme catalyzed hydrolysis of Prol  $\beta$ -NA. The current response was found to be proportional to the substrate concentration (Nagy *et al.*, 1998). Figure 4.2A shows the current-time profile that was observed before and after addition of PIP enzyme to a substrate-

containing solution. Nicely visible is the current step that was induced through merging the enzyme and substrate.

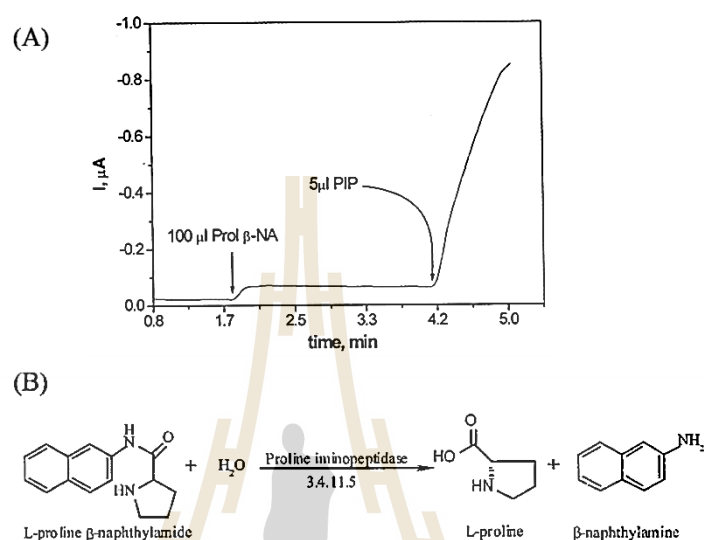


**Figure 4.2** (A) Current-time profiles in a buffer solution containing the Prol  $\beta$ -NA, the current increase after added PIP enzyme to the substrate solution and (B) Enzymatic reaction of prolineiminopeptidase (Nagy *et al.*, 1998).

Here, the pronounced redox activity of (4-MU) labels of  $\beta$ -N-acetylglucosaminidase substrate was explored for electrochemical enzyme assay establishment. 4-MU is a member of the collection of coumarins, which are benzopyrones and either available as natural plant ingredients or as product of tailored organic synthesis. 4-MU is actually widely used as drug for the treatment of cholecystitis, gallstones, cancer, *etc.* (L. Wang *et al.*, 2015). Because of their good light absorption properties mainly spectroscopic methods have been suggested for the determination of 4-MU, including UV-photometry, fluorimetry and high-performance

liquid chromatography (HPLC) (Carrazón *et al.*, 1989). Attached as optical label to oligosaccharides 4MU served in spectroscopic enzyme assays as reporter of enzyme activity. A simplified schematic of this analytical procedure is presented in Figure 4.3. The action of enzyme on (4-MU)-labeled chitosugars leads to 4-MU liberation into measuring buffer and the steady rise in the concentration of the label is followed via sensitive spectroscopy.

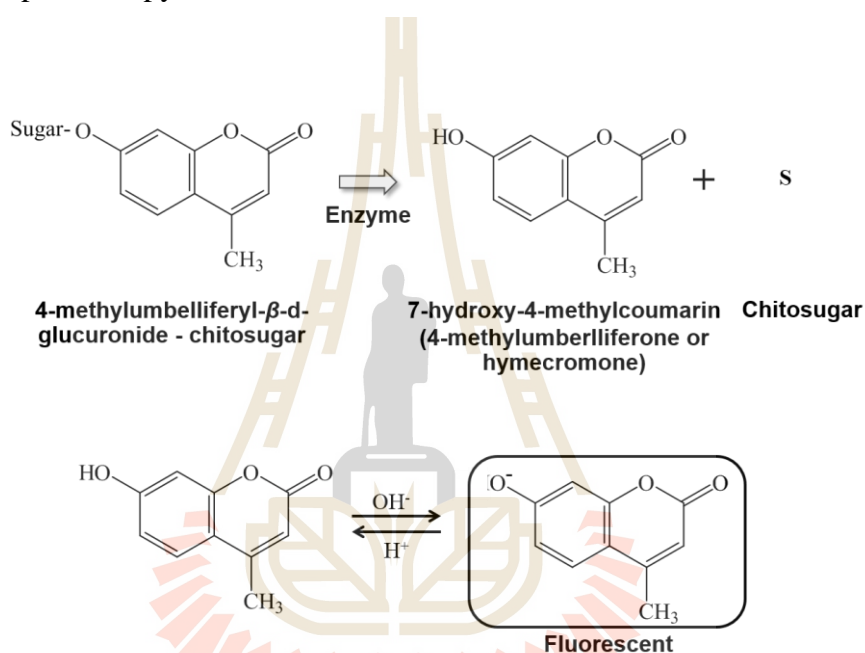


**Figure 4.3** Enzyme kinetic assay utilizing 4-MU label attachment to sugar substrates and fluorescent spectrophotometry for visualization and determination of substrate/enzyme interaction. Measured as indicator of ongoing enzyme activity is the buffer levels of free 4-MU. 4-MU calibration curves allow translation of absorption values into concentration and construction of quantitative enzyme kinetic activity plots.

There are some reports regarding the electroanalysis of 4-MU or similar coumarin derivatives. Wu and Dewald, for instance, studied the voltammetry behavior of various coumarins by cyclic voltammetry, differential pulse voltammetry and

chronocoulometry (Q. Wu and Dewald, 2001). In another publication, Wang and coworker studied the redox character of 7-hydroxy-4-methylcoumarin by electrochemical measurement (L. Wang *et al.*, 2015). However so far unexplored was the possibility to use an electrochemical detection of 4-MU as basis of a quantitative electrochemical enzyme activity assay that delivers Michaelis-Menten-type of enzyme kinetic plots and this particular exploration was addressed here.

## 4.2 Experimental and methods

### 4.2.1 Chemicals

4-methylumbelliferyl *N*-acetyl- $\beta$ -d-glucosaminide and 4-methylumbelliferone, 4-MU, which is also known as 7-Hydroxy-4-methylcoumarin, were both obtained through Italmar (Thailand) Co., Ltd. (Bangkok, Thailand) as analytical grade product of Sigma-Aldrich® (St. Louis, MO, USA). All other chemicals were Sigma-Aldrich® products and of analytical grade. Routinely, aqueous solution preparation used ultrapure de-ionized water. Supporting electrolyte for all experiments tests was 0.1 M phosphate buffer solutions, pH 7.0.

### 4.2.2 Electrochemical instruments

Cyclic voltammetry (CV), Differential pulse voltammetry (DPV) and chronoamperometry measurements were carried out with a computer controlled potentiostat, electrochemical workstation from Gamry Instruments (potentiostat Model Reference 600®, Gamry Instruments, Warminster, PA USA). A conventional three-electrode set-up was used. A 3-mm-diameter disk-shaped boron doped diamond

(BDD) electrode was used as working electrode, platinum wire and Ag/AgCl wire were used as counter electrode and reference electrode, respectively.

### 4.3 Results and discussion

#### 4.3.1 Voltammetry and amperometry of dissolved 7-hydroxy-4-methylcoumarin (4-MU)

4-MU is a phenolic compound and it is known that the products of an anodic phenol oxidation – which takes place in course of the determination of 4-MU at a positively polarized electrode – have the tendency to stick to the detecting surface and cause electrode poisoning/loss of sensitivity. Among the common electrode materials, boron-doped diamond (BDD) is known to be most resistive against that adverse effect (Luong *et al.*, 2009; Pecková *et al.*, 2009). Preliminary sensor tests were carried out with disk-shaped glassy carbon, platinum and BDD electrodes and in agreement with literature best 4-MU detection was obtained with 3 mm disk-shaped BDD electrodes and they were thus selected as working electrode for all further experiments towards realization of the (4-MU)-based electrochemical enzyme assay.

Cyclic voltammetric measurements were conducted at the bare BDD with and without 4-MU present in 0.1 M phosphate buffer solution, pH 7.0. As shown in Figure 4.4A in the positive potential scan direction, no redox signal was observed in phosphate buffer solution (pH7.0) in the absence of 4-MU (black curve), while a well-shaped single oxidation peak was observed in the presence of 4-MU (blue curve). The scan started at 0.3 V vs. Ag/AgCl (saturated), moved into the positive direction to 1.2 V and went back to starting point. The peak for the anodic oxidation came up at

about 0.74 V, but no reduction wave or peak corresponding to the anodic wave was observed for the scan in cathodic direction, at least not up to the lower scan limit of 0.3 V vs. reference. This indicated that oxidation peak should be attributed to the oxidation of 4MU. Figure 4.4B show the results of bulk solution without 4MU at black curve, while red curve and green curve represent oxidation of low and high 4MU concentrations which investigated at 40 and 400  $\mu\text{M}$ , respectively.

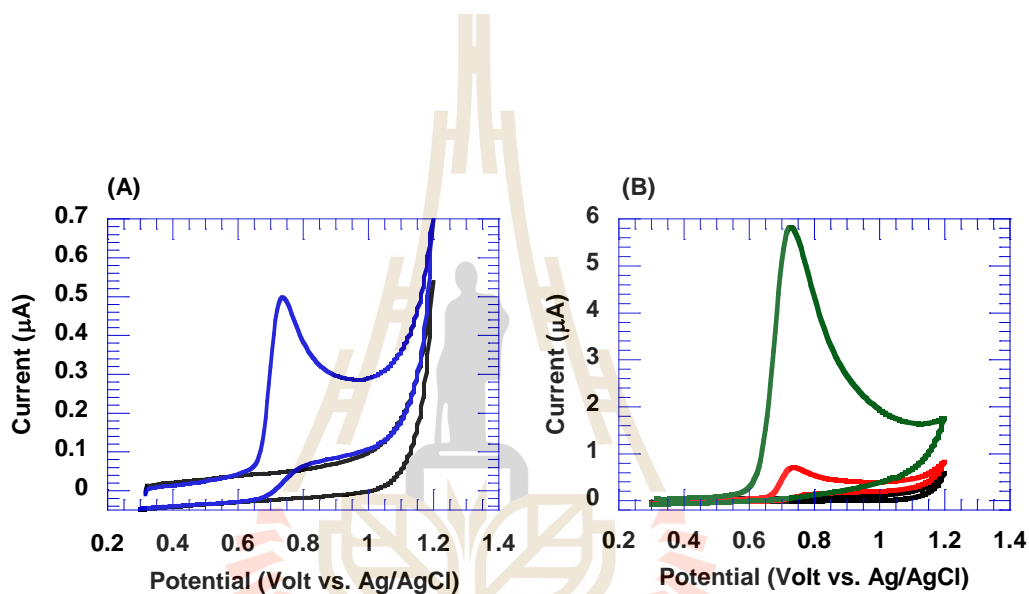


**Figure 4.4** (A) Cyclic voltammograms responses of 4-MU obtained at a 3 mm disk-shaped boron doped diamond electrode, in the absence (black curve) and presence (20  $\mu\text{M}$ , blue curve) of 4-MU. (B) Cyclic voltammograms responses of 4-MU at different concentrations, in the absence (black curve) low (40  $\mu\text{M}$ , red curve) and high (400  $\mu\text{M}$ , green curve). All experiments were performed in 0.1 M phosphate buffer (pH 7.0) with scan rate 50  $\text{mV}\cdot\text{s}^{-1}$ .

Though the BBD electrodes were best for the detection of 4-MU they were not fully protected against surface contamination with polymerized 4-MU

oxidation products and indeed they lost sensitivity during use, in particular when measuring larger concentrations repeatedly. This undesirable effect is demonstrated in Figure 4.5 for repeated acquisition of cyclic voltammograms with a 3mm disk-shaped BDD electrode in an electrolyte containing 100  $\mu\text{M}$  4-MU in 0.1 M phosphate buffer solution (pH 7.0). In course of ten successive voltammetric scans the CV current peak decreased significantly from above 2 to about 0.5  $\mu\text{A}$ , as result of electrode surface coverage with polymeric oxidation products. For the reliable assessment of calibration curves it was thus decided to polish and clean the surface of the BDD disk in between individual measurements of voltammograms (e.g. DPVs) for different 4-MU concentrations.

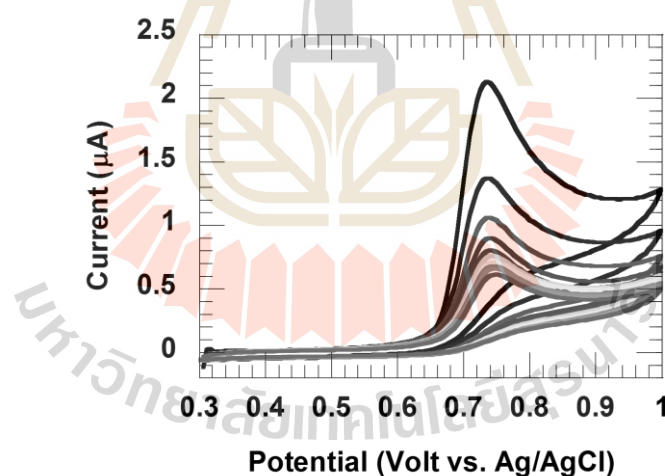


**Figure 4.5** Cyclic voltammograms responses of 100  $\mu\text{M}$  4-MU as obtained at boron doped diamond electrode (BDD, 3-mm of diameter). Shown are 10 repetitive scans in 0.1 M phosphate buffer solution (pH 7.0) with scan rate 50  $\text{mV s}^{-1}$ .

Differential pulse voltammetry (DPV) was used for calibration of the anodic BDD 4-MU response and reveal a relationship between the solution

concentrations of 4-MU and electrochemical signal. As evident from the collection of DPVs in Figure 4.6A, no redox signal was observed in pure phosphate buffer solution (pH 7.0) without 4-MU (curve for the blank), while a well-shaped concentration-dependent oxidation peak was observed for increasing levels of dissolved 4-MU (peaks of increasing amplitude at 0.74 V vs. reference). Extraction of peak heights and their plot against 4-MU solution level (Figure 4.6B) revealed a linear relationship for concentrations between 1 and 40  $\mu\text{M}$ . The linear regression equation was actually  $i_{\text{pa}} (\mu\text{A}) = 0.0539c (\mu\text{M}) - 0.0135$  ( $R^2 = 0.998$ ).

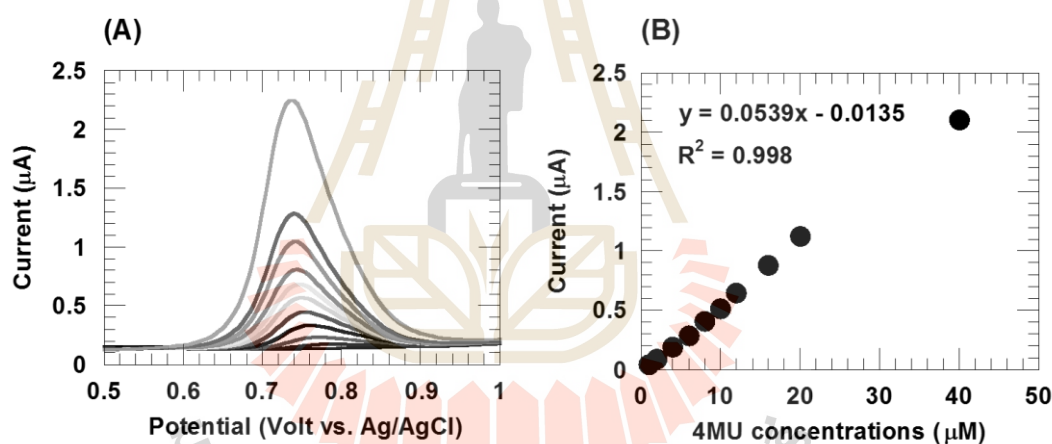


**Figure 4.6** (A) Collection of differential pulse voltammograms from a voltammetric 4-MU calibration trial with a disk-shaped boron-doped diamond electrode of 3 mm diameter. 4-MU was measured in 0.1 M phosphate buffer solution, pH 7.0 at concentrations of 1, 2, 4, 6, 8, 10, 12, 16, 20 and 40  $\mu\text{M}$ . (B) Plot of 4-MU DPV peak currents as function of 4-MU electrolyte concentration.

Chronoamperometric measurements of 4-MU at detection potentials of +700 mV vs, reference were also conducted to evaluate whether in the current

recordings clearly visible rises in anodic currents would be triggered through 4-MU additions of different strength. Please note that as for the DPV calibration trial BBD disks were carefully re-polished between acquisitions of the individual amperograms to avoid a bad influence of electrode poisoning. Figure 4.7A shows a typical set of amperometric current-time traces that were recorded in of such a trial with 0.5, 1, 2, 4, 6, 8, 10 and 16  $\mu\text{M}$  being the choice of test concentration. Figure 4.7B represent the amperometric 4-MU calibration curve that was constructed from the raw data of the current-time traces in Figure 4.7A. Linearity of the amperometric calibration plot stretched up to the tested 16  $\mu\text{M}$  (equation for the regression line:  $y (\mu\text{A}) = 0.0098x (\mu\text{M}) - 0.0054$ ; regression coefficient  $R^2=0.983$ ).

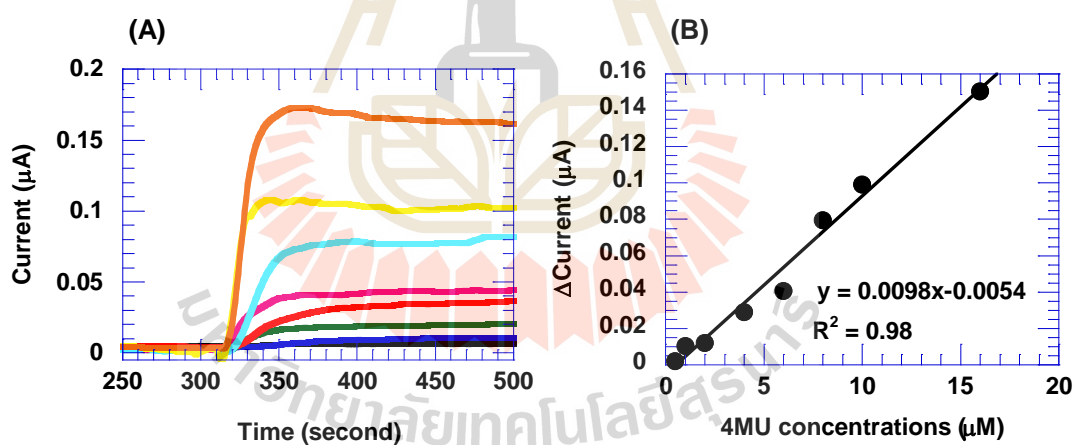


**Figure 4.7** (A) Collection of 4-MU amperograms, acquired with a boron doped diamond electrode of diameter at + 700 mV vs. reference electrode, for different 4-MU levels of concentrations in 0.1 M phosphate buffer solution (pH 7.0) (0.5, 1, 2, 4, 6, 8, 10, and 16  $\mu\text{M}$ ). (B) The linear relationship between anodic peak current and hymecromone concentration.

### 4.3.2 The amperometric *VhGlcNAcase* activity assay

4-MU amperometry as devised in the previous sub-section was then used as a screening tool for the liberation of the compound from an impact of *VhGlcNAcase* on (4-MU)-labeled *N*-acetyl- $\beta$ -D-glucosaminide. Figure 4.8A displays a set of typical current-time traces that were recorded in an amperometric trial in 0.1 M phosphate buffer solution (pH 7.0) with 0.05  $\mu$ M *VhGlcNAcase* for 4-MU-*N*-acetyl- $\beta$ -D-glucosaminide concentrations 0.5, 1, 2, 3, 4, 6, 8, 10, 16 and 20  $\mu$ M. Figure 4.8B represents the Michaelis-Menten type plot which can be constructed by plotting the slope of the initial phase of the original amperograms in Figure 4.8A versus 4-MU solution level. The shape of the plot well resembles the one obtained via optical analysis of the enzyme activity with 4-MU spectroscopy in charge for the quantification of cleaved label. The apparent, electrochemically assessed,  $V_{max}$  and  $K_m$  values are 1.37  $\mu$ M sec<sup>-1</sup> and 10.79  $\mu$ M (n=3), respectively. With these values and the known enzyme and substrate concentrations rate of the reaction,  $k_{cat}$ , is calculated as 27.48 sec<sup>-1</sup>.

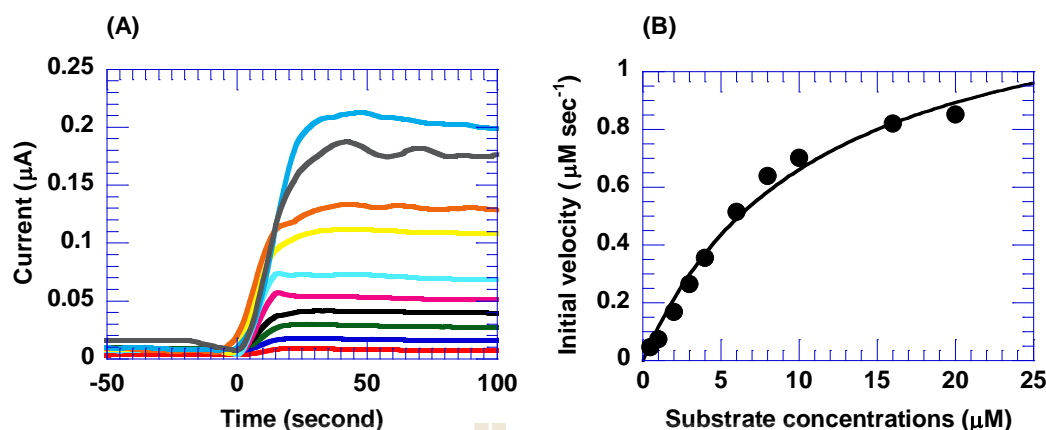


**Figure 4.8** (A) Amperometric recordings of *VhGlcNAcase* cleavage activity on (4-MU)-labeled *N*-acetyl- $\beta$ -D-glucosaminide. *VhGlcNAcase* electrolyte level was 0.05  $\mu$ M and substrate concentrations were 0.5, 1, 2, 3, 4, 6, 8, 10, 16 and 20  $\mu$ M. (B) The electrochemically derived Michaelis-Menten plot as extract with the data in (A). Individual amperometric measurements were performed in 0.1 M phosphate buffer solution (pH 7.0), with freshly polished boron-doped diamond disk electrode of 3 mm diameter held at +700 mV vs. reference for anodic 4-MU detection.

#### 4.4 Conclusions

In summary 4-MU amperometry at boron-doped diamond electrodes offered indeed a sensitive electrochemical assay for monitoring the interaction of a sugar-hydrolyzing enzyme with (4-MU)-labeled corresponding substrate. The data of the assay allowed construction of Michaelis-Menten-type of enzyme activity fingerprints as plots of the rate of enzymatic substrate reaction (slope of the initial phase of current) vs. time, just as usually obtained via standard optical analysis. Together with the outcome of two previously published studies utilizing redox-active 1-naphthol- (Pemberton *et al.*, 2001) and *p*-Nitrophenol (Tanguaram *et al.*, 2006) as functional

enzyme labels, evidence has thus been produced that a highly sensitive, rapid and simple electrochemical assay for glycosidase activity measurements is possible based on inspections of the particular biocatalyst with appropriately labeled glycoside substrates and corresponding amperometric or voltammetric detection of the released redox tag. Glycosidase activity analysis depends on substrates which are prepared via customized organic synthesis with measurable tags. The manifestation of amperometry/voltammetry as alternative readout is a valuable accomplishment as the restriction of an optical label activity was overcome and a larger number of molecular labels became feasible for custom biocatalyst conjugation. Further advantages of the opportunity of working with an electrochemical enzyme activity readout are the potential for assay miniaturization through use of micro- or nanoelectrodes as detector in microfluidic devices and capacity to be developed into easy portable assay system via assay operation with cigarette box-sized computerized potentiostats.

**CHAPTER V**

**CATALYTIC REACTION OF 4MU-GLCNAC**

**DEPENDENT BY  $\beta$ -N-ACETYL GLUCOSAMINIDASE**

**FROM *VIBRIO HARVEYI***

$\beta$ -N-acetylglucosaminidases are commonly occurring enzymes involved in the degradation of polysaccharides and glycoconjugates containing N-acetylglucosamine residues. *VhGlcNAcase* is a  $\beta$ -N-acetylglucosaminidase that has been purified from *Vibrio Harveyi* 650. The enzyme has a molecular mass of 75 kDa. In this study, enzyme activity and kinetic experiments have been studied using 4-methylumbelliferyl N-acetyl- $\beta$ -D-glucosaminide (4MU-GlcNAc) as substrate. The fluorimetric assay monitored substrate hydrolysis by using stopped-flow and fluorescence measurements by determining the liberating 4-methylumbelliferone. Based on results obtained from stopped-flow measurements, the enzyme reacts with the 4MU-substrate, forming 4-methylumbelliferone (phenolic form) with a rate constant of  $53 \pm 4 \text{ s}^{-1}$ . The apparent  $k_{cat}$  at saturating concentrations of 4MU-GlcNAc is  $11.5 \text{ s}^{-1}$ . Pre-steady state and steady-state kinetic data were used to construct the catalytic cycle of the reaction as will be shown later.

## 5.1 Literature review

*Vibrio harveyi*  $\beta$ -*N*-acetylglucosaminidase (*VhGlcNAcase*) is a new member of the family GH20 glycoside hydrolase, responsible for the complete degradation of chitin fragments, with *N*-acetylglucosamine (GlcNAc) monomers being released as the final products (Meekrathok *et al.*, 2015a). Chitin is a homopolysaccharide composed of  $\beta$ -1,4-linked *N*-acetyl-D-glucosamine units. It is one of the most highly abundant organic compounds in marine environments, occurring in the structural skeletons of crustaceans (e.g. crabs and shrimps), as well as in the interal shells of cephalopods, including squid and octopus. The complete degradation pathway of chitin by the marine bacterium *Vibrio harveyi* involves the successive action of two classes of chitinolytic enzymes; 1) GH18 endochitinase A (*VhChiA*, EC 3.2.1.14), which hydrolyzes chitin, generating chitooligosaccharide fragments that are readily transported into the cell and subsequently broken down and produced GlcNAc monomers by 2) GH20 exo  $\beta$ -*N*-acetylglucosaminidase (*VhGlcNAcases*, EC 3.2.1.52). The model chitinolytic cascade is presented in Figure 5.1 (Cohen-Kupiec and Chet, 1998; Kadokura *et al.*, 2007; Kubota *et al.*, 2004; Meekrathok and Suginta, 2016; Rinaudo, 2006; Sirimontree *et al.*, 2015).

Based on CAZy (Carbohydrate-Active enZymes Database; <http://www.cazy.org>), GlcNAcases are classified into glycoside hydrolase family 3 (GH-3) and family 20 (GH-20), based on the amino acid sequence similarity of their catalytic domains and the mode of enzyme action (Henrissat and Bairoch, 1993; Henrissat and Davies, 1997; H. Li *et al.*, 2002). Family 3 glycoside hydrolases include  $\beta$ -D-glucosidases (EC 3.2.1.21),  $\beta$ -D-xylopyranosidases (EC 3.2.1.37),  $\beta$ -N-

acetylglucosaminidases (GlcNAcases) (EC 3.2.1.52), and  $\alpha$ -L-arabinofuranosidases (EC 3.2.1.55) (Harvey *et al.*, 2000). Family 20 glycoside hydrolases include  $\beta$ -N-acetylglucosaminidases (GlcNAcases) (EC 3.2.1.52) and  $\beta$ -hexosaminidases ( $\beta$ -N-acetylhexosaminidases) (EC 3.2.1.52). While, GlcNAcases hydrolyze  $\beta$ -1,4 linkages *N*-acetylglucosamine oligomers,  $\beta$ -hexosaminidases also hydrolyze  $\beta$ -1,4 linkages between *N*-acetylgalactosamine and galactosamine moieties (Tews *et al.*, 1996). Most of bacterial GlcNAcases are grouped into family 20 GlcNAcases, such as chitobiase from *Serratia marcescense* (Tews *et al.*, 1996),  $\beta$ -hexosaminidase from *Streptomyces plicatus* (Mark *et al.*, 2001), disperin B ( $\beta$ -1,6-*N*-acetylglucosaminidase) from *Actinobacillus actinomycetemcomitans* (Ramasubbu *et al.*, 2005), *N*-acetyl- $\beta$ -D-glucosaminidase from *Streptococcus gordonii* (Langley *et al.*, 2008),  $\beta$ -N-acetylhexosaminidase from *Paenibacillus sp.* (Sumida *et al.*, 2009), and  $\beta$ -N-acetylglucosaminidases from *Vibrio harveyi* 650 (Suginta *et al.*, 2010). While, only five bacterial GH-3 GlcNAcases have been characterized, including ExoII or NagZ from *Vibrio furnissii* (Chitlaru and Roseman, 1996), Nag3A from *Clostridium paraputrificum* M-21 (H. Li *et al.*, 2002), NagA from *Streptomyces thermoviolaceus* OPV-520 (Kubota *et al.*, 2004), NagA from *Thermotoga maritima*, and CbsA from *T. neapolitana* (Choi *et al.*, 2009). The mode of enzyme action of family 3 GlcNAcases has been proposed to be the double-displacement retaining mechanism, while the mode of enzyme action of family 20 GlcNAcases employs the substrate-assisted retaining mechanism, which is similar to family 18 chitinases (Vocadlo and Withers, 2005).

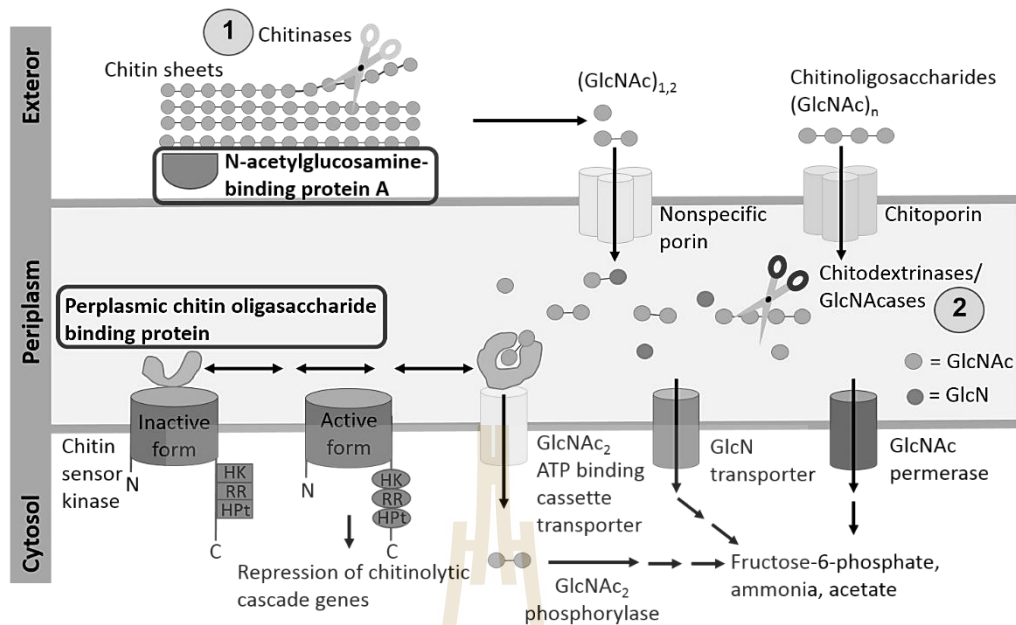


**Figure 5.1** Chitin degradation pathway of *Vibrio harveyi* class involves the successive action of two classes of chitinolytic enzymes 1) *VhChiA* and 2) *VhGlcNAcase* (Hjerde *et al.*, 2008; Xibing Li and Roseman, 2004; Xibing Li *et al.*, 2007; Suginta *et al.*, 2013a).

The catalytic mechanism of family 20 GlcNAcase employs the substrate-assisted retaining mechanism, involving the carbonyl of the 2-acetamido group that acts as a nucleophile to displace the aglycon leaving group with the net result being the formation of an oxazolinium ion intermediate. Afterwards, a water molecule attacks the anomeric center, breaking down the oxazolinium ring to generate the hemiacetal product with retained stereochemistry (Figure 5.2) (Vocadlo and Withers, 2005). The two key catalytic residues of family 20 glycoside hydrolases were identified previously by both structural and kinetic studies.

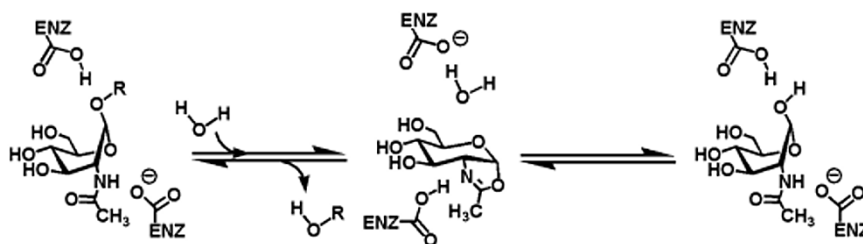


**Figure 5.2** The catalytic mechanism of GlcNAcase. Family 20 GlcNAcases use the 2-acetamido group of the substrate to act as nucleophile to form an oxazolinium ion intermediate (modified from Vocadlo and Withers, 2005).

According to the catalytic cycle of  $\beta$ -*N*-acetylglucosaminidase employs the Asp-Glu catalytic pair, where the aspartate and glutamate residues are immediately adjacent to each other in the sequence (Çetinbaş et al., 2006). Asp437 and Glu438 were shown to act as the catalytic pair of *Vh*GlcNAcase. The work studied by Meekrathok et al (SUT thesis, 2015) is presented in Figure 5.3.

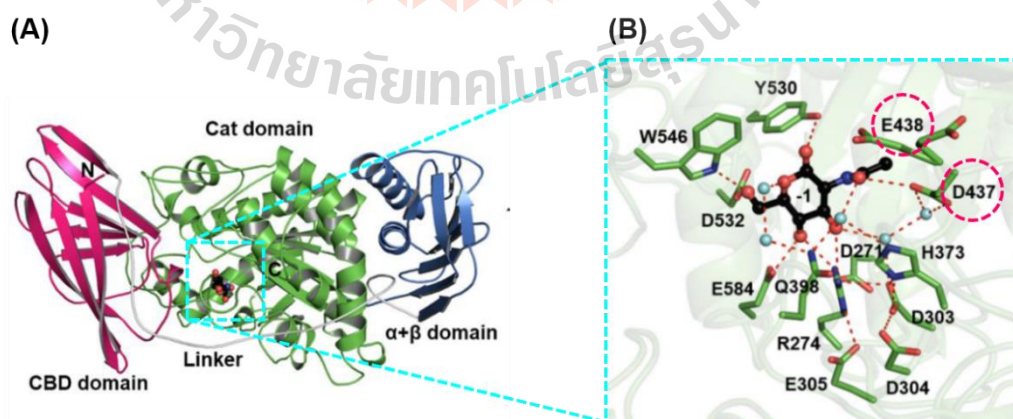


**Figure 5.3** Overall structure of GH20 *Vh*GlcNAcase consists of three domains. The N-terminal carbohydrate-binding domain is presented in dark pink, the  $\alpha$ + $\beta$  domain is



## 5.2 Material and methods

### 5.2.1 Materials

The genes encoding  $\beta$ -*N*-acetylglucosaminidase (*VhGlcNAcase*) was isolated from the genome of the marine bacterium *Vibrio harveyi*, cloned into pQE60 expression vector and expressed in *E. coli* M15 (pREP) type strain as described elsewhere (Suginta *et al.*, 2010). In this study, DNA constructs, namely and pQE60/*GlcNAcase* were used for high-level expression of *VhGlcNAcase*. The pQE60 plasmid contains an ampicillin resistance maker. Chemicals and reagents used for protein expression, purification and characterization were of analytical grade. *p*-Nitrophenol (*pNP*), *p*-nitrophenyl-*N*-acetyl-glucosaminide (*pNP-GlcNAc*) and 4-methylumbelliferyl *N*-acetyl- $\beta$ -D-glucosaminide (4MU-*GlcNAc*) were obtained through Italmar (Thailand) Co., Ltd. (Bangkok, Thailand) as a product of Sigma-Aldrich® (St. Louis, MO, USA). Phosphate buffer solution was prepared by mixing 0.1 M stock solutions of Na<sub>2</sub>HPO<sub>4</sub> and NaH<sub>2</sub>PO<sub>4</sub> to achieve the desired pH. The concentrations of *pNP* and 4MU are determined according to extinction coefficients of  $\epsilon_{405} = 18.5 \times 10^3 \text{ M}^{-1}\text{cm}^{-1}$  and  $\epsilon_{320} = 13.8 \times 10^3 \text{ M}^{-1}\text{cm}^{-1}$ , respectively.

### 5.2.2 Bacterial culture

The expression vector pQE60/*GlcNAcase* was transformed into expression host *E. coli* M15. The transformed cells were selected on LB agar containing 50  $\mu\text{g/mL}$  ampicillin and 25  $\mu\text{g/mL}$  kanamycin. The cells contains a kanamycin resistance maker. The colony of transformed cells was inoculated into 50 ml of a starting LB medium (in 250 ml Erlenmeyer flask). The culture contained 50  $\mu\text{g/ml}$  ampicillin, 25  $\mu\text{g/ml}$  kanamycin, and incubated overnight in an orbital shaker at 37°C,

200 rpm. The overnight culture of 10 ml was inoculated into large-scale cell culture of 1 liter for 6 liters of the LB medium containing 50 µg/mL ampicillin, 25 µg/ml kanamycin. The freshly inoculated culture was diluted to a ratio of 1:100 with LB broth medium, containing the same concentrations of ampicillin and kanamycin, and further grown at 37°C. The enzyme expression was induced with 0.4 mM isopropyl thio-β-D-galactoside (IPTG) when cell density is around 1.2 of absorbance at 600 nm. After adding IPTG, the temperature was lower to be 20°C, and the culture was further incubated overnight. The cells were harvested and the pellet cell was kept at -80°C until used.

### 5.2.3 Protein purification

The cell pellet was re-suspended in lysis buffer (60 µM phenylmethylsulfonyl fluoride (PMSF), 5% imidazole and 20 mM Tris-HCl buffer, pH 8.0 containing 150 mM NaCl). The cell debris was removed by centrifuge at 18,000 rpm at 4°C for 1 hours, while supernatant containing recombinant proteins was collected for purification.

Affinity chromatography was used in the first step of protein purification, *VhGlcNAcase*. The recombinant protein was expressed in *E. coli* M15 (pREP) cells with hexa-histidine tag attached at their C-terminal ends to aid purification by affinity chromatography. The cell suspension breakage was carried out using a 750 W ultrasonic processor Vibra cell model. Purification of the recombinant proteins was carried out initially using Ni-based immobilized metal affinity chromatography (IMAC) at 4°C. The supernatant containing soluble was gravitationally applied onto a Ni-based IMAC affinity column. The column was equilibrated with the equilibration

buffer (20 mM Tris-HCl, pH 8.0 containing 150 mM NaCl). After sample loading, the column was washed thoroughly with 200 mL of the equilibration buffer containing 20 mM imidazole and then eluted with 250 mM imidazole. The eluted fractions were concentrated to 5 mL using amicon cut off 10 kDa. Eluted fractions of 5 mL were collected and 15  $\mu$ L of each fraction was analyzed by 12 % SDS-PAGE, based on the method reported by Laemmli (Laemmli, 1970), to confirm the purity of the protein. The final protein concentration was determined using extinction coefficients at 280 nm (based on amino acid sequence) of  $119,500 \text{ M}^{-1} \text{ cm}^{-1}$ .

#### 5.2.4 Spectroscopic Studies

To determine an apparent catalytic constant ( $k_{cat}$ ), various concentrations of *p*NP-GlcNAc substrate were incubated with *Vh*GlcNAc, which was fixed at 0.05  $\mu$ M. Substrate concentrations of 1-320  $\mu$ M was prepared in 1 mL total volume of the reaction mixture. The absorbance of the releasing *p*NP product were measured by spectrophotometer at 405 nm. UV-visible absorbance spectra and fluorescence intensity were recorded using a Shimadzu 2550 spectrophotometer and Cary Eclipse spectrofluorometer, respectively. The catalytic activity of the enzyme was also performed using fluorescence properties of product 4-MU from the cleavage of the substrate 4MU-GlcNAc. All reactions were made in 100 mM phosphate buffer, pH 7.0 at 25°C. The fluorescence intensities were measured at a fixed excitation (slit width of 5 nm) and emission (slit width of 1 nm) wavelength of 324 nm and 448 nm, respectively.

Steady-state kinetic parameters were obtained using a continuous fluorescence spectrophotometric assay. To determine a catalytic constant ( $k_{cat}$ ) and  $K_m$ ,

various concentrations in the range of 1-40  $\mu\text{M}$  of 4MU-GlcNAc were used with enzyme concentration of 0.01  $\mu\text{M}$ . The concentrations of the fluorescence product were determined from a standard curve of in a range of concentrations of 0-12  $\mu\text{M}$ . The values of kinetic parameter were evaluated from three independent sets of data using the nonlinear regression function obtained from the KaleidaGraph 4.0 (Synergy Software, Reading, PA).

### 5.2.5 Pre-steady state kinetics

To investigate kinetic mechanism of *VhGlcNAc*, rapid kinetics were studied using stopped-flow spectrophotometry. The 4MU-GlcNAc (2  $\mu\text{M}$ ) was mixed with various *VhGlcNAc* enzyme concentrations. The reactions were performed in 100 mM phosphate buffer, pH 7.0. The single turnover catalytic reaction was monitored under enzyme concentrations that were at least 5-fold greater than substrate concentration. The reaction was monitored by following the fluorescence intensity change over 360 nm (cut off filter) with excitation wavelength of 324 nm. The observed rate constants and amplitudes of kinetic traces were analyzed using the Kinetic Studio software (TgK Scientific, Bradford-on-Avon, UK). The observed rate constants were plotted against enzyme concentrations to obtain the reaction mechanism. Alternatively, the raw data was imported into the computer program KaleidaGraph (Synergy Software, Reading, PA) and fit using similar equations. Fluorescence amplitude changes for a single-exponential transients obtained from the stopped-flow instrument.

## 5.3 Results

### 5.3.1 Steady-State Kinetics of *Vh*GlcNAc with fluorescence substrate

The reaction contained 0.01  $\mu\text{M}$  of *Vh*GlcNAc enzyme with various substrate concentrations; 1, 2, 4, 8, 16, 20 and 40  $\mu\text{M}$ , respectively. Figure 5.4A represents fluorescence intensity at 448 nm that was monitored as a function of time (time course) over a range of 0-100 sec. The Michaelis constant ( $K_m$ ), the apparent catalytic constant ( $k_{\text{cat}}$ ) and the maximum velocity ( $V_{\text{max}}$ ) were obtained from the experiments by using Michaelis-Menten equation, which showed a plot of hyperbolic curve. Figure 5.4B represents a hyperbolic curve that was constructed by the analysis of the experiments in Figure 5.4A. The  $V_{\text{max}}$  and  $K_m$  for the 4MU-GlcNAc catalyzed by *Vh*GlcNAc is 0.1148  $\mu\text{M sec}^{-1}$  and 21.20  $\mu\text{M}$ , respectively. Consequently, 11.48  $\text{sec}^{-1}$  is estimated for  $k_{\text{cat}}$  which was obtained by calculation with total enzyme concentration 0.01  $\mu\text{M}$ .

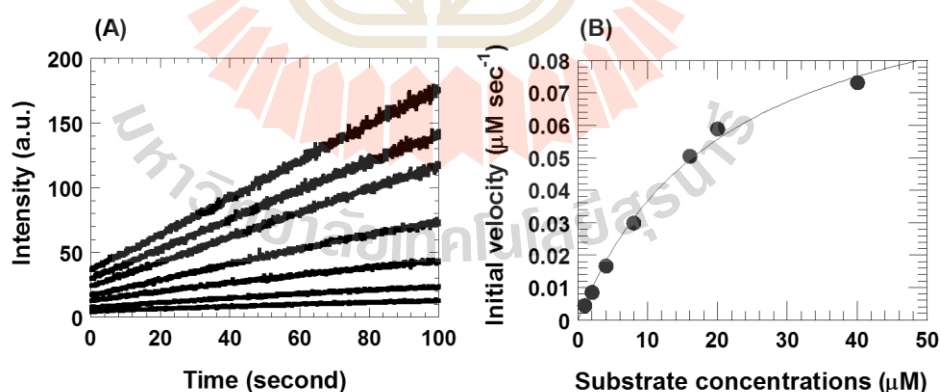


**Figure 5.4** The steady-state kinetic of *Vh*GlcNAc with 4MU-GlcNAc. The reactions contained 0.01  $\mu\text{M}$  enzyme with varied substrate concentrations of 1, 2, 4, 8, 16, 20 and 40  $\mu\text{M}$ . The initial velocity was monitored fluorescence intensity change at 448 nm (A). The plot of initial velocity and substrate concentrations allowed the determination of the  $V_{\text{max}}$ ,  $K_m$  and  $k_{\text{cat}}$  (B).

### 5.3.2 Pre-steady state kinetic and reaction mechanism with fluorescence substrate

The catalytic mechanism of *Vh*GlcNAc with 4MU-GlcNAc was studied using stopped-flow spectrophotometer in fluorescence mode. The 4MU-GlcNAc concentration of 2  $\mu\text{M}$  was mixed with various enzyme concentrations of 10, 20, 40, 80 and 113  $\mu\text{M}$  under pseudo-first order condition. Enzyme and substrate solution were contained in separate syringes before mixing. The concentrations as described were after mixing concentrations. The kinetic traces showed an increase in emission intensity greater than 360 nm from hydrolysis of glycosidic bond between 4MU and GlcNAc with producing of fluorophore substrate (4MU). The kinetic traces in Figure 5.5 from the lowest to the most upper traces are according to the lowest to the highest concentrations. The intensity change was analyzed as a single exponential curve. The observed rate constants were hyperbolically dependent on enzyme concentrations (inset of Figure 5.5). The non-linear plot between %intensity *versus* time indicated that the reaction mechanism of *Vh*GlcNAc with 4MU-GlcNAc is two-step process. The first step is rapid binding of enzyme to 4MU-GlcNAc following the catalytic bond cleavage to produce free fluorophore according to Figure 5.6.

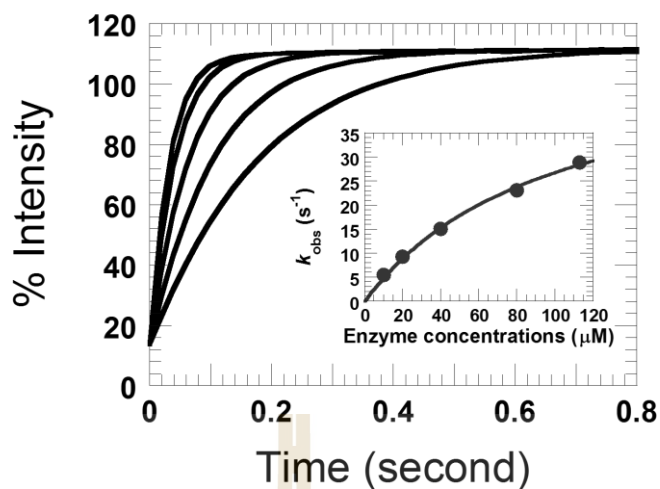


**Figure 5.5** Pre-steady state kinetics of *VhGlcNAc* with 4MU-GlcNAc. The 4MU-GlcNAc concentration of 2 μM was mixed with varied *VhGlcNAc* concentrations of 10, 20, 40, 80 and 113 μM (from lower to upper kinetic traces). All concentrations were after mixing concentrations. The reactions were performed in 100 mM phosphate buffer pH 7.0 at 25°C. The reaction was monitored the fluorescence intensity change (cut off  $\geq 360$  nm). The kinetic trace was analyzed as single exponential. A plot of observed rate constants versus enzyme concentrations was hyperbolically dependent (inset).

The hyperbolic dependence of the observed rate constants with enzyme concentrations was fitted according to Equation 5.2. The enzyme concentration that gives a half-saturation value of the plot which is equivalent to the  $K_d$  (Figure 5.5) for binding of 4MU-GlcNAc to the *VhGlcNAc* is 99 μM. The observed rate constant approaches the limiting value of  $53 \pm 4$  s<sup>-1</sup> indicates for glycosidic bond cleavage ( $k_2$  in Figure 5.6).

$$k_{obs} = \frac{k_2[E]}{K_d + [E]} \quad \text{Equation 5.2}$$

The  $k_{cat}$  value of  $11.5 \text{ s}^{-1}$  obtained from steady-state turnover of enzyme was slightly less than the rate constant for glycosidic bond cleavage. This demonstrated that the steps of glycosidic bond cleavage and GlcNAc product release are partially-rate limiting step ( $k_3$  in Figure 5.6). Based on rapid-equilibrium binding of enzyme and substrate, the  $k_3$  of product releasing step was calculated from the  $k_{cat}$  as described in Equation 5.3.

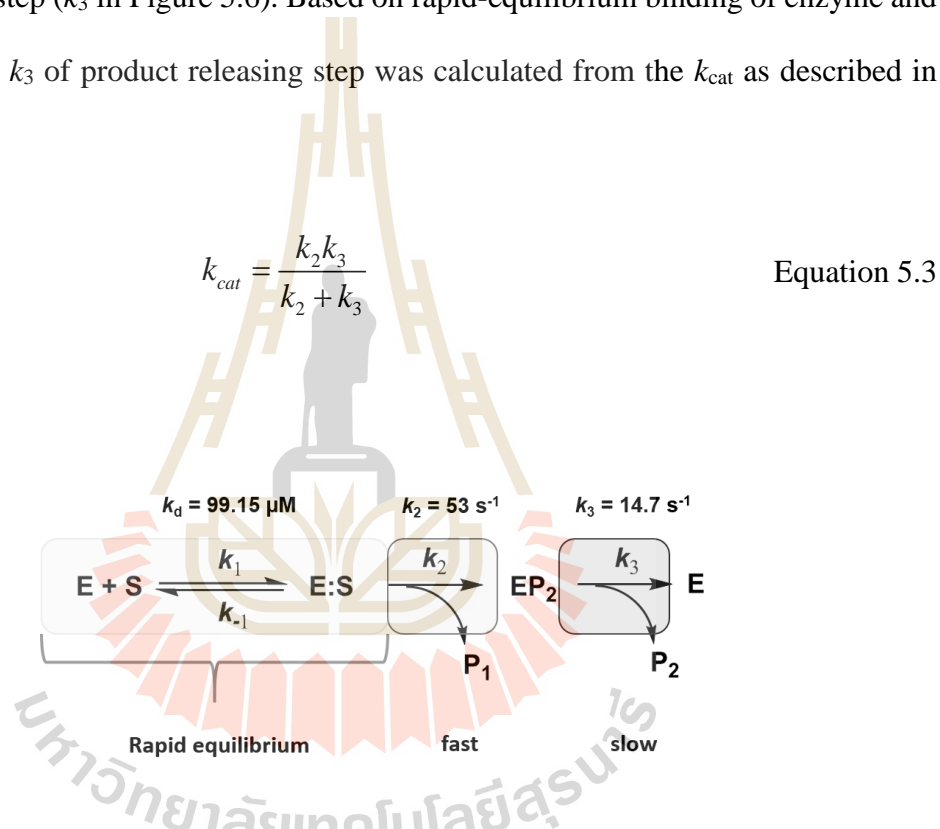


**Figure 5.6** The catalytic mechanism of  $\beta$ -*N*-acetylglucosaminidase enzyme toward 4MU-GlcNAc substrate.

### 5.3.3 Steady-State Kinetics of *Vh*GlcNAc with *p*NP-GlcNAc

The effects on kinetic properties of *Vh*GlcNAc enzyme toward the 4-nitrophenyl *N*-acetyl- $\beta$ -D-glucosaminide (*p*NP-GlcNAc) substrate. The experiments were carried out in 0.1 M phosphate buffer solution, pH 7.0. A reaction mixture was

prepared in a cuvette (1 mL) and contained constant concentration of *Vh*GlcNAc enzyme with various substrate concentration; 1, 2, 4, 8, 16, 20, 40, 80, 160 and 320  $\mu\text{M}$ , respectively. Figure 5.7 is Michaelis-Menten type plot that was constructed by the analysis of the absorbance value plot as a function of time. The  $V_{max}$  and  $K_m$  values determination for the *p*NP-GlcNAc are 0.06  $\mu\text{M s}^{-1}$  and 51  $\mu\text{M}$ , respectively. The turnover number ( $k_{cat}$ ) is calculated based on total enzyme concentration of 0.05  $\mu\text{M}$  is 1.2  $\text{s}^{-1}$ .

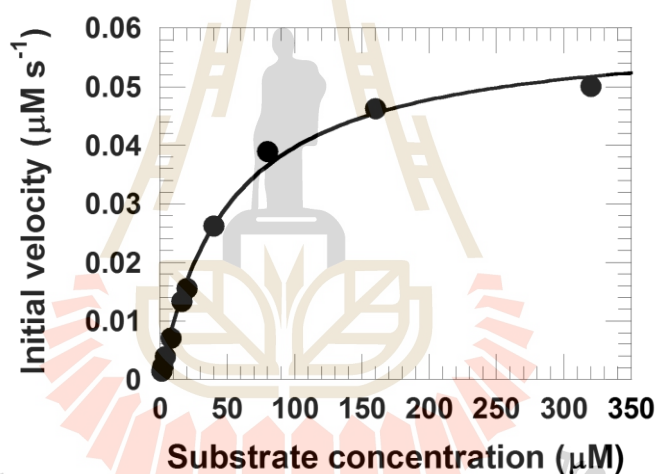


**Figure 5.7** The steady-state kinetic of *Vh*GlcNAc with *p*NP-GlcNAc. The reaction contained 0.05  $\mu\text{M}$  enzyme and varied *p*NP-GlcNAc concentrations of 1, 2, 4, 6, 8, 16, 20, 40, 80, 160 and 320  $\mu\text{M}$ . The initial velocity was monitored absorbance change at 405 nm. The plot of initial velocity and substrate concentrations determined the  $V_{max}$ ,  $K_m$  and catalytic constant ( $k_{cat}$ ).

## 5.4 Discussion

This study reports the kinetics action of mechanism of  $\beta$ -*N*-acetylglucosaminidase from *Vibrio harveyi* (*VhGlcNAcase*) enzyme using pre-steady state and steady-state experiment. The pre-steady state using stopped-flow spectrophotometer in fluorescence mode and steady-state using fluorometric assay, both of them were conducted using the substrate analogue, 4-methylumbelliferyl-*N*-acetyl- $\beta$ -D-glucosaminide (4MU-GlcNAc). The hydrolysis of this substrate was followed continuously at pH7.0 by measuring the production of the free fluorophore.

The results reveal for the first time the catalytic features of 4MU-GlcNAc by GH20 *VhGlcNAcase*. The data reported here help to understand the catalytic step introduced in the mechanism of the enzyme presented in Figure 5.8. The  $k_{cat}$  obtained from the stopped-flow experiments ( $53 \pm 4 \text{ s}^{-1}$ ) was compared to the  $k_{cat}$  determined in steady state studies ( $11.5 \text{ s}^{-1}$ ) with the same substrate analogue; the two rates were found to be distinguishable within experiment but not much. In previous report, Jones and Kosman (1980) studied the kinetics action of mechanism of  $\beta$ -*N*-acetylglucosaminidase from *Aspergillus niger* in a different condition from our work. They discovered that the catalytic step was a sequential mechanism. The enzymatic hydrolysis were conducted continuously in sodium citrate (pH4.6) using the substrate analogue, 2,4-diNP- $\beta$ GlcNAc. The  $k_{cat}$  obtained from the stopped-flow experiments ( $1958 \pm 150 \text{ min}^{-1}$ ) was compared to the  $k_{cat}$  determined in steady state studies ( $2300 \pm 250 \text{ min}^{-1}$ ) with the same substrate analogue; the two rates were found to be indistinguishable within experiment.

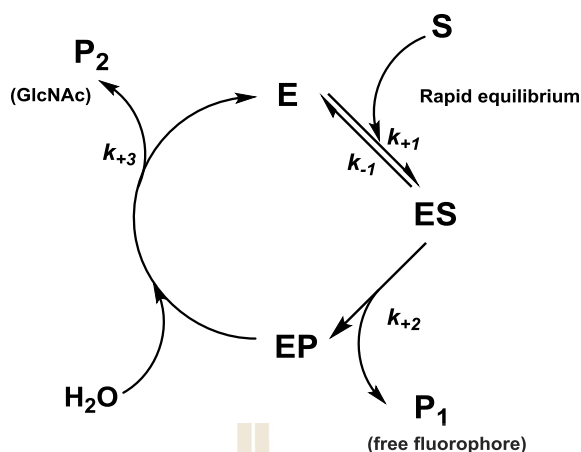


**Figure 5.8** The kinetic mechanism for the reaction of *VhGlcNAcase* catalyzed fluorogenic substrate.

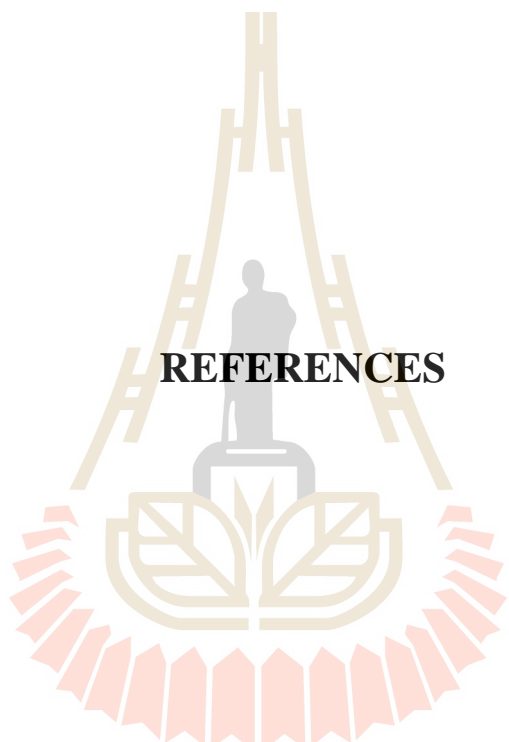
In steady state, absorption substrate was studied in order to find out the kinetic parameters, there is the *pNP*-GlcNAc substrate catalysis by GH20 *VhGlcNAcase* in the same measuring buffer condition. The  $k_{cat}$  obtained from the absorption experiments ( $1.2 \text{ s}^{-1}$ ) was compared to the  $k_{cat}$  determined in fluorescence studies ( $11.5 \text{ s}^{-1}$ ), the value show distinguish value which indicated that *VhGlcNAcase* enzyme have specific activity with 4MU-GlcNAc better than *pNP*-GlcNAc. The study by Jones and Kosman (1980) was obtained the  $k_{cat}$  in steady state studies ( $2300 \pm 250 \text{ min}^{-1}$ ) with the 2,4-diNP- $\beta$ GlcNAc substrate, when compared with our work the enzyme can convert substrate to product faster than 4MU-GlcNAc and *pNP*-GlcNAc.

The steady-state kinetic studies from Jones and Kosman (1980) established a  $K_m$  value of 0.27 mM for the 2,4-diNP- $\beta$ GlcNAc substrate found the comparable value with *pNP*- $\beta$ GlcNAc substrate (0.34 mM) of their experiments. In the previous studies, Suginta and co-worker (2010) established the  $K_m$  value of 0.077 mM for *pNP*-GlcNAc

substrate catalyzed by *VhGlcNAcase* (GH20). In our experiment, we obtained a  $K_m$  value of 0.051 mM with the same substrate and enzyme as Suginta studied, thus demonstrating a substrate concentration dependence comparable to that observed for the *p*-nitrophenyl derivative for the same enzyme and the substrate.

## 5.5 Conclusions

This part of work has elucidated the reaction mechanism of  $\beta$ -N-acetylglucosaminidase from *Vibrio harveyi* (*VhGlcNAc*). The results clearly show that the reaction mechanism of *VhGlcNAc* with 4MU-GlcNAc is two-step process. The first step is rapid binding of enzyme to 4MU-GlcNAc following the catalytic bond cleavage to produce free fluorophore, for the glycosidic bond cleavage and GlcNAc product is released in partially-rate limiting step.



**REFERENCES**

มหาวิทยาลัยเทคโนโลยีสุรนารี

## REFERENCES

- Afreen, S., Muthoosamy, K., Manickam, S., and Hashim, U. (2015). Functionalized Fullerene (C60) as a Potential Nanomediator in the Fabrication of Highly Sensitive Biosensors. **Biosensors and bioelectronics**. 63: 354-364.
- Agüí, L., Yáñez-Sedeño, P., and Pingarrón, J. M. (2008). Role of Carbon Nanotubes in Electroanalytical Chemistry: A Review. **Analytica Chimica Acta**. 622(1-2): 11-47.
- Ahammad, A., Lee, J.-J., and Rahman, M. A. (2009). Electrochemical Sensors Based on Carbon Nanotubes. **Sensors**. 9(4): 2289-2319.
- Ajayan, P. (1999). Nanotubes from Carbon. **Chemical reviews**. 99(7): 1787-1800.
- Alizadeh, T., Ganjali, M. R., Norouzi, P., Zare, M., and Zeraatkar, A. (2009). A Novel High Selective and Sensitive Para-Nitrophenol Voltammetric Sensor, Based on a Molecularly Imprinted Polymer–Carbon Paste Electrode. **Talanta**. 79(5): 1197-1203.
- Alpat, Ş., and Telefoncu, A. (2010). Development of an Alcohol Dehydrogenase Biosensor for Ethanol Determination with Toluidine Blue O Covalently Attached to a Cellulose Acetate Modified Electrode. **Sensors**. 10(1): 748-764.
- Arslan, F., Ustabaş, S., and Arslan, H. (2011). An Amperometric Biosensor for Glucose Determination Prepared from Glucose Oxidase Immobilized in Polyaniline-Polyvinylsulfonate Film. **Sensors**. 11(8): 8152-8163.

- Arvinte, A., Mahosenaho, M., Pinteala, M., Sesay, A.-M., and Virtanen, V. (2011). Electrochemical Oxidation of P-Nitrophenol Using Graphene-Modified Electrodes, and a Comparison to the Performance of Mwnt-Based Electrodes. **Microchimica Acta**. 174(3-4): 337-343.
- Balasubramanian, K., and Burghard, M. (2006). Biosensors Based on Carbon Nanotubes. **Analytical and bioanalytical chemistry**. 385(3): 452-468.
- Batra, B., Narwal, V., and Pundir, C. S. (2016). An Amperometric Lactate Biosensor Based on Lactate Dehydrogenase Immobilized onto Graphene Oxide Nanoparticles-Modified Pencil Graphite Electrode. **Engineering in Life Sciences**. 16(8): 786-794.
- Batra, B., and Pundir, C. (2013). An Amperometric Glutamate Biosensor Based on Immobilization of Glutamate Oxidase onto Carboxylated Multiwalled Carbon Nanotubes/Gold Nanoparticles/Chitosan Composite Film Modified Au Electrode. **Biosensors and bioelectronics**. 47: 496-501.
- Boujtita, M., Hart, J. P., and Pittson, R. (2000). Development of a Disposable Ethanol Biosensor Based on a Chemically Modified Screen-Printed Electrode Coated with Alcohol Oxidase for the Analysis of Beer. **Biosensors and bioelectronics**. 15(5-6): 257-263.
- Boussema, F., Gross, A. J., Hmida, F., Ayed, B., Majdoub, H., Cosnier, S., Maaref, A., and Holzinger, M. (2018). Dawson-Type Polyoxometalate Nanoclusters Confined in a Carbon Nanotube Matrix as Efficient Redox Mediators for Enzymatic Glucose Biofuel Cell Anodes and Glucose Biosensors. **Biosensors and bioelectronics**. 109: 20-26.

- Brena, B., González-Pombo, P., and Batista-Viera, F. (2013). Immobilization of Enzymes: A Literature Survey. In **Immobilization of Enzymes and Cells**. (pp. 15-31): Springer.
- Brondani, D., Dupont, J., Spinelli, A., and Vieira, I. C. (2009). Development of Biosensor Based on Ionic Liquid and Corn Peroxidase Immobilized on Chemically Crosslinked Chitin. **Sensors and Actuators B: Chemical**. 138(1): 236-243.
- Brooks, H. B., and Davidson, V. L. (1993). A Method for Extracting Rate Constants from Initial Rates of Stopped-Flow Kinetic Data: Application to a Physiological Electron-Transfer Reaction. **Biochemical journal**. 294(1): 211-213.
- Bullock, C. (1995). Immobilized Enzymes. **Science Progress**. 78: 119-134.
- Cai, C., and Chen, J. (2004). Direct Electron Transfer of Glucose Oxidase Promoted by Carbon Nanotubes. **Analytical biochemistry**. 332(1): 75-83.
- Cai, C., Chen, J., and Lu, T. (2004). Direct Electron Transfer of Glucose Oxidase on the Carbon Nanotube Electrode. **Science in China Series B: Chemistry**. 47(2): 113-119.
- Carrazón, J. P., Vergara, A. G., Garcia, A. R., and Diez, L. P. (1989). Determination of Coumarins by Voltammetric Techniques in Micellar and Emulsified Media. **Analytica Chimica Acta**. 216: 231-242.
- Cass, A. E., Davis, G., Francis, G. D., Hill, H. A. O., Aston, W. J., Higgins, I. J., Plotkin, E. V., Scott, L. D., and Turner, A. P. (1984). Ferrocene-Mediated Enzyme Electrode for Amperometric Determination of Glucose. **Analytical Chemistry**. 56(4): 667-671.

- Castillo, J., Gáspár, S., Leth, S., Niculescu, M., Mortari, A., Bontidean, I., Soukharev, V., Dorneanu, S., Ryabov, A., and Csöregi, E. (2004). Biosensors for Life Quality: Design, Development and Applications. **Sensors and Actuators B: Chemical**. 102(2): 179-194.
- Çetinbaş, N., Macauley, M. S., Stubbs, K. A., Drapala, R., and Vocadlo, D. J. (2006). Identification of Asp174 and Asp175 as the Key Catalytic Residues of Human O-GlcNacase by Functional Analysis of Site-Directed Mutants. **Biochemistry**. 45(11): 3835-3844.
- Cha, S. (1968). A Simple Method for Derivation of Rate Equations for Enzyme-Catalyzed Reactions under the Rapid Equilibrium Assumption or Combined Assumptions of Equilibrium and Steady State. **Journal of Biological Chemistry**. 243(4): 820-825.
- Chaplin, M. F., and Bucke, C. (1990). **Enzyme Technology**. CUP Archive.
- Chaubey, A., Gerard, M., Singhal, R., Singh, V., and Malhotra, B. (2001). Immobilization of Lactate Dehydrogenase on Electrochemically Prepared Polypyrrole–Polyvinylsulphonate Composite Films for Application to Lactate Biosensors. **Electrochimica Acta**. 46(5): 723-729.
- Chaubey, A., and Malhotra, B. (2002). Mediated Biosensors. **Biosensors and bioelectronics**. 17(6-7): 441-456.
- Che, X., Yuan, R., Chai, Y., Li, J., Song, Z., and Li, W. (2010). Amperometric Glucose Biosensor Based on Prussian Blue–Multiwall Carbon Nanotubes Composite and Hollow Ptco Nanochains. **Electrochimica Acta**. 55(19): 5420-5427.
- Che, X., Yuan, R., Chai, Y., Li, J., Song, Z., Li, W., and Zhong, X. (2011). A Glucose Biosensor Based on Chitosan–Prussian Blue–Multiwall Carbon Nanotubes–

- Hollow Ptco Nanochains Formed by One-Step Electrodeposition. **Colloids and Surfaces B: Biointerfaces**. 84(2): 454-461.
- Chen, W. R. (2013). Chitin, Chitosan, and Glycated Chitosan Regulate Immune Responses: The Novel Adjuvants for Cancer Vaccine. **Clinical and Developmental Immunology**. 2013.
- Chen, X., Jia, J., and Dong, S. (2003). Organically Modified Sol-Gel/Chitosan Composite Based Glucose Biosensor. **Electroanalysis**. 15(7): 608-612.
- Chitlaru, E., and Roseman, S. (1996). Molecular Cloning and Characterization of a Novel B-N-Acetyl-D-Glucosaminidase from *Vibrio Furnissii*. **Journal of Biological Chemistry**. 271(52): 33433-33439.
- Choi, K.-H., Seo, J. Y., Park, K.-M., Park, C.-S., and Cha, J. (2009). Characterization of Glycosyl Hydrolase Family 3 B-N-Acetylglucosaminidases from *Thermotoga Maritima* and *Thermotoga Neapolitana*. **Journal of bioscience and bioengineering**. 108(6): 455-459.
- Claussen, J. C., Franklin, A. D., ul Haque, A., Porterfield, D. M., and Fisher, T. S. (2009). Electrochemical Biosensor of Nanocube-Augmented Carbon Nanotube Networks. **ACS nano**. 3(1): 37-44.
- Cogal, S., Celik Cogal, G., and Oksuz, A. U. (2018). Plasma-Modified Multiwalled Carbon Nanotubes with Polyaniline for Glucose Biosensor Applications. **International Journal of Polymeric Materials and Polymeric Biomaterials**. 67(7): 454-461.
- Cohen-Kupiec, R., and Chet, I. (1998). The Molecular Biology of Chitin Digestion. **Current opinion in biotechnology**. 9(3): 270-277.

- Comba, F. N., Romero, M. R., Garay, F. S., and Baruzzi, A. M. (2018). Mucin and Carbon Nanotube-Based Biosensor for Detection of Glucose in Human Plasma. **Analytical biochemistry**. 550: 34-40.
- Copeland, R. A. (1997). Enzymes: A Practical Introduction to Structure, Mechanism, and Data Analysis. **Biomedicine & Pharmacotherapy**. 4(51): 187.
- Copeland, R. A. (2004). **Enzymes: A Practical Introduction to Structure, Mechanism, and Data Analysis**. John Wiley & Sons.
- Cosnier, S. (1999). Biomolecule Immobilization on Electrode Surfaces by Entrapment or Attachment to Electrochemically Polymerized Films. A Review. **Biosensors and bioelectronics**. 14(5): 443-456.
- Cui, X., Li, C. M., Zang, J., and Yu, S. (2007). Highly Sensitive Lactate Biosensor by Engineering Chitosan/Pvi-Os/Cnt/Lod Network Nanocomposite. **Biosensors and bioelectronics**. 22(12): 3288-3292.
- Datta, S., Christena, L. R., and Rajaram, Y. R. S. (2013). Enzyme Immobilization: An Overview on Techniques and Support Materials. **3 Biotech**. 3(1): 1-9.
- Devasenathipathy, R., Mani, V., Chen, S.-M., Huang, S.-T., Huang, T.-T., Lin, C.-M., Hwa, K.-Y., Chen, T.-Y., and Chen, B.-J. (2015). Glucose Biosensor Based on Glucose Oxidase Immobilized at Gold Nanoparticles Decorated Graphene-Carbon Nanotubes. **Enzyme and microbial technology**. 78: 40-45.
- Dong, S., Wang, B., and Liu, B. (1992). Amperometric Glucose Sensor with Ferrocene as an Electron Transfer Mediator. **Biosensors and bioelectronics**. 7(3): 215-222.
- Fan, P., Liu, L., Guo, Q., Wang, J., Yang, J., Guan, X., Chen, S., and Hou, H. (2017). Three-Dimensional N-Doped Carbon Nanotube@ Carbon Foam Hybrid: An

- Effective Carrier of Enzymes for Glucose Biosensors. **RSC Advances**. 7(43): 26574-26582.
- Fatoni, A., Numnuam, A., Kanatharana, P., Limbut, W., Thammakhet, C., and Thavarungkul, P. (2013). A Highly Stable Oxygen-Independent Glucose Biosensor Based on a Chitosan-Albumin Cryogel Incorporated with Carbon Nanotubes and Ferrocene. **Sensors and Actuators B: Chemical**. 185: 725-734.
- Frascione, N., Pinto, V., and Daniel, B. (2012). Development of a Biosensor for Human Blood: New Routes to Body Fluid Identification. **Analytical and bioanalytical chemistry**. 404(1): 23-28.
- Frasco, M. F., and Chaniotakis, N. (2009). Semiconductor Quantum Dots in Chemical Sensors and Biosensors. **Sensors**. 9(9): 7266-7286.
- Freire, R. S., Pessoa, C. A., Mello, L. D., and Kubota, L. T. (2003). Direct Electron Transfer: An Approach for Electrochemical Biosensors with Higher Selectivity and Sensitivity. **Journal of the Brazilian Chemical Society**. 14(2): 230-243.
- Frew, J. E., and Hill, H. A. O. (1988). Direct and Indirect Electron Transfer between Electrodes and Redox Proteins. **The FEBS Journal**. 172(2): 261-269.
- Garcia, A., Peniche-Covas, C., Chico, B., Simpson, B. K., and Villalonga, R. (2007). Ferrocene Branched Chitosan for the Construction of a Reagentless Amperometric Hydrogen Peroxide Biosensor. **Macromolecular bioscience**. 7(4): 435-439.
- Gavalas, V. G., and Chaniotakis, N. A. (2000). [60] Fullerene-Mediated Amperometric Biosensors. **Analytica Chimica Acta**. 409(1-2): 131-135.
- Gooding, J. J., Chou, A., Liu, J., Losic, D., Shapter, J. G., and Hibbert, D. B. (2007). The Effects of the Lengths and Orientations of Single-Walled Carbon

Nanotubes on the Electrochemistry of Nanotube-Modified Electrodes. **Electrochemistry Communications**. 9(7): 1677-1683.

Gorton, L., Lindgren, A., Larsson, T., Munteanu, F., Ruzgas, T., and Gazaryan, I. (1999). Direct Electron Transfer between Heme-Containing Enzymes and Electrodes as Basis for Third Generation Biosensors. **Analytica Chimica Acta**. 400(1-3): 91-108.

Grieshaber, D., MacKenzie, R., Voeroes, J., and Reimhult, E. (2008). Electrochemical Biosensors-Sensor Principles and Architectures. **Sensors**. 8(3): 1400-1458.

Gülce, H., Gülce, A., Kavanoz, M., Coşkun, H., and Yıldız, A. (2002). A New Amperometric Enzyme Electrode for Alcohol Determination. **Biosensors and bioelectronics**. 17(6-7): 517-521.

Guo, Y., Li, J., and Dong, S. (2011). Hemin Functionalized Graphene Nanosheets-Based Dual Biosensor Platforms for Hydrogen Peroxide and Glucose. **Sensors and Actuators B: Chemical**. 160(1): 295-300.

Gupta, S., Murthy, C., and Prabha, C. R. (2017). Recent Advances in Carbon Nanotube Based Electrochemical Biosensors. **International journal of biological macromolecules**. 108: 687-703.

Guzsvany, V., Anojcic, J., Radulovic, E., Vajdle, O., Stankovic, I., Madarasz, D., Konya, Z., and Kalcher, K. (2017). Screen-Printed Enzymatic Glucose Biosensor Based on a Composite Made from Multiwalled Carbon Nanotubes and Palladium Containing Particles. **Microchimica Acta**. 184(7): 1987-1996.

- Guzsvány, V., Anojčić, J., Radulović, E., Vajdle, O., Stanković, I., Madarász, D., Kónya, Z., and Kalcher, K. (2017). Screen-Printed Enzymatic Glucose Biosensor Based on a Composite Made from Multiwalled Carbon Nanotubes and Palladium Containing Particles. **Microchimica Acta**. 184(7): 1987-1996.
- Harris, T., and Keshwani, M. (2009). Measurement of Enzyme Activity. In **Methods in Enzymology**. (Vol. 463, pp. 57-71): Elsevier.
- Harvey, A. J., Hrmova, M., De Gori, R., Varghese, J. N., and Fincher, G. B. (2000). Comparative Modeling of the Three-Dimensional Structures of Family 3 Glycoside Hydrolases. **Proteins: Structure, Function, and Bioinformatics**. 41(2): 257-269.
- Hasan, F., Shah, A. A., and Hameed, A. (2009). Methods for Detection and Characterization of Lipases: A Comprehensive Review. **Biotechnology advances**. 27(6): 782-798.
- Heller, I., Kong, J., Williams, K. A., Dekker, C., and Lemay, S. G. (2006). Electrochemistry at Single-Walled Carbon Nanotubes: The Role of Band Structure and Quantum Capacitance. **Journal of the American Chemical Society**. 128(22): 7353-7359.
- Henrissat, B., and Bairoch, A. (1993). New Families in the Classification of Glycosyl Hydrolases Based on Amino Acid Sequence Similarities. **Biochemical journal**. 293(3): 781-788.
- Henrissat, B., and Davies, G. (1997). Structural and Sequence-Based Classification of Glycoside Hydrolases. **Current opinion in structural biology**. 7(5): 637-644.

- Herschkovitz, Y., Eshkenazi, I., Campbell, C., and Rishpon, J. (2000). An Electrochemical Biosensor for Formaldehyde. **Journal of Electroanalytical Chemistry**. 491(1-2): 182-187.
- Hjerde, E., Lorentzen, M. S., Holden, M. T., Seeger, K., Paulsen, S., Bason, N., Churcher, C., Harris, D., Norbertczak, H., and Quail, M. A. (2008). The Genome Sequence of the Fish Pathogen *Aliivibrio Salmonicida* Strain Lfi1238 Shows Extensive Evidence of Gene Decay. **BMC genomics**. 9(1): 616.
- Hu, H., Feng, M., and Zhan, H. (2015). A Glucose Biosensor Based on Partially Unzipped Carbon Nanotubes. **Talanta**. 141: 66-72.
- Ibrahim, A. A., Umar, A., Ahmad, R., Kumar, R., and Baskoutas, S. (2016). Fabrication and Characterization of Highly Sensitive and Selective Glucose Biosensor Based on ZnO Decorated Carbon Nanotubes. **Nanoscience and Nanotechnology Letters**. 8(10): 853-858.
- Jones, C. S., and Kosman, D. (1980). Purification, Properties, Kinetics, and Mechanism of Beta-N-Acetylglucosamidase from *Aspergillus Niger*. **Journal of Biological Chemistry**. 255(24): 11861-11869.
- Jose, M. V., Marx, S., Murata, H., Koepsel, R. R., and Russell, A. J. (2012). Direct Electron Transfer in a Mediator-Free Glucose Oxidase-Based Carbon Nanotube-Coated Biosensor. **Carbon**. 50(11): 4010-4020.
- Joshi, P. P., Merchant, S. A., Wang, Y., and Schmidtke, D. W. (2005). Amperometric Biosensors Based on Redox Polymer– Carbon Nanotube– Enzyme Composites. **Analytical Chemistry**. 77(10): 3183-3188.

- Kadokura, K., Sakamoto, Y., Saito, K., Ikegami, T., Hirano, T., Hakamata, W., Oku, T., and Nishio, T. (2007). Production of a Recombinant Chitin Oligosaccharide Deacetylase from *Vibrio Parahaemolyticus* in the Culture Medium of *Escherichia Coli* Cells. **Biotechnology letters**. 29(8): 1209.
- Kamyabi, M. A., Hajari, N., Turner, A. P. F., and Tiwari, A. (2016). A High-Performance Glucose Biosensor Using Covalently Immobilised Glucose Oxidase on a Poly(2,6-Diaminopyridine)/Carbon Nanotube Electrode (Vol 116, Pg 801, 2013). **Talanta**. 153: 414-415.
- Kang, X., Wang, J., Wu, H., Aksay, I. A., Liu, J., and Lin, Y. (2009). Glucose Oxidase–Graphene–Chitosan Modified Electrode for Direct Electrochemistry and Glucose Sensing. **Biosensors and bioelectronics**. 25(4): 901-905.
- Kaushik, A., Khan, R., Solanki, P. R., Pandey, P., Alam, J., Ahmad, S., and Malhotra, B. (2008). Iron Oxide Nanoparticles–Chitosan Composite Based Glucose Biosensor. **Biosensors and bioelectronics**. 24(4): 676-683.
- Kitchen, B., Middleton, G., and Salmon, M. (1978). Bovine Milk N-Acetyl-B-D-Glucosaminidase and Its Significance in the Detection of Abnormal Udder Secretions. **Journal of Dairy Research**. 45(1): 15-20.
- Kittle, J. D., Wang, C., Qian, C., Zhang, Y., Zhang, M., Roman, M., Morris, J. R., Moore, R. B., and Esker, A. R. (2012). Ultrathin Chitin Films for Nanocomposites and Biosensors. **Biomacromolecules**. 13(3): 714-718.
- Kong, T., Chen, Y., Ye, Y., Zhang, K., Wang, Z., and Wang, X. (2009). An Amperometric Glucose Biosensor Based on the Immobilization of Glucose Oxidase on the ZnO Nanotubes. **Sensors and Actuators B: Chemical**. 138(1): 344-350.

- Krajewska, B. (2004). Application of Chitin-and Chitosan-Based Materials for Enzyme Immobilizations: A Review. **Enzyme and microbial technology**. 35(2-3): 126-139.
- Krapf, D., Quinn, B. M., Wu, M.-Y., Zandbergen, H. W., Dekker, C., and Lemay, S. G. (2006). Experimental Observation of Nonlinear Ionic Transport at the Nanometer Scale. **Nano letters**. 6(11): 2531-2535.
- Kricka, L. J., Voyta, J. C., and Bronstein, I. (2000). Chemiluminescent Methods for Detecting and Quantitating Enzyme Activity.
- Kubota, T., Miyamoto, K., Yasuda, M., Inamori, Y., and Tsujibo, H. (2004). Molecular Characterization of an Intracellular B-N-Acetylglucosaminidase Involved in the Chitin Degradation System of *Streptomyces Thermoviolaceus* Opc-520. **Bioscience, biotechnology, and biochemistry**. 68(6): 1306-1314.
- Kurzawa, C., Hengstenberg, A., and Schuhmann, W. (2002). Immobilization Method for the Preparation of Biosensors Based on Ph Shift-Induced Deposition of Biomolecule-Containing Polymer Films. **Analytical Chemistry**. 74(2): 355-361.
- Laemmli, U. K. (1970). Cleavage of Structural Proteins During the Assembly of the Head of Bacteriophage T4. **Nature**. 227(5259): 680.
- Langley, D. B., Harty, D. W., Jacques, N. A., Hunter, N., Guss, J. M., and Collyer, C. A. (2008). Structure of N-Acetyl-B-D-Glucosaminidase (Gna) from the Endocarditis Pathogen *Streptococcus Gordonii* and Its Complex with the Mechanism-Based Inhibitor Nag-Thiazoline. **Journal of molecular biology**. 377(1): 104-116.

- Laviron, E. (1979). General Expression of the Linear Potential Sweep Voltammogram in the Case of Diffusionless Electrochemical Systems. **Journal of Electroanalytical Chemistry and Interfacial Electrochemistry**. 101(1): 19-28.
- Li, H., Morimoto, K., Katagiri, N., Kimura, T., Sakka, K., Lun, S., and Ohmiya, K. (2002). A Novel B-N-Acetylglucosaminidase of *Clostridium Paraputrificum* M-21 with High Activity on Chitobiose. **Applied microbiology and biotechnology**. 60(4): 420-427.
- Li, L., Sheng, Q., Zheng, J., and Zhang, H. (2008). Facile and Controllable Preparation of Glucose Biosensor Based on Prussian Blue Nanoparticles Hybrid Composites. **Bioelectrochemistry**. 74(1): 170-175.
- Li, X., and Roseman, S. (2004). The Chitinolytic Cascade in *Vibrios* Is Regulated by Chitin Oligosaccharides and a Two-Component Chitin Catabolic Sensor/Kinase. **Proceedings of the National Academy of Sciences of the United States of America**. 101(2): 627-631.
- Li, X., Wang, L.-X., Wang, X., and Roseman, S. (2007). The Chitin Catabolic Cascade in the Marine Bacterium *Vibrio Cholerae*: Characterization of a Unique Chitin Oligosaccharide Deacetylase. **Glycobiology**. 17(12): 1377-1387.
- Li, X., Zhou, Y., Zheng, Z., Yue, X., Dai, Z., Liu, S., and Tang, Z. (2009). Glucose Biosensor Based on Nanocomposite Films of Cdte Quantum Dots and Glucose Oxidase. **Langmuir**. 25(11): 6580-6586.
- Liang, B., Zhang, S., Lang, Q., Song, J., Han, L., and Liu, A. (2015). Amperometric L-Glutamate Biosensor Based on Bacterial Cell-Surface Displayed Glutamate Dehydrogenase. **Analytica Chimica Acta**. 884: 83-89.

- Lin, Y., Lu, F., Tu, Y., and Ren, Z. (2004). Glucose Biosensors Based on Carbon Nanotube Nanoelectrode Ensembles. **Nano letters**. 4(2): 191-195.
- Linko-Löppönen, S., and Mäkinen, M. (1985). A Microtiter Plate Assay for N-Acetyl-B-D-Glucosaminidase Using a Fluorogenic Substrate. **Analytical biochemistry**. 148(1): 50-53.
- Liu, J., Sun, S., Shang, H., Lai, J., and Zhang, L. (2016). Electrochemical Biosensor Based on Bienzyme and Carbon Nanotubes Incorporated into an Os-Complex Thin Film for Continuous Glucose Detection in Human Saliva. **Electroanalysis**. 28(9): 2016-2021.
- Liu, Q., Lu, X., Li, J., Yao, X., and Li, J. (2007). Direct Electrochemistry of Glucose Oxidase and Electrochemical Biosensing of Glucose on Quantum Dots/Carbon Nanotubes Electrodes. **Biosensors and bioelectronics**. 22(12): 3203-3209.
- Liu, Y., Wang, M., Zhao, F., Xu, Z., and Dong, S. (2005). The Direct Electron Transfer of Glucose Oxidase and Glucose Biosensor Based on Carbon Nanotubes/Chitosan Matrix. **Biosensors and bioelectronics**. 21(6): 984-988.
- Liu, Y., Yu, D., Zeng, C., Miao, Z., and Dai, L. (2010). Biocompatible Graphene Oxide-Based Glucose Biosensors. **Langmuir**. 26(9): 6158-6160.
- Lo, J.-T., Mukerji, K., Awasthi, Y., Hanada, E., Suzuki, K., and Srivastava, S. (1979). Purification and Properties of Sphingolipid Beta-Galactosidases from Human Placenta. **Journal of Biological Chemistry**. 254(14): 6710-6715.
- Luo, X., Morrin, A., Killard, A. J., and Smyth, M. R. (2006). Application of Nanoparticles in Electrochemical Sensors and Biosensors. **Electroanalysis**. 18(4): 319-326.

- Luong, J. H., Male, K. B., and Glennon, J. D. (2009). Boron-Doped Diamond Electrode: Synthesis, Characterization, Functionalization and Analytical Applications. **Analyst**. 134(10): 1965-1979.
- Lyons, M. E., and Keeley, G. P. (2008). Carbon Nanotube Based Modified Electrode Biosensors. Part 1: Electrochemical Studies of the Flavin Group Redox Kinetics at Swcnt/Glucose Oxidase Composite Modified Electrodes. **International Journal of Electrochemical Science**. 3: 819-853.
- Mani, V., Devadas, B., and Chen, S.-M. (2013). Direct Electrochemistry of Glucose Oxidase at Electrochemically Reduced Graphene Oxide-Multiwalled Carbon Nanotubes Hybrid Material Modified Electrode for Glucose Biosensor. **Biosensors and bioelectronics**. 41: 309-315.
- Mark, B. L., Vocadlo, D. J., Knapp, S., Triggs-Raine, B. L., Withers, S. G., and James, M. N. (2001). Crystallographic Evidence for Substrate-Assisted Catalysis in a Bacterial B-Hexosaminidase. **Journal of Biological Chemistry**. 276(13): 10330-10337.
- Mason, M., Longo, E., and Scampicchio, M. (2016). Monitoring of Glucose in Beer Brewing by a Carbon Nanotubes Based Nylon Nanofibrous Biosensor. **Journal of Nanomaterials**.
- Masoomi-Godarzi, S., Khodadadi, A., Vesali-Naseh, M., and Mortazavi, Y. (2014). Highly Stable and Selective Non-Enzymatic Glucose Biosensor Using Carbon Nanotubes Decorated by Fe<sub>3</sub>O<sub>4</sub> Nanoparticles. **Journal of The Electrochemical Society**. 161(1): B19-B25.

- Meekrathok, P., Bürger, M., Porfetye, A. T., Vetter, I. R., and Suginta, W. (2015a). Expression, Purification, Crystallization and Preliminary Crystallographic Analysis of a Gh20 B-N-Acetylglucosaminidase from the Marine Bacterium *Vibrio Harveyi*. **Acta Crystallographica Section F: Structural Biology Communications**. 71(4): 427-433.
- Meekrathok, P., Porfetye, A. T., Bürger, M., Vetter, I. R., and Suginta, W. (2015b). Functional and Structural Analysis of a Gh20  $\beta$ -N-Acetylglucosaminidase from the Marine Bacterium *Vibrio Harveyi*: Pe-007. **Protein Science**. 24: 105-106.
- Meekrathok, P., and Suginta, W. (2016). Probing the Catalytic Mechanism of *Vibrio Harveyi* Gh20 B-N-Acetylglucosaminidase by Chemical Rescue. **PLoS one**. 11(2): e0149228.
- Mincea, M., Negrulescu, A., and Ostafe, V. (2012). Preparation, Modification, and Applications of Chitin Nanowhiskers: A Review. **Reviews On Advanced Materials Science**. 30(3): 225-242.
- Monošík, R., Stred'anský, M., and Šturdík, E. (2012). Biosensors-Classification, Characterization and New Trends. **Acta Chimica Slovaca**. 5(1): 109-120.
- Nagy, G., Xu, C. X., Buck, R. P., Lindner, E., and Neuman, M. R. (1998). Amperometric Microcell for Enzyme Activity Measurements. **Analytical Chemistry**. 70(10): 2156-2162.
- Nakorn, P. N. (2017). Chitin Nanowhisker and Chitosan Nanoparticles in Protein Immobilization for Biosensor Applications. **Journal of Metals, Materials and Minerals**. 18(2): 73-77.
- Newman, J. D., and Turner, A. P. (1992). Biosensors: Principles and Practice. **Essays in biochemistry**. 27: 147-159.

- Newman, J. D., and Turner, A. P. (2005). Home Blood Glucose Biosensors: A Commercial Perspective. **Biosensors and bioelectronics**. 20(12): 2435-2453.
- Niraj, G., Varshney, H., Pandey, S., and Singh, S. (2012). Sensors for Diabetes. Glucose Biosensors by Using Different Newer Techniques: A Review. **International Journal of Therapeutic Applications**. 6: 28-37.
- Odaci, D., Telefoncu, A., and Timur, S. (2008). Pyranose Oxidase Biosensor Based on Carbon Nanotube (Cnt)-Modified Carbon Paste Electrodes. **Sensors and Actuators B: Chemical**. 132(1): 159-165.
- Ohashi, E., and Karube, I. (1995). Development of a Thin Membrane Glucose Sensor Using B-Type Crystalline Chitin for Implantable Biosensor. **Journal of biotechnology**. 40(1): 13-19.
- Ohashi, E., and Koriyama, T. (1992). Simple and Mild Preparation of an Enzyme-Immobilized Membrane for a Biosensor Using B-Type Crystalline Chitin. **Analytica Chimica Acta**. 262(1): 19-25.
- Oliveira, J. E., Mattoso, L. H. C., Medeiros, E. S., and Zucolotto, V. (2012). Poly (Lactic Acid)/Carbon Nanotube Fibers as Novel Platforms for Glucose Biosensors. **Biosensors**. 2(1): 70-82.
- Palanisamy, S., Vilian, A. E., and Chen, S.-M. (2012). Direct Electrochemistry of Glucose Oxidase at Reduced Graphene Oxide/Zinc Oxide Composite Modified Electrode for Glucose Sensor. **International Journal of Electrochemical Science**. 7(3): 2153-2163.
- Palmer, T. (1991). **Understanding Enzymes**. E. Horwood.
- Palmer, T., and Bonner, P. L. (2007). **Enzymes: Biochemistry, Biotechnology, Clinical Chemistry**. Elsevier.

- Pandey, P., Upadhyay, S., Shukla, N., and Sharma, S. (2003). Studies on the Electrochemical Performance of Glucose Biosensor Based on Ferrocene Encapsulated Ormosil and Glucose Oxidase Modified Graphite Paste Electrode. **Biosensors and bioelectronics**. 18(10): 1257-1268.
- Paredes, P. A., Parellada, J., Fernández, V. M., Katakis, I., and Domínguez, E. (1997). Amperometric Mediated Carbon Paste Biosensor Based on D-Fructose Dehydrogenase for the Determination of Fructose in Food Analysis. **Biosensors and bioelectronics**. 12(12): 1233-1243.
- Pecková, K., Musilová, J., and Barek, J. (2009). Boron-Doped Diamond Film Electrodes—New Tool for Voltammetric Determination of Organic Substances. **Critical Reviews in Analytical Chemistry**. 39(3): 148-172.
- Pemberton, R., Hart, J., and Mottram, T. (2001). An Assay for the Enzyme N-Acetyl-B-D-Glucosaminidase (Nagase) Based on Electrochemical Detection Using Screen-Printed Carbon Electrodes (Spces). **Analyst**. 126(11): 1866-1871.
- Periasamy, A. P., Chang, Y.-J., and Chen, S.-M. (2011). Amperometric Glucose Sensor Based on Glucose Oxidase Immobilized on Gelatin-Multiwalled Carbon Nanotube Modified Glassy Carbon Electrode. **Bioelectrochemistry**. 80(2): 114-120.
- Perumal, V., and Hashim, U. (2014). Advances in Biosensors: Principle, Architecture and Applications. **Journal of Applied Biomedicine**. 12(1): 1-15.
- Pilehvar, S., and De Wael, K. (2015). Recent Advances in Electrochemical Biosensors Based on Fullerene-C60 Nano-Structured Platforms. **Biosensors**. 5(4): 712-735.

- Pillai, C., Paul, W., and Sharma, C. P. (2009). Chitin and Chitosan Polymers: Chemistry, Solubility and Fiber Formation. **Progress in polymer science**. 34(7): 641-678.
- Prashanth, K. H., and Tharanathan, R. (2007). Chitin/Chitosan: Modifications and Their Unlimited Application Potential—an Overview. **Trends in food science & technology**. 18(3): 117-131.
- Prodromidis, M. I., and Karayannis, M. I. (2002). Enzyme Based Amperometric Biosensors for Food Analysis. **Electroanalysis**. 14(4): 241.
- Pumera, M., Sanchez, S., Ichinose, I., and Tang, J. (2007). Electrochemical Nanobiosensors. **Sensors and Actuators B: Chemical**. 123(2): 1195-1205.
- Qiu, J.-D., Zhou, W.-M., Guo, J., Wang, R., and Liang, R.-P. (2009). Amperometric Sensor Based on Ferrocene-Modified Multiwalled Carbon Nanotube Nanocomposites as Electron Mediator for the Determination of Glucose. **Analytical biochemistry**. 385(2): 264-269.
- Ramasubbu, N., Thomas, L., Raguinath, C., and Kaplan, J. (2005). Structural Analysis of Dispersin B, a Biofilm-Releasing Glycoside Hydrolase from the Periodontopathogen *Actinobacillus Actinomycetemcomitans*. **Journal of molecular biology**. 349(3): 475-486.
- Raof, J. B., Ojani, R., and Kolbadinezhad, M. (2009). Voltammetric Sensor for Glutathione Determination Based on Ferrocene-Modified Carbon Paste Electrode. **Journal of Solid State Electrochemistry**. 13(9): 1411.

- Razmi, H., and Mohammad-Rezaei, R. (2013). Graphene Quantum Dots as a New Substrate for Immobilization and Direct Electrochemistry of Glucose Oxidase: Application to Sensitive Glucose Determination. **Biosensors and bioelectronics**. 41: 498-504.
- Ren, X., Chen, Z., Chen, X., Liu, J., and Tang, F. (2014). Sensitive Optical Detection of Alkaline Phosphatase Activity with Quantum Dots. **Journal of Luminescence**. 145: 330-334.
- Rinaudo, M. (2006). Chitin and Chitosan: Properties and Applications. **Progress in polymer science**. 31(7): 603-632.
- Rivas, G. A., Rubianes, M. D., Rodriguez, M. C., Ferreyra, N. F., Luque, G. L., Pedano, M. L., Miscoria, S. A., and Parrado, C. (2007). Carbon Nanotubes for Electrochemical Biosensing. **Talanta**. 74(3): 291-307.
- Robinson, P. K. (2015). Enzymes: Principles and Biotechnological Applications. **Essays in biochemistry**. 59: 1-41.
- Sapsford, K. E., Pons, T., Medintz, I. L., and Mattoussi, H. (2006). Biosensing with Luminescent Semiconductor Quantum Dots. **Sensors**. 6(8): 925-953.
- Schlittler, R., Seo, J. W., Gimzewski, J., Durkan, C., Saifullah, M., and Welland, M. (2001). Single Crystals of Single-Walled Carbon Nanotubes Formed by Self-Assembly. **Science**. 292(5519): 1136-1139.
- Scouten, W. H., Luong, J. H., and Brown, R. S. (1995). Enzyme or Protein Immobilization Techniques for Applications in Biosensor Design. **Trends in biotechnology**. 13(5): 178-185.

- Şenel, M., and Nergiz, C. (2012). Novel Amperometric Glucose Biosensor Based on Covalent Immobilization of Glucose Oxidase on Poly (Pyrrole Propylic Acid)/Au Nanocomposite. **Current Applied Physics**. 12(4): 1118-1124.
- Sett, A., Das, S., Sharma, P., and Bora, U. (2012). Aptasensors in Health, Environment and Food Safety Monitoring. **Open Journal of Applied Biosensor**. 1(02): 9.
- Shrestha, B. K., Ahmad, R., Mousa, H. M., Kim, I. G., Kim, J. I., Neupane, M. P., Park, C. H., and Kim, C. S. (2016). High-Performance Glucose Biosensor Based on Chitosan-Glucose Oxidase Immobilized Polypyrrole/Nafion/Functionalized Multi-Walled Carbon Nanotubes Bio-Nanohybrid Film. **Journal of Colloid and Interface Science**. 482: 39-47.
- Shrestha, B. K., Ahmad, R., Shrestha, S., Park, C. H., and Kim, C. S. (2017). Globular Shaped Polypyrrole Doped Well-Dispersed Functionalized Multiwall Carbon Nanotubes/Nafion Composite for Enzymatic Glucose Biosensor Application. **Scientific Reports**. 7.
- Shukla, S. K., Mishra, A. K., Arotiba, O. A., and Mamba, B. B. (2013). Chitosan-Based Nanomaterials: A State-of-the-Art Review. **International journal of biological macromolecules**. 59: 46-58.
- Sirimontree, P., Fukamizo, T., and Suginta, W. (2015). Azide Anions Inhibit Gh-18 Endochitinase and Gh-20 Exo B-N-Acetylglucosaminidase from the Marine Bacterium *Vibrio Harveyi*. **The Journal of Biochemistry**. 159(2): 191-200.
- Sirimontree, P., Suginta, W., Sritho, N., Kanda, Y., Shinya, S., Ohnuma, T., and Fukamizo, T. (2014). Mutation Strategies for Obtaining Chitooligosaccharides with Longer Chains by Transglycosylation Reaction of Family Gh18 Chitinase. **Bioscience, biotechnology, and biochemistry**. 78(12): 2014-2021.

- So, H.-M., Won, K., Kim, Y. H., Kim, B.-K., Ryu, B. H., Na, P. S., Kim, H., and Lee, J.-O. (2005). Single-Walled Carbon Nanotube Biosensors Using Aptamers as Molecular Recognition Elements. **Journal of the American Chemical Society**. 127(34): 11906-11907.
- Solanki, P. R., Kaushik, A., Agrawal, V. V., and Malhotra, B. D. (2011). Nanostructured Metal Oxide-Based Biosensors. **NPG Asia Materials**. 3(1): 17.
- Song, Y., Shen, Y., Gong, C., Chen, J., Xu, M., Wang, L., and Wang, L. (2017). A Novel Glucose Biosensor Based on Tb@ Mesoporous Metal-Organic Frameworks/Carbon Nanotube Nanocomposites. **Chemelectrochem**. 4(6): 1457-1462.
- Sotiropoulou, S., and Chaniotakis, N. A. (2003). Carbon Nanotube Array-Based Biosensor. **Analytical and bioanalytical chemistry**. 375(1): 103-105.
- Sritho, N., and Suginta, W. (2012). Role of Tyr-435 of Vibrio Harveyi Chitinase a in Chitin Utilization. **Applied biochemistry and biotechnology**. 166(5): 1192-1202.
- Stoica, L., Lindgren-Sjölander, A., Ruzgas, T., and Gorton, L. (2004). Biosensor Based on Cellobiose Dehydrogenase for Detection of Catecholamines. **Analytical Chemistry**. 76(16): 4690-4696.
- Sugawara, K., Takano, T., Fukushi, H., Hoshi, S., Akatsuka, K., Kuramitz, H., and Tanaka, S. (2000). Glucose Sensing by a Carbon-Paste Electrode Containing Chitin Modified with Glucose Oxidase. **Journal of Electroanalytical Chemistry**. 482(1): 81-86.
- Suginta, W., Chuenark, D., Mizuhara, M., and Fukamizo, T. (2010). Novel B-N-Acetylglucosaminidases from Vibrio Harveyi 650: Cloning, Expression,

- Enzymatic Properties, and Subsite Identification. **BMC biochemistry**. 11(1): 40.
- Suginta, W., Chumjan, W., Mahendran, K. R., Janning, P., Schulte, A., and Winterhalter, M. (2013a). Molecular Uptake of Chitooligosaccharides through Chitoporin from the Marine Bacterium *Vibrio Harveyi*. **Public Library of Science one**. 8(1): e55126.
- Suginta, W., Khunkaewla, P., and Schulte, A. (2013b). Electrochemical Biosensor Applications of Polysaccharides Chitin and Chitosan. **Chemical reviews**. 113(7): 5458-5479.
- Sumida, T., Ishii, R., Yanagisawa, T., Yokoyama, S., and Ito, M. (2009). Molecular Cloning and Crystal Structural Analysis of a Novel B-N-Acetylhexosaminidase from *Paenibacillus* Sp. Ts12 Capable of Degrading Glycosphingolipids. **Journal of molecular biology**. 392(1): 87-99.
- Tan, X., Li, M., Cai, P., Luo, L., and Zou, X. (2005). An Amperometric Cholesterol Biosensor Based on Multiwalled Carbon Nanotubes and Organically Modified Sol-Gel/Chitosan Hybrid Composite Film. **Analytical biochemistry**. 337(1): 111-120.
- Tang, L., Zhu, Y., Xu, L., Yang, X., and Li, C. (2007). Amperometric Glutamate Biosensor Based on Self-Assembling Glutamate Dehydrogenase and Dendrimer-Encapsulated Platinum Nanoparticles onto Carbon Nanotubes. **Talanta**. 73(3): 438-443.
- Tangkuaram, T., Gerlach, J. Q., Xiang, Y., Kawde, A.-N., Dai, Z., Bhavanandan, V. P., La Belle, J. T., Veerasai, W., Joshi, L., and Wang, J. (2006). Sensitive and Rapid Electrochemical Bioassay of Glycosidase Activity. **Analyst**. 131(8): 889-891.

- Taylor, K. B. (2002). **Enzyme Kinetics and Mechanisms**. (Vol. 64): Springer Science & Business Media.
- TermehYousefi, A., Bagheri, S., Kadri, N. A., Mahmood, M. R., and Ikeda, S. (2015). Constant Glucose Biosensor Based on Vertically Aligned Carbon Nanotube Composites. **International Journal of Electrochemical Science**. 10(5): 4183-4192.
- Tews, I., Perrakis, A., Oppenheim, A., Dauter, Z., Wilson, K. S., and Vorgias, C. E. (1996). Bacterial Chitobiase Structure Provides Insight into Catalytic Mechanism and the Basis of Tay–Sachs Disease. **Nature Structural and Molecular Biology**. 3(7): 638.
- Tischer, W., and Wedekind, F. (1999). **Immobilized Enzymes: Methods and Applications**. In *Biocatalysis-from Discovery to Application* (pp. 95-126): Springer.
- Tkac, J., Whittaker, J. W., and Ruzgas, T. (2007). The Use of Single Walled Carbon Nanotubes Dispersed in a Chitosan Matrix for Preparation of a Galactose Biosensor. **Biosensors and bioelectronics**. 22(8): 1820-1824.
- Trivedi, U., Lakshminarayana, D., Kothari, I., Patel, P., and Panchal, C. (2009). Amperometric Fructose Biosensor Based on Fructose Dehydrogenase Enzyme. **Sensors and Actuators B: Chemical**. 136(1): 45-51.
- Umemoto, J., Matta, K., Barlow, J., and Bhavanandan, V. (1978). Action of Endo-A-N-Acetyl-D-Galactosaminidase on Synthetic Glycosides Including Chromogenic Substrates. **Analytical biochemistry**. 91(1): 186-193.
- Uwimbabazi, E., Mukasekuru, M. R., and Sun, X. (2017). Glucose Biosensor Based on a Glassy Carbon Electrode Modified with Multi-Walled Carbon Nanotubes-

- Chitosan for the Determination of Beef Freshness. **Food Analytical Methods**. 10(8): 2667-2676.
- Van Dorst, B., Mehta, J., Bekaert, K., Rouah-Martin, E., De Coen, W., Dubruel, P., Blust, R., and Robbens, J. (2010). Recent Advances in Recognition Elements of Food and Environmental Biosensors: A Review. **Biosensors and bioelectronics**. 26(4): 1178-1194.
- Velmurugan, M., Sakthinathan, S., Chen, S.-M., and Karuppiah, C. (2015). Direct Electron Transfer of Glucose Oxidase and Electrocatalysis of Glucose Based on Gold Nanoparticles/Electroactivated Graphite Nanocomposite. **International Journal of Electrochemical Science**. 10: 6663-6671.
- Vocadlo, D. J., Mayer, C., He, S., and Withers, S. G. (2000). Mechanism of Action and Identification of Asp242 as the Catalytic Nucleophile of Vibrio Furnisii N-Acetyl-B-D-Glucosaminidase Using 2-Acetamido-2-Deoxy-5-Fluoro-A-L-Idopyranosyl Fluoride. **Biochemistry**. 39(1): 117-126.
- Vocadlo, D. J., and Withers, S. G. (2005). Detailed Comparative Analysis of the Catalytic Mechanisms of B-N-Acetylglucosaminidases from Families 3 and 20 of Glycoside Hydrolases. **Biochemistry**. 44(38): 12809-12818.
- Wang, J. (2005). Carbon-Nanotube Based Electrochemical Biosensors: A Review. **Electroanalysis**. 17(1): 7-14.
- Wang, J. (2008). Electrochemical Glucose Biosensors. **Chemical reviews**. 108(2): 814-825.
- Wang, J., and Musameh, M. (2003). Carbon Nanotube/Teflon Composite Electrochemical Sensors and Biosensors. **Analytical Chemistry**. 75(9): 2075-2079.

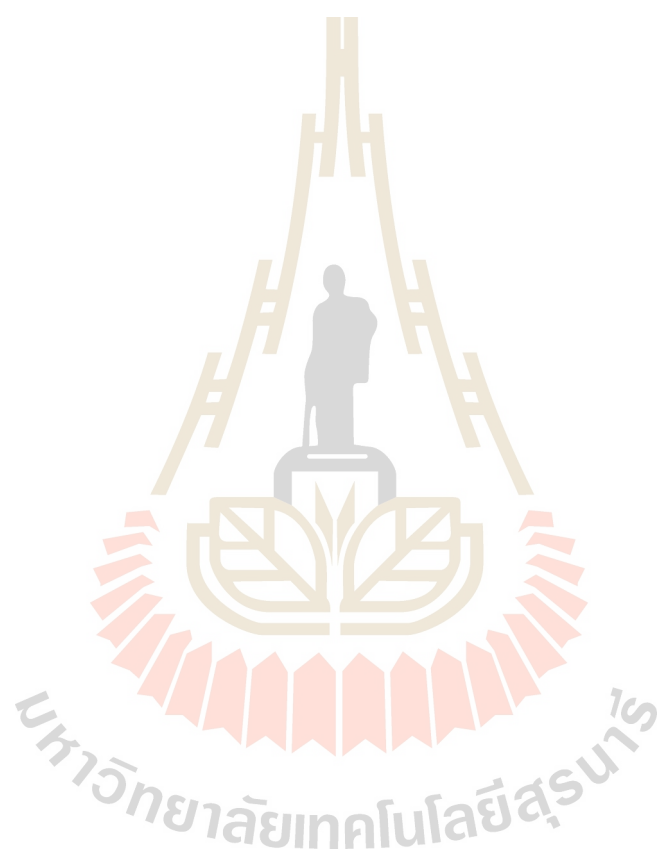
- Wang, L., Li, Y., Li, G., Xie, Z., and Ye, B. (2015). Electrochemical Characters of Hymecromone at the Graphene Modified Electrode and Its Analytical Application. **Analytical Methods**. 7(7): 3000-3005.
- Wang, S., Zhang, Q., Wang, R., and Yoon, S. (2003). A Novel Multi-Walled Carbon Nanotube-Based Biosensor for Glucose Detection. **Biochemical and biophysical research communications**. 311(3): 572-576.
- Wang, Y., and Yao, Y. (2012). Direct Electron Transfer of Glucose Oxidase Promoted by Carbon Nanotubes Is without Value in Certain Mediator-Free Applications. **Microchimica Acta**. 176(3-4): 271-277.
- Wang, Y., Yuan, R., Chaia, Y., Li, W., Zhuo, Y., Yuan, Y., and Li, J. (2011). Direct Electron Transfer: Electrochemical Glucose Biosensor Based on Hollow Pt Nanosphere Functionalized Multiwall Carbon Nanotubes. **Journal of Molecular Catalysis B: Enzymatic**. 71(3-4): 146-151.
- Woodley, J. (1992). Immobilized Biocatalysts. **Solid Supports Catal Org Synth**. 21: 254-271.
- Wu, Q., and Dewald, H. D. (2001). Voltammetry of Coumarins. **Electroanalysis: An International Journal Devoted to Fundamental and Practical Aspects of Electroanalysis**. 13(1): 45-48.
- Wu, Y., and Hu, S. (2007). Biosensors Based on Direct Electron Transfer in Redox Proteins. **Microchimica Acta**. 159(1-2): 1-17.
- Yakovleva, M., Buzas, O., Matsumura, H., Samejima, M., Igarashi, K., Larsson, P.-O., Gorton, L., and Danielsson, B. (2012). A Novel Combined Thermometric and Amperometric Biosensor for Lactose Determination Based on Immobilised Cellobiose Dehydrogenase. **Biosensors and bioelectronics**. 31(1): 251-256.

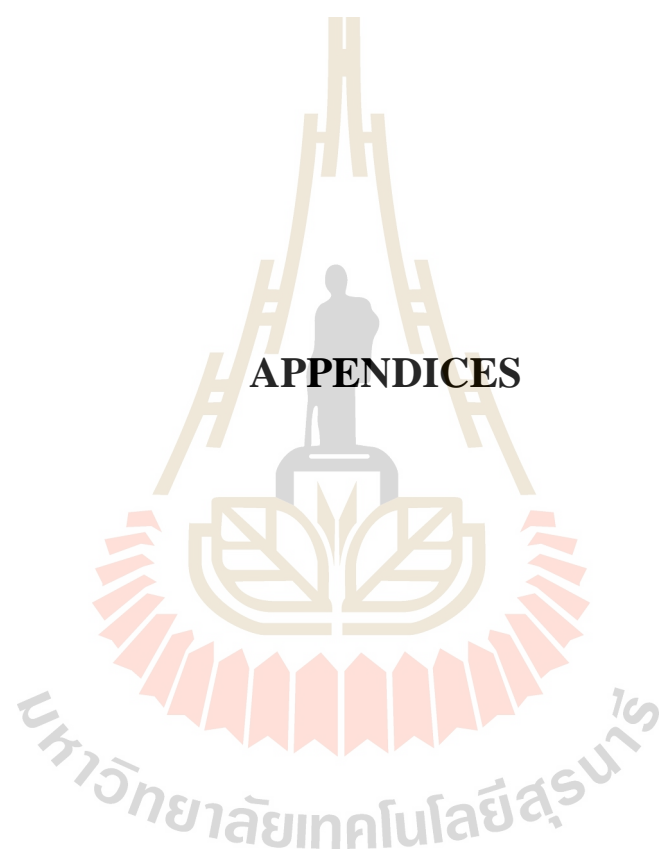
- Yang, C.-Y., Chen, S.-M., Tsai, T.-H., and Unnikrishnan, B. (2012). Poly (Diphenylamine) with Multi-Walled Carbon Nanotube Composite Film Modified Electrode for the Determination of Phenol. **International Journal of Electrochemical Science**. 7: 12796-12807.
- Yang, H., Gong, C., Miao, L., and Xu, F. (2017). A Glucose Biosensor Based on Horseradish Peroxidase and Glucose Oxidase Co-Entrapped in Carbon Nanotubes Modified Electrode. **International Journal of Electrochemical Science**. 12: 4958-4969.
- Yang, N., Chen, X., Ren, T., Zhang, P., and Yang, D. (2015). Carbon Nanotube Based Biosensors. **Sensors and Actuators B: Chemical**. 207: 690-715.
- Yang, W., Ratinac, K. R., Ringer, S. P., Thordarson, P., Gooding, J. J., and Braet, F. (2010). Carbon Nanomaterials in Biosensors: Should You Use Nanotubes or Graphene? **Angewandte Chemie International Edition**. 49(12): 2114-2138.
- Yang, W., Thordarson, P., Gooding, J. J., Ringer, S. P., and Braet, F. (2007a). Carbon Nanotubes for Biological and Biomedical Applications. **Nanotechnology**. 18(41): 412001.
- Yang, W., Zhou, H., and Sun, C. (2007b). Synthesis of Ferrocene-Branched Chitosan Derivatives: Redox Polysaccharides and Their Application to Reagentless Enzyme-Based Biosensors. **Macromolecular rapid communications**. 28(3): 265-270.
- Yılmaz, Ö., Demirkol, D. O., Gülcemal, S., Kılınc, A., Timur, S., and Çetinkaya, B. (2012). Chitosan–Ferrocene Film as a Platform for Flow Injection Analysis Applications of Glucose Oxidase and Gluconobacter Oxydans Biosensors. **Colloids and Surfaces B: Biointerfaces**. 100: 62-68.

- Yin, H., Zhou, Y., Ai, S., Liu, X., Zhu, L., and Lu, L. (2010). Electrochemical Oxidative Determination of 4-Nitrophenol Based on a Glassy Carbon Electrode Modified with a Hydroxyapatite Nanopowder. **Microchimica Acta**. 169(1-2): 87-92.
- Yoo, E.-H., and Lee, S.-Y. (2010). Glucose Biosensors: An Overview of Use in Clinical Practice. **Sensors**. 10(5): 4558-4576.
- Zhang, F.-F., Wan, Q., Wang, X.-L., Sun, Z.-D., Zhu, Z.-Q., Xian, Y.-Z., Jin, L.-T., and Yamamoto, K. (2004a). Amperometric Sensor Based on Ferrocene-Doped Silica Nanoparticles as an Electron Transfer Mediator for the Determination of Glucose in Rat Brain Coupled to in Vivo Microdialysis. **Journal of Electroanalytical Chemistry**. 571(2): 133-138.
- Zhang, M., Smith, A., and Gorski, W. (2004b). Carbon Nanotube– Chitosan System for Electrochemical Sensing Based on Dehydrogenase Enzymes. **Analytical Chemistry**. 76(17): 5045-5050.
- Zhang, S., Wang, N., Yu, H., Niu, Y., and Sun, C. (2005). Covalent Attachment of Glucose Oxidase to an Au Electrode Modified with Gold Nanoparticles for Use as Glucose Biosensor. **Bioelectrochemistry**. 67(1): 15-22.
- Zhang, W., and Li, G. (2004). Third-Generation Biosensors Based on the Direct Electron Transfer of Proteins. **Analytical sciences**. 20(4): 603-609.
- Zhao, S., Zhang, K., Bai, Y., Yang, W., and Sun, C. (2006). Glucose Oxidase/Colloidal Gold Nanoparticles Immobilized in Nafion Film on Glassy Carbon Electrode: Direct Electron Transfer and Electrocatalysis. **Bioelectrochemistry**. 69(2): 158-163.
- Zhilei, W., Zaijun, L., Xiulan, S., Yinjun, F., and Junkang, L. (2010). Synergistic Contributions of Fullerene, Ferrocene, Chitosan and Ionic Liquid Towards

Improved Performance for a Glucose Sensor. **Biosensors and bioelectronics.**

25(6): 1434-1438.





**APPENDICES**

## **APPENDIX A**

### **STANDARD CURVE**

#### **A.1 Standard curve of 4-methylumbelliferyl *N*-acetyl- $\beta$ -d-glucosaminide**

The standard curve from the product of the 4-methylumbelliferyl *N*-acetyl- $\beta$ -d-glucosaminide (4MU-GlcNAc) catalyzed by *Vh*GlcNAc enzyme was examined by fluorescence spectroscopy, the experiments were carried out in an aqueous 0.1 M phosphate buffer solution, pH 7.0. Figure A.1 represent an emission spectra at excitation wavelength of 324 nm, increasing intensity following 4MU-GlcNAc substrate was increased; 1, 2, 4, 6, 8, 10 and 12  $\mu$ M, respectively. The standard curve from product of 4MU-GlcNAc which show in Figure A.2 was constructed by the analysis of the fluorescence experiments. A curve was fitted linearity with zero-interception in the range of 1 – 12  $\mu$ M with a good regression coefficient ( $R^2=0.99$ ) following by equation  $y = 18.83x$ .

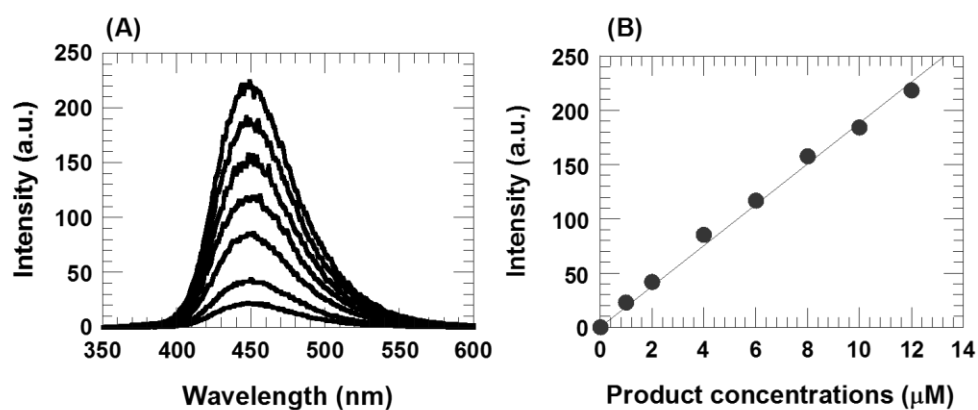


**Figure A.1** Standard curve measurement from various product concentrations of 4MU-GlcNAc. (A) Emission spectra of various 4MU-GlcNAc concentrations; 1, 2, 4, 6, 8, 10 and 12  $\mu\text{M}$ , respectively. (B) Linear range of the emission intensity in the range of 1-12  $\mu\text{M}$  concentrations of product.

## APPENDIX B

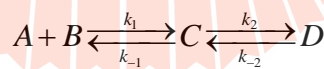
### DERIVATION OF MECHANISM

#### B.1 Pre-steady state kinetics

The hyperbolic dependent of observed rate constant ( $k_{\text{obs}}$ ) is interpreted as the simplest model as two-step reaction mechanism of which the first step is rapid binding and dissociating to reach the equilibrium prior to the second step is occurred as shown in equation B.1



This is compared to the following scheme (E = A, S = B, C = ES, D = EP)



Based on rate law, the change of A, B, C and D are described as

$$\frac{-dC_A}{dt} = k_1 C_A C_B - k_{-1} C_C$$

$$\frac{-dC_B}{dt} = k_1 C_A C_B - k_{-1} C_C$$

$$\frac{-dC_C}{dt} = k_1 C_A C_B - k_{-2} C_D + (k_{-1} + k_2) C_C$$

$$\frac{-dC_D}{dt} = k_2 C_C + k_{-2} C_D$$

Law of mass balance

$$\Delta C_A = \Delta C_B$$

$$-\Delta C_A - \Delta C_C = \Delta C_D$$

$$-\Delta C_B - \Delta C_C = \Delta C_D$$

The time dependent can be expressed as

$$C_A = \bar{C}_A + \Delta C_A$$

$$C_B = \bar{C}_B + \Delta C_B$$

$$C_C = \bar{C}_C + \Delta C_C$$

$$C_D = \bar{C}_D + \Delta C_D$$

In rapid-equilibrium, the rate of  $k_1(\bar{C}_A + \bar{C}_B) + k_{-1} \gg k_2, k_{-2}$ , and it is assumed that during the change of D, the species of A, B and C are in equilibrium.

$$K_1 = \frac{C_C}{C_A C_B} \quad K_1 = \frac{\bar{C}_C}{\bar{C}_A \bar{C}_B}$$

With assumed rapid-equilibrium

$$\frac{C_C}{C_A C_B} = \frac{\bar{C}_C}{\bar{C}_A \bar{C}_B}, \text{ therefore } \frac{(\Delta C_C + \bar{C}_C)}{(\Delta C_A + \bar{C}_A)(\Delta C_B + \bar{C}_B)} = K_1$$

$$\Delta C_C + \bar{C}_C = K_1 \left[ \Delta C_A \Delta C_B + \bar{C}_A \Delta C_B + \bar{C}_B \Delta C_A + \bar{C}_A \bar{C}_B \right]$$

$$\Delta C_A = \Delta C_B$$

$$\Delta C_C + \bar{C}_C = K_1 \left[ \Delta C_A^2 + \bar{C}_A \Delta C_A + \bar{C}_B \Delta C_A + \bar{C}_A \bar{C}_B \right]$$

$$\Delta C_C = K_1 (\bar{C}_A + \bar{C}_B) \Delta C_A$$

$$-\Delta C_A - \Delta C_C = \Delta C_D$$

Substitution of  $\Delta C_C$  into  $\Delta C_A$ , therefore  $-\left( \frac{\Delta C_C}{K_1 (\bar{C}_A + \bar{C}_B)} + \Delta C_C \right) = \Delta C_D$

Under pseudo-first order condition  $[B] \gg [A]$

$$\Delta C_C = -\frac{K_1 [B]}{1 + K_1 [B]} \Delta C_D$$

From rate law of the change of  $C_d$

$$\frac{-d\Delta C_D}{dt} = -k_2 (\Delta C_C + \bar{C}_C) + k_{-2} (\Delta C_D + \bar{C}_D)$$

$$k_2 \bar{C}_C = k_{-2} \bar{C}_D$$

$$\frac{-d\Delta C_D}{dt} = -k_2 \Delta C_C + k_{-2} \Delta C_D, \text{ substitution of } \Delta C_C = -\frac{K_1 [B]}{1 + K_1 [B]} \Delta C_D$$

$$\frac{-d\Delta C_D}{dt} = \left( k_2 \frac{K_1 [B]}{1 + K_1 [B]} + k_{-2} \right) \Delta C_D$$

$$k_{obs} = k_2 \frac{K_1 [B]}{1 + K_1 [B]} + k_{-2}; K_1 = \frac{k_{-1}}{k_1} = \frac{1}{K_d}$$

and in case of no reversible rate constant of  $k_{-2}$

$$k_{obs} = \frac{k_2 [B]}{K_d + [B]} + k_{-2}$$

## B.2 Steady state kinetics (Taylor, 2002)

The chemical model for an enzyme-catalyzed reaction that is ordinarily presented in the equation B.4 of a linear process following as:

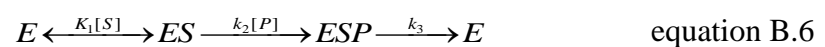


The net-rate-constant method is recognized, since a proportion of the reversible in each step actually goes on to product, an irreversible rate constant is associated with each step. Assume initially that all of the steps are irreversible as show in equation B.5



where  $K'_1 = k_1 / k_{-1}$ ,  $K'_2 = k_2 / k_{-2}$  and  $K'_3 = k_3$

Equation B.6 represent the bisubstrate, sequential, ordered, rapid equilibrium substrate addition following equation B.5 as:



In a model equation B.6 the enzyme complex with S, ES dissociates back to free enzyme, E, and substrate, S, faster than the complex adds the second substrate, P. Thus the magnitude of  $k_2$ , implicit  $K_1$ , is greater than that of  $k_3$ . The conventions for derivation of model with rapid equilibrium steps described by Cha (Cha, 1968), are that a rapid equilibrium segment can be treated as a single enzyme form. The rapid equilibrium will be regarded as a single species with a total concentration of enzyme intermediates  $E'$  which represent in equation B.7.

$$[E'] = [E] + [ES] \quad \text{equation B.7}$$

From equation B.6 can rearrange following as:



The steady-state approximation specifies the rates of all steps in equation B.8 are equal to each other. The rate is also equal to the initial velocity which represent in equation B.9. Division of each of the expressions in equation B.9 by  $(E_t)$  results in the set of equations B.10.

$$v = k_2[E'] = k_3[EP] \quad \text{equation B.9}$$

$$\frac{v}{E_t} = \frac{k_2[E']}{E_t} \quad \text{equation B.10}$$

$$\frac{v}{E_t} = \frac{k_3[EP]}{E_t}$$

in the set of equation B.10 by the net rate constant results represent in equation B.11

$$\frac{1}{k_2} \cdot \frac{v}{E_t} = \frac{[E']}{E_t}$$

equation B.11

$$\frac{1}{k_3} \cdot \frac{v}{E_t} = \frac{[EP]}{E_t}$$

The sum of the two equation B.11, and also the conservation of enzyme of the sum is equal to 1.0

$$\frac{v}{E_t} \cdot \left( \frac{1}{k_2} + \frac{1}{k_3} \right) = \frac{[E'] + [EP]}{E_t}$$

equation B.12

Finally division of both side of equation B.12 by the sum of the reciprocals of the net rate constants results in equation B.13

$$\frac{v}{E_t} = \frac{1}{\frac{1}{k_2} + \frac{1}{k_3}}$$

equation B.13

From  $k_{cat} = V_{max} / E_t$

Equation B.13 can rearrange to obtained catalytic constant following equation B.14

$$k_{cat} = \frac{k_2 k_3}{k_2 + k_3}$$

equation B.14

## APPENDIX C

### LIST OF PRESENTATION

**Waraporn Rernglit**, Wipa Suginta and Albert Schulte. Amperometric enzyme biosensors with long life-time of glucose oxidase in colloidal chitin-soaked nanoporous carbon nanotube thin films as biocompatible immobilization matrix. The 5<sup>th</sup> Asia Pacific Protein Association (APPA) Conference and the 12th International Symposium for the Protein Society of Thailand, The Tide Resort, Bangsaen, Chon Buri, Thailand, July 11<sup>st</sup>-14<sup>th</sup>, 2017. **P199**, *Poster presentation.*

**Waraporn Rernglit**, Wipa Suginta and Albert Schulte. Amperometric enzyme biosensors with long life-time of glucose oxidase in colloidal chitin-soaked nanoporous carbon nanotube thin films as biocompatible immobilization matrix. The 5<sup>th</sup> Thailand International Nanotechnology Conference, Greenery Resort Khao Yai Hotel, Nakhon Ratchasima, Thailand, November 27<sup>th</sup>-29<sup>th</sup>, 2016. **P159**, *Poster presentation.*

**Waraporn Rernglit**, Wipa Suginta and Albert Schulte. Hybrid redox recycling of glucose oxidase in thin-film chitosan-carbon nanotube sensor coatings. The 10<sup>th</sup> International Symposium of the Protein Society of Thailand, Chulabhorn Research Institute Convention Center, Bangkok, Thailand, July 15<sup>th</sup>-17<sup>th</sup>, 2015. **P83**, *Poster presentation*.

**Waraporn Rernglit**, Wipa Suginta and Albert Schulte. Prototyping an electrochemical readout for para-nitrophenol-based enzyme activity assays. 7<sup>th</sup> Asia Oceania Human Proteome Organization (AOHUPO) Congress and 9<sup>th</sup> International Symposium of the Protein Society of Thailand “Frontiers in Protein and Proteomic Research”, Miracle Grand Convention Hotel, Bangkok, Thailand, August 6<sup>th</sup>-8<sup>th</sup>, 2014. **P208**, *Poster presentation*.

**Waraporn Rernglit**, Wipa Suginta and Albert Schulte. An electrochemical enzyme activity assay working with *p*-nitrophenol as redox marker. The 8<sup>th</sup> International Symposium of the Protein Society of Thailand, Chulabhorn Research Institute Convention Center, Bangkok, Thailand, August 5<sup>th</sup>-7<sup>th</sup>, 2013. **P97**, *Poster presentation*.

**Waraporn Rernglit**, Piyanuch Kullawong, Wipa Suginta and Albert Schulte. Carbon Nanotube-Chitin Blends as Easy-To-Form but Well-Working Enzyme Biosensor Immobilization Matrices. 13<sup>th</sup> FAOBMB (Federation of National Societies of Biochemistry and Molecular Biology) Congress, “Discovery of Life Processes: From Biomolecules to Systems Biology”, Bangkok International Trade and Exhibition Center (BITEC), Bangkok, Thailand, August 25<sup>th</sup>-29<sup>th</sup>, 2012. **P219-P220**, *Poster presentation*.

## APPENDIX D

### PUBLICATIONS

#### D.1 Submitted:

**Rernglit, W.**, Suginta, W. and Schulte, A. (2018) Plain carbon nanotube scaffolds with polymer glaze: An easy-to-make capped nanoporous sponge for durable oxidase biosensors with wide dynamic range. **Advanced Functional Materials**

#### D.2 In preparations:

**Rernglit, W.**, Sucharitakul, J., Schulte, A., Jaiyen, P. and Suginta, W. (2018) Catalytic mechanism of 4MU-GlcNAc dependent by  $\beta$ -N-acetyl glucosaminidase from *Vibrio Harveyi* (VhGlcNacase).

**Rernglit, W.**, Suginta, W. and Schulte, A. (2018) Establishment of an electrochemical readout for  $\beta$ -N-acetyl glucosaminidase enzyme activity assays.

## CURRICULUM VITAE

**NAME:** Miss Waraporn Rernglit

**STATUS:** Ph.D. candidate (Chemistry)

**DATE OF BIRTH:** 8th November 1979

**PLACE OF BIRTH:** Chaiyaphum, Thailand

**NATIONALITY:** Thai

### EDUCATIONS:

- 1993, High school  
Suranareewittaya School, Nakhon Ratchasima, Thailand.
- 1998, B.Sc., Chemical Engineering  
Faculty of Engineering, Srinakharinwirot University, Bangkok, Thailand.
- 2002, M.Sc., Chemical Technology  
Faculty of Science, Chulalongkhon University, Bangkok, Thailand.
- 2012 – 2018 start as Ph.D. student  
School of Chemistry, Institute of Science, Suranaree University of  
Technology, Nakhon Ratchasima, Thailand.